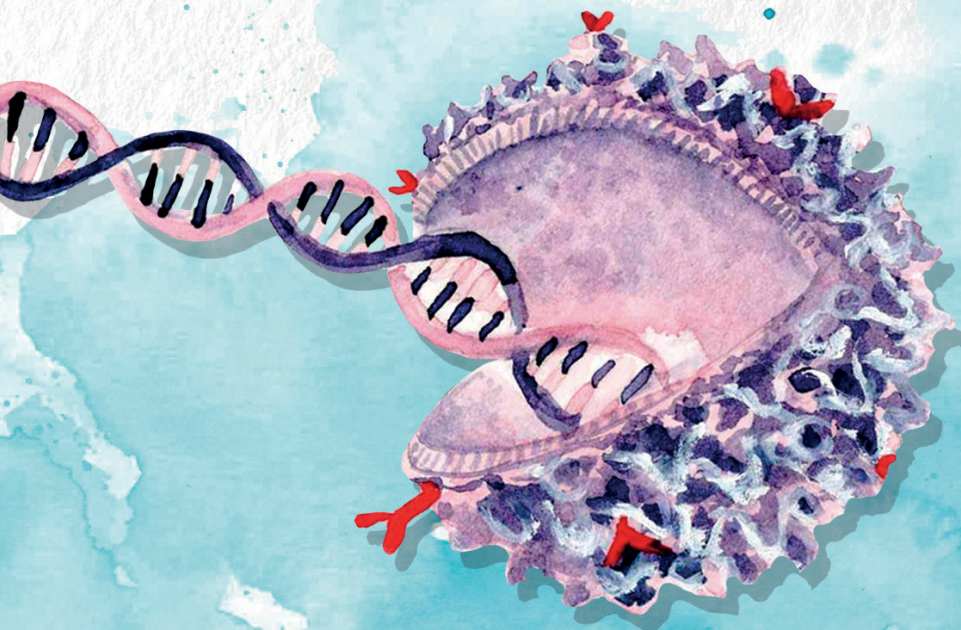


Engineering the next-generation of T cell-based cancer immunotherapies

Patricia Hernández López



Engineering the next-generation of T cell-based cancer immunotherapies

Patricia Hernández López

ISBN: 978-94-6483-699-8

Cover design: Eva Blasco – www.acuarelasomteha.com

Print: Ridderprint – www.ridderprint.nl

©Copyright 2024: Patricia Hernández López, Utrecht, The Netherlands
All rights reserved. No part of this publication may be reproduced, stored in a retrieval system, or transmitted in any form or by any means, electronic, mechanical, by photocopying, recording, or otherwise, without the prior written permission of the author.

Printing of this thesis was financially supported by Infection and Immunity Utrecht

Engineering the next-generation of T cell-based cancer immunotherapies

Bouwen aan de T cel therapie van morgen

(met een samenvatting in het Nederlands)

Proefschrift

ter verkrijging van de graad van doctor aan de
Universiteit Utrecht
op gezag van de
rector magnificus, prof.dr. H.R.B.M. Kummeling,
ingevolge het besluit van het college voor promoties
in het openbaar te verdedigen op

dinsdag 13 februari 2024 des middags te 12.15 uur

door

Patricia Hernández López

geboren op 11 mei 1994

te Madrid

Promotor

Prof. dr. J.H.E. Kuball

Co-promotors

Dr. D. Beringer

Dr. Z Sebestyen

Beoordelingscommissie:

prof. dr. P.J. Coffe (voorzitter)

prof. dr. S. Minguet

prof. dr. L. Meyaard

prof. dr. J.J. Molenaar

dr. J.M.L. Roodhart

Contents

Chapter 1	General introduction.Strategies to improve $\gamma\delta$ TCRs engineered T-cell therapies for the treatment of solid malignancies <i>Frontiers in Immunology, 2023</i>	9
Chapter 2	Thesis outline	27
Chapter 3	Gamma delta TCR anti-CD3 bispecific molecules (GABs) as novel immunotherapeutic compounds <i>The Journal for ImmunoTherapy of Cancer, 2021</i>	33
Chapter 4	Impact of CD3 binding affinity on the potency of Gamma delta TCR Anti-CD3 Bispecific T cell engagers (GABs) <i>Manuscript in preparation</i>	71
Chapter 5	Adding help to an HLA-A*24:02 tumor reactive $\gamma\delta$ TCR increases tumor control <i>Frontiers in Immunology, 2021</i>	97
Chapter 6	Dual-targeting of cancer-metabolome and stress antigens impacts transcriptomic heterogeneity and efficacy of engineered T-cells <i>Nature Immunology, 2023</i> <i>Patent application: EP23188032.9CD277 TARGETING COSTIMULATORYRECEPTOR (Hernández co-inventor)</i>	135
Chapter 7	Characterization and modulation of anti- $\alpha\beta$ TCR antibodies and their respective binding sites at the β TCR chain to enrich engineered T cells. <i>Molecular Therapy - Methods & Clinical Development, 2021</i>	201
Chapter 8	Summarizing discussion.	237
Appendices	Summary Nederlandse samenvatting Acknowledgement/agradecimientos List of publications Curriculum vitae	251



CHAPTER 1

General introduction

Strategies to improve $\gamma\delta$ TCRs engineered
T-cell therapies for the treatment of solid
malignancies

A. D. Meringa^{1†}, P. Hernández-López^{1†}, A. Cleven^{1†}, M. de Witte^{1,2}, T. Straetemans^{1,2}, J. Kuball^{1,2}, D. X. Beringer¹, Z. Sebestyen¹

¹Center for Translational Immunology, University Medical Center Utrecht, Utrecht University, Utrecht, Netherlands

²Department of Hematology, University Medical Center Utrecht, Utrecht University, Utrecht, Netherlands

† Equally contributed

Frontiers in Immunology, 2023

Introduction

After the overwhelming clinical success of targeting hematological malignancies with CAR-T cells¹, the first signals of treatment are seen for solid tumors targeted by engineered immune cells². However, targeting solid tumors with this kind of immunotherapy still remains a challenge^{3,4}. There are multiple mechanisms that make it difficult for adoptive cellular therapies to effectively target solid tumors.

First, most solid tumors lack homogeneous expression of a tumor-specific antigen making it difficult to find appropriate receptors to target them⁵. The selection of targetable tumor antigens needs careful consideration to avoid targeting of healthy tissue, especially when considering engineered cellular therapies against solid cancers, where potent and safe antigens are rare⁶. Additionally, the microenvironment of solid tumors holds unique features such as expression of immunosuppressive molecules and hypoxia that have a huge impact on T cell fitness^{4,7,8}. Finally, a combination of extracellular matrix deposition and anti-inflammatory signals, like attracting mesenchymal derived suppressor cells (MDSCs), prevent effective infiltration of T cells towards the tumor site⁹.

In this article we will further discuss the roadblocks facing successful implementation of T cell therapies for the treatment of solid malignancies focusing on $\gamma\delta$ T cells and their receptors since they provide a new avenue to target novel tumor antigens. Characterization of these cells and their receptors holds the potential to generate novel strategies for targeting cancer and provide new engineering strategies to potentially overcome these hurdles.

Gamma delta T cells as source of novel tumor-targeting receptors

The infiltration of $\gamma\delta$ T cell in tumors has been associated in many studies to have a favorable impact on patient survival¹⁰⁻¹⁶, while some other studies made in murine models report that interleukin-17 (IL-17) producing $\gamma\delta$ T cells are tumor promoting^{17, 18}. While these data are very insightful, it has to be carefully handled when translating it to human clinical practices given that

human and mouse $\gamma\delta$ T cell repertoires and functions are not fully compatible. Regardless of the ultimate effector function, activation of $\gamma\delta$ T cells is contingent upon the engagement of their surface receptors with antigens on the tumor cell. $\gamma\delta$ T cells can be divided into two groups, $V\delta 2^+$ and $V\delta 2^-$, with $V\delta 1$ forming the majority of $V\delta 2^-$ T-cells. $V\delta 2^-$ T cells are predominantly found in peripheral tissue and have also been shown to be enriched in carcinomas^{11, 19-21}. Multiple studies reported a correlating favorable clinical outcome either with the presence of $V\delta 2^-$ T-cells^{12, 13} or with $\gamma\delta$ T in general²². This tissue-association might be advantageous for targeting and infiltrating solid tumors when using $V\delta 1$ TCRT cells as effector cells. $V\delta 2^-$ TCRs can recognize a wide variety of ligands that are expressed on infected and malignant cells²³. A large number of studies have shown that numerous $V\delta 2^-$ TCRs can recognize nonpolymorphic MHC I-like molecules MR1 and CD1^{24, 25}. Most CD1 isoforms, CD1a, CD1b, and CD1c, are mainly found on cells of hematological origin and declassify them as potential ligands for solid tumors²⁶, but both MR1 as CD1d have been found to be expressed on solid tumors^{26, 27}. Other $\gamma\delta$ TCR ligands expressed on solid tumors and are recognized by specific $V\delta 2^-$ TCR clones are endothelial protein C receptor (EPCR)²⁸, Annexin A2²⁹, and EphA2³⁰. Based on the wide breath of ligands recognized by $V\delta 2^-$ TCRs²³, it is to be expected that many more ligands for this subset will be identified in the future. While many of these $V\delta 2^-$ TCR ligands are also expressed on the surface healthy cells, such as EPCR on endothelial cells³¹ and CD1d on APCs³², no major safety concerns have been reported. For example, a study demonstrating that while an EPCR reactive $V\delta 2^-$ TCR clone recognized cytomegalovirus (CMV)-infected or malignant endothelial cells it was not reactive against normal endothelial cells, due to increased expression of immune modulating molecules such as CD54 and CD58²⁸. Additionally, to avoid toxicity towards healthy, antigen presenting cells (APCs), lipid-specific CD1d reactive $V\delta 2^-$ TCRs can be used³³.

Unlike above discussed $V\delta 2^-$ T cells, $V\delta 2^+$ T cells, also referred as $V\gamma 9V\delta 2$ T cells are mainly present in blood and their role of cancer immune surveillance have been studied the most among all $\gamma\delta$ T cells³⁴. The process of identifying the ligand complex for the invariant $V\gamma 9V\delta 2$ TCRs has been a long and winding path, that started with the identification of phosphoantigens³⁵ that are bound by the intracellular domain of butrophylin 3A1 (BTN3A1)³⁶. This process leads

to a re-localization of BTN3A1 to the cell surface^{37, 38}, where it can form a complex with BTN2A1³⁹⁻⁴¹. Only when this phosphoantigen driven complex of BTN3A1 and BTN2A1 is formed on the plasma membrane, V γ 9V δ 2 TCRs can be activated. This multistep ligand complex formation serves a safety threshold that prevents V γ 9V δ 2 TCR mediated toxicity towards healthy tissue but enables the eradication of tumors in many preclinical models⁴²⁻⁴⁴.

While $\gamma\delta$ T cells have their natural potential to target cancer, as described above, the most clinical trials to date, that have assessed the efficacy and safety of $\gamma\delta$ T cells as adoptive cellular therapy did show moderate clinical efficacy⁴⁵⁻⁴⁸ where only incidentally e.g. prolonged survival of patients has been reported⁴⁷. However, the potential of natural, tumor infiltrating $\gamma\delta$ T cells has recently been demonstrated in colorectal cancer¹⁰ and kidney cancer¹⁶, supporting the idea to further investigate the details of receptors present on $\gamma\delta$ T cells for the treatment of cancer. While providing an emerging universe of tumor specific receptors, one has to carefully assess possible toxicity against healthy tissues in advanced 3-dimensional preclinical models^{42, 43, 49} that resemble the homeostatic environment of the human body.

Improving T-cell fitness for durable tumor control

T cell dysfunction has been one of the major causes of failure of CAR-T cell treatments as it results in poor T cell expansion and short-term persistence resulting in reduced anti-tumor efficacy^{8, 50}. Despite efforts to improve CAR designs, CAR-T cell exhaustion remains one of the main limitations of this kind of therapy⁵¹⁻⁵³. Thus, although CAR-T field has significantly growth in the last years, some studies advocate for the use of natural TCR signaling to reduce exhaustion of T cells^{54, 55}. The main reason for this is that CAR's artificial design accelerates exhaustion of T cells when compared to TCR based therapies, mostly due to the described tonic signaling in the absence of antigen⁵⁵⁻⁵⁷. In this line, several designs have been explored to make CAR more TCR-like, such as HLA-independent TCR (HIT) or synthetic TCR and antigen receptor (STAR)^{58, 59}. The CAR scFv sequence in these receptors is fused to the constant domains of an $\alpha\beta$ TCR, thereby preserving TCR signaling while using the CAR's ability to recognize tumors in an HLA independent way. An elegant alternative

to these designs is engineering $\alpha\beta$ T cells to express tumor-reactive V γ 9V δ 2 TCRs (called TEGs)^{42, 60}. In this way, the use of $\gamma\delta$ TCRs in T cell therapy appear to be advantageous when compared with CARs or $\alpha\beta$ TCRs, as they supply T cells with natural TCR signaling while preserving the ability of recognize tumors in an HLA-independent way⁴⁵.

Optimal co-stimulation has been described as key to overcome exhaustion and improve T cell fitness and persistence in the context of cancer⁶¹⁻⁶³. Therefore, as costimulatory signals are highly involved in T cell metabolic reprogramming^{64, 65} and T cell exhaustion is closely related with metabolic dysfunction, manipulation of co-stimulation in T cell therapies will result in improved metabolic T cell fitness, which is key to achieve robust anti-tumor responses⁶⁴. One example is the addition of co-stimulatory domains to the first generation of CARs, which has shown to improve persistence of these cells^{66, 67}. This led to the development of second and third generation of CARs with improved proliferation ability. Therefore, combining natural TCR signaling properties, by using $\gamma\delta$ TCRs to target tumors, with improved co-stimulation might be the answer to CAR-T limitations.

One way to improve the co-stimulation of T cells can be achieved by expressing chimeric costimulatory receptors (CCRs) in combination with a CAR or a TCR⁶⁸⁻⁷¹. These receptors preserve the structure of conventional second-generation CARs but lack the CD3 ζ domain, therefore providing only costimulatory signals to the T cell. Uncoupling of signal 1 (CD3 signal) and signal 2 (co-stimulation) by this dual targeting has been shown to be beneficial⁷²⁻⁷⁴ as T cells will only activate once synergistic signals are delivered upon encounter of both antigens. While these receptors improve T cell proliferation, they also reduce exhaustion⁷² thereby improving T cell persistence in the tumor niche and leading to an improved therapeutic effect^{72, 75}.

A type of CCRs are the so-called switch chimeric co-receptors⁷⁶⁻⁷⁹, which use the extracellular domain of a described inhibitory receptor (such as PD-1 or TIGIT) and link it to the intracellular domain of activating costimulatory receptors (such as CD28 or 4-1BB) or eventually DAP10, when expressed in

$\gamma\delta$ T cells⁷¹. Thus, these receptors turn inhibitory signals, that would normally induce exhaustion of T cells, into activating signals. This strategy improves not only T cell fitness, by improving co-stimulation, but also makes engineered T cells resistant to tumor microenvironment immunosuppressive factors.

Finally, it is important to further investigate the mechanisms that impact T cell fitness as not all the T cells subsets respond equal to the same stimulus. For example, TGF- β has been shown to improve cytotoxic activity of V δ 2⁺ T cells⁸⁰ while it is been described to suppress $\alpha\beta$ T cells function⁸¹. Furthermore, IL-15 has been shown to improve tumor killing capacity of $\gamma\delta$ T cells isolated from AML patients⁸². Therefore, comprehensive studies and rational engineering it is key to develop effective therapies. In conclusion, to achieve durable anti-tumor responses the next generation of T cell-based immunotherapies should include fine-tuning of co-stimulation, to preserve T cell fitness, ensure persistence, and skew the T cells to the most potent phenotype.

Tackling the tumor microenvironment

The lack of efficacy observed for different T cell treatments targeting various antigens in solid tumors suggest the presence of general barriers that inhibit the efficacy of these immunotherapies. The cellular and extra-cellular composition of the tumor microenvironment can influence the tumor biology and response to immune therapy⁸³. The dense extracellular matrix (ECM) of solid tumors is a physical barrier for T cells to penetrate leading to low numbers of infiltrating, endogenous T cells in solid tumors⁴. Meanwhile, immunosuppressive cells such as myeloid-derived suppressive cells and regulatory T cells in the tumor microenvironment (TME) inhibit antitumor activity of T cells that do infiltrate in the TME⁸⁴. Different engineering strategies are being developed to overcome these general barriers of T-cell therapies in solid malignancies.

Modulation of the chemokine signaling of the tumor-reactive T cells can lead to improved T cell infiltration by increasing chemotaxis towards the tumor site. For example, expression of the colony stimulating factor receptor (CSF-R) in CAR-T cells improved migration towards solid tumor models producing CSF⁸⁵.

Arming T cells with other chemokine receptors have shown similar results where CCR4, CCR2b and CXCR3 overexpression in the T cell products led to increased infiltration in the TME and thereby increased tumor targeting⁸⁶⁻⁸⁸.

Upon infiltration of immune cells in the TME, multiple mechanisms can render the T cells inactive via expression of immunosuppressive molecules. Well-known checkpoint molecules such as PD-1 and TIM3 are not only affecting $\alpha\beta$ T cells but also act on $\gamma\delta$ T cells as has been recently shown¹⁰ in colorectal cancer. However, $\gamma\delta$ T cells are also often regulated by unique sets of inhibitory natural killer (NK) receptors: for example, tumor and stromal cells can express ligands for immune checkpoints in T cells like HLA-E binding NKG2A on $\gamma\delta$ tumor infiltrating lymphocytes (TILs)⁸⁹. To overcome this, numerous cytokines have been tested to make armed CAR-T cells also known as T cell redirected for antigen-unrestricted cytokine-initiated killing (TRUCKs)⁹⁰. CAR-T cells targeting different solid tumor models were shown to improve their anti-tumor activity, increase their resistance to regulatory T cell signaling and improve local proliferation upon arming the T cells with IL-12 expression⁹¹⁻⁹³. Expression of other cytokines such as IL-7, IL-15 and IL-18 have shown to provide similar results by increasing therapy efficacy via increasing local inflammation in the TME⁹³⁻⁹⁵. Chemokine and cytokine arming of $\gamma\delta$ TCR based T cell therapies could increase efficacy since other T cell engineering approaches for CAR-T cells.

Additionally, CAR-T cells can be engineered to express ECM-modifying enzymes to facilitate better penetration to the tumor site. Heparinase expressing GD2 CAR-T cells improved their infiltrating capacity in solid tumor models compared to CAR-T cells lacking heparin expression^{96, 97}. Arming CAR-T cell with prolyl endopeptidase is another approach for targeting the ECM in the TME⁹⁸. Expression of prolyl endopeptidase in CAR-T cells improved their anti-tumor activity, however some toxicity towards healthy tissue was observed with both ECM targeting approaches. Introducing these types of modifications could be very promising for improving the therapeutic effect of $\gamma\delta$ TCR T cells in solid tumors.

Future Perspectives

Current developments in the field of engineered adoptive cellular therapies, especially CAR-T cell therapies show promising results in the treatment of haematological malignancies; more specifically B cell-derived tumors. However, adapting these T cells therapies to solid tumor treatments options requires overcoming certain impediments posed by solid malignancies and their TME (Figure 1). Fortunately, these T cells-based therapies allow for *ex vivo* modifications of the treatment to address these tumor-specific challenges posed in the TME of solid tumors where lesson learned from tumor specific $\gamma\delta$ T may provide a possible solution.

Selection of the tumor-reactive receptor and the tumor specific/associated antigen remains the first important step in optimizing T cell therapies in solid tumors. To this end, $\gamma\delta$ TCRs are an interesting option due to their unique recognition patterns. Secondly, the addition of a co-stimulatory signal, especially in combination with a naturally low affinity $\gamma\delta$ TCR can help improve T cell fitness via either one of the three suggested signalling approaches. Expressing a chimeric costimulatory receptor to mimic signal 2 will help the T cells to retain their anti-tumor activity upon prolonged exposure in the TME. Furthermore, the induction of inflammation via secretion of cytokines such as at the tumor site can help the tumor infiltrating $\gamma\delta$ TCR T cells to overcome the immunosuppressive signals present in the TME. Finally, expression of chemokine(receptors) or ECM modifying molecules can help increase T cell infiltration in the solid tumor microenvironment.

In conclusion, promising approaches for improving the efficacy and scope of T cell therapies are being developed to overcome the current roadblocks in the treatment of solid malignancies. Using $\gamma\delta$ TCRs as tumor-reactive receptors, and combining these with appropriate co-stimulation via expression of additional chimeric costimulatory receptor to improve fitness and providing additional mechanisms to improve $\gamma\delta$ TCR T-cell infiltration like boosting chemotaxis, will be key assets to enhance efficacy of T cell therapies for solid malignancies. While further modifying the T cells does contain risks, these

solutions will help to optimize efficacy of engineered T cell therapies and introduce this technology for a more widespread use in anticancer therapy.

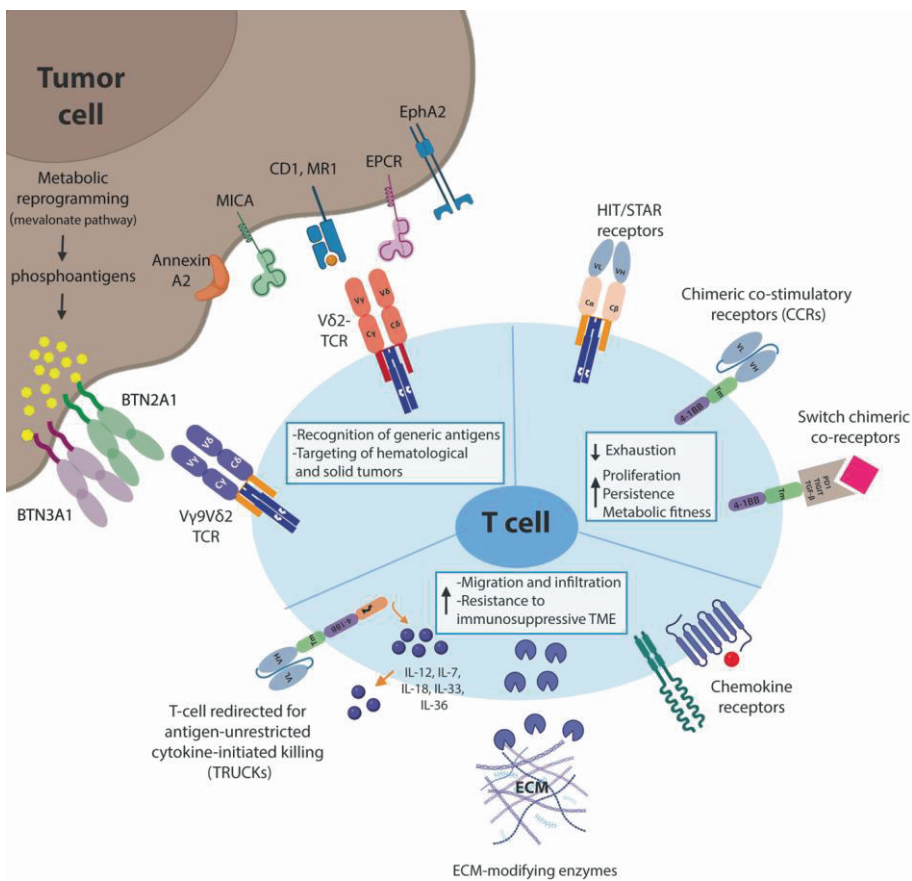


Figure 1. Schematic representation of T-cell engineering approaches. Biological mechanisms that prevent effective adoption of gd T-cell therapies for the treatment of solid malignancies and suggested engineering strategies to overcome these hurdles are shown

Author contributions

All authors listed have made a substantial, direct, and intellectual contribution to the work and approved it for publication.

Funding

This work was supported by grants KWF 11979, KWF 11393, KWF 12586, KWF 13043, KWF 13493 to authors JK, ZS and DB from the Dutch Cancer Society KWF

Conflict of interest

JK, ZS and DB are inventors on various patents regarding T cell immune therapies, JK is shareholder at Gadeta BV. The remaining authors declare that the research was conducted in the absence of any commercial or financial relationships that could be construed as a potential conflict of interest.

References

1. Roschewski, M., D.L. Longo, and W.H. Wilson, *CAR T-Cell Therapy for Large B-Cell Lymphoma - Who, When, and How?* N Engl J Med, 2022. **386**(7): p. 692-696.
2. Majzner, R.G., et al., *GD2-CAR T cell therapy for H3K27M-mutated diffuse midline gliomas.* Nature, 2022. **603**(7903): p. 934-941.
3. Marofi, F., et al., *CAR T cells in solid tumors: challenges and opportunities.* Stem Cell Res Ther, 2021. **12**(1): p. 81.
4. Hou, A.J., L.C. Chen, and Y.Y. Chen, *Navigating CAR-T cells through the solid-tumour microenvironment.* Nat Rev Drug Discov, 2021. **20**(7): p. 531-550.
5. Wagner, J., et al., *CAR T Cell Therapy for Solid Tumors: Bright Future or Dark Reality?* Mol Ther, 2020. **28**(11): p. 2320-2339.
6. Bailey, S.R., et al., *Four challenges to CAR T cells breaking the glass ceiling.* Eur J Immunol, 2022: p. e2250039.
7. Gao, T.A. and Y.Y. Chen, *Engineering Next-Generation CAR-T Cells: Overcoming Tumor Hypoxia and Metabolism.* Annu Rev Chem Biomol Eng, 2022. **13**: p. 193-216.
8. Gumber, D. and L.D. Wang, *Improving CAR-T immunotherapy: Overcoming the challenges of T cell exhaustion.* EBioMedicine, 2022. **77**: p. 103941.
9. Lanitis, E., et al., *Mechanisms regulating T-cell infiltration and activity in solid tumors.* Ann Oncol, 2017. **28**(suppl_12): p. xii18-xii32.
10. de Vries, N.L., et al., *gammadelta T cells are effectors of immunotherapy in cancers with HLA class I defects.* Nature, 2023. **613**(7945): p. 743-750.
11. Gherardin, N.A., et al., *gammadelta T Cells in Merkel Cell Carcinomas Have a Proinflammatory Profile Prognostic of Patient Survival.* Cancer Immunol Res, 2021. **9**(6): p. 612-623.
12. Donia, M., et al., *Analysis of Vdelta1 T cells in clinical grade melanoma-infiltrating lymphocytes.* Oncoimmunology, 2012. **1**(8): p. 1297-1304.
13. Gentles, A.J., et al., *The prognostic landscape of genes and infiltrating immune cells across human cancers.* Nat Med, 2015. **21**(8): p. 938-945.
14. Zakeri, N., et al., *Characterisation and induction of tissue-resident gamma delta T-cells to target hepatocellular carcinoma.* Nat Commun, 2022. **13**(1): p. 1372.
15. Rosso, D.A., et al., *Glioblastoma cells potentiate the induction of the Th1-like profile in phosphoantigen-stimulated gammadelta T lymphocytes.* J Neurooncol, 2021. **153**(3): p. 403-415.
16. Rancan, C., et al., *Exhausted intratumoral Vdelta2(-) gammadelta T cells in human kidney cancer retain effector function.* Nat Immunol, 2023.
17. Coffelt, S.B., et al., *IL-17-producing gammadelta T cells and neutrophils conspire to promote breast cancer metastasis.* Nature, 2015. **522**(7556): p. 345-348.
18. Lo Presti, E., et al., *Squamous Cell Tumors Recruit gammadelta T Cells Producing either IL17 or IFNgamma Depending on the Tumor Stage.* Cancer Immunol Res, 2017. **5**(5): p. 397-407.

19. Hidalgo, J.V., et al., *Histological Analysis of gammadelta T Lymphocytes Infiltrating Human Triple-Negative Breast Carcinomas*. *Front Immunol*, 2014. **5**: p. 632.
20. Dadi, S., et al., *Cancer Immunosurveillance by Tissue-Resident Innate Lymphoid Cells and Innate-like T Cells*. *Cell*, 2016. **164**(3): p. 365-77.
21. Janssen, A., et al., *gammadelta T-cell Receptors Derived from Breast Cancer-Infiltrating T Lymphocytes Mediate Antitumor Reactivity*. *Cancer Immunol Res*, 2020. **8**(4): p. 530-543.
22. Gentles, A.J., et al., *The prognostic landscape of genes and infiltrating immune cells across human cancers*. *Nat Med*, 2015. **21**(8): p. 938-45.
23. Willcox, B.E. and C.R. Willcox, *gammadelta TCR ligands: the quest to solve a 500-million-year-old mystery*. *Nat Immunol*, 2019. **20**(2): p. 121-128.
24. Van Rhijn, I. and J. Le Nours, *CD1 and MR1 recognition by human gammadelta T cells*. *Mol Immunol*, 2021. **133**: p. 95-100.
25. Castro, C.D., et al., *Diversity in recognition and function of human gammadelta T cells*. *Immunol Rev*, 2020. **298**(1): p. 134-152.
26. Consonni, M., P. Dellabona, and G. Casorati, *Potential advantages of CD1-restricted T cell immunotherapy in cancer*. *Mol Immunol*, 2018. **103**: p. 200-208.
27. Crowther, M.D., et al., *Genome-wide CRISPR-Cas9 screening reveals ubiquitous T cell cancer targeting via the monomorphic MHC class I-related protein MR1*. *Nat Immunol*, 2020. **21**(2): p. 178-185.
28. Willcox, C.R., et al., *Cytomegalovirus and tumor stress surveillance by binding of a human gammadelta T cell antigen receptor to endothelial protein C receptor*. *Nat Immunol*, 2012. **13**(9): p. 872-9.
29. Marlin, R., et al., *Sensing of cell stress by human gammadelta TCR-dependent recognition of annexin A2*. *Proc Natl Acad Sci U S A*, 2017. **114**(12): p. 3163-3168.
30. Harly, C., et al., *Human gammadelta T cell sensing of AMPK-dependent metabolic tumor reprogramming through TCR recognition of EphA2*. *Sci Immunol*, 2021. **6**(61).
31. Laszik, Z., et al., *Human protein C receptor is present primarily on endothelium of large blood vessels: implications for the control of the protein C pathway*. *Circulation*, 1997. **96**(10): p. 3633-40.
32. Brigl, M. and M.B. Brenner, *CD1: antigen presentation and T cell function*. *Annu Rev Immunol*, 2004. **22**: p. 817-90.
33. Luoma, A.M., et al., *Crystal structure of Vdelta1 T cell receptor in complex with CD1d-sulfatide shows MHC-like recognition of a self-lipid by human gammadelta T cells*. *Immunity*, 2013. **39**(6): p. 1032-42.
34. Sebestyen, Z., et al., *Translating gammadelta (gammadelta) T cells and their receptors into cancer cell therapies*. *Nat Rev Drug Discov*, 2020. **19**(3): p. 169-184.
35. Tanaka, Y., et al., *Natural and synthetic non-peptide antigens recognized by human gamma delta T cells*. *Nature*, 1995. **375**(6527): p. 155-8.
36. Harly, C., et al., *Key implication of CD277/butyrophilin-3 (BTN3A) in cellular stress sensing by a major human gammadelta T-cell subset*. *Blood*, 2012. **120**(11): p. 2269-79.

37. Vantourout, P., et al., *Heteromeric interactions regulate butyrophilin (BTN) and BTN-like molecules governing gammadelta T cell biology*. Proc Natl Acad Sci U S A, 2018. **115**(5): p. 1039-1044.
38. Vyborova, A., et al., *gamma9delta2T cell diversity and the receptor interface with tumor cells*. J Clin Invest, 2020. **130**(9): p. 4637-4651.
39. Rigau, M., et al., *Butyrophilin 2A1 is essential for phosphoantigen reactivity by gammadelta T cells*. Science, 2020. **367**(6478).
40. Karunakaran, M.M., et al., *Butyrophilin-2A1 Directly Binds Germline-Encoded Regions of the Vgamma9Vdelta2 TCR and Is Essential for Phosphoantigen Sensing*. Immunity, 2020. **52**(3): p. 487-498 e6.
41. Hsiao, C.C., et al., *Ligand-induced interactions between butyrophilin 2A1 and 3A1 internal domains in the HMBPP receptor complex*. Cell Chem Biol, 2022. **29**(6): p. 985-995 e5.
42. Johanna, I., et al., *Evaluating in vivo efficacy - toxicity profile of TEG001 in humanized mice xenografts against primary human AML disease and healthy hematopoietic cells*. J Immunother Cancer, 2019. **7**(1): p. 69.
43. van Diest, E., et al., *Gamma delta TCR anti-CD3 bispecific molecules (GABs) as novel immunotherapeutic compounds*. J Immunother Cancer, 2021. **9**(11).
44. De Gassart, A., et al., *Development of ICT01, a first-in-class, anti-BTN3A antibody for activating Vgamma9Vdelta2 T cell-mediated antitumor immune response*. Sci Transl Med, 2021. **13**(616): p. eabj0835.
45. Sebestyen, Z., et al., *Translating gammadelta ($\gamma\delta$) T cells and their receptors into cancer cell therapies*. Nat Rev Drug Discov, 2020. **19**(3): p. 169-184.
46. Mensurado, S., R. Blanco-Dominguez, and B. Silva-Santos, *The emerging roles of gammadelta T cells in cancer immunotherapy*. Nat Rev Clin Oncol, 2023.
47. Xu, Y., et al., *Allogeneic Vgamma9Vdelta2 T-cell immunotherapy exhibits promising clinical safety and prolongs the survival of patients with late-stage lung or liver cancer*. Cell Mol Immunol, 2021. **18**(2): p. 427-439.
48. Fournie, J.J., et al., *What lessons can be learned from gammadelta T cell-based cancer immunotherapy trials?* Cell Mol Immunol, 2013. **10**(1): p. 35-41.
49. Braham, M.V.J., et al., *Cellular immunotherapy on primary multiple myeloma expanded in a 3D bone marrow niche model*. Oncoimmunology, 2018. **7**(6): p. e1434465.
50. Fraietta, J.A., et al., *Determinants of response and resistance to CD19 chimeric antigen receptor (CAR) T cell therapy of chronic lymphocytic leukemia*. Nat Med, 2018. **24**(5): p. 563-571.
51. Kouro, T., H. Himuro, and T. Sasada, *Exhaustion of CAR T cells: potential causes and solutions*. J Transl Med, 2022. **20**(1): p. 239.
52. Whery, E.J. and M. Kurachi, *Molecular and cellular insights into T cell exhaustion*. Nat Rev Immunol, 2015. **15**(8): p. 486-99.
53. Poorebrahim, M., et al., *Counteracting CAR T cell dysfunction*. Oncogene, 2021. **40**(2): p. 421-435.

54. Salter, A.I., et al., *Comparative analysis of TCR and CAR signaling informs CAR designs with superior antigen sensitivity and in vivo function*. *Sci Signal*, 2021. **14**(697).
55. Wachsmann, T.L.A., et al., *Comparing CAR and TCR engineered T cell performance as a function of tumor cell exposure*. *Oncoimmunology*, 2022. **11**(1): p. 2033528.
56. Calderon, H., M. Mamonkin, and S. Guedan, *Analysis of CAR-Mediated Tonic Signaling*. *Methods Mol Biol*, 2020. **2086**: p. 223-236.
57. Gomes-Silva, D., et al., *Tonic 4-1BB Costimulation in Chimeric Antigen Receptors Impedes T Cell Survival and Is Vector-Dependent*. *Cell Rep*, 2017. **21**(1): p. 17-26.
58. Mansilla-Soto, J., et al., *HLA-independent T cell receptors for targeting tumors with low antigen density*. *Nat Med*, 2022. **28**(2): p. 345-352.
59. Liu, Y., et al., *Chimeric STAR receptors using TCR machinery mediate robust responses against solid tumors*. *Sci Transl Med*, 2021. **13**(586).
60. Marcu-Malina, V., et al., *Redirecting alphabeta T cells against cancer cells by transfer of a broadly tumor-reactive gammadeltaT-cell receptor*. *Blood*, 2011. **118**(1): p. 50-9.
61. Long, A.H., et al., *4-1BB costimulation ameliorates T cell exhaustion induced by tonic signaling of chimeric antigen receptors*. *Nat Med*, 2015. **21**(6): p. 581-90.
62. Guedan, S., et al., *Enhancing CAR T cell persistence through ICOS and 4-1BB costimulation*. *JCI Insight*, 2018. **3**(1).
63. Kowolik, C.M., et al., *CD28 costimulation provided through a CD19-specific chimeric antigen receptor enhances in vivo persistence and antitumor efficacy of adoptively transferred T cells*. *Cancer Res*, 2006. **66**(22): p. 10995-1004.
64. Pellegrino, M., et al., *Manipulating the Metabolism to Improve the Efficacy of CAR T-Cell Immunotherapy*. *Cells*, 2020. **10**(1).
65. Kawalekar, O.U., et al., *Distinct Signaling of Coreceptors Regulates Specific Metabolism Pathways and Impacts Memory Development in CAR T Cells*. *Immunity*, 2016. **44**(2): p. 380-90.
66. Tokarew, N., et al., *Teaching an old dog new tricks: next-generation CAR T cells*. *Br J Cancer*, 2019. **120**(1): p. 26-37.
67. Imai, C., et al., *Chimeric receptors with 4-1BB signaling capacity provoke potent cytotoxicity against acute lymphoblastic leukemia*. *Leukemia*, 2004. **18**(4): p. 676-84.
68. Katsarou, A., et al., *Combining a CAR and a chimeric costimulatory receptor enhances T cell sensitivity to low antigen density and promotes persistence*. *Sci Transl Med*, 2021. **13**(623): p. eabh1962.
69. Krause, A., et al., *Antigen-dependent CD28 signaling selectively enhances survival and proliferation in genetically modified activated human primary T lymphocytes*. *J Exp Med*, 1998. **188**(4): p. 619-26.
70. Sadelain, M., R. Brentjens, and I. Rivière, *The basic principles of chimeric antigen receptor design*. *Cancer Discov*, 2013. **3**(4): p. 388-98.
71. Fisher, J., et al., *Engineering gammadeltaT cells limits tonic signaling associated with chimeric antigen receptors*. *Sci Signal*, 2019. **12**(598).

72. Wilkie, S., et al., *Dual targeting of ErbB2 and MUC1 in breast cancer using chimeric antigen receptors engineered to provide complementary signaling*. J Clin Immunol, 2012. **32**(5): p. 1059-70.
73. Liao, Q., et al., *PD-L1 chimeric costimulatory receptor improves the efficacy of CAR-T cells for PD-L1-positive solid tumors and reduces toxicity in vivo*. Biomark Res, 2020. **8**(1): p. 57.
74. Lanitis, E., et al., *Chimeric antigen receptor T Cells with dissociated signaling domains exhibit focused antitumor activity with reduced potential for toxicity in vivo*. Cancer Immunol Res, 2013. **1**(1): p. 43-53.
75. Halim, L., et al., *Engineering of an Avidity-Optimized CD19-Specific Parallel Chimeric Antigen Receptor That Delivers Dual CD28 and 4-1BB Co-Stimulation*. Front Immunol, 2022. **13**: p. 836549.
76. Vienot, A., et al., *Chemokine switch regulated by TGF- β 1 in cancer-associated fibroblast subsets determines the efficacy of chemo-immunotherapy*. Oncoimmunology, 2022. **11**(1): p. 2144669.
77. Supimon, K., et al., *Cytotoxic activity of anti-mucin 1 chimeric antigen receptor T cells expressing PD-1-CD28 switch receptor against cholangiocarcinoma cells*. Cytotherapy, 2022.
78. Chen, C., et al., *Construction of PD1/CD28 chimeric-switch receptor enhances anti-tumor ability of c-Met CAR-T in gastric cancer*. Oncoimmunology, 2021. **10**(1): p. 1901434.
79. Hoogi, S., et al., *A TIGIT-based chimeric co-stimulatory switch receptor improves T-cell anti-tumor function*. J Immunother Cancer, 2019. **7**(1): p. 243.
80. Peters, C., et al., *TGF- β enhances the cytotoxic activity of V δ 2 T cells*. Oncoimmunology, 2019. **8**(1): p. e1522471.
81. Dahmani, A. and J.S. Delisle, *TGF- β in T Cell Biology: Implications for Cancer Immunotherapy*. Cancers (Basel), 2018. **10**(6).
82. Van Acker, H.H., et al., *Interleukin-15 enhances the proliferation, stimulatory phenotype, and antitumor effector functions of human gamma delta T cells*. J Hematol Oncol, 2016. **9**(1): p. 101.
83. Junttila, M.R. and F.J. de Sauvage, *Influence of tumour micro-environment heterogeneity on therapeutic response*. Nature, 2013. **501**(7467): p. 346-54.
84. Verma, N.K., et al., *Obstacles for T-lymphocytes in the tumour microenvironment: Therapeutic challenges, advances and opportunities beyond immune checkpoint*. EBioMedicine, 2022. **83**: p. 104216.
85. Lo, A.S., et al., *Harnessing the tumour-derived cytokine, CSF-1, to co-stimulate T-cell growth and activation*. Mol Immunol, 2008. **45**(5): p. 1276-87.
86. Di Stasi, A., et al., *T lymphocytes coexpressing CCR4 and a chimeric antigen receptor targeting CD30 have improved homing and antitumor activity in a Hodgkin tumor model*. Blood, 2009. **113**(25): p. 6392-402.

87. Nagarsheth, N., M.S. Wicha, and W. Zou, *Chemokines in the cancer microenvironment and their relevance in cancer immunotherapy*. *Nat Rev Immunol*, 2017. **17**(9): p. 559-572.
88. Craddock, J.A., et al., *Enhanced tumor trafficking of GD2 chimeric antigen receptor T cells by expression of the chemokine receptor CCR2b*. *J Immunother*, 2010. **33**(8): p. 780-8.
89. Cazzetta, V., et al., *NKG2A expression identifies a subset of human Vdelta2 T cells exerting the highest antitumor effector functions*. *Cell Rep*, 2021. **37**(3): p. 109871.
90. Chmielewski, M., A.A. Hombach, and H. Abken, *Of CARs and TRUCKs: chimeric antigen receptor (CAR) T cells engineered with an inducible cytokine to modulate the tumor stroma*. *Immunol Rev*, 2014. **257**(1): p. 83-90.
91. Pegram, H.J., et al., *Tumor-targeted T cells modified to secrete IL-12 eradicate systemic tumors without need for prior conditioning*. *Blood*, 2012. **119**(18): p. 4133-41.
92. Koneru, M., et al., *IL-12 secreting tumor-targeted chimeric antigen receptor T cells eradicate ovarian tumors in vivo*. *Oncoimmunology*, 2015. **4**(3): p. e994446.
93. Yeku, O.O., et al., *Armored CAR T cells enhance antitumor efficacy and overcome the tumor microenvironment*. *Sci Rep*, 2017. **7**(1): p. 10541.
94. Hoyos, V., et al., *Engineering CD19-specific T lymphocytes with interleukin-15 and a suicide gene to enhance their anti-lymphoma/leukemia effects and safety*. *Leukemia*, 2010. **24**(6): p. 1160-70.
95. Chmielewski, M. and H. Abken, *CAR T Cells Releasing IL-18 Convert to T-Bet(high) FoxO1(low) Effectors that Exhibit Augmented Activity against Advanced Solid Tumors*. *Cell Rep*, 2017. **21**(11): p. 3205-3219.
96. Caruana, I., et al., *Heparanase promotes tumor infiltration and antitumor activity of CAR-redirection T lymphocytes*. *Nat Med*, 2015. **21**(5): p. 524-9.
97. Mardomi, A. and S. Abediankenari, *Matrix Metalloproteinase 8: Could it Benefit the CAR-T Cell Therapy of Solid Tumors?- a Commentary on Therapeutic Potential*. *Cancer Microenviron*, 2018. **11**(1): p. 93-96.
98. Tran, E., et al., *Immune targeting of fibroblast activation protein triggers recognition of multipotent bone marrow stromal cells and cachexia*. *J Exp Med*, 2013. **210**(6): p. 1125-35.



CHAPTER 2

Thesis outline

As outlined in our review in **Chapter 1** promising approaches for improving the efficacy and scope of T-cell therapies are being developed to overcome the current roadblocks in the treatment of solid malignancies. Using $\gamma\delta$ TCRs as tumor-reactive receptors, and combining these with appropriate co-stimulation via expression of additional chimeric costimulatory receptor to improve T-cell fitness will be key assets to enhance efficacy of T-cell therapies for solid malignancies. While further modifying the T-cells does contain risks, it will help to optimize efficacy of engineered T-cell therapies and introduce engineered T-cell therapies for a more widespread use in anticancer therapy. In this thesis, we aimed to develop new T-cell based therapies by harnessing the capacity of $\gamma\delta$ TCRs to target tumor cells. We explored different designs, either as soluble formats, by developing bispecific T-cell engagers (**chapters 3 and 4**), or membrane embedded formats (**chapters 5 and 6**), by co-expression of different $\gamma\delta$ TCRs together with natural or chimeric co-receptors in $\alpha\beta$ T cells. Finally, inspired by a concept originally developed for $\gamma\delta$ TCRs, we aimed to further improve product purity when using $\alpha\beta$ TCRs to engineer $\alpha\beta$ T cells (**chapter 7**).

In **Chapter 3** we developed a novel bispecific T-cell engager by fusing the extracellular domains of a tumor reactive $\gamma\delta$ TCR to an anti-scFV-CD3, creating $\gamma\delta$ TCR anti-CD3 bispecific molecules (GABs). GABs are able to bind $\alpha\beta$ T-cells through their anti-CD3 domain and redirect them to recognize tumor cells through their $\gamma\delta$ TCR domain. GABs were able to target both hematological and solid tumors *in vitro* without harming healthy tissues, and decreased tumor outgrowth in a subcutaneous multiple myeloma xenograft model. Thereby we harness the potential of $\gamma\delta$ TCR to target a broad range of tumor cells, and combine it with the advantage of an off-the-shelf treatment such as a bispecific molecule, thus shortening the time to infusion as well as treatment cost when compared with other therapies like CAR-T cells.

In **Chapter 4** we study the impact of the affinity of the anti-CD3 arm on GABs efficacy. We demonstrated that increasing the affinity of the anti-CD3 scFV improves GABs efficacy *in vitro*. Moreover, GABs containing a high affinity anti-CD3 increased tumor control in a multiple myeloma xenograft model and were found to be bound longer to T-cells *in vivo*.

In **Chapter 5** we aimed to improve TEG011 ($\alpha\beta$ T-cells engineered to express an allo-HLA-A*24:02-restricted V γ 5V δ 1-TCR called FE11) efficacy by co-expressing CD8 α . FE11-TCR activity has been shown to be CD8 α -dependent. Introduction of CD8 α into TEG011 CD4 $^{+}$ cells improved *in vivo* persistence and tumor infiltration of these cells, resulting in enhanced tumor control.

In **Chapter 6** we describe a novel strategy to target tumors from different origin by combining targeting of tumor metabolic reprogramming and stress ligands. To do this, we harness the metabolic sensing of V γ 9 δ 2-TCRs to target a large variety of tumors by using the clinical candidate TEG001 ($\alpha\beta$ T-cells expressing the V γ 9 δ 2-TCR called Cl5), combined with a NKG2D or anti-CD277 based chimeric co-receptor that recognizes the stress ligands and provide co-stimulation once TCR is engaged. NKG2D-CD28 and NKG2D-4-1BB chimeric co-receptors were able to increase tumor control in a multiple myeloma xenograft model. Moreover, NKG2D-4-1BB chimera increased proliferation *in vivo*, decreased tumor outgrowth in a head and neck subcutaneous xenograft model and transcriptionally reprogrammed CD4 $^{+}$ TEG001 towards a less exhausted phenotype. On the other hand, the anti-CD277 chimeric co-receptor (103-4-1BB) reprogrammed both CD4 $^{+}$ and CD8 $^{+}$ cells and induced the eradication of liquid and solid tumors *in vivo*. Combining targeting of tumors through V γ 9 δ 2-TCRs with either NKG2D-4-1BB chimera or anti-CD277 chimera relies on the targeting of two types of universal tumor-associated antigens, and therefore it increases the number of tumors that can be treated with one single therapy when compared to other T-cell based therapies such as CARs, opening a broad range of opportunities to improve already existing T-cell based therapies.

In **Chapter 7** we describe a method to increase the product purity for $\alpha\beta$ TCR-based therapies, in which two amino acids in the constant domain of the $\alpha\beta$ TCR are exchanged by their mouse counterpart. Modifying binding sites at the $\alpha\beta$ TCR was inspired by an isolation strategy using $\gamma\delta$ TCR^{1,2}. Mutation of these two amino acids abrogate the binding of a GMP-grade human anti- $\alpha\beta$ TCR antibody, which can be used to deplete the non-engineered or poorly engineered T-cells resulting in significantly increased percentage of engineered T-cells in the total product. Moreover, mutation of seven extra

amino acids in the constant region allowed for the depletion of engineered T-cells by using an anti-mouse $\alpha\beta$ TCR antibody, which could be exploited in the future to specifically eliminate engineered T-cells *in vivo*.

Chapter 8 summarizes and discusses the findings of the previous chapters in the context of the latest literature within the field of the $\gamma\delta$ and $\alpha\beta$ T-cell immunotherapies.

References

1. Straetemans, T., et al., *GMP-Grade Manufacturing of T Cells Engineered to Express a Defined gammadeltaTCR*. *Front Immunol*, 2018. **9**: p. 1062.
2. Straetemans, T., et al., *Untouched GMP-Ready Purified Engineered Immune Cells to Treat Cancer*. *Clin Cancer Res*, 2015. **21**(17): p. 3957-68.



CHAPTER 3

Gamma delta TCR Anti-CD3 Bispecific molecules (GABs) as novel immunotherapeutic compounds

Eline van Diest^{1,*}, Patricia Hernández López^{1,*}, Angelo Meringa¹, Anna Vyborova¹, Effrosyni Karaiskaki¹, Sabine Heijhuurs¹, Jan Gumathi Bormin¹, Sanne van Dooremalen¹, Mara Nicolassen¹, Lucrezia Gatti¹, Inez Johanna¹, Trudy Straetemans¹, Zsolt Sebestyén¹, Dennis X. Beringer^{1,#} and Jürgen Kuball^{1,2,#}

¹Center for Translational Immunology, University Medical Center Utrecht, Utrecht University, 3584 CX Utrecht, The Netherlands

²Department of Hematology, University Medical Center Utrecht, Utrecht University, 3584 CX Utrecht, The Netherlands

* EVD and PHL contributed equally

Shared senior authors

Journal for Immunotherapy of Cancer, 2021

Abstract

Background: $\gamma\delta$ T cells hold great promise as cancer therapeutics because of their unique capability of reacting to metabolic changes with tumor cells. However, it has proven very difficult to translate this promise into clinical success.

Methods: In order to better utilize the tumor reactivity of $\gamma\delta$ T cells and combine this with the great potential of T cell engager molecules, we developed a novel bispecific molecule by linking the extracellular domains of tumor-reactive $\gamma\delta$ TCRs to a CD3-binding moiety, creating gamma delta TCR anti-CD3 bispecific molecules (GABs). GABs were tested *in vitro* and *in vivo* for ability to redirect T lymphocytes to a variety of tumor cell lines and primary patient material.

Results: GABs utilizing naturally occurring high affinity $\gamma\delta$ TCRs efficiently induced $\alpha\beta$ T cell mediated phosphoantigen-dependent recognition of tumor cells. Reactivity was substantially modulated by variations in the V δ 2 CDR3-region and the BTN2A1-binding HV4-region between CDR2 and CDR3 of the γ -chain was crucial for functionality. GABs redirected $\alpha\beta$ T cells against a broad range of hematopoietic and solid tumor cell lines and primary acute myeloid leukemia. Furthermore, they enhanced infiltration of immune cells in a 3D bone marrow niche and left healthy tissues intact, while eradicating primary multiple myeloma cells. Lastly, GABs constructed from natural high affinity $\gamma\delta$ TCR sequences significantly reduced tumor growth *in vivo* in a subcutaneous myeloma xenograft model.

Conclusions: We conclude that GABs allow for the introduction of metabolic targeting of cancer cells to the field of T cell engagers.

Introduction

Among all immunological subtypes, $\gamma\delta$ T cells stand out in an unbiased computational analysis for their association with improved overall survival of patients with many different tumor types¹. $\gamma\delta$ T cells are innate like T cells that are present in both blood and tissue, and are known to be important for recognition of foreign pathogens, stress signatures of infected cells, and of cancer cells². *In vitro*, $\gamma\delta$ T cells display very potent and broad tumor recognition; they can target and lyse cancer cells of both hematological and solid origin^{3,4}. In contrast to $\alpha\beta$ T cells, $\gamma\delta$ T cells do not rely on HLA for target cell recognition⁵. $\gamma\delta$ 2 T cells, a $\gamma\delta$ subset mainly present in the blood, are known to recognize an increase in intracellular phosphoantigens (pAg), which can be caused by microbial infections but are also found in many cancers⁶. Recognition of intracellular pAg levels by $\gamma\delta$ 2 TCRs relies on an inside out mechanism involving RhoB, BTN3A1, and BTN2A1⁷⁻¹¹. The metabolic targeting of tumor cells by $\gamma\delta$ 2 cells paves the way for novel tumor antigens for immunotherapy¹². Unfortunately, the adoptive transfer of *ex vivo* expanded polyclonal $\gamma\delta$ T cells associates so far with few clinical responses¹³, most likely because of a significantly underestimated diversity, and many mechanisms of tolerance in advanced cancer patients that act against this particular immune subset^{12,14}. Most recently, restoring the $\alpha\beta$ / $\gamma\delta$ 2 T cell balance by BTN3A1 blocking antibodies has been suggested to hold great therapeutic promise as a new checkpoint inhibitor¹⁵; but only a fraction of tumors is infiltrated by $\gamma\delta$ 2 T cells¹. T cells engineered to express a defined $\gamma\delta$ TCR (TEGs) have been proposed as an alternative strategy^{11,16-24} in line with the development of chimeric antigen receptor transduced T cells (CAR-T)^{25,26}. However, advanced therapy medicinal products (ATMPs) such as genetically engineered T cells are delivered to patients with a substantial price tag²⁷, and production processes, as well as clinical implementation are cumbersome²⁸.

To avoid the practical and economic challenges of ATMPs while still utilizing the immune system to attack cancer, an alternative strategy is currently employed for classical antigens like CD19. Bispecific antibodies (bsAb) have been developed, fusing a tumor-targeting domain to a T cell binding domain, to recruit cytotoxic T cells to tumors. Such a bispecific T cell engager (BiTE)

combining an anti-CD19 and anti-CD3 domain is now used in daily clinical practice²⁹, and many other bsAb for cancer immunotherapy are in various phases of clinical development³⁰. The selection of suitable tumor-associated target antigens for these novel therapies, however, remains very challenging currently limiting the broad application of CAR-T and bsAb therapy³¹.

An alternative T cell engager strategy arose by linking the extracellular domain of an $\alpha\beta$ TCR as a tumor antigen binding domain to a single chain variable fragment (scFv) of a CD3 antibody³². These $\alpha\beta$ TCR-bispecifics recognize intracellular peptides presented by MHC molecules, creating the possibility of targeting novel tumor-specific antigens that are not expressed at the cell surface. HLA restriction, however, also limits the use of such $\alpha\beta$ TCR-bispecifics to tumors with high mutational loads and defined HLA-types. Furthermore, down-regulation of HLA is observed as an immune-escape mechanism in approximately 40 to 90% of all human tumors³³, thereby greatly limiting the applicability of therapies based on $\alpha\beta$ TCR mediated tumor recognition.

To overcome these limitations and to combine the tumor specificity and therapeutic potential of $\gamma\delta$ T cells with the recent success of T cell engagers, we fused the extracellular domain of a $\gamma\delta$ 2TCR to an anti-CD3 scFv. We demonstrate that these **G**dTCR **A**nti-CD3 **B**ispecific molecules (GABs) with natural high affinity $\gamma\delta$ 2TCR can mimic the rather complex more pattern-like mode of action mediated by a $\gamma\delta$ 2TCR^{7, 8, 34} without the need of additional affinity maturation. GABs efficiently redirect $\alpha\beta$ T cells towards several tumor cell lines of both hematologic and solid origin, as well as primary patient material *in vitro*. Furthermore, we show significant reduction of tumor growth after GAB treatment in a subcutaneous myeloma xenograft model. We conclude that GABs open an avenue towards metabolic cancer targeting tumors with a bispecific format.

Material and Methods

Generation of Bispecific constructs

A customized pcDNA3-NEO vector, which allows consecutive expression of

two genes of interest under their own CMV promoter, was a kind gift of Jan Meeldijk (LTI protein facility, UMC Utrecht, The Netherlands). First the antiCD3-scFv (OKT3)³⁵ gene was cloned into multiple cloning site one. In addition to the antiCD3-scFv gene, the DNA fragment also contained bases encoding a (G₄S)₃ flexible linker at the 5' end and poly histidine tag on the 3' end. At the 5' end of the flexible linker a BsiWI restriction site was present for the subsequent introduction of the TCR gamma chain in the vector, resulting in the TCR gamma-CD3scFv fusion gene. The TCR delta chain was cloned into the second multiple cloning site. TCR domain boundaries were used as in Allison et al.³⁶. Most γ 9 and δ 2 TCR sequences were reported previously^{11, 24, 36}, while other $\gamma\delta$ TCR sequences were obtained from randomly picked clones (Table 1).

Expression and purification of Bispecifics

His-tagged GABs were expressed in 293 F cells. 293 F cells were cultured in Gibco Freestyle Expression medium, as transfection reagent Polyethylenimine (PEI) (25 kDa linear PEI, Polysciences, Germany) was used. Transfection was done using 293 F cells at a density of 1.10×10^6 cells/ml mixed with 1.25 μ g DNA and 3.75 μ g PEI per million cells. DNA and PEI were pre-mixed in freestyle medium (1/30 of transfection volume), incubated for 20 minutes, and added dropwise to the cell cultures. The cultures were maintained shaking at 37 °C 5% CO₂. Cell culture supernatant was harvested after 5 days and filtered through a 0.22 μ m filter top (Milipore, United States). Supernatant was adjusted to 25 mM Tris (Sigma Aldrich, Germany), 150 mM NaCl (Sigma Aldrich, Germany) and 15 mM Imidazole (Merck, Germany) (pH 8). Supernatant was loaded on a 1 ml HisTrap FF column (GE healthcare, United States) using the ÄKTA start purification system (GE healthcare, United States). Column was washed with IMAC loading buffer (25 mM Tris, 150 mM NaCl 15 mM Imidazole (pH 8), and protein was eluted using a linear imidazole gradient from 21 to 300 mM in 20 CV. Fractions containing the GAB were pooled, concentrated and buffer exchanged to TBS (25 mM tris, 150 mM NaCl, pH 8) using vivaspin 4 10 kD spin columns (Sartorius, Germany). Protein was diluted 100 times in IEX loading buffer (25 mM Tris pH 8), and loaded onto a HiTrap Q HP 1 ml column (GE healthcare, United states) using the ÄKTA start purification system, for a second purification step. Column was washed

with 10 column volumes IEX loading buffer, and protein was eluted using a linear NaCl gradient from 50 to 300 mM in 25 CV. Fractions containing the GAB were pooled, concentrated using vivaspin 4 10 kD spin columns (Sartorius, Germany) and examined by SDS-PAGE and staining with Instant blue protein stain (Sigma Aldrich, Germany). Protein concentration was measured by absorbance on Nanodrop and corrected for the Extinction coefficients. Protein was snap frozen and stored at -80°C and thawed before use.

Cell lines, Flow cytometry, IFN γ Elispot, CD107 degranulation assay, luciferase based cytotoxicity and the animal model are reported in supplementary methods.

In vitro bone-marrow model

The 3D model was previously described in detail ²⁰. In short: primary CD138+ were selected from the mononuclear cells (MNCs) of myeloma bone marrow from two patients by MACS separation using microbeads (Miltenyi Biotec, Germany). The CD138+ cells and the RPMI 8226 tumor cells were stained with Vybrant DiO (Thermo Fisher, United States) and seeded in Matrigel (Corning, United States) together with multipotent mesenchymal stromal cells (MSCs) and endothelial progenitor cells (EPCs), both stained with Vybrant DiD (Thermo Fisher, United States). After four days, T cells were stained with Vybrant Dil (Thermo Fisher, United States) and administered to the model together with CL5 or LM1 GAB (30 μ g/ml) and 10 μ M PAM (Calbiochem, United States). One day later the culture medium was refreshed with medium containing 30 μ g/ml GAB. Tumor-, T- and stromal cells within and surrounding the matrigel were visualized two days later by confocal imaging. Afterwards, the Matrigel was dissolved using Dispase (Corning, United States) to retrieve the cells from the model. The cells were quantified by FACS using Flow count Fluorospheres (Beckman Coulter, United States), and normalized to mock treatment.

Results

Production of highly pure GABs

In line with the observation that not only antibodies but also high affinity $\alpha\beta$ TCR

can be linked to anti-CD3scFvs to redirect T cells to tumor cells ³², we assessed whether the $\gamma\delta$ 2TCR CL5 (Table 1) was able to mediate anti-tumor reactivity in a bispecific format. **G**dTCR **A**nti-CD3 **B**ispecific molecules (GABs) were cloned with an anti-CD3scFv derived from the anti-CD3 ϵ antibody OKT3 linked to the C terminus of the gamma chain of a soluble $\gamma\delta$ 2TCR, using a flexible (G₄S)₃ linker (Figure 1A).

Table 1 GAB sequences. Depicted are sequences used for generation of GABs

GAB	REF	CDR3 δ	CDR3 γ
CL5	²⁴	CACDALKRTDTDKLIFF	CALWEIQELGKKIKVF
6_2	this report	CACDTLPGAGGADKLIFF	CALWEVQELGKKIKVF
CL13	²⁴	CACVPLLADTDKLIFF	CALWEVIELGKKIKVF
G115	³⁶	CACDTLGMGGEYTDKLIFF	CALWEAQQELGKKIKVF
AJ8	this report	CACDTAGGSWDTRQMFF	CALWEAQQELGKKIKVF
A1	¹¹	CACDTLLLLGDSSDKLIFF	CALWEAQQELGKKIKVF
A3	¹¹	CACDAWGHTDKLIFF	CALWEAQQELGKKIKVF
A4	¹¹	CACDALGDTGSDKLIFF	CALWEAQQELGKKIKVF
C1	¹¹	CACDPVPSIHDTDKLIFF	CALWEAQQELGKKIKVF
C3	¹¹	CACDTVSGGYQYTDKLIFF	CALWEAQQELGKKIKVF
C4	¹¹	CACDTLALGDTDKLIFF	CALWEAQQELGKKIKVF
C5	¹¹	CACDLLAPGDTSFDTKLIFF	CALWEAQQELGKKIKVF
C7	¹¹	CACDMGDASSWDTRQMFF	CALWEAQQELGKKIKVF
LM1	²⁴	CACDTLLATDKLIFF	CALWEAQQELGKKIKVF
DLC4	⁴⁶	CACDPAILGDELSWDTRQMFF	CALWEVRQELGKKIKVF
MOP	³⁸	CACDPVVLGDTGYTDKLIFF	CALKELGKKIKVF
RIG1	⁹	CACDPVQVTGGYKVDKLIFF	CALWEVHELGKKIKVF
RIG6	⁹	CACDPLIGSERLGDTGIDKLIFF	CALWESQELGKKIKVF
DGSF68	⁴⁵	CACDTVAHGGGTDKLIFF	CALWEVGELGKKIKVF

CL5 GAB was expressed in mammalian freestyle 293F cells as secreted protein, and purified from the culture supernatant using His-tag purification, followed by a second ion exchange purification step, to ensure a highly pure protein product. As expected, the two different chains of the GAB, ectoGamma-CD3scFv and ectoDelta, were both clearly visible on gel (Figure 1B). This indicates that during expression, the two separate chains of the GAB associate properly, resulting in a heterodimeric bispecific molecule.

GABs bind to $\alpha\beta$ T cells

To further address proper folding of GABs, we employed a flow cytometry based analysis. $\alpha\beta$ T cells were incubated with CL5 GAB, followed by a secondary staining using fluorochrome labeled antibodies against V δ 2, V γ 9 or pan $\gamma\delta$ -TCR (Figure 1C). A strong and specific staining could be observed with all three antibodies, further indicating that the CD3scFv and both TCR chains are properly associated and folded. Following GAB binding on the cell surface of T lymphocytes that were coated with CL5 GAB over time, shows GAB binding up to four days after initial binding to CD3 (Figure 1D), with a declining signal after 2 days implying, as for other bispecific molecules 37, that continuous presence of the molecule will be needed to maintain efficacy.

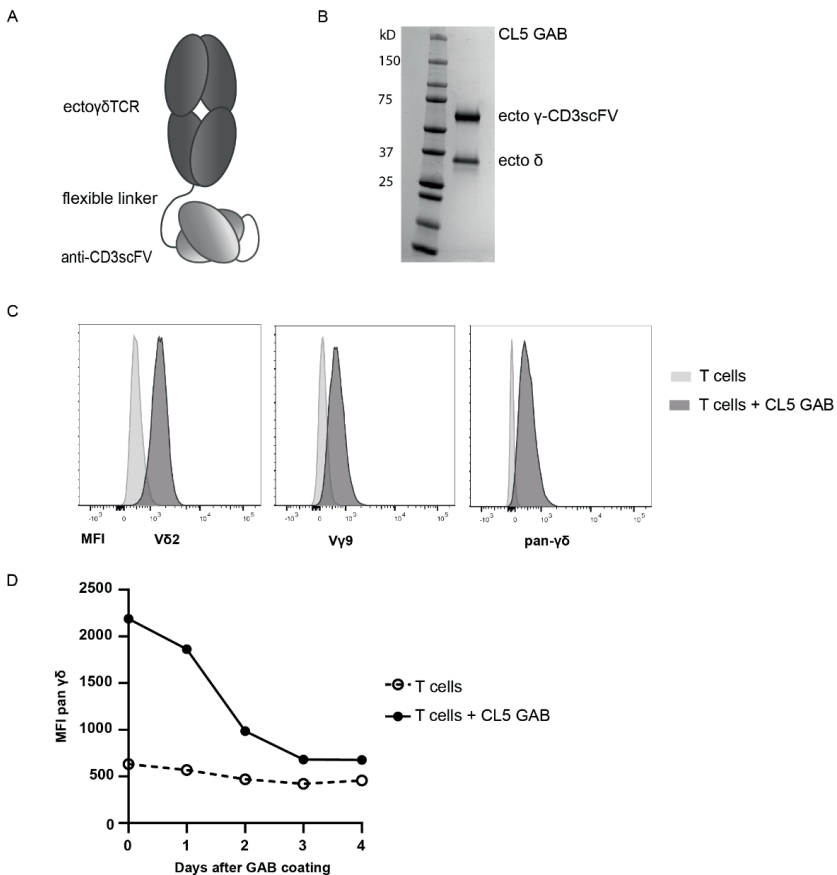


Figure 1. GAB design and binding to CD3+T cells. (A) Schematic representation of the GAB design, showing the extracellular $\gamma\delta$ TCR domain linked to an anti-CD3 scFv via a flexible linker. (B) Purified GAB

was run on SDS-page gel and stained with Coomassie brilliant blue protein stain, visualizing the ectoy-CD3scFv and ecto δ -chain. (C,D) Coating of $\alpha\beta$ T cells with GAB (10 $\mu\text{g}/\text{mL}$ (C) or 90 $\mu\text{g}/\text{mL}$ (D)), followed by staining with fluorochrome labeled anti-V γ 9, V δ 2 or pan $\gamma\delta$ antibodies. MFI was measured by flow cytometry and represented in histograms. GAB, gamma delta TCR anti-CD3 bispecific molecules

GABs induce pAg-dependent tumor recognition by $\alpha\beta$ T cells which is influenced by variations in the V δ 2 TCR chain

$\gamma\delta$ 2T cells are known to recognize SCC9 cells, a squamous cell carcinoma cell line. This recognition can be enhanced by treating tumor cells with pamidronate (PAM), which causes an increase in the intracellular phosphoantigen (pAg) levels by inhibiting the mevalonate pathway²⁴. To test whether GABs can also induce recognition of this cell line, $\alpha\beta$ T cells and SCC9 target cells were co-incubated with and without PAM, and CL5 or LM1 GAB. LM1 GAB was generated to serve as negative control, LM1 GAB harbors a $\gamma\delta$ 2 TCR where the CDR3 region of the δ chain is replaced by a single alanine, making the $\gamma\delta$ 2 TCR non-functional.²⁴ As anticipated, CL5 - but not LM1 GAB, induced recognition of SCC9 target cells by $\alpha\beta$ T cell in the presence of PAM (Figure 2A), suggesting that the mode of recognition by GABs is comparable to recognition mediated by $\gamma\delta$ 2TCRs expressed at a cell membrane¹¹.

We^{11, 24} and others³⁸⁻⁴⁰ reported on the impact of changes in the CDR3 region of δ 2TCR chains on TCR function. To assess the impact of variations in the CDR3 region of the δ 2TCR chain on GAB activity, we generated a larger panel of GABs, derived from previously published $\gamma\delta$ 2TCRs^{11, 24, 36} and randomly picked $\gamma\delta$ 2T cell clones, varying in CDR3 δ -chain (Table 1). To assess activity, the different GABs were co-incubated with $\alpha\beta$ T cells and SCC9 target cells in the presence of PAM. Most GABs efficiently induced an IFN γ response, though activity substantially differed between different constructs (Figure 2B), although all showed similar binding to $\alpha\beta$ T cells (Figure S1). GABs in which the CDR3 δ was reduced to one alanine (LM1) did not induce IFN γ production at any concentration (Figure 2B). Titrating GAB concentrations allowed for further analysis of the differences in efficacy between the different CDR3 δ sequences. We observed large differences in GAB activity with an EC₅₀ of 0.8 $\mu\text{g}/\text{ml}$ for the best performing GAB to an EC₅₀ of 25 $\mu\text{g}/\text{ml}$ for the lowest activity. EC₅₀ of several non- or very low active receptors could not formally be assessed (Figure 2B and Table 2).

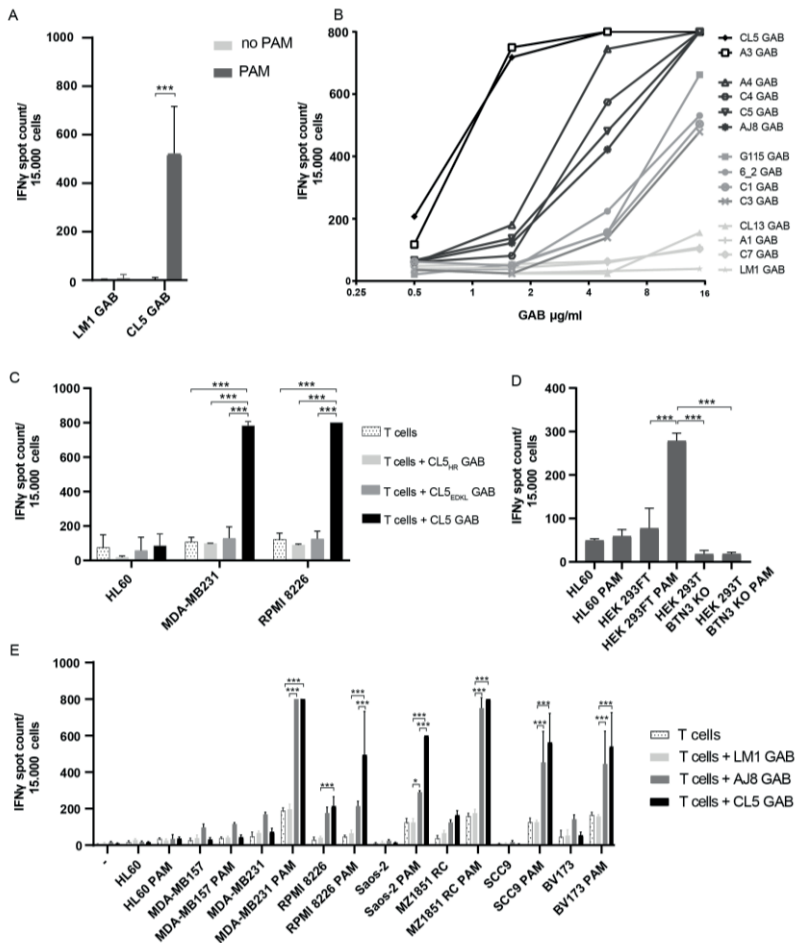


Figure 2. GABs induce pAg dependent tumor recognition by $\alpha\beta$ T cells. (A–E) IFN γ production was measured by elispot, if separate spots could not be distinguished, spot count was set to a maximum value of 800. (A) $\alpha\beta$ T cells were co-incubated with SCC9 target cells in the presence or absence of PAM (100 μ M) and LM1 or CL5 GAB (10 μ g/mL), values are corrected for T cells only (n=4). (B) T cells were incubated with SCC9 target cells, PAM (100 μ M) and an increasing concentration of GABs derived from different γ 9V δ 2TCRs. A representative experiment is shown. (C) γ -chain HV4 mutations shown to hamper TCR binding were tested in the GAB format, $\alpha\beta$ T cells and target cells were co-incubated with the wildtype or mutant GABs (10 μ g/mL) and PAM (100 μ M) n=2. (D) AJ8 GAB (10 μ g/mL) was co-cultured with T lymphocytes, HL60, HEK293FT WT or BTN3A1 knockout cells with and without PAM (100 μ M) n=1 in duplo. (E) CL5 and AJ8 GAB (10 μ g/mL) were tested in a coculture of T cells and a larger panel of target cell lines with and without the addition of PAM (100 μ M), and compared with mock GAB LM1 n=2. Error bars represent SD, significance was calculated using a multiple T test (A) or one-way ANOVA (C–E). * P<0.05, **p<0.001, ***p<0.0001. ANOVA, analysis of variance; GAB, gamma delta TCR anti-CD3 bispecific molecules; PAM, pamidronate.

Table 2. EC50 of GAB for IFN γ release. EC50 of GABs was calculated from Figure 2A. n.d. not determined.

GAB	EC50 ($\mu\text{g/ml}$)	Confidence interval ($\mu\text{g/ml}$)	R2
CL5	0.7524	0.6285 to 0.9086	0.9956
A3	0.8344	0.7055 to 0.9888	0.9637
A4	2.417	2.038 to 2.882	0.9851
C4	3.528	2.934 to 4.198	0.9916
C5	4.028	3.304 to 4.818	0.9801
AJ8	4.586	3.816 to 5.444	0.9777
G115	8.537	7.127 to 10.23	0.9923
6_2	9.811	7.777 to 12.17	0.9267
C1	11.46	9.356 to 13.81	0.9471
C3	12.30	10.14 to 14.74	0.9740
CL13	27.70	21.50 to 42.50	0.9301
A1	n.d.	n.d.	n.d.
C7	n.d.	n.d.	n.d.
LM1	n.d.	n.d.	n.d.

γ -TCR loop and BTN3A are critical for GAB mediated $\alpha\beta$ T cell activation

The HV4 region between the CDR2 and the CDR3 of the γ -chain is critical for $\gamma\delta$ 2TCR activity by binding to BTN2A1 expressed on target cells⁹⁻¹¹. To assess whether GABs also depend on this mode of action, we focused on GAB CL5, one of the most active TCR sequences from the tested panel, and introduced two mutations in the γ HV4 region of CL5 GAB (E₇₀D₇₂→K₇₀L₇₂ (CL5_{EDKL}GAB) and H₈₅→R₈₅ (CL5_{HR}GABs)), reported to cause loss of activity in membrane expressed $\gamma\delta$ 2TCRs⁴¹. CL5, CL5_{EDKL} and CL5_{HR} GABs were added to a co-culture of $\alpha\beta$ T cells with the well-described breast cancer cell line (MDA-MB231) or multiple myeloma cell line (RPMI 8226)^{11, 24} in the presence of PAM. CL5_{EDKL} and CL5_{HR} GAB lost activity, assessed by IFN γ production, when compared to the wild type CL5 GAB (Figure 2C), highlighting the importance of the γ HV4 region for target cell engagement by GABs.

BTN3A has also been recognized as a crucial factor in phosphoantigen dependent $\gamma\delta$ 2TCR reactivity. Loss of BTN3A membrane expression on target cell leads to a complete loss of membrane-bound $\gamma\delta$ 2TCR reactivity

to pAgs^{11, 42}. By testing GAB mediated recognition of HEK293FT WT and BTN3A knock-out, we confirmed that GAB induced recognition after PAM treatment also depends on BTN3A expression (Figure 2D). These findings support the assumption that there is a similar binding mode between membrane-expressed $\gamma\delta 2$ TCRs and GABs, both depending on encounter of BTN2A1 through the γ -chain and a second signal, which is pAg and BTN3A depended.

GABs retarget $\alpha\beta$ T cells to a wide variety of tumor cells

Next, we addressed whether GABs can redirect $\alpha\beta$ T cells to a broader variety of tumor cells, and whether GABs with different EC_{50} against SCC9 target cells also have different activities against a broader range of hematological and solid tumor cells. GABs with lower (AJ8) and higher (CL5) EC_{50} or the negative control LM1 GAB were co-incubated with $\alpha\beta$ T cells, and previously defined panel of tumors targets cells⁴³. A significant increase in IFN γ production was observed for CL5 and AJ8 GABs against most tumor targets except for HL60 and MDA-MB157, while LM1 GAB did not induce cytokine secretion (Figure 2E). For most cell lines, CL5 GAB had a slightly higher activity compared to AJ8 GAB, although not always significant. Isolated CD4⁺ and CD8⁺ $\alpha\beta$ T cells induced IFN γ release after co-incubation with CL5 GAB (Figure S2A). However, as expected we observed that the relative contribution of CD4⁺ and CD8⁺ $\alpha\beta$ T cells differed between donors and target cells, with CD4⁺ $\alpha\beta$ T cells producing more cytokines in general.

As in blood up to 5% of the CD3⁺ T lymphocytes are comprised of $V\delta 2$ ⁺ T cells, we next investigated GAB activity in combination with $V\delta 2$ ⁺ and $\alpha\beta$ T cells side by side. $V\delta 2$ ⁺ and $\alpha\beta$ T cells were isolated from a healthy donor and IFN γ release was measured after a co-culture with two recognized (RPMI8226, SCC9) and one unrecognized cell line (ML-1) with and without CL5 GAB and in the absence or presence of PAM (Figure S2B). LM1 GAB was added as extra control to the $V\delta 2$ ⁺ T cells. As expected, the $V\delta 2$ ⁺ T cells alone recognized the positive target cell lines after PAM treatment, surprisingly however this recognition was lower compared to $\alpha\beta$ T cells co-incubated with CL5 GAB. Activity of $V\delta 2$ ⁺ T cells was not blocked by the addition of the mock LM1 GAB, and addition of GAB CL5 did not lead to a further increase in activation of the

V δ 2+ T cells. These data imply that GABs will most likely not activate V δ 2+ T cells, which could be a consequence of the differences in CD3 composition of V δ 2+ T cells versus α β T cells⁴⁴. This is also in line with the previous observation that V δ 2+T cell expansion protocols usually do not use CD3 engagers, but rather rely on agents that directly engage the TCR, such as phytohaemagglutinin (PHA)^{4, 43}.

To this point, IFN γ production was used as a read out for GAB activity. However, the clinical activity of bispecific molecules comes through their ability to mediate killing of target cells. Therefore, as the next step, we assessed CD8+ α β T cell-mediated toxicity by utilizing a degranulation assay detecting surface expression of the lysosomal-associated membrane glycoprotein-1 (LAMP-1/CD107a) by FACS. α β T cells were co-cultured with three different target cell lines and CL5, AJ8 or negative control LM1 GAB, with and without PAM for 7 hours (Figure 3A). As an extra control, α β T cells and GABs were incubated together without target cells. Similar to the IFN γ release data, GABs induced degranulation of CD8+ α β T cells upon binding to a target cell line in a PAM dependent manner, while no upregulation of CD107a was observed when co-incubated with the negative control cell line HL60. To formally assess the ability of GABs to kill tumor targets, we employed a luciferase-based cytotoxicity assay. RPMI 8226 and SCC9 tumor cells stably transduced with a luciferase gene were co-cultured with GABs and α β T cells at different effector to target (E:T) ratios. After a co-culture of 16 hours, the bioluminescence was measured by adding beetle luciferin to the co-culture. The amount of viable cells was determined by comparing the bioluminescence signal to untreated target cells (Figure 3B). Both CL5 and AJ8 GAB efficiently induced up to 60-80% lysis of the tumor cells at the lower effector to target cell ratios, while LM1 GAB had as little activity as α β T cells alone.

To extend our findings to GABs harboring sequences published by others^{9, 38, 45, 46}, a second set of five GABs were generated (Table 1) and tested for ability to induce target cell lysis after co-incubation with α β T lymphocytes and the multiple myeloma target cell line RPMI 8226¹¹ in the presence of PAM. As benchmark we used the previously identified GABs with lower (AJ8) and higher

(CL5) EC₅₀ and as negative control LM1 GAB. Again, we observed differences in activity, GABs harboring sequences from CL5 were superior to all other tested GABs. Only the GABs derived from DGSG68 and MOP TCR were not significantly different from the lysis induced by AJ8 GAB, while the other 3 tested GABs were inferior to the AJ8 GAB (Figure S3).

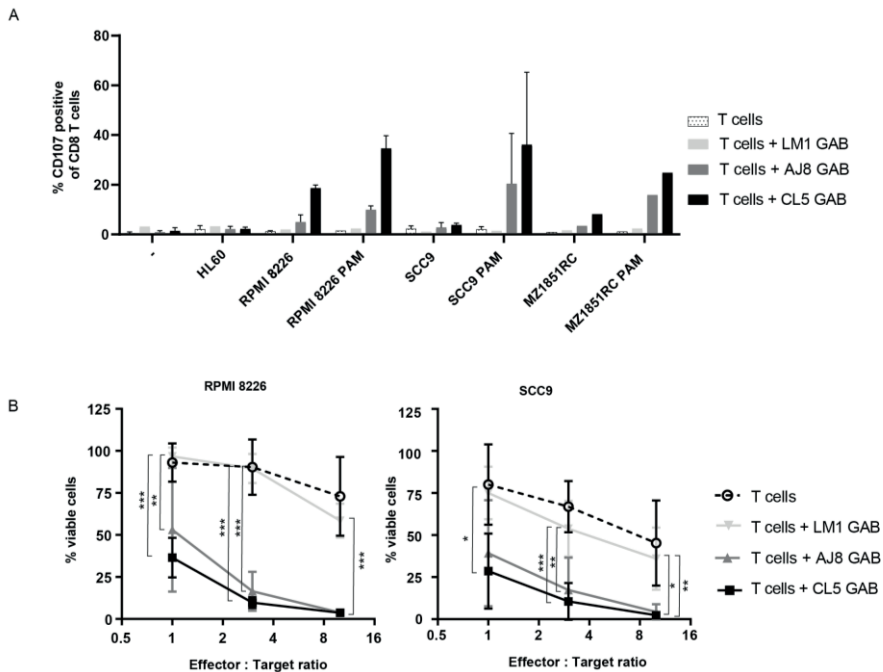


Figure 3. GABs induce T cell mediated lysis of cancer cell lines. (A) CD8+T cell degranulation was measured by staining with CD107a antibody during a 7-hour co-incubation of T cell effector and three different target cell lines in the presence and absence of GAB (10 $\mu\text{g}/\text{mL}$) and PAM (100 μM). Golgistop was added during the incubation. N=2 (for LM1 GAB and MZ1851RC N=1) significance was not calculated because of amount of data points. (B) T effector and luciferase transduced RPMI 8226 and SCC9 target cells were co-incubated for 16 hours in the presence and absence of GAB (10 $\mu\text{g}/\text{mL}$) and PAM (100 μM) at different E:T ratios. Percentage viable cells were determined by comparing luminescence signal to untreated target cells, representing 100% viability. N=3, error bars represent SD, significance was calculated using a one-way ANOVA. * $P < 0.05$, ** $p < 0.001$, *** $p < 0.0001$. ANOVA, analysis of variance; GAB, gamma delta TCR anti-CD3 bispecific molecules

GABs are active against primary leukemia but not against primary healthy tissues

To test whether GABs can mediate recognition of not only tumor cell lines, but also of primary tumors such as primary AML, $\alpha\beta$ T cells were co-cultured with AJ8 GAB and primary AML blasts of 4 patients, with and without PAM. GABs induced a significant increase in IFN γ production upon PAM treatment against two out of the four patient samples (Figure 4A).

Given the broad activity of GABs, we next assessed their ability to sense healthy tissues in a resting or stressed situation. To this end, we isolated B cells, monocytes and CD34+ cells from a healthy donor, and tested reactivity of CL5 and LM1 GAB against these cells and against healthy donor-derived fibroblasts in an IFN γ release assay. Recognition of the cells was tested in resting, but also activated or stressed conditions, such as after irradiation or chemotherapy treatment. Neither CL5 nor LM1 GAB induced recognition of healthy cells, in resting, activated or stressed conditions, while the positive control, RPMI 8226 tumor cells, induced cytokine release when incubated with CL5 GAB (Figure 4B).

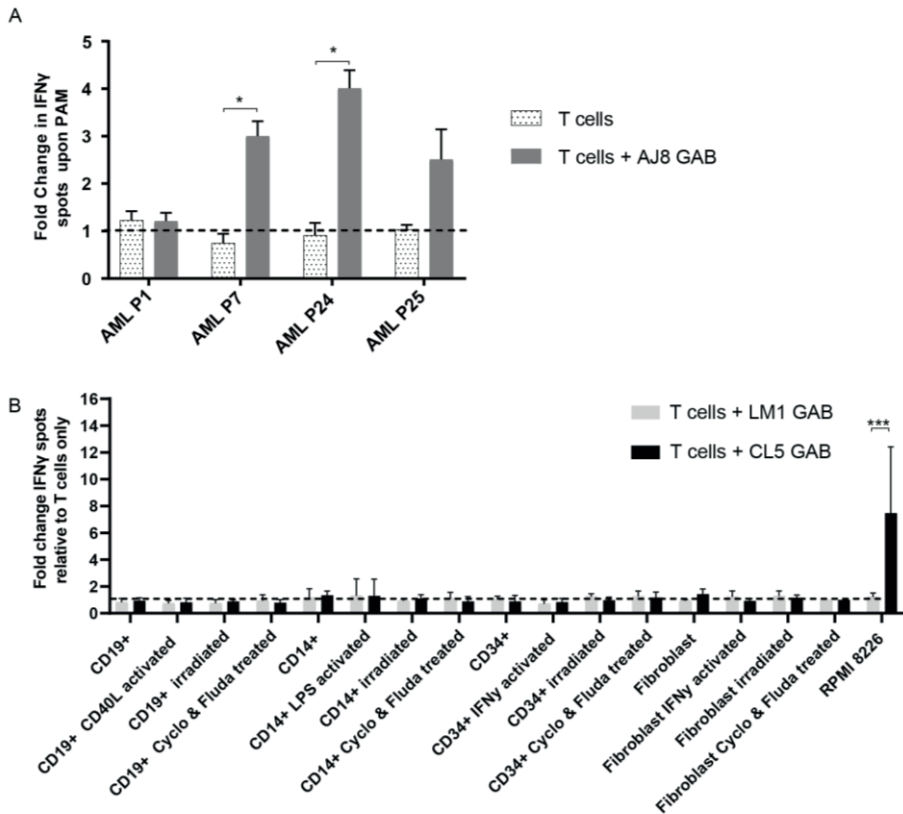


Figure 4. GABs induce recognition of primary AML samples but not of healthy hematopoietic cells or fibroblasts. (A) $\alpha\beta$ T cells were incubated with AML blasts with or without 100 μ M PAM, and 10 μ g/mL AJ8 GAB. IFN γ production was measured by elispot after 24 hours. Fold change in IFN γ production on addition of pamidronate was calculated N=1. (B) $\alpha\beta$ T cells were co-cultured with healthy hematopoietic cells or fibroblasts and LM1 or CL5 GAB (10 μ g/mL). Target cells were activated as indicated, or stressed by irradiation or a combination treatment with cyclophosphamide (Cyclo) and fludarabine (Fluda). IFN γ release was measured by elispot. The figure represents pooled data from four different target cell donors (CD19+ and CD14+) or two donors (CD34+ and fibroblasts). $\alpha\beta$ T effector cells were derived from four different donors (CD19+ and CD14+) or two donors (CD34+ and fibroblasts). Error bars represent SD, significance was calculated using a multiple T test. * P<0.05, **p<0.001, ***p<0.0001. GAB, gamma delta TCR anti-CD3 bispecific molecules.

Favorable efficacy toxicity profile of GABs in the bone marrow niche

In vivo, the tumor microenvironment is often important for survival and proliferation of tumor cells. Therefore, we tested whether GABs can also eradicate primary tumor material without harming healthy tissues in a more natural environment, using a previously described 3D bone marrow niche

model ²⁰. In this model, mesenchymal stem cells (MSC) and endothelial progenitor cells (EPC) are used as stromal support for the growth of a multiple myeloma (MM) cell line (RPMI 8226) or primary CD138+ MM cells derived from patients. CD138+ MM cells from two patients, and the MM cell line RPMI 8226 were stained and seeded in matrigel together with MSCs and EPCs. After four days, labeled $\alpha\beta$ T cells, together with CL5 or LM1 GAB and PAM were added to the model. One day later fresh medium with GABs was added to the model to ensure constant GAB coating on the $\alpha\beta$ T cells. After two days visualizing $\alpha\beta$ T cells infiltrated into the tumor bearing matrigel by confocal microscopy indicated an increased $\alpha\beta$ T cell infiltration in the presence of CL5, but not LM1 GAB (Figure 5A). This observation was supported by a subsequent FACs based quantification of the $\alpha\beta$ T cells present in the matrigel (Figure 5B). To further study specific $\alpha\beta$ T cell activation by GABs, we measured several cytokines in the supernatant of the 3D model containing primary MM tumor cells. Next to IFN γ , we also observed a significant increase in the levels of other Th1 cytokines, IL2 and TNF α for the CL5 GAB condition (Figure 5C).

The most important measurement remains the elimination of tumor cells. Therefore, the amount of tumor cells remaining in the model after CL5 GAB treatment was determined by FACs analysis and cell numbers were normalized to treatment with mock LM1 GAB. Treatment with CL5 GAB induced a significant reduction of CD138+ MM cells compared to the mock treatment with LM1 GAB, for both patient samples and the MM cell line RPMI 8226. (Figure 5D). Healthy stromal cells were also quantified, showing no differences between CL5 or LM1 GAB treatment (Figure 5D), suggesting that surrounding healthy tissues are not affected by the treatment with active GAB.

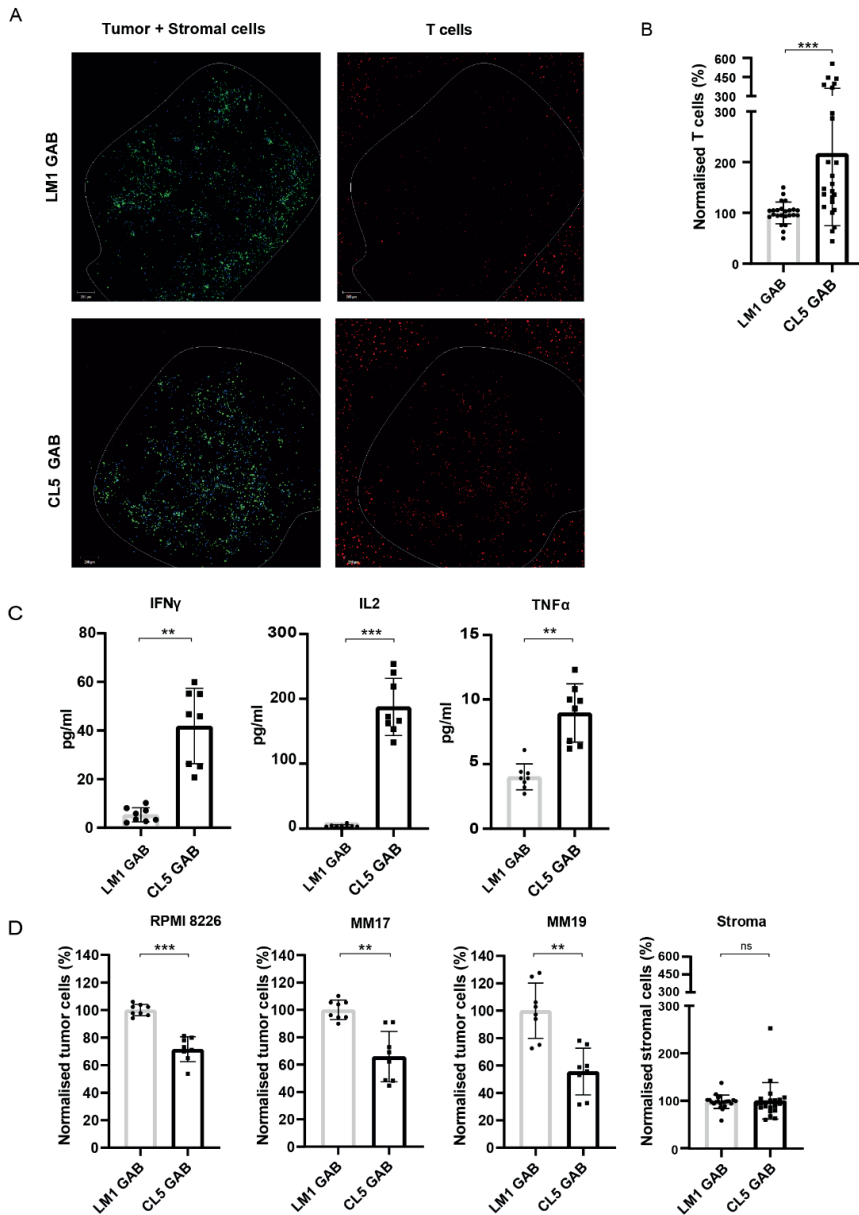


Figure 5. GABs mediate recognition and lysis of primary multiple myeloma in a 3D model. The RPMI 8226 tumor cell line or primary MM patient material was cultured in a 3D bone marrow niche consisting of matrigel and stromal cells. After 4 days, α β T cells were added together with PAM (10 μ M PAM) and GAB (30 μ g/mL). (A) Confocal images showing cell localization within and around the 3D model (boundaries indicated by the white line) with the tumor and stromal cells, respectively, in green and blue and T cells in

red. (B) Two days after addition of the T cells, the matrigel was dissolved to retrieve the cells from the model. $\alpha\beta$ T lymphocytes were quantified by flow cytometry and normalized to mock treatment. (C) Cytokines were measured in the supernatant by luminex. (D) Tumor and stromal cells were collected from the dissolved matrigel and quantified by flow cytometry. Cell numbers were normalized to mock treatment. Significance was calculated by a paired T test. * $P < 0.05$, ** $p < 0.001$, *** $p < 0.0001$. $N = 4$ with technical duplo's. GAB, gamma delta TCR anti-CD3 bispecific molecules

GABs control tumor growth in vivo

To test whether treatment with GABs can also affect tumor growth *in vivo*, we established a xenograft model by injecting RPMI 8226 multiple myeloma cells subcutaneously (s.c) into NSG mice. For this *in vivo* experiment we generated RPMI 8226 B2M knock-out cells that we injected s.c, as in previous experiments i.v injected WT RPMI 8226 cells were rejected when co-engrafted with human PBMC, most likely due to allo-reactivity (Figure S4). One week after tumor cell injection, mice received an i.v injection of human PBMCs (Figure 6A). Next, the mice were randomized over two groups, based on tumor size, and received treatment for 7 consecutive days with CL5 GAB or the mock LM1 GAB. Moreover, an additional group in which mice received tumor and PBMCs but no GABs was included as extra control to monitor co-engraftment of PBMCs and tumor in NSG mice. Tumor volume was measured three times per week for 30 days. Treatment with CL5 GAB significantly decreased tumor growth compared to the control group treated with LM1 GAB (Figure 6B). Furthermore, mice treated with LM1 GAB showed similar tumor outgrowth compared to the PBMC only group. Persistence of GABs bound to $\alpha\beta$ T cells in the blood was determined by flow cytometry 1, 2 and 8 days after GAB injection by calculating absolute number of $\alpha\beta$ TCR- and $\alpha\beta$ TCR/ $\gamma\delta$ TCR double positive (GAB coated) T cells. Figure 6C shows that 24 hours after the first GAB injection (day 10), and 48 hours after the last GAB injection (day 17), around 30% of the total $\alpha\beta$ TCR positive cells are $\alpha\beta$ TCR/ $\gamma\delta$ TCR double positive, meaning that there are still GABs bound to the T cells. Furthermore, we found that 8 days after the last GAB injection (day 23) this double positive population was no longer present.

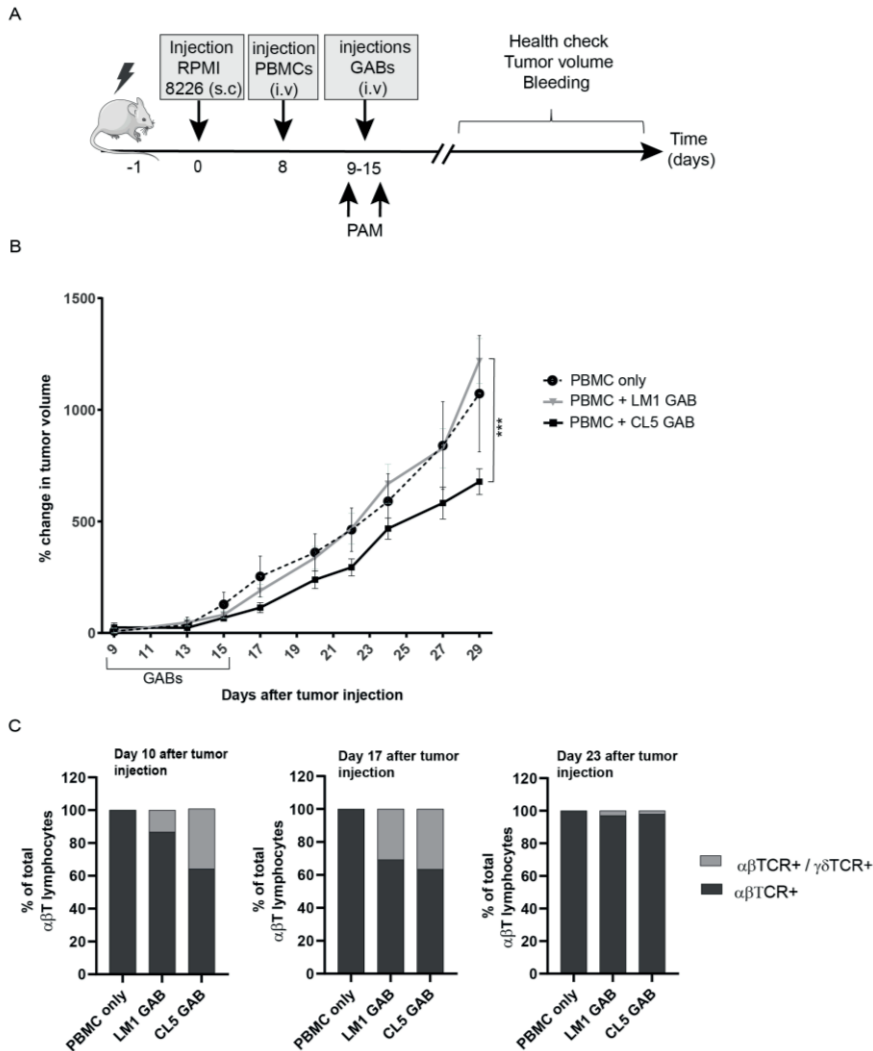


Figure 6. In vivo control of tumor growth by GABs. (A) Schematic representation of experimental design. NSG mice were irradiated at day -1 , and injected subcutaneous (s.c) with 10×10^6 RPMI 8226 tumor cells 1 day later. After 7 days, the mice were randomized over three groups, based on tumor size ($N=10$). From day 9 to 15, mice in two groups were treated with one intravenous injection per day of CL5 or LM1 GAB ($2,7$ mg/kg). Tumor size was measured three times per week for 3 weeks after start of the GAB treatment (B) and is plotted as percent change in tumor volume compared with the initial tumor volume at the start of the GABs treatment. (C) Amount of $\alpha\beta$ TCR single positive and $\alpha\beta$ TCR/ $\gamma\delta$ TCR double positive cells in the mice was determined by flow cytometry on day 10, 17 and 23 after tumor injection, which corresponds to 24 hours after the first GAB injection and 48 hours and 8 days after the last GAB injection. Data are shown as mean of percentage of total $\alpha\beta$ TCR positive cells. PBMC only $N=4$, LM1/CL5 GAB $N=10$. Error bars represent SEM, significance was calculated by mixed-effects model with repeated measures. * $P < 0.05$, ** $p < 0.001$, *** $p < 0.0001$. GAB, gamma delta TCR anti-CD3 bispecific molecules.

Discussion

In this study we developed a novel bispecific T cell engager format, **G**dTCR **A**nti-CD3 **B**ispecific molecules (GABs), based on the fusion of a soluble $\gamma 9\delta 2$ TCR to an anti-CD3 scFv. With GABs, we introduce the targeting of cancer as a metabolic disease to the field of bispecific T cell engagers. GAB activity against tumor but not healthy tissues was observed when utilizing naturally occurring high affinity $\gamma 9\delta 2$ TCR and relied, as for membrane bound $\gamma 9\delta 2$ TCR, on the complex orchestration of BTN2A1 and BTN3A1 and was modified by intracellular phosphoantigen levels ^{8, 11, 12}.

Most T cell engagers use tumor targeting domains with binding affinities in the nanomolar range, a 10-100 fold affinity maturation has been reported to further enhance activity ^{37, 47}. For T cell engagers with an $\alpha\beta$ TCR as tumor binding domain, affinity maturation from the micromolar to picomolar range is needed to overcome the rather low overall avidity mediated by a low density of tumor associated molecules within the context of MHC molecules, in order to create functional T cell engagers ⁴⁸. Therefore, it was initially surprising that a $\gamma 9\delta 2$ TCR is active in the bispecific format without artificial affinity maturation, while natural $\alpha\beta$ TCR showed only a little activity ³². Most recent studies estimated the binding affinity of the $\gamma 9$ chain to BTN2A1 to be around $40 \mu\text{M}$ ⁹ which is in the range of $\alpha\beta$ TCRs ⁴⁹. However, the number of BTN2A1 molecules that are present on the cell surface for binding to the $\gamma 9$ TCR chain is most likely substantially higher compared to tumor associated antigens in HLA complexes, potentially generating a higher avidity for $\gamma 9\delta 2$ TCR based T cell engagers compared to $\alpha\beta$ TCRs. This however does not explain why, in our data set, only a selected group of defined $\gamma 9\delta 2$ TCR clones was active in the GAB format.

The reported affinity of the $\gamma 9$ chain to BTN2A1 ⁹ is presumably an underestimation of the binding affinity of the $\gamma 9\delta 2$ TCR to its complete interacting complex, as the TCR binding is not solely mediated by the $\gamma 9$ -chain. This assumption is supported by our previous observation that apart from the γ -chain, variations in the CDR3 region of the $\delta 2$ chain also contribute substantially to the overall functional avidity of $\gamma 9\delta 2$ TCRs once expressed in

a T cell^{11, 24}. δ 2TCR sequences that were previously reported to mediate high overall efficacy when expressed at the cell membrane¹¹, also mediated high activity when used in the GAB format, e.g. CL5 and A3. Vice versa, sequences which mediated lower efficacy in the TEG format were even poorer performers in the GAB format, e.g. A1. Thus, as both the γ 9- and δ 2-chain contribute to the affinity of a γ 9 δ 2 TCR to its complex, a careful selection of δ 2TCR sequences is needed guarantee a functional GAB.

Transforming cold- into hot tumors is a key success factor for immune therapies.⁵⁰ Novel $\alpha\beta$ TCR based biologics have been reported to warm “cold” tumors⁵¹. By using a 3D bone marrow niche model for primary MM cells²⁰, we provide evidence that γ 9 δ 2TCR, when provided in the GAB format, can initiate infiltration of immune cells into the tumor microenvironment. This was further confirmed by the *in vivo* model, showing that GABs can reduce tumor growth of a subcutaneously growing RPMI 8226 tumor.

Furthermore, as the utilized 3D model was comprised of healthy MSC and EPC to guarantee survival and proliferation of MM cells *in vitro*²⁰, this model also allowed us to assess the impact of GABs on healthy tissues, and extended our *in vitro* safety data for GAB. This current data confirms the previously reported lack of toxicity of targeting BTN2A1 and BTN3A1 when utilizing a high affinity γ 9 δ 2TCR in the TEG format^{17, 20, 23, 24} or when administering BTN3A1 targeting antibodies¹⁵.

In this report we tested the reactivity of GABs to patient material from several AML patients, and found that GABs were reactive to two out of the four samples. This observation is in line with our previous report assessing larger tumor panels, including 16 AML patients, which suggest that approximately 50% of all tumor cells are recognized by primary $\gamma\delta$ T cells or TEGs²³. Mode of action studies investigating requirements for γ 9 δ 2TCR mediated tumor cell recognition, conducted in order to elucidate this differential tumor recognition, pointed to multiple factors such as pAg dependent rearrangement of the BTN2-BTN3 complex involving RhoB and the intracellular B30.1 domain of BTN3A1⁹⁻¹¹. However, these studies also imply that a yet to be defined second ligand, binding to the CDR3 δ is most likely involved. Thus, although a lot of

knowledge has been obtained over the past years, tumor recognition mediated by a $\gamma\delta$ TCR cannot be fully explained and predicted yet ¹¹. Therefore, further investigation into the complex $\gamma\delta$ TCR mediated target cell recognition, and the identification of novel biomarkers that can help identifying patient populations that are susceptible to $\gamma\delta$ based therapies will be key for a successful clinical translation ¹².

The GAB format outperformed natural $\gamma\delta$ T cells, as reported previously for TEGs ^{11, 43}, most likely reflecting the careful selection of a high affinity $\gamma\delta$ TCR in the GAB or TEG design. Despite this superior activity, a limiting factor for $\gamma\delta$ TCR mediated target cell recognition remains the requirement for pAg accumulation, also GAB mediated recognition of many cancer cells required additional treatment with amino-bisphosphonates to increase pAg levels. To elucidate why tumor cells differ in the dependence on PAM to enhance $\gamma\delta$ TCR recognition further investigation will be needed, but it is most likely a consequence of different availabilities of all the characterized key components for $\gamma\delta$ TCR binding, including, but not limited to, the intracellular accumulation of pAgs. The dependence on increased intracellular pAg levels for recognition of many tumors, does however imply that $\gamma\delta$ TCR based therapeutic strategies most likely need to be combined with amino-bisphosphonate treatment, a state of the art drug safely combined with many different treatments including $\gamma\delta$ T infusions ¹².

In conclusion, we have shown that a $\gamma\delta$ TCR bispecific format can mimic the rather complex metabolic cancer targeting usually mediated by membrane bound $\gamma\delta$ TCR ^{7, 8, 34}, though requires a very careful selection of the used sequences and then allows for the introduction of the unique tumor targeting potential of $\gamma\delta$ T cells to the field of bispecific T cell engagers. Our findings imply also that, in contrast to previously reported data for $\alpha\beta$ TCR derived bispecifics, selecting an endogenously occurring high affinity $\gamma\delta$ TCR for use in a bispecific format could omit the need for affinity maturation. Since the use of affinity matured TCRs poses the risk of altering the TCR specificity or introducing cross-reactivity ^{52, 53}, using a therapy based on the endogenous TCR affinity could be a preferred strategy. This approach might overcome cumbersome engineering efforts, and provide with GABs and TEGs, two

complementary or even additive strategies as reported for CAR-T.

Acknowledgements

We thank the staff of the Flow Core Facility and the Multiplex Core Facility at the UMC Utrecht. We kindly thank Prof. Erin Adams (The University of Chicago) for providing the CD277 KO HEK293T cell line and Halvard Boenig (Institute for Transfusion Medicine and Immunohematology, Goethe University, Frankfurt a. M., Germany) for providing feeder cells.

Funding

Funding for this study was provided by ZonMW 43400003 and VIDI-ZonMW 917.11.337, KWF 2013-6426, 2014-6790 2015-7601, 2018-11393, 2018-11979, 2020-13403 to J.K., KWF 2018-11393 2020-13403 to Z.S., KWF 11979 and Marie Curie 749010 to D.X.B.,

Conflict-of-interest statement:

J.K. is shareholder of Gadeta (www.gadeta.nl). Jürgen Kuball, Zsolt Sebestyen, Dennis X Beringer, Anna Vyborova, and Eline van Diest are authors on several patent applications.

References:

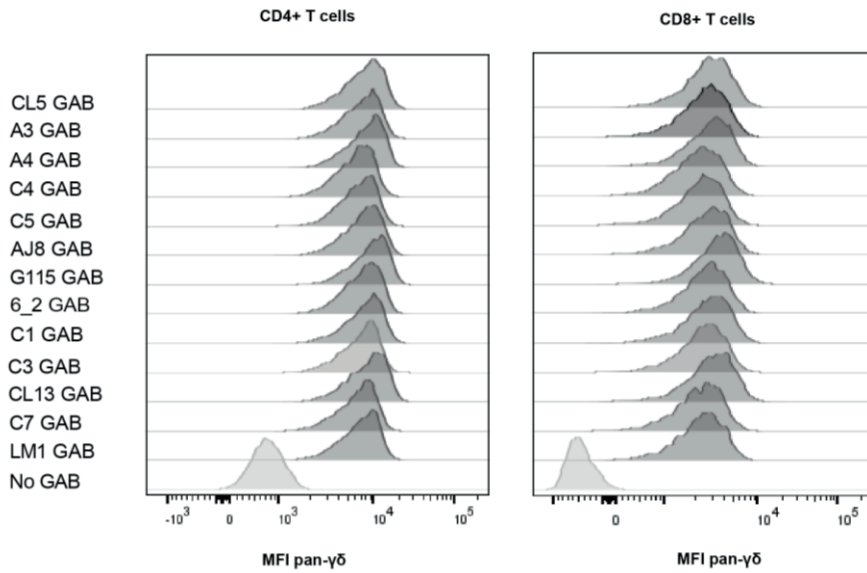
1. Gentles AJ, Newman AM, Liu CL, Bratman SV, Feng W, Kim D, et al. The prognostic landscape of genes and infiltrating immune cells across human cancers. *Nat Med*. 2015;21(8):938-45.
2. Bonneville M, O'Brien RL, Born WK. Gammadelta T cell effector functions: a blend of innate programming and acquired plasticity. *Nat Rev Immunol*. 2010;10(7):467-78.
3. Scheper W, Grunder C, Straetemans T, Sebestyen Z, Kuball J. Hunting for clinical translation with innate-like immune cells and their receptors. *Leukemia*. 2014;28(6):1181-90.
4. Scheper W, van Dorp S, Kersting S, Pietersma F, Lindemans C, Hol S, et al. gammadeltaT cells elicited by CMV reactivation after allo-SCT cross-recognize CMV and leukemia. *Leukemia*. 2013;27(6):1328-38.
5. Simões AE, Di Lorenzo B, Silva-Santos B. Molecular Determinants of Target Cell Recognition by Human $\gamma\delta$ T Cells. *Front Immunol*. 2018;9:929.
6. Gober HJ, Kistowska M, Angman L, Jenö P, Mori L, De Libero G. Human T cell receptor gammadelta cells recognize endogenous mevalonate metabolites in tumor cells. *J Exp Med*. 2003;197(2):163-8.
7. Gu S, Sachleben JR, Boughter CT, Nawrocka WI, Borowska MT, Tarrasch JT, et al. Phosphoantigen-induced conformational change of butyrophilin 3A1 (BTN3A1) and its implication on Vgamma9Vdelta2 T cell activation. *Proc Natl Acad Sci U S A*. 2017;114(35):E7311-E20.
8. Sebestyen Z, Scheper W, Vyborova A, Gu S, Rychnavska Z, Schifferl M, et al. RhoB Mediates Phosphoantigen Recognition by Vgamma9Vdelta2 T Cell Receptor. *Cell Rep*. 2016;15(9):1973-85.
9. Rigau M, Ostrouska S, Fulford TS, Johnson DN, Woods K, Ruan Z, et al. Butyrophilin 2A1 is essential for phosphoantigen reactivity by gammadelta T cells. *Science*. 2020;367(6478).
10. Karunakaran MM, Willcox CR, Salim M, Paletta D, Fichtner AS, Noll A, et al. Butyrophilin-2A1 Directly Binds Germline-Encoded Regions of the Vgamma9Vdelta2 TCR and Is Essential for Phosphoantigen Sensing. *Immunity*. 2020;52(3):487-98.e6.
11. Vyborova A, Beringer DX, Fasci D, Karaiskaki F, van Diest E, Kramer L, et al. gamma9delta2T cell diversity and the receptor interface with tumor cells. *J Clin Invest*. 2020.
12. Sebestyen Z, Prinz I, Dechanet-Merville J, Silva-Santos B, Kuball J. Translating gammadelta (gammadelta) T cells and their receptors into cancer cell therapies. *Nat Rev Drug Discov*. 2020;19(3):169-84.
13. Deniger DC, Moyes JS, Cooper LJ. Clinical applications of gamma delta T cells with multivalent immunity. *Front Immunol*. 2014;5:636.
14. Scheper W, Sebestyen Z, Kuball J. Cancer Immunotherapy Using gammadeltaT Cells: Dealing with Diversity. *Front Immunol*. 2014;5:601.

15. Payne KK, Mine JA, Biswas S, Chaurio RA, Perales-Puchalt A, Anadon CM, et al. BTN3A1 governs antitumor responses by coordinating alphabeta and gammadelta T cells. *Science*. 2020;369(6506):942-9.
16. Johanna I, Hernandez-Lopez P, Heijhuurs S, Bongiovanni L, de Bruin A, Beringer D, et al. TEG011 persistence averts extramedullary tumor growth without exerting off-target toxicity against healthy tissues in a humanized HLA-A*24:02 transgenic mice. *J Leukoc Biol*. 2020;107(6):1069-79.
17. Johanna I, Straetmans T, Heijhuurs S, Aarts-Riemens T, Norell H, Bongiovanni L, et al. Evaluating in vivo efficacy - toxicity profile of TEG001 in humanized mice xenografts against primary human AML disease and healthy hematopoietic cells. *J Immunother Cancer*. 2019;7(1):69.
18. Kierkels GJJ, Scheper W, Meringa AD, Johanna I, Beringer DX, Janssen A, et al. Identification of a tumor-specific allo-HLA-restricted gammadeltaTCR. *Blood Adv*. 2019;3(19):2870-82.
19. Straetmans T, Janssen A, Jansen K, Doorn R, Aarts T, van Muyden ADD, et al. TEG001 Insert Integrity from Vector Producer Cells until Medicinal Product. *Mol Ther*. 2020;28(2):561-71.
20. Braham MVJ, Minnema MC, Aarts T, Sebestyen Z, Straetmans T, Vyborova A, et al. Cellular immunotherapy on primary multiple myeloma expanded in a 3D bone marrow niche model. *Oncoimmunology*. 2018;7(6):e1434465.
21. Straetmans T, Kierkels GJJ, Doorn R, Jansen K, Heijhuurs S, Dos Santos JM, et al. GMP-Grade Manufacturing of T Cells Engineered to Express a Defined gammadeltaTCR. *Front Immunol*. 2018;9:1062.
22. Kierkels GJ, Straetmans T, de Witte MA, Kuball J. The next step toward GMP-grade production of engineered immune cells. *Oncoimmunology*. 2016;5(2):e1076608.
23. Straetmans T, Gründer C, Heijhuurs S, Hol S, Slaper-Cortenbach I, Bönig H, et al. Untouched GMP-Ready Purified Engineered Immune Cells to Treat Cancer. *Clin Cancer Res*. 2015;21(17):3957-68.
24. Grunder C, van DS, Hol S, Drent E, Straetmans T, Heijhuurs S, et al. gamma9 and delta2CDR3 domains regulate functional avidity of T cells harboring gamma9delta2TCRs. *Blood*. 2012;120(26):5153-62.
25. June CH, O'Connor RS, Kawalekar OU, Ghassemi S, Milone MC. CAR T cell immunotherapy for human cancer. *Science*. 2018;359(6382):1361-5.
26. Singh AK, McGuirk JP. CAR T cells: continuation in a revolution of immunotherapy. *Lancet Oncol*. 2020;21(3):e168-e78.
27. Chabannon C, Kuball J, McGrath E, Bader P, Dufour C, Lankester A, et al. CAR-T cells: the narrow path between hope and bankruptcy? *Bone Marrow Transplant*. 2017;52(12):1588-9.
28. McGrath E, Chabannon C, Terwel S, Bonini C, Kuball J. Opportunities and challenges associated with the evaluation of chimeric antigen receptor T cells in real-life. *Curr Opin Oncol*. 2020;32(5):427-33.

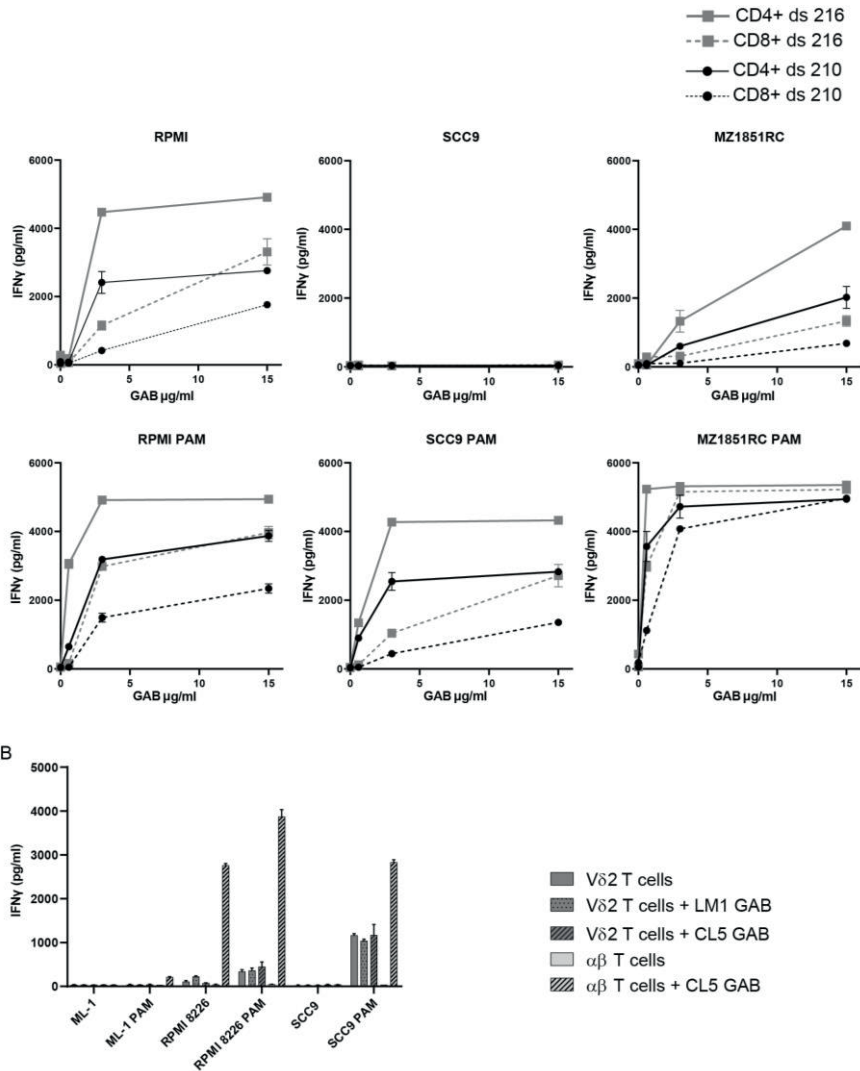
29. Batlevi CL, Matsuki E, Brentjens RJ, Younes A. Novel immunotherapies in lymphoid malignancies. *Nat Rev Clin Oncol.* 2016;13(1):25-40.
30. Krishnamurthy A, Jimeno A. Bispecific antibodies for cancer therapy: A review. *Pharmacol Ther.* 2018;185:122-34.
31. Abbott RC, Cross RS, Jenkins MR. Finding the Keys to the CAR: Identifying Novel Target Antigens for T Cell Redirection Immunotherapies. *Int J Mol Sci.* 2020;21(2).
32. Liddy N, Bossi G, Adams KJ, Lissina A, Mahon TM, Hassan NJ, et al. Monoclonal TCR-redirecated tumor cell killing. *Nat Med.* 2012;18(6):980-7.
33. Bubenik J. Tumour MHC class I downregulation and immunotherapy (Review). *Oncol Rep.* 2003;10(6):2005-8.
34. Sandstrom A, Peigne CM, Leger A, Crooks JE, Konczak F, Gesnel MC, et al. The intracellular B30.2 domain of butyrophilin 3A1 binds phosphoantigens to mediate activation of human Vgamma9Vdelta2 T cells. *Immunity.* 2014;40(4):490-500.
35. Arakawa F, Kuroki M, Kuwahara M, Senba T, Ozaki H, Matsuoka Y, et al. Cloning and sequencing of the VH and V kappa genes of an anti-CD3 monoclonal antibody, and construction of a mouse/human chimeric antibody. *J Biochem.* 1996;120(3):657-62.
36. Allison TJ, Winter CC, Fournie JJ, Bonneville M, Garboczi DN. Structure of a human gammadelta T-cell antigen receptor. *Nature.* 2001;411(6839):820-4.
37. Goebeler ME, Bargou RC. T cell-engaging therapies - BiTEs and beyond. *Nat Rev Clin Oncol.* 2020;17(7):418-34.
38. Starick L, Riano F, Karunakaran MM, Kunzmann V, Li J, Kreiss M, et al. Butyrophilin 3A (BTN3A, CD277)-specific antibody 20.1 differentially activates Vgamma9Vdelta2 TCR clonotypes and interferes with phosphoantigen activation. *Eur J Immunol.* 2017;47(6):982-92.
39. Wang H, Fang Z, Morita CT. Vgamma2Vdelta2 T Cell Receptor recognition of prenyl pyrophosphates is dependent on all CDRs. *J Immunol.* 2010;184(11):6209-22.
40. Yamashita S, Tanaka Y, Harazaki M, Mikami B, Minato N. Recognition mechanism of non-peptide antigens by human gammadelta T cells. *Int Immunol.* 2003;15(11):1301-7.
41. Willcox CR, Vantourout P, Salim M, Zlatareva I, Melandri D, Zanardo L, et al. Butyrophilin-like 3 Directly Binds a Human Vgamma4(+) T Cell Receptor Using a Modality Distinct from Clonally-Restricted Antigen. *Immunity.* 2019.
42. Harly C, Guillaume Y, Nedellec S, Peigné CM, Mönkkönen H, Mönkkönen J, et al. Key implication of CD277/butyrophilin-3 (BTN3A) in cellular stress sensing by a major human $\gamma\delta$ T-cell subset. *Blood.* 2012;120(11):2269-79.
43. Marcu-Malina V, Heijhuurs S, van Buuren M, Hartkamp L, Strand S, Sebestyen Z, et al. Redirecting $\alpha\beta$ T cells against cancer cells by transfer of a broadly tumor-reactive $\gamma\delta$ T-cell receptor. *Blood.* 2011;118(1):50-9.
44. Morath A, Schamel WW. $\alpha\beta$ and $\gamma\delta$ T cell receptors: Similar but different. *J Leukoc Biol.* 2020;107(6):1045-55.

45. Tanaka Y, Morita CT, Tanaka Y, Nieves E, Brenner MB, Bloom BR. Natural and synthetic non-peptide antigens recognized by human gamma delta T cells. *Nature*. 1995;375(6527):155-8.
46. De Libero G, Casorati G, Giachino C, Carbonara C, Migone N, Matzinger P, et al. Selection by two powerful antigens may account for the presence of the major population of human peripheral gamma/delta T cells. *J Exp Med*. 1991;173(6):1311-22.
47. Ellerman D. Bispecific T-cell engagers: Towards understanding variables influencing the in vitro potency and tumor selectivity and their modulation to enhance their efficacy and safety. *Methods*. 2019;154:102-17.
48. Li Y, Moysey R, Molloy PE, Vuidepot AL, Mahon T, Baston E, et al. Directed evolution of human T-cell receptors with picomolar affinities by phage display. *Nat Biotechnol*. 2005;23(3):349-54.
49. Birnbaum ME, Mendoza JL, Sethi DK, Dong S, Glanville J, Dobbins J, et al. Deconstructing the peptide-MHC specificity of T cell recognition. *Cell*. 2014;157(5):1073-87.
50. Duan Q, Zhang H, Zheng J, Zhang L. Turning Cold into Hot: Firing up the Tumor Microenvironment. *Trends Cancer*. 2020;6(7):605-18.
51. Lowe KL, Cole D, Kenefeck R, I OK, Lepore M, Jakobsen BK. Novel TCR-based biologics: mobilising T cells to warm 'cold' tumours. *Cancer Treat Rev*. 2019;77:35-43.
52. Riley TP, Baker BM. The intersection of affinity and specificity in the development and optimization of T cell receptor based therapeutics. *Semin Cell Dev Biol*. 2018;84:30-41.
53. Cameron BJ, Gerry AB, Dukes J, Harper JV, Kannan V, Bianchi FC, et al. Identification of a Titin-Derived HLA-A1-Presented Peptide as a Cross-Reactive Target for Engineered MAGE A3-Directed T Cells. *SciTranslMed*. 2013;5(197):197ra03.
54. Choi BD, Yu X, Castano AP, Bouffard AA, Schmidts A, Larson RC, et al. CAR-T cells secreting BiTEs circumvent antigen escape without detectable toxicity. *Nat Biotechnol*. 2019;37(9):1049-58.

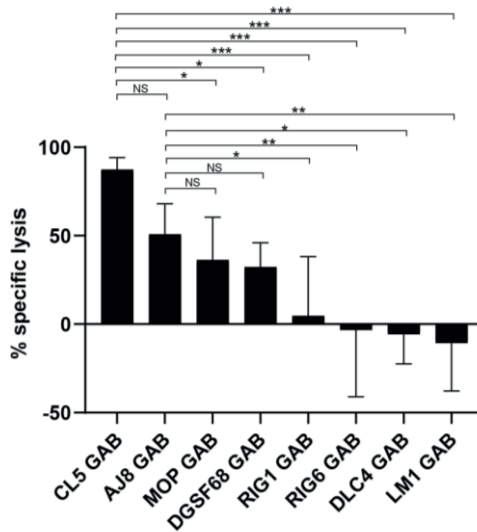
Supplementary Figures



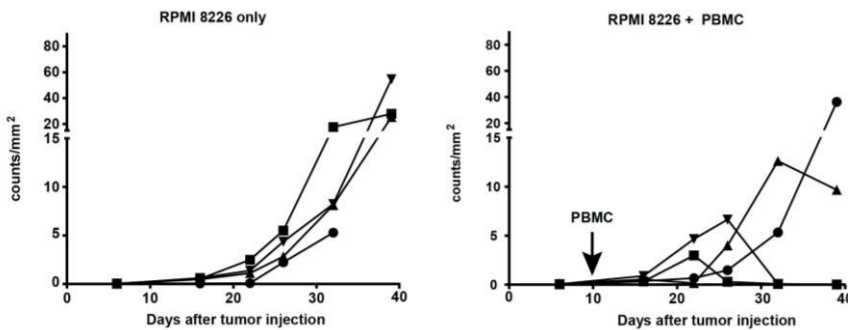
Supplementary Figure 1. GAB coating of CD4 and CD8+ $\alpha\beta$ T cells. Coating of $\alpha\beta$ T cells with GAB (90 $\mu\text{g/ml}$), followed by staining with fluorochrome labeled anti pan $\gamma\delta$, CD4 and CD8 antibodies. MFI was measured by flow cytometry, histograms represent MFI for $\gamma\delta$ for CD4+ and CD8+ T lymphocytes.



Supplementary Figure 2. Differential GAB mediated activation of CD4+, CD8+ $\alpha\beta$ T cells and V δ 2+ T cells. IFN γ release was measured using ELISA after a co-culture of (A) MACS separated CD4 and CD8 $\alpha\beta$ T cells from 2 different T cells donors with 3 different target cells in the presence of different concentration of CL5 GAB, with and without PAM (100 μ M). (B) bulk $\alpha\beta$ T cells or bulk V δ 2+ T cells with 2 recognized (RPMI 8226 + SCC9) and 1 unrecognized cell line (ML-1) with and without LM1/CL5 GAB (15 μ g/ml) and PAM (100 μ M). N=1 error bars represent SD from technical duplicates.



Supplementary Figure 3. Higher activity CL5 GAB compared to GABs derived from publicly available $\gamma 9\delta 2$ TCRs. A) T effector and luciferase transduced RPMI 8226 cells were co-incubated for 16 hours in the presence of GABs (10 $\mu\text{g}/\text{ml}$) derived from different $\text{V}\gamma 9\text{V}\delta 2$ TCRs and PAM (30 μM) at 10:1 E:T ratio. Percentage specific lysis was determined by comparing luminescence signal to untreated target cells, representing 100% viability. N=2, with technical duplos error bars represent SD, significance was calculated using a one-way ANOVA; * $P < 0.05$, ** $P < 0.001$, *** $P < 0.0001$



Supplementary Figure 4. Poor outgrowth of IV injected RPMI 8226 in NSG mice when co-engrafted with huPBMCs. NSG mice were irradiated at day -1, and injected intra venous (i.v) with 10^6 RPMI 8226 tumor cells one day later, after 10 days the mice were randomized over two groups. One group was injected i.v with 10^6 huPBMCs (n=5 right panel) while the other group received no further treatment (n=4 left panel). Tumor growth was monitored by bioluminescence imaging (BL) once a week and plotted overtime, each line represents one mouse.

Supplementary Material and Methods

Cells, Cell lines, and Primary Material.

PBMCS were isolated by Ficoll-Paque (GE Healthcare, Eindhoven, The Netherlands) from buffy coats obtained from Sanquin Blood Bank (Amsterdam, The Netherlands). $\alpha\beta$ T cells were expanded from PBMCs using CD3/CD28 dynabeads (Thermo Fisher scientific, United States) and (1.7×10^3 IU/ml of MACS GMP Recombinant Human interleukin (IL)-7 (Miltenyi Biotec, Germany), and 1.5×10^2 IU/ml MACS GMP Recombinant Human IL-15 (Miltenyi Biotec, Germany). CD4⁺ and CD8⁺ $\alpha\beta$ T cells were selected using MACS isolation with CD4- and CD8- microbeads respectively (Miltenyi Biotec, Germany). $\gamma\delta$ T cells were first selected from PBMCs by MACS isolation using TCR $\gamma\delta$ ⁺ isolation kit (Miltenyi Biotec, Germany), after which the V δ 2⁺ T cells were isolated via FACS sort based on positive staining for V δ 2-FITC (clone B6, Biolegend). V δ 2⁺ cells were expanded using the previously described rapid expansion protocol ¹ RPMI 8226 stably expressing GFP-luciferase was generated by a previously described retroviral transduction protocol ². The plasmid containing the GFP and luciferine transgenes was kindly provided by Jeanette Leusen (UMC Utrecht, Utrecht, Netherlands). The following cell lines were obtained from ATCC between 2010 and 2018, HL60 (CCL-240), ML-1 (CVCL_0436), MDA-MB231 (HTB-26), RPMI 8226 (CCL-155), Saos-2 (HTB-85), SCC9 (CRL-1629), HEK293T (CRL-3216). HEKBTN3 knock-out was a gift from Erin Adams (Chicago, United States). BV173 (ACC 20) was obtained from DSMZ. MZ1851RC was a kind gift from Barbara Seliger (University Halle, Germany). MDA-MB157 was kindly provided in 2016 by Thordur Oskarsson (Deutschen Krebsforschungszentrum, Heidelberg, Germany). Freestyle 293-F cells (R790-07) were obtained from Invitrogen (United States). HL60, RPMI 8226 ML-1 and BV173 were cultured in RPMI (Gibco, United states), 10% FCS (Bodinco, Alkmaar, The Netherlands), 1% Pen/Strep (Invitrogen, United States). Freestyle 293-F in Freestyle expression medium (Gibco). All other cell lines in DMEM, 10% FCS, 1% Pen/Strep. RPMI 8226 B2M knockout was created using Alt-R Crispr-CAS9 system (IDT, United States) according to the manufacturers protocol, with guide RNA sequence AAGTCAACTTCAATGTCCGA. Transfection was done with Neon Transfection system (Thermo Fisher Scientific) using the following settings: pulse voltage

1050 V, pulse width 20, 3 pulses.

Primary Material

Primary acute myeloid leukemia and multiple myeloma blasts were obtained from the biobank of the University Medical Center, Utrecht in accordance with good clinical practice and the Declaration of Helsinki regulations. All patients gave their consent prior to storage in the biobank (TCBio 16-088). B cells and monocytes were isolated from PBMCs by MACS-separation using CD19 and CD14-microbeads (Miltenyi Biotec, Germany) respectively, according to the manufacturers' protocol. Fibroblasts were a kind gift from Marieke Griffioen (Leiden University Medical Centre, Leiden, The Netherlands) and cultured in DMEM medium containing 10% FCS, 100 U/ml penicillin and 100 µg/ml streptomycin. Multipotent mesenchymal stromal cells (MSCs) were isolated from healthy bone marrow (Hematology Department, UMC Utrecht, The Netherlands) by adherence to tissue culture flasks, and cultured in MSC-medium; α -minimal essential media (Gibco, USA) containing 0.2 mM L-ascorbic acid 2-phosphate, 10% FCS, 100 U/ml penicillin and 100 µg/ml streptomycin. Endothelial progenitor cells (EPCs) were isolated from healthy umbilical cord blood by density-gradient centrifugation using Ficoll-paque. The isolated MNCs were seeded on collagen I-coated tissue flasks and expanded in EGM-2 medium (Lonza, Switzerland) containing 10% FCS, 100 U/ml penicillin and 100 µg/ml streptomycin. CD34+ were isolated from human umbilical cord blood using magnetic bead selection (Miltenyi Biotec, Germany). Umbilical cord blood was obtained after informed consent and approval by the ethics committee of the University Medical Center Utrecht (TC-bio 15-345). To induce stress, cells were irradiated with 3500 cGy, or treated with 5mM cyclophosphamide (Sigma Aldrich, Germany) and 20 µM fludarabine (Sigma Aldrich). Activation was done with huCD40LT (Miltenyi Biotec, Germany) 400 ng/ml for 72 hours prior to assay (CD19+), IFN γ (R&D systems, Canada) 1000 IU/ml 16 hours prior to assay (CD34+, Fibroblasts), LPS 100ng/ml (Invitrogen, United States) added during the assay (CD14+).

Flow cytometry

0.2×10^6 T cells were incubated with GAB (10 µg/ml if not indicated differently) in 20 µl FACS buffer (PBS, 1% BSA (Sigma Aldrich, Germany), 0.01

% sodium azide (Severn Biotech Ltd, United Kingdom) for 30 minutes at room temperature. Cells were washed once in FACS buffer and incubated with the appropriate secondary antibody mix for 30 minutes at room temperature. Cells were washed 2 times in FACS buffer and fixed in 1% paraformaldehyde (Merck, Germany) in PBS. Data acquisition was done on FACS Canto and analyzed using FACS Diva software (BD, United States) or FlowJo. Antibodies that were used are pan- $\gamma\delta$ TCR-PE (Beckman Coulter, United States, clone IMMU510, 1:10), pan- $\gamma\delta$ TCR-APC (BD Pharmingen, United States, clone B1,1:5), V δ 2-FITC (Biolegend, United States, clone B6, 1:10) and V γ 9-PE (BD pharmingen, clone B3, 1:25).

IFN γ Elispot

15.000 effector cells and 50.000 target cells were incubated together, with or without GAB (10 μ g/ml if not indicated differently) for 16 hours at 37 °C 5% CO₂. In PAM conditions, 100 μ M PAM (Calbiochem, United States) was added to the cells. The co-culture was done in nitrocellulose-bottomed 96-well plates (Millipore, United States) pre-coated with α -IFN γ antibody (clone 1-D1K) (Mabtech, Sweden). After 16 hours, the plates were washed with PBS and incubated with mAb7-B6-1 (II; Mabtech, Sweden) followed by Streptavidin-HRP (Mabtech, Sweden) IFN γ spots were visualized with TMB substrate (Mabtech, Sweden) and analyzed using A.EL.VIS ELISPOT wscanner and analysis software (A.EL.VIS, Germany).

CD107 degranulation assay

300.000 target cells were incubated with 100.000 T cells, GAB (10 μ g/ml) and 100 μ M PAM (Calbiochem, United States) in the presence of aCD107 α -PE (BD, United States, clone AB4, 1:200) for 7 hours, after 2 hours Golgistop (BD, United States) was added (1:1500). After 7 hours, cells were washed in FACS buffer and stained with aCD3-eFluor450 (eBioscience, United states, clone OKT3, 1:50) and aCD8-PerCP-Cy5.5 (Biolegend, United States, clone RPA-T8, 1:1000). Cells were washed 2 times in FACS buffer and fixed in 1% paraformaldehyde (Merck, Germany) in PBS. Data acquisition was done on FACS Canto and analyzed using FACS Diva software (BD)

Luciferase based cytotoxicity

5000 RPMI 8226 target cells stably expressing luciferase were incubated with T cells at different E:T ratios (1:1 to 1:30), with or without 10 µg/ml GAB in the presence of 0.1 mM PAM (calbiochem, United States). After 16 hours, beetle luciferin (Promega, United States) was added to the wells (125 µg/ml) and bioluminescence was measured on SoftMax Pro plate reader. The signal in treatment wells was normalized to the signal measured for untreated targets, which was assumed to represent 100% living cells.

Animal model

NOD.Cg-PrkdcscidIl2rgtm1Wjl/SzJ (NSG) mice were obtained from Jackson Laboratory (Bar Harbor, ME, USA). Experiments were conducted under institutional guidelines after permission from the local Ethical Committee and in accordance with the current Dutch laws on Animal Experimentation. Mice were housed in sterile conditions using an individually ventilated cage (IVC) system and fed with sterile food and water. Irradiated mice were given sterile water with antibiotic ciproxin for the duration of the experiment. Adult female mice (16 weeks old) received sublethal total body irradiation (1.75 Gy) on Day -1. For the iv model, mice received a subcutaneous injection of 10×10^6 RPMI 8226-luc cells in PBS on day 0. Ten days later, mice were randomized into two groups of 4 or 5 mice and one group was intravenously injected with 10×10^6 huPBMCs. Tumor growth was measured once a week by bioluminescence imaging (BLI). For the subcutaneous model, mice received a subcutaneous injection of 10×10^6 RPMI 8226-luc B2M knockout cells in PBS, on day 0. One week later, mice were randomized based on tumor volume into two groups of 10 mice and intravenously injected with 10×10^6 huPBMCs. Next, mice received 7 consecutive injections of either CL5 GAB or LM1 GAB (2,7 mg/kg body weight). Pamidronate (10 mg/kg body weight) was injected together with the GABs on days 9 and 12. Moreover, an extra group (n=4) that received tumor and huPBMCs but no GABs was included as additional control. Tumor volume was measured three times a week as primary outcome measure. Percent change in tumor volume was calculated using the formula: $(V_f - V_0)/V_0 \times 100$, where V_0 = volume at the beginning of the treatment, and V_f = final volume. Mouse peripheral blood samples were obtained via cheek vein (maximum 50–80 µl/mouse) once a week. Red blood cell lysis was performed for blood

samples using 1× RBC lysis buffer (Biolegend) before cell staining. Blood samples were stained with $\gamma\delta$ TCR-PE (clone RPA-T4, Biolegend), $\alpha\beta$ TCR-FITC (Clone IP26, Invitrogen), huCD45-PB (Clone HI30, Sony). The persistence of GABs bound to $\alpha\beta$ T cells was measured in peripheral blood by quantifying the absolute $\alpha\beta$ TCR positive and $\alpha\beta$ TCR⁺/ $\gamma\delta$ TCR double positive cell number by flow cytometry using Flow-count Fluorospheres (Beckman Coulter).

Supplementary references

1. Marcu-Malina V, Heijhuurs S, van Buuren M, Hartkamp L, Strand S, Sebestyen Z, *et al.* Redirecting $\alpha\beta$ T cells against cancer cells by transfer of a broadly tumor-reactive $\gamma\delta$ T-cell receptor. *Blood* 2011;118:50-9
2. Grunder C, van DS, Hol S, Drent E, Straetemans T, Heijhuurs S, *et al.* gamma9 and delta2CDR3 domains regulate functional avidity of T cells harboring gamma9delta2TCRs. *Blood* 2012;120:5153-62



CHAPTER 4

Impact of CD3 binding affinity on the potency of Gamma delta TCR Anti-CD3 Bispecific T cell engagers (GABs)

Eline van Diest¹⁺, Patricia Hernández-López¹⁺, Mara Nicolassen¹, Laura Bongiovani², Alain de Bruin^{2,3}, Effrosyni Karaiskaki¹, Koen Bots¹, Sabine Heijhuurs¹, Anita Kumari¹, Trudy Straetemans¹, Dennis X Beringer^{1*}, Jürgen Kuball^{1,4*}

¹Center for Translational Immunology, University Medical Center Utrecht, The Netherlands

²Department of Biomolecular Health Sciences, Dutch Molecular Pathology Center, Faculty of Veterinary Medicine, Utrecht University, Utrecht, Netherlands.

³Department of Pediatrics, University Medical Center Groningen, University of Groningen, Groningen, Netherlands.

⁴Department of Hematology, University Medical Center Utrecht, The Netherlands

+Shared first authors

*Equally contributed

Manuscript in preparation

Abstract

We previously developed a novel T cell engager construct: **G**amma **D**elta TCR **A**nti-CD3 **B**ispecific T cell engager molecule (GAB), by fusing the ectodomains of a V γ 9V δ 2 TCR to an anti-CD3 single chain variable fragment (scFv). GABs mirror the unique tumor sensing capacity of V γ 9V δ 2T cells, which is mediated by BTN2A1, and a phosphoantigen- and RhoB-dependent orchestration of BTN3A1 at the cell membrane of target cells. Amongst various variables, the binding affinity of the anti-CD3 scFv has been identified as an important determinant of *in vitro* and *in vivo* potency of bispecific T cell engagers. In this light, we explored the effect of several anti-CD3scFvs, with different binding characteristics, on GAB effectivity. We show that *in vitro* GAB potency correlated with CD3 binding strength, and that increasing CD3 binding strength also increased GAB-induced IFN γ release and tumor cell killing. Within this context we describe a V γ 9V δ 2TCR-aCD3scFv combination that, *in vitro*, observed a low EC50 for tumor cell killing, and a 10-fold higher EC50 for cytokine secretion. GABs comprised of a high affinity anti-CD3scFv and a high affinity anti-CD3 binding arm also showed improved efficacy *in vivo* in a xenograft model. We detected prolonged GAB binding to T cells *in vivo* for this construct, which might have contributed to the increased efficacy, but was, however, also accompanied by a temporary lymphopenia that resolved over time. In conclusion, we show that increasing CD3 binding affinity in combination with a high affinity V γ 9V δ 2 TCR increases the potency of the GAB molecules, both *in vitro* and *in vivo*, with an acceptable safety toxicity profile.

Introduction

A variety of immunotherapeutic strategies are currently being developed for the treatment of cancer, including checkpoint inhibitors, adoptive T cell transfer of TCR or CAR-engineered T cells, and bispecific T cell engagers. Bispecific T cell engagers (TCEs) combine a tumor targeting domain with a T cell binding domain, often specific for CD3, and can thereby redirect T lymphocytes to tumor cells, independent of specific TCR-MHC binding^{1, 2}. Blinatumomab and tebentafusp are currently the only two FDA-approved TCE constructs^{3, 4}, but many other TCEs are under development². However, other difficulties are currently hampering further TCE development, including the identification of novel suitable target antigens, and the occurrence of treatment related toxicities, like, for example, cytokine release syndrome.

We previously developed a novel T cell engager construct: **Gamma Delta TCR Anti-CD3 Bispecific T cell engager molecule (GAB)**, by fusing the ectodomains of a V γ 9V δ 2TCR to an anti-CD3 single chain variable fragment (scFv)⁵. GABs duplicate the unique tumor sensing capacity of V γ 9V δ 2T cells, which is mediated by the direct interaction of the V γ 9V δ 2TCR, with BTN2A1 further modulated by the phosphoantigen-dependent orchestration of BTN3A at the cell membrane of target cells⁶⁻⁸. Phosphoantigen accumulation is found in infected cells, but is also often seen during transformation of tumor cells⁹, and orchestrates BTN3A turnover together with RhoB¹⁰. GABs can efficiently induce $\alpha\beta$ T cell mediated phosphoantigen-dependent recognition of tumor cells, and redirect $\alpha\beta$ T cells against a broad range of hematopoietic and solid tumor cell lines, and primary acute myeloid leukemia or multiple myeloma⁵. Affinity of V γ 9V δ 2TCR to their ligand complex can, however, substantially differ^{8, 11}. We have shown that selection of naturally occurring higher affinity V γ 9V δ 2TCR is important for GAB effectivity⁵, which is in line with the consensus that higher affinity target cell engagement is preferred, to achieve potent T cell redirection¹². It was nonetheless surprising that GABs are functional when using V γ 9V δ 2TCR. Though GABs constructed with V γ 9V δ 2TCR were considered as high affinity within the context of V γ 9V δ 2TCR, their binding affinity is substantially lower (in the μ M range) when compared to $\alpha\beta$ TCR based TCEs, for which affinity maturation to the pM range is necessary

to create potent TCEs¹³. Different requirements of TCR affinity for $\gamma\delta$ - and $\alpha\beta$ TCR based TCEs might simply reflect the higher expression of the respective ligands, as the total amount of surface expressed V γ 9V δ 2TCR ligand complex likely exceeds the amount of MHC presented peptides for a specific $\alpha\beta$ TCR.

In addition to the target binding arm, the choice of CD3 binding domain, often an scFv derived from an anti-CD3 monoclonal Ab (mAb), has also been reported to influence effectivity of TCEs¹². The interest in determining the optimal anti-CD3 scFv for TCEs originated from the first clinical trials using bispecific T cell engagers, showing only a short therapeutic window, due to early occurrence of cytokine release syndrome (CRS), which was at least partially attributed to the high affinity binding of the TCE's to CD3¹⁴. Many of the several subsequent reports on the effect of CD3 binding affinity on TCE effectivity and tolerability concluded that lowering CD3 binding affinity improved *in vivo* biodistribution, tumor control, toxicity, and kinetics of several TCE formats¹⁵⁻¹⁹. Another interesting report showed that, by careful anti-CD3 scFv selection, it was possible to completely uncouple the TCE mediated tumor cell lysis from cytokine release, which would significantly reduce the risk for CRS²⁰.

Most of such CD3scFv affinity studies with TCEs were conducted with TCEs that combine the CD3 engaging arm with a very high affinity tumor target binding domain, which might not reflect the situation in which a lower affinity target binding domain is used, like, for example the V γ 9V δ 2TCR in the GABs. Thus, more studies are needed to assess the right balance when the affinity of the tumor binding arm is lower, as biological properties of both arms are likely to contribute to overall TCE potency^{12, 21}.

In this report, we investigated how different anti-CD3 scFvs in the GAB format influence GAB potency *in vitro* and *in vivo*. We showed superior T cell activation and tumor cell lysis by GABs with a higher affinity anti-CD3 scFv *in vitro*, which demonstrated improved tumor control *in vivo*, when combined with a higher affinity V γ 9V δ 2TCR.

Material and methods

Generation and production of GABs

The construction of the GAB molecule was described earlier⁵. The different CD3scFv were interchanged in the GAB-containing vector using a 5' FSEI site and 3' SALI site. The scFvs sequence were constructed by linking the 3' variable heavy chain via a flexible 3(G₄S) linker to the variable light chain (TR66, 7196,7232 and OKT3) or in the opposite order (UCHT1). The scFv sequences can be found in Table 1. TCR domain boundaries were used as in Allison et al.²². The $\gamma 9$ and $\delta 2$ TCR sequences used were reported previously AJ8⁵ as low affinity TCR ($\gamma\delta$ TCR_{LO}), and high affinity A3 *in vitro*⁸, and CL5 for the *in vivo* experiments ($\gamma\delta$ TCR_{HI})²³. GAB expression and purification have been extensively described⁵.

Cells and Cell lines

PBMCS were isolated by Ficoll-Paque (GE Healthcare, Eindhoven, The Netherlands) from buffy coats obtained from Sanquin Blood Bank (Amsterdam, The Netherlands). $\alpha\beta$ T cells were expanded from PBMCs using CD3/CD28 dynabeads (Thermo Fisher scientific, United States) and 1.7×10^3 IU/ml of MACS GMP Recombinant Human interleukin (IL)-7 (Miltenyi Biotec, Germany), and 1.5×10^2 IU/ml MACS GMP Recombinant Human IL-15 (Miltenyi Biotec, Germany). Mock TCR transduced T cells and RPMI 8226 and SCC9 stably expressing GFP-luciferase were generated via a retroviral transduction protocol described earlier²³. The plasmid containing the GFP and luciferine transgenes was kindly provided by Jeanette Leusen (UMC Utrecht, Utrecht, Netherlands). The following cell lines were obtained from ATCC between 2010 and 2018, HL60 (CCL-240), RPMI 8226 (CCL-155), SCC9 (CRL-1629), K562 (CCL-243) and MDA-MB231 (HTB-26). Freestyle 293-F cells (R790-07) were obtained from Invitrogen (United States). HL60, RPMI 8226 and K562 were cultured in RPMI (Gibco, United states), 10% FCS (Bodinco, Alkmaar, The Netherlands), 1% Pen/Strep (Invitrogen, United States). Freestyle 293-F in Freestyle expression medium (Gibco). SCC9 and MDA-MB231 in DMEM, 10% FCS, 1% Pen/Strep.

Flow cytometry

0.2×10^6 bulk $\alpha\beta$ T cells were incubated with GAB at different concentrations, in 20 μ l FACS buffer PBS, 1% BSA (Sigma Aldrich, Germany), 0.01% sodium azide (Severn Biotech Ltd, United Kingdom) for 30 minutes at room temperature. Cells were washed once in FACS buffer, and incubated with pan- $\gamma\delta$ TCR-PE (Beckman Coulter, United States, clone IMMU510, 1:10) for 30 minutes at room temperature. Cells were washed 1 time in FACS buffer and fixed in 1% paraformaldehyde (Merck, Germany) in PBS. Data acquisition was done on FACS Canto and analyzed using FACS Diva software (BD, United States).

IFN γ ELISA

50.000 effector cells and 50.000 target cells were incubated together, with or without GAB (different concentrations, as indicated) for 16 hours at 37 °C 5% CO₂, 0.1 mM PAM (calbiochem) was added to the target cells. The supernatant was harvested after 16 hours, and the level of IFN γ was determined using the IFN gamma Human Uncoated ELISA Kit (Invitrogen).

Luciferase-based cytotoxicity

5000 target cells stably expressing luciferase were incubated with T cells transduced with a mock TCR at 3:1 target cell ratio, with different GAB concentrations (as indicated) in the presence of 0.1 mM PAM (calbiochem, United States). After 16 hours, beetle luciferin (Promega, United States) was added to the wells (125 μ g/ml) and bioluminescence was measured on SoftMax Pro plate reader. The signal in treatment wells was normalized to the signal measured for targets and T cells only, which was assumed to represent 100% living cells.

Animal model, *in vivo* cytokine analyses and mouse pathology

NOD.Cg-Prkdcscid1l2rgtm1Wjl/SzJ (NSG) mice were obtained from Jackson Laboratory (Bar Harbor, ME, USA). Experiments were conducted under institutional guidelines after permission from the local Ethical Committee and in accordance with the current Dutch laws on animal experimentation. Mice were housed in sterile conditions using an individually ventilated cage (IVC) system, and fed with sterile food and water. Irradiated mice were given sterile

water with antibiotic ciproxin for the duration of the experiment. Adult female mice (13 weeks old) received sublethal total body irradiation (1.75 Gy) on Day -1. Mice received a subcutaneous injection of 10×10^6 RPMI 8226-luc B2M KO cells in PBS on day 0. For the tumor treatment model, the mice were randomized, based on tumor size, into three groups of 10 mice on day 7, and were intravenously injected with 10×10^6 huPBMCs. Next, mice received 7 GAB injections every other day, starting at day 8 (2.7 mg/kg body weight). Pamidronate (10 mg/kg body weight) was injected together with the GABs on days 8 and 14. Moreover, an extra group (n=5) that received tumor and huPBMCs, but no GABs was included as an additional control. Tumor volume was measured three times a week as the primary outcome measure. For the second, short mouse model, mice were randomized over four groups of 5 mice, and received two GAB injections on day 8 and 10. Peripheral blood samples were obtained via cheek vein (maximum 50–80 μ l/mouse) on indicated days. Red blood cell lysis was performed for blood samples using $1 \times$ RBC lysis buffer (Biolegend) before cell staining. Blood samples were stained with $\gamma\delta$ TCR-PE (clone IMMU510, Beckman Coulter), $\alpha\beta$ TCR-FITC (Clone IP26, Invitrogen), huCD45-PB (Clone HI30, Sony), CD4-APC (clone RPA-T4, Biolegend) and CD8 (clone RPA-T8, Biolegend). The persistence of GABs bound to $\alpha\beta$ T cells was measured in peripheral blood by quantifying the absolute $\alpha\beta$ TCR positive and $\alpha\beta$ TCR⁺/ $\gamma\delta$ TCR double positive cell number by flow cytometry, using Flow-count Fluorospheres (Beckman Coulter). Plasma was collected and luminex was performed to measure cytokine levels for IL2, IL6, IL10, TNF α , IFN γ , MCP1, MIP1 α , MIP1 β , CXCL1, and IP10. Tumors were collected at the end of the experiment (day 12) and fixed in formalin. Fixed tumors were embedded in paraffin and cut into 4 μ m sections, and hematoxylin and eosin (H&E) staining were performed, following the previously described protocol²⁴. The following histologic features were evaluated: number of mitotic figures and apoptotic cells: expressed as a range per high-power fields (HPFs), calculated in the same, randomly selected 5 HPFs, 40 \times); extension of the necrotic tumor tissue was expressed as the percentage considering the entire tumor mass. Images were taken using an Olympus BX45 microscope with the Olympus DP25 camera, and analyzed using DP2-BSW (version.2.2) software. T cell infiltration was determined using immunofluorescent (IF) staining. For IF, after deparaffinization and

dehydration, slides were pretreated with 10 mM citrate buffer pH 6.0 for 15 min, followed by cooling at room temperature for 30 min. Staining was done using anti-human Anti-Nuclei Antibody (clone 3E1.3, Merck Millipore BV) and anti-human CD3 polyclonal antibody (Agilent Technologies). Slides were mounted in VECTASHIELD Antifade Mounting Medium with DAPI (Vector Laboratories). Slides were scanned by an Olympus VS200 research slide scanner and analyzed by the Olyvia (Olympus) imaging software. The total number of double positive cells was counted in the entire tissue section, and expressed as a number.

Results

CD3scFv panel with different CD3 binding affinity

To study the effect of CD3 binding affinity on GAB activity, we selected five anti-CD3 scFvs (α CD3) to couple to the previously characterized low affinity $V\gamma 9V\delta 2$ TCR AJ8 (TCR_{LO})⁵. The selected scFvs were derived from three anti-CD3 antibodies that have been historically used in different TCEs, listed from low to high CD3 affinity: TR66, OKT3 and UCHT1 (Supplementary Table 1)²⁵. In addition, two CD3scFv sequences, 7195 and 7232, were chosen based on their binding kinetics²⁶. 7195 is a high affinity scFv with a long half-life of 117 minutes, while the intermediate affinity scFv 7232 has a short half-life of only 7 minutes. After expression and purification, the different TCR_{LO}- α CD3 GABs were analyzed on SDS gel, all showing similar bands for the TCR δ _{LO}- and TCR γ _{LO}- α CD3 chain, confirming proper expression of all constructs (Figure 1A).

We first assessed T cell binding of the TCR_{LO}- α CD3 GABs by flow cytometry. GABs were titrated and incubated with T lymphocytes and the T cells bound by GABs were assessed using a pan- $\gamma\delta$ TCR antibody (Figure 1B). Titration of GABs allowed us to determine EC₅₀ values, showing, in line with earlier reports, that GABs containing one of the high affinity scFvs UCHT1 and 7195 were the strongest binders, with an EC₅₀ of 0.2-0.3 μ g/ml (Table 1). GABs containing one of the intermediate affinity scFvs 7232 and OKT3 showed similar intermediate binding with an EC₅₀ around 1 μ g/ml, and GABs constructed with the low affinity TR66 had the lowest EC₅₀ at 2.2 μ g/ml. Based

on these data, we selected three scFvs with different CD3 binding affinity for further functional testing: the high affinity scFv UCHT1 (α CD3_{HI}), OKT3 as intermediate binder (α CD3_{MED}) and TR66 with low binding affinity (α CD3_{LO}).

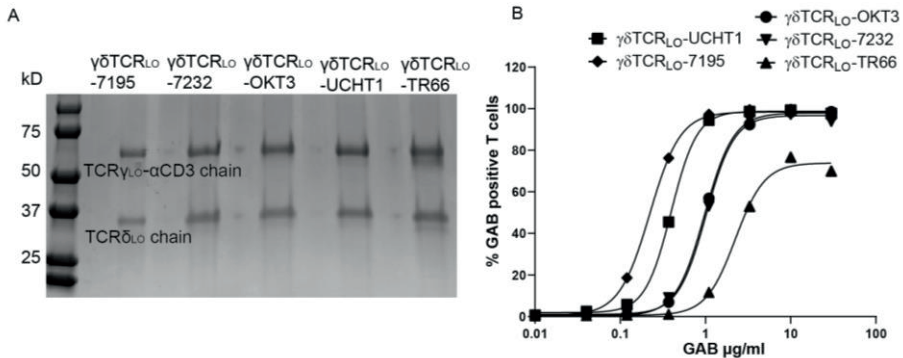


Figure 1. Expression and T cell binding of the GAB molecules with different anti-CD3 scFvs (A) After HIS-tag purification, the GABs containing a low affinity $\gamma\delta$ TCR with different anti-CD3 scFvs ($\gamma\delta$ TCR_{LO}- α CD3) were run on SDS gel, and visualized with Coomassie brilliant blue protein stain. Showing a band for the TCR _{γ} - α CD3 chain at 59 kD and the TCR _{δ} chain at 24 kD (B) Coating of T lymphocytes with GABs containing the different α CD3 scFvs, followed by staining with fluorochrome labeled anti pan- $\gamma\delta$ antibody, percentage positive T cells was determined by flow cytometry. The EC₅₀ was calculated using a non-linear regression model, depicted in the table as μ g/ml and mol/L (M) for each anti-CD3 scFv. N=2, a representative figure is shown

Table 1. EC₅₀ of GABs with different CD3scFvs in T cell binding in (μ g/ml) and (M)

CD3scFv	EC ₅₀ (μ g/ml) T cell binding	EC ₅₀ (M) T cell binding
UCHT1	0.396 μ g/ml	4.7 * 10 ⁻⁹ M
7195	0.222 μ g/ml	2.6 * 10 ⁻⁹ M
OKT3	0.979 μ g/ml	1.2 * 10 ⁻⁸ M
7232	1.017 μ g/ml	1.2 * 10 ⁻⁸ M
TR66	2.241 μ g/ml	2.7 * 10 ⁻⁸ M

GABs using a high affinity CD3scFv are more potent in inducing IFN γ release by T cells, mainly when combined with a lower affinity $\gamma\delta$ TCR

To test impact of the anti-CD3 scFv binding affinity on in vitro potency of the GABs, we first assessed the TCR_{LO}- α CD3_{HI}/MED/LO GABs in an IFN γ release assay. The GABs were titrated in a co-culture of T lymphocytes and

the recognized target cell lines MDA-MB231 and SCC9. There was a clear impact of the different anti-CD3 scFvs on GAB potency against both cell lines, $\gamma\delta$ TCRLO- α CD3HI GAB could already induce IFN γ release at low concentrations, starting from 0.1 μ g/ml. $\gamma\delta$ TCRLO- α CD3MED and $\gamma\delta$ TCRLO- α CD3LO were only able to induce IFN γ release at the higher concentrations, from 10 μ g/ml against SCC9 or 1 μ g/ml against MDA-MB231, and did not reach a plateau (Figure 2A).

The different anti-CD3 scFvs were also tested in combination with a higher affinity TCR ($\gamma\delta$ TCRHI) 5. There was again a difference in potency between $\gamma\delta$ TCRHI- α CD3HI and $\gamma\delta$ TCRHI- α CD3LO GAB. Combining the $\gamma\delta$ TCRHI with the α CD3MED, resulted in a GAB with intermediate potency (Figure 2B). $\gamma\delta$ TCRHI- α CD3HI induced more IFN γ release at concentrations below 10 μ g/ml compared to $\gamma\delta$ TCRHI α CD3MED, but at higher concentrations, the GAB with α CD3MED induced similar or even higher levels of IFN γ against both targeted cell lines.

To test whether activation of T cells through GABs occurs only in the presence of the molecular target and is not due to the higher affinity CD3 binding only, GABs with the different anti-CD3 scFvs were incubated at a fixed concentration of 10 μ g/ml with HEK293T-BTN3KO cells, a cell line which lacks one of the ligands crucial for V γ 9V δ 2TCR mediated activation. RPMI 8226 was used as a positive control, and IFN γ release was assessed (Figure 2C). Overall, none of the GABs induced IFN γ when co-incubated with the negative target cell line HEK293T-BTN3AKO, while they did induce recognition when co-incubated with the positive control cell line RPMI 8226. This confirms that for all of the anti-CD3 scFvs used here, single T cell engagement is not sufficient to induce cytokine release.

GABs using higher affinity CD3scFvs are more potent in inducing tumor cell lysis, and increase the EC₅₀ ratio between killing and cytokine secretion

Creating a more favorable balance for induction of tumor cell killing is the most important aspect for TCEs. Therefore, we tested all of the different TCR_{HI}- α CD3 GABs for their ability to induce tumor cell lysis, using two recognized

tumor cell lines: RPMI 8226 and SCC9. The amount of living cells was determined after a co-culture of T cells, target cells and GABs at different concentrations. In line with the IFN γ release data, $\gamma\delta$ TCR $_{HI}$ - α CD3 $_{HI}$ was most

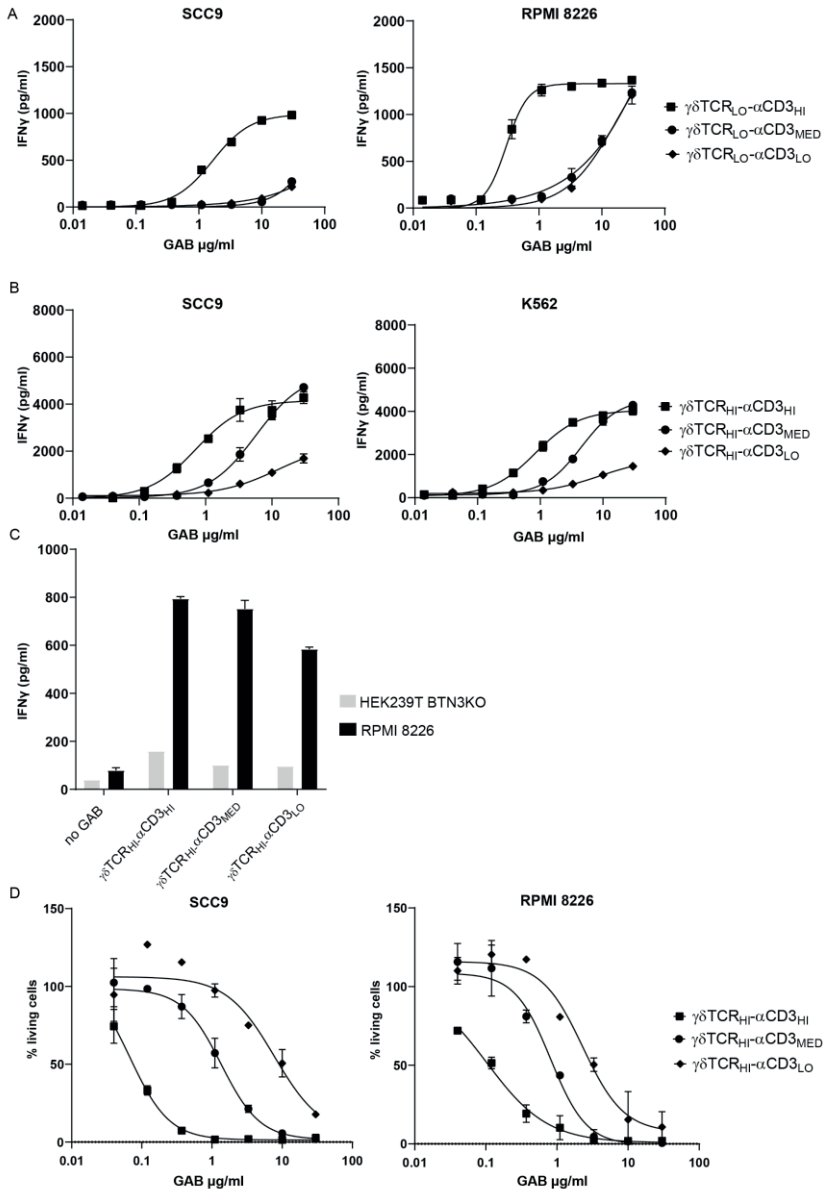


Figure 2. GAB with higher affinity CD3 binding is more potent in induction of IFN γ release and tumor

cell lysis. (A+B) IFN γ release was determined after 16 hours 1:1 co-culture of T cells (A) with RPMI 8226 or SCC9 target cells and a titration of GABs with a lower affinity $\gamma\delta$ TCR ($\gamma\delta$ TCR_{LO}) combined with an anti-CD3 scFv with high (α CD3_{HI}), intermediate (α CD3_{MED}) or low affinity (α CD3_{LO}) in the presence of PAM (100 μ M). (B) or with K562 and SCC9 target cells and a titration of GABs with high affinity $\gamma\delta$ TCR ($\gamma\delta$ TCR_{HI}) coupled to α CD3_{HI}/ α CD3_{MED}/ α CD3_{LO} in the presence of PAM (100 μ M). (C) GABs with $\gamma\delta$ TCR_{HI} coupled to α CD3_{HI}/ α CD3_{MED}/ α CD3_{LO} (10 μ g/ml) were incubated with HEK293T BTN3KO or RPMI 8226 target cells and T cells, and IFN γ release was measured after 16 hours. (D) T lymphocytes and luciferase transduced RPMI 8226 and SCC9 target cells were co-incubated for 16 hours with $\gamma\delta$ TCR_{HI} coupled to α CD3_{HI}/ α CD3_{MED}/ α CD3_{LO} at different concentrations and PAM (30 μ M) at an E:T ratio of 3:1. Percentage viable cells was determined by comparing luminescence signal to the no-GAB condition, representing 100% viability. N=1 Error Bars represent SD from technical duplicates.

potent in inducing tumor cell lysis, inducing killing at concentrations as low as 0.1 μ g/ml (Figure 2D). Again $\gamma\delta$ TCR_{HI}- α CD3_{MED} GAB displayed an intermediate phenotype, able to efficiently induce lysis, but at a higher concentration compared to the GABs with a high affinity scFvs. GABs with the α CD3_{LO} were able to induce lysis only at the highest concentrations.

Toxicity of TCE is frequently induced by excessive cytokine secretion, and therefore TCE's with reduced cytokine secretion relative to killing capacity are developed^{19, 27, 28}. Within this context, we analyzed EC₅₀ in target cell lysis and IFN γ release for the $\gamma\delta$ TCR_{HI}- α CD3 GABs with high, medium or low CD3 affinity, using the target cell line SCC9 (Table 2). Interestingly, the EC₅₀ for target cell lysis was substantially lower compared to IFN γ release for all tested anti-CD3 scFvs. The largest difference in EC₅₀ values was observed for $\gamma\delta$ TCR_{HI}- α CD3_{HI}, with 10-fold less GABs needed for target cell killing when compared to IFN γ release, while the other tested GABs had smaller differences, a 4.4 fold difference for $\gamma\delta$ TCR_{HI}- α CD3_{MED} and a 1.5 fold difference $\gamma\delta$ TCR_{HI}- α CD3_{LO}. Our data imply that, despite having the strongest activity for both killing and cytokine secretion, $\gamma\delta$ TCR_{HI}- α CD3_{HI} could have the best therapeutic efficacy/toxicity window for later clinical application.

Table 2 EC50 $\gamma\delta$ _{HI}- α CD3_{HI/MED/LO} GABs IFN γ release and target cell lysis with SCC9 target cells

	EC ₅₀ IFN γ release	EC ₅₀ Target cell lysis
$\gamma\delta$ _{HI} - α CD3 _{HI}	0.712 μ g/ml	0.068 μ g/ml
$\gamma\delta$ _{HI} - α CD3 _{MED}	5.722 μ g/ml	1.350 μ g/ml
$\gamma\delta$ _{HI} - α CD3 _{LO}	12.18 μ g/ml	7.755 μ g/ml

GABs with the high affinity anti-CD3 scFv show better *in vivo* tumor control compared to GABs with an intermediate affinity.

Others reported that selecting the most potent *in vitro* T cell engager does not necessarily result in the best *in vivo* efficacy in mice ¹⁶. Therefore, we tested whether the most potent GAB, with the best efficacy-toxicity profile when assessed *in vitro* ($\gamma\delta\text{TCR}_{\text{HI}}\text{-}\alpha\text{CD3}_{\text{HI}}$), was superior *in vivo* when compared to the less potent GAB *in vitro* ($\gamma\delta\text{TCR}_{\text{HI}}\text{-}\alpha\text{CD3}_{\text{MED}}$). To this end, NSG mice were injected with the multiple myeloma cell line RPMI 8226- β 2M KO subcutaneously, and human PBMC intravenously one week later to reconstitute the human immune system (Figure 3A) as described previously ⁵. Starting from day 8, the mice received injections with $\gamma\delta\text{TCR}_{\text{HI}}\text{-}\alpha\text{CD3}_{\text{HI}}$, $\gamma\delta\text{TCR}_{\text{HI}}\text{-}\alpha\text{CD3}_{\text{MED}}$, or $\gamma\delta\text{TCR}_{\text{MOCK}}\text{-}\alpha\text{CD3}_{\text{MED}}$, with mock TCR LM1 ²³ coupled to $\alpha\text{CD3}_{\text{MED}}$ as a negative control, every second day until day 20. Tumor size was determined until day 35, showing that both $\gamma\delta\text{TCR}_{\text{HI}}\text{-}\alpha\text{CD3}_{\text{HI}}$ and $\gamma\delta\text{TCR}_{\text{HI}}\text{-}\alpha\text{CD3}_{\text{MED}}$ significantly reduced tumor size compared $\gamma\delta\text{TCR}_{\text{MOCK}}\text{-}\alpha\text{CD3}_{\text{MED}}$, while the mock group did not differ significantly from the PBMC only group (Figure 3B). Moreover, the GAB with $\alpha\text{CD3}_{\text{HI}}$ was significantly better in tumor control, compared to the $\alpha\text{CD3}_{\text{MED}}$.

Superior *in vivo* performance of $\gamma\delta\text{TCR}_{\text{HI}}\text{-}\alpha\text{CD3}_{\text{HI}}$ could be due not only to its increased killing efficacy (e.g. Table 2), but also potentially to extend persistence in the bloodstream due to prolonged binding to T cells. To investigate this hypothesis, mice were bled on day 9,10 and 21, 22 and 24, corresponding to 24 plus 48 hours after the first GAB injection and 24, 48 and 96 hours after the seventh and last GAB injection respectively. Total human T lymphocytes per ml of blood was determined, and these T cells were divided in T cells that stained single for positive for $\alpha\beta\text{TCR}$, and $\alpha\beta\text{TCR}/\gamma\delta\text{TCR}$ double positive, corresponding to T cells coated with GAB protein (Figure 3C). $\gamma\delta\text{TCR}_{\text{HI}}\text{-}\alpha\text{CD3}_{\text{HI}}$ showed higher and longer *in vivo* T cell coating compared to the other groups. Almost all T cells were still bound by GABs 48 hours after the first or the last injection in this group. Strikingly, the total T cell numbers in the group treated with $\gamma\delta\text{TCR}_{\text{HI}}\text{-}\alpha\text{CD3}_{\text{HI}}$ was consistently lower compared to either $\alpha\text{CD3}_{\text{MED}}$ GAB or PBMCs-only group, with a strong drop within the first 24 hours after each injection, and did not differ between CD4+ or CD8+ T cells (Figure 3C and Figure S1A and B).

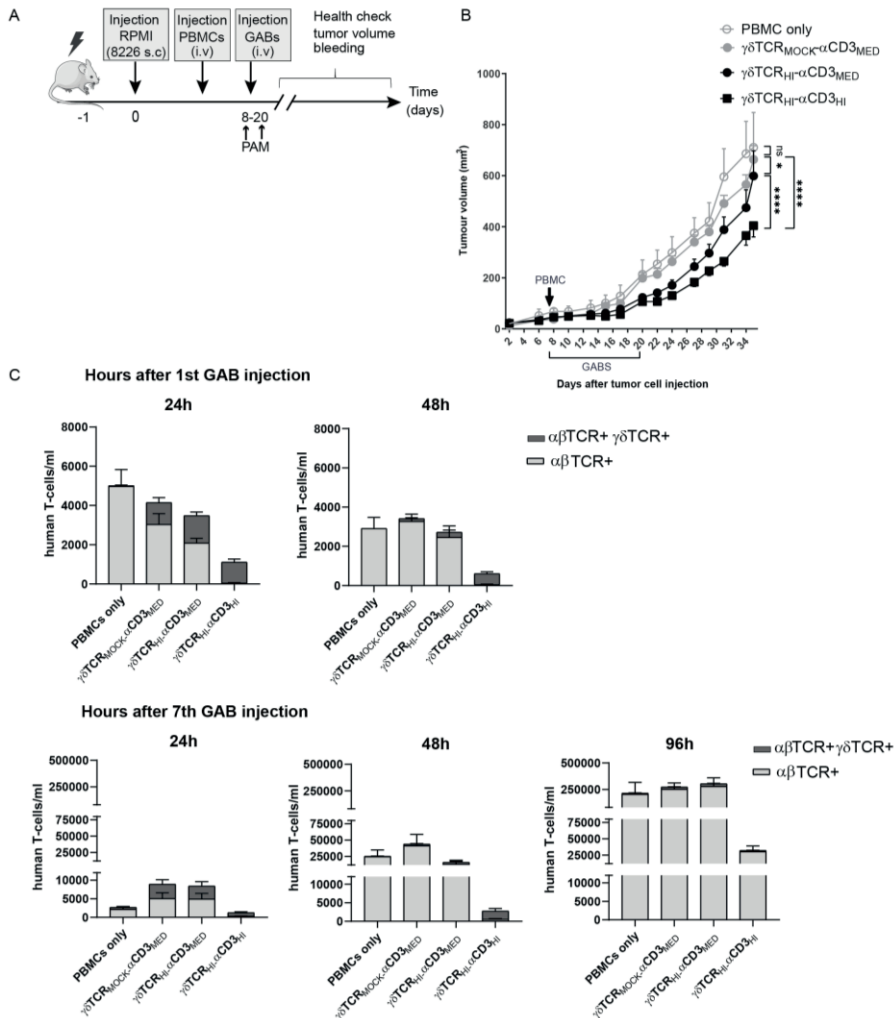


Figure 3. Superior *in vivo* tumor control and T cell coating by GABs with higher affinity CD3 binding (A) Schematic representation of experimental design. NSG mice were irradiated at day -1, and injected subcutaneously (s.c) with $10^6 \times 10^6$ RPMI 8226 tumor cells one day later. After 7 days the mice were randomized over three groups of 10 and one group of 5 (PBMC only), based on tumor size. All groups were injected with $10^6 \times 10^6$ huPBMCs i.v on day 7. From day 8 to 20 three groups were treated with i.v injections of $\gamma\delta\text{TCR}_{\text{HI}}-\alpha\text{CD3}_{\text{HI}}$, $\gamma\delta\text{TCR}_{\text{HI}}-\alpha\text{CD3}_{\text{MED}}$ or $\gamma\delta\text{TCR}_{\text{MOCK}}-\alpha\text{CD3}_{\text{MED}}$ every other day for a total of 7 injections (2,7 mg/kg). The PBMC only group did not receive additional treatment (B) Tumor size was measured three times a week for five weeks after tumor cell injection. (C) Amount of $\alpha\beta\text{TCR}$ single positive and $\alpha\beta\text{TCR}/\gamma\delta\text{TCR}$ double positive cells in the mice was determined by flow cytometry on day 9, 10, 21, 22 and 24 after tumor injection, which corresponds to 24 and 48h after the first GAB injection and 24, 48 and 96 hours after the last GAB injection respectively. PBMC only N=5, $\gamma\delta\text{TCR}_{\text{HI}}-\alpha\text{CD3}_{\text{HI}}$, $\gamma\delta\text{TCR}_{\text{HI}}-\alpha\text{CD3}_{\text{MED}}$ or $\gamma\delta\text{TCR}_{\text{MOCK}}-\alpha\text{CD3}_{\text{MED}}$ N=10. Error bars represent SEM, significance was calculated by mixed-effects model with repeated measures. * P<0.05, ** P<0.001, *** P<0.0001.

However, 96 hours after $\gamma\delta\text{TCR}_{\text{HI}}\text{-}\alpha\text{CD3}_{\text{HI}}$ injections, T cell counts started to recover. We also monitored weight loss and survival of the mice until the end of the experiment at day 35, as these factors could indicate toxicity due to overstimulation of T cells, and we saw no significant differences between the groups (Figure S1 C and D) in line with the favorable toxicity and efficacy profile observed *in vitro*.

GABs with the high affinity anti-CD3 scFv do not induce enhanced cytokine release or T cell infiltration compared to GABs with an intermediate affinity *in vivo*.

To further investigate the different *in vivo* treatment effects of GABs with either $\text{-}\alpha\text{CD3}_{\text{MED}}$ or $\text{-}\alpha\text{CD3}_{\text{HI}}$, we performed a second, two-week mouse model in which, after tumor and PBMC injection, GABs were injected twice, and blood and tumor were collected. The potential risk of T cell overstimulation by high affinity CD3 binding, was addressed by determining the presence of 10 cytokines and chemokines, associated with cytokine release syndrome (CRS), 4 and 48 hours after injection of $\gamma\delta\text{TCR}_{\text{HI}}\text{-}\alpha\text{CD3}_{\text{MED}}$ and $\gamma\delta\text{TCR}_{\text{HI}}\text{-}\alpha\text{CD3}_{\text{HI}}$. For four of the selected cytokines and chemokines, $\text{IFN}\gamma$, MCP1, MIP1 β , and CXCL1, the plasma levels were below the detection limit of the luminex assay in all samples. Overall, for the other six cytokines and chemokines, 4 hours after GAB injection, we observed no significant differences between mice injected with mock- or functional GAB, nor between mice injected with GAB with $\text{-}\alpha\text{CD3}_{\text{MED}}$ or $\text{-}\alpha\text{CD3}_{\text{HI}}$ (Figure 4B). We only observed a decrease in IP-10 level in mice treated with $\gamma\delta\text{TCR}_{\text{MOCK}}\text{-}\alpha\text{CD3}_{\text{HI}}$ mice compared to $\gamma\delta\text{TCR}_{\text{MOCK}}\text{-}\alpha\text{CD3}_{\text{MED}}$, which was, however, not seen for the groups treated with $\gamma\delta\text{TCR}_{\text{HI}}\text{-}\alpha\text{CD3}_{\text{MED}}$ or $\gamma\delta\text{TCR}_{\text{HI}}\text{-}\alpha\text{CD3}_{\text{HI}}$. This low level of induced cytokines by the different GABs was also observed 48 hours after the second GAB injection (Figure S2).

To assess whether we observed either a difference in T cell infiltration after GAB injection, or an enhanced killing of tumors between different groups, histopathologic analysis of tumor sections were performed. We observed a significant decrease in mitotic figures and apoptotic cells in mice treated with functional GAB ($\gamma\delta\text{TCR}_{\text{HI}}$), compared to mock treatment ($\gamma\delta\text{TCR}_{\text{MOCK}}$), while there were no differences observed between $\alpha\text{CD3}_{\text{MED}}$ or $\text{-}\alpha\text{CD3}_{\text{HI}}$ treated

groups or in the percentage necrosis between all the groups. These data implied, in line with the recently described apoptotic paradox ²⁹, an improved tumor control early after functional GAB injections, though no differences in tumor control were observed between different active GABs at this early time point. We also did not observe any significant differences in T cell infiltration between the different treatment groups, implying that GABs do not attract T cells to the tumor site during this early treatment phase, and that the improved tumor control of $\gamma\delta\text{TCR}_{\text{HI}}\text{-}\alpha\text{CD3}_{\text{HI}}$ might be a consequence of longer exposure over time with GAB-coated T cells, rather than of an increase in effector cell infiltration.

In conclusion, we show that $\gamma\delta\text{TCR}_{\text{HI}}\text{-}\alpha\text{CD3}_{\text{HI}}$ has the most favorable efficacy toxicity profile, with improved tumor control *in vivo*, with no signs of increased inflammation or treatment related toxicity.

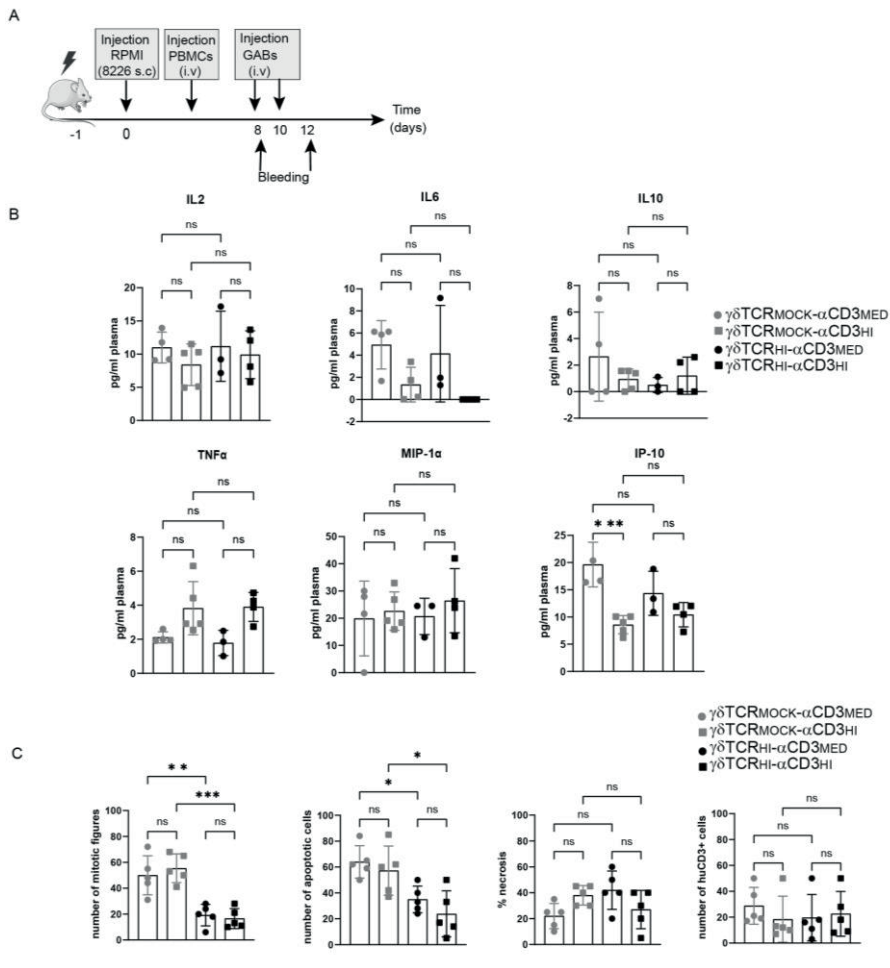


Figure 4. GABs with high affinity CD3 binding do not increase production of cytokines associated with cytokine release syndrome or tumor T cell infiltration (A) Schematic representation of experimental design. NSG mice were irradiated at day -1, and injected subcutaneously (s.c) with $10^6 \times 10^6$ RPMI 8226 tumor cells one day later. After 7 days the mice were randomized over four groups of 5 mice and injected with $10^6 \times 10^6$ huPBMCs (i.v), and day 8 and 10 the mice were injected with $\gamma\delta$ TCR^{HI/MOCK}- α CD3^{MED/HL} (B) blood was drawn on day 8 (4 hours after the first GAB injection) and cytokine levels were measured using luminex. (C) Tumor tissue was collected on day 12 and the number of mitotic figures, amount of apoptotic cells and % necrosis was determined based and HE staining. Tumor infiltrated human T cells were visualized and quantified using HNF and CD3 staining and immunofluorescent microscopy. N=3,4 or 5, error bars represent SD, significance was calculated using one way ANOVA. * P<0.05, ** P<0.001, ***P<0.0001

Discussion

During the pre-clinical development of bispecific T cell engagers, many factors can be optimized to create the molecule with most beneficial properties^{12, 21}, and over the past several years, interest in the selection of CD3 binding domains with optimal properties to incorporate in TCEs has increased significantly¹⁴. A factor considered to be important for this selection is the relative potency of the TCE in induction of tumor cell lysis versus cytokine release, with the overall goal to reduce the risk of cytokine release syndrome^{20, 28}. But the *in vivo* biodistribution of the TCE is also considered, with the assumption that the relative binding affinities of the tumor- and T cell binding arm will have a large impact on distribution and thereby potency of the TCE *in vivo*^{15, 18}.

Within this context, we further developed our most recently described TCE concept of GABs⁵ and describe now a next generation of GAB that is optimized for the balance between the tumor binding- $\text{V}\gamma 9\text{V}\delta 2\text{TCR}$ ectodomain, and the anti-CD3 scFv T cell binding affinity.

To accomplish this goal, in this report we tested the influence of different binding strengths of the CD3 arm in the GABs, in combination with different $\text{V}\gamma 9\text{V}\delta 2\text{TCR}$ affinities, on the *in vitro* and *in vivo* potency. We found a strong correlation between CD3 binding affinity and *in vitro* potency of the GAB. GABs incorporating a higher affinity CD3scFv more efficiently induced cytokine release as well as tumor cell lysis. However, in addition to an overall increase in potency, we also observed a change in the window between the relative EC_{50} for induction of $\text{IFN}\gamma$ release versus lysis, as reported by others^{17, 20, 30}. This observation would allow for the treatment of patients with a lower amount of GAB protein, and thereby allow for a better distinction dissection between toxicity and cytokine secretion. We could not, however, identify specific $\text{V}\gamma 9\text{V}\delta 2\text{TCR}$ -CD3scFv combinations where cytokine secretion was abolished, while tumor toxicity was maintained.

Part of the success was also testing different anti-CD3 scFvs with either a high- ($\text{V}\delta_{\text{HI}}$) or lower affinity ($\text{V}\delta_{\text{LO}}$) $\text{V}\gamma 9\text{V}\delta 2\text{TCR}$. The loss of potency when using

lower affinity anti-CD3 scFvs, although observed for both GABs, seemed more pronounced in the $\gamma\delta_{LO}$ GAB, and mainly reduced the window between EC_{50} for induction of IFN γ release versus lysis. This observation is in line with a report showing that decreased binding avidity of the tumor engaging arm of HER2-CD3 TCEs, by using a tumor cell line with low HER2 expression, resulted in greater differences in TCE potency, while in a high avidity situation, by using a HER2 high tumor cell line, CD3 affinity did not affect the TCE potency²⁷.

In line with our *in vitro* assays, we also found superior *in vivo* tumor control by $\gamma\delta TCR_{HI}$ - $\alpha CD3_{HI}$ compared to $\gamma\delta TCR_{HI}$ - $\alpha CD3_{MED}$. This finding is in contrast to recent reports showing that TCEs with higher CD3 binding affinity, regardless of *in vitro* potency, do not show improved tumor control *in vivo*^{18, 19}. Non-optimal biodistribution of the TCEs, bound to T cells, to lymph nodes and secondary lymphoid organs rather than to the tumor, is one of the concerns when using high binding affinity to CD3 *in vivo*¹⁵. We also observed a rapid decline in T cells in the blood after $\gamma\delta TCR_{HI}$ - $\alpha CD3_{HI}$ treatment. However, this phenomenon was only temporary, did not associate with cytokine release, and did not impair, but rather associated with improved efficacy. Thus, while for other TCE's, strong binding to T cells is viewed as sub-optimal, this might not be the case for the GAB molecules, which need to overcome low affinity binding of the $\gamma\delta TCR$ to the tumor, which is even with "higher affinity" $\gamma\delta TCR$ most likely in the μM range. Therefore, prolonged circulation when binding on T cells might be important to achieve long term exposure of tumor tissues to GABs, as suggested by our observation that in the early phase, we neither observed increased T cell infiltration between all GABs, nor differences in mitotic or apoptotic signals between functional GABs at the tumor site in mice. Increasing the binding affinity of the $\gamma\delta TCR$ to its ligand complex could still be an interesting alternative strategy to improve GAB potency, though it could be challenging, given the lack of understanding of the full composition of the TCR-ligand complex.

In conclusion, here we show that increasing the binding affinity of the anti-CD3 scFv in the GAB format, in combination with a high affinity to $\gamma\delta TCR$, leads to increased potency *in vitro* and *in vivo*. Though *in vivo* temporary drops in T cell counts were observed as compared to other constructs, this did not associate

with increased toxicity, but rather with improved tumor control, most likely through increased killing and a prolonged exposure of tumor cells to GAB coated T cells.

References

1. Goebeler ME, Bargou RC. T cell-engaging therapies - BiTEs and beyond. *Nat Rev Clin Oncol.* 2020;17(7):418-34.
2. Trabolsi A, Arumov A, Schatz JH. T Cell-Activating Bispecific Antibodies in Cancer Therapy. *J Immunol.* 2019;203(3):585-92.
3. Przepiorka D, Ko CW, Deisseroth A, Yancey CL, Candau-Chacon R, Chiu HJ, et al. FDA Approval: Blinatumomab. *Clin Cancer Res.* 2015;21(18):4035-9.
4. Dhillon S. Tebentafusp: First Approval. *Drugs.* 2022;82(6):703-10.
5. van Diest E, Hernández López P, Meringa AD, Vyborova A, Karaiskaki F, Heijhuurs S, et al. Gamma delta TCR anti-CD3 bispecific molecules (GABs) as novel immunotherapeutic compounds. *J Immunother Cancer.* 2021;9(11).
6. Karunakaran MM, Willcox CR, Salim M, Paletta D, Fichtner AS, Noll A, et al. Butyrophilin-2A1 Directly Binds Germline-Encoded Regions of the Vgamma9Vdelta2 TCR and Is Essential for Phosphoantigen Sensing. *Immunity.* 2020;52(3):487-98.e6.
7. Rigau M, Ostrouska S, Fulford TS, Johnson DN, Woods K, Ruan Z, et al. Butyrophilin 2A1 is essential for phosphoantigen reactivity by gammadelta T cells. *Science.* 2020;367(6478).
8. Vyborova A, Beringer DX, Fasci D, Karaiskaki F, van Diest E, Kramer L, et al. $\gamma\delta$ 2 T cell diversity and the receptor interface with tumor cells. *J Clin Invest.* 2020.
9. Gober HJ, Kistowska M, Angman L, Jenö P, Mori L, De Libero G. Human T cell receptor gammadelta cells recognize endogenous mevalonate metabolites in tumor cells. *J Exp Med.* 2003;197(2):163-8.
10. Sebestyen Z, Scheper W, Vyborova A, Gu S, Rychnavska Z, Schiffler M, et al. RhoB Mediates Phosphoantigen Recognition by Vgamma9Vdelta2 T Cell Receptor. *Cell Rep.* 2016;15(9):1973-85.
11. Vyborova A, Janssen A, Gatti L, Karaiskaki F, Yonika A, van Dooremalen S, et al. $\gamma\delta$ 2 T-Cell Expansion and Phenotypic Profile Are Reflected in the CDR3 δ Repertoire of Healthy Adults. *Front Immunol.* 2022;13:915366.
12. Ellerman D. Bispecific T-cell engagers: Towards understanding variables influencing the in vitro potency and tumor selectivity and their modulation to enhance their efficacy and safety. *Methods.* 2019;154:102-17.
13. Liddy N, Bossi G, Adams KJ, Lissina A, Mahon TM, Hassan NJ, et al. Monoclonal TCR-redirecated tumor cell killing. *Nat Med.* 2012;18(6):980-7.
14. Vafa O, Trinklein ND. Perspective: Designing T-Cell Engagers With Better Therapeutic Windows. *Front Oncol.* 2020;10:446.

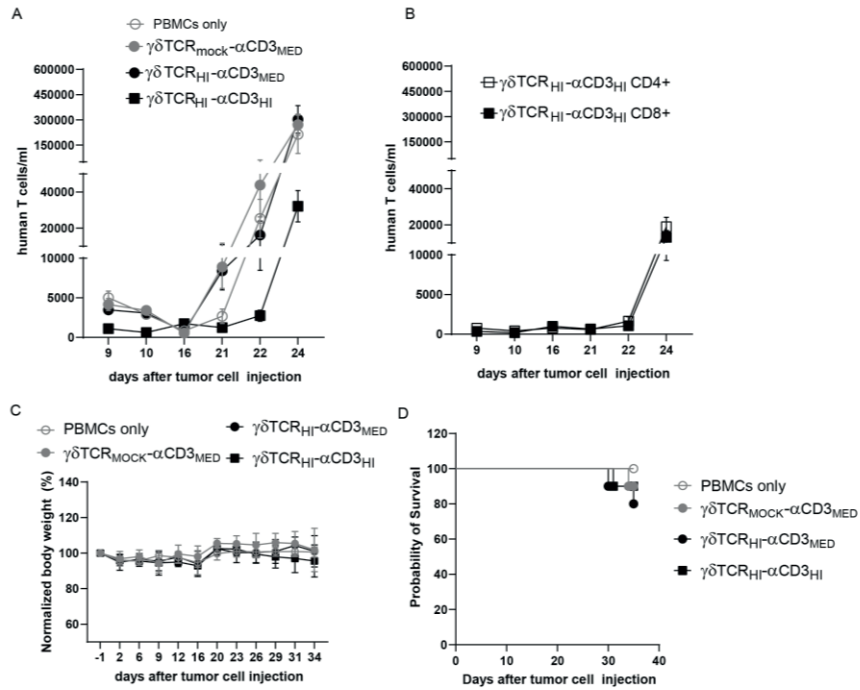
15. Mandikian D, Takahashi N, Lo AA, Li J, Eastham-Anderson J, Slaga D, et al. Relative Target Affinities of T-Cell-Dependent Bispecific Antibodies Determine Biodistribution in a Solid Tumor Mouse Model. *Mol Cancer Ther.* 2018;17(4):776-85.
16. Leong SR, Sukumaran S, Hristopoulos M, Totpal K, Stainton S, Lu E, et al. An anti-CD3/anti-CLL-1 bispecific antibody for the treatment of acute myeloid leukemia. *Blood.* 2017;129(5):609-18.
17. Dang K, Castello G, Clarke SC, Li Y, Balasubramani A, Boudreau A, et al. Attenuating CD3 affinity in a PSMAxCD3 bispecific antibody enables killing of prostate tumor cells with reduced cytokine release. *J Immunother Cancer.* 2021;9(6).
18. Haber L, Olson K, Kelly MP, Crawford A, DiLillo DJ, Tavaré R, et al. Generation of T-cell-redirecting bispecific antibodies with differentiated profiles of cytokine release and biodistribution by CD3 affinity tuning. *Sci Rep.* 2021;11(1):14397.
19. Staffin K, Zuch de Zafra CL, Schutt LK, Clark V, Zhong F, Hristopoulos M, et al. Target arm affinities determine preclinical efficacy and safety of anti-HER2/CD3 bispecific antibody. *JCI Insight.* 2020;5(7).
20. Trinklein ND, Pham D, Schellenberger U, Buelow B, Boudreau A, Choudhry P, et al. Efficient tumor killing and minimal cytokine release with novel T-cell agonist bispecific antibodies. *MAbs.* 2019;11(4):639-52.
21. Chen W, Yang F, Wang C, Narula J, Pascua E, Ni I, et al. One size does not fit all: navigating the multi-dimensional space to optimize T-cell engaging protein therapeutics. *MAbs.* 2021;13(1):1871171.
22. Allison TJ, Winter CC, Fournie JJ, Bonneville M, Garboczi DN. Structure of a human gammadelta T-cell antigen receptor. *Nature.* 2001;411(6839):820-4.
23. Grunder C, van DS, Hol S, Drent E, Straetemans T, Heijhuurs S, et al. gamma9 and delta2CDR3 domains regulate functional avidity of T cells harboring gamma9delta2TCRs. *Blood.* 2012;120(26):5153-62.
24. Johanna I, Hernández-López P, Heijhuurs S, Bongiovanni L, de Bruin A, Beringer D, et al. TEG011 persistence averts extramedullary tumor growth without exerting off-target toxicity against healthy tissues in a humanized HLA-A*24:02 transgenic mice. *J Leukoc Biol.* 2020;107(6):1069-79.
25. Wu Z, Cheung NV. T cell engaging bispecific antibody (T-BsAb): From technology to therapeutics. *Pharmacol Ther.* 2018;182:161-75.
26. Smith E, inventor anti-CD3 antibodies, bispecific antigen-binding molecules that bind CD3 and CD20, and used thereof 2017.
27. Poussin M, Sereno A, Wu X, Huang F, Manro J, Cao S, et al. Dichotomous impact of affinity on the function of T cell engaging bispecific antibodies. *J Immunother Cancer.* 2021;9(7).
28. Li J, Piskol R, Ybarra R, Chen YJ, Li J, Slaga D, et al. CD3 bispecific antibody-induced cytokine release is dispensable for cytotoxic T cell activity. *Sci Transl Med.* 2019;11(508).
29. Morana O, Wood W, Gregory CD. The Apoptosis Paradox in Cancer. *Int J Mol Sci.* 2022;23(3).

30. Zuch de Zafra CL, Fajardo F, Zhong W, Bernett MJ, Muchhal US, Moore GL, et al. Targeting Multiple Myeloma with AMG 424, a Novel Anti-CD38/CD3 Bispecific T-cell-recruiting Antibody Optimized for Cytotoxicity and Cytokine Release. *Clin Cancer Res.* 2019;25(13):3921-33.

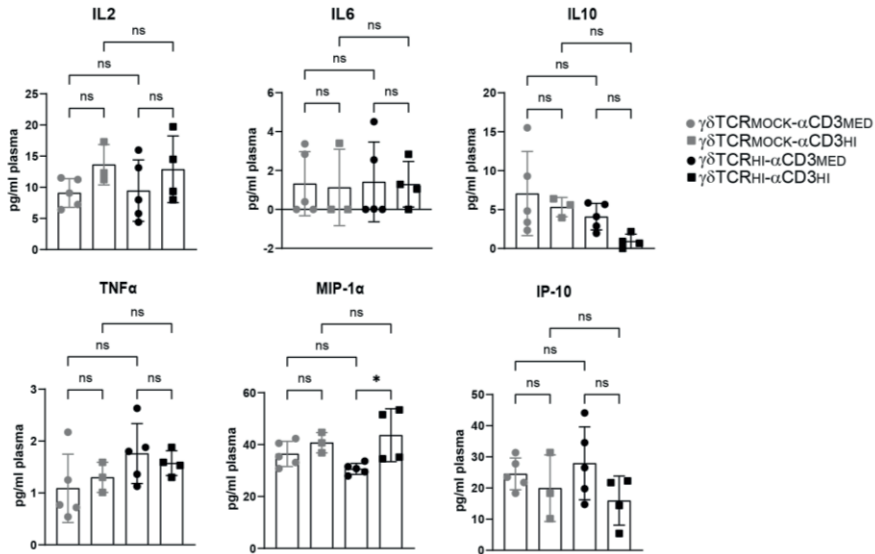
Supplementary Figures and Tables

Supplementary Table 1. Anti-CD3 scFv sequence and reported affinity

Anti-CD3 scFv	Amino acid sequence	Reported K_D single arm
UCHT1	DIQMTQTSSLSASLGDRVTISCRASQDIRNYLNWYQQKP DGTVKLLIYTSRLHSGVPSKFSGSGSGTDYSLTISNLEQE DIATYFCQQGNTLPWFAGGTKLEIKGGGGSGGGSGG GGSQVQLQQSGPELVKPGASMKISCKASGYSFTGYTMN WVKQSHGKNLEWMGLINPYKGVSTYNQKFKDKATLTV KSSSTAYMELLSLTSSESAVYYCARSYYGSDWYFDVW GQGTTLTVFSVD	$51 * 10^{-9} M^1$
OKT3	QVQLVQSGGGVVPGRSLRLSCKASGYTFTRYTMHWVR QAPGKGLEWIGYINPSRGTNYNQKFKDRFTISRDNKNT AFLQMDSLRPEDTGVYFCARYDDHYCLDYWGQGTPTV VSSGGGSGGGGGGGGGGGGGSIQMTQSPSSLSASVGDRT ITCSASSSVSYMNWYQQTPGKAPKRWIYDTSKLASGVPS RFSGSGSGTDYFTFISLQ PEDIATYYCQQWSSNPFTFGQGTKLQITRVD	$2.73 * 10^{-6} M^2$
TR66	QIQLVQSGAEVAKPGASVKVSCASGYTFTRYTMHWVRQ RPGQGLEWIGYINPSRGTNYNQKFKDRATLTDKSTSTA YMESSLTSEDTAVYYCARYDDHYCLDYWGQGTPTVVS SGGGGSGGGGGGGGGGGGGSDIQLTQSPSSLSASVGDRTITC RASSSVSYMNWYQQKSGTAPKRWIYDTSKVASGVPIRFS GSGSGTSYLTISLQPEDAATYYCQQWSSNPFTFGGGTK VEIKVD	$2.6 * 10^{-7} M^3$
7195	QVQLVESGGGLVQPGRSLRLSCAASGFTFADYTMHWVR QAPGKGLEWVSDISWNSGSIAYADSVKGRFTISRDNANK SLYLQMNSLRTEDTAFYYCAKDSRGYGHYKYLGLDVWGQ GTTVTVSSGGGGSGGGGGGGGGGGSDIQLTQSPSSLSASV GDRVTITCRASQSISSYLNWYQQKPGKAPKLLIYAASLQS GVPSRFSGSGSGTDFTLTISLQPEDFATYYCQQSYSTPPI TFGQGRLEIKV D	$3.19 * 10^{-9} M^4$
7232	QVQLVESGGGLVHPGRSLRLSCAASGFTFDDYTMHWVR QAPGKGLEWVSDISWNSGSRGYADSVKGRFTISRDNANK SLYLQMNSLRAEDTALYYCAKDKSGYGHYHYAMDVWG QGTTVTVSSGGGGSGGGGGGGGGGGSDIQLTQSPSSLSAS VGDRTITCRASQSISSYLNWYQQKPGKAPKLLIYAASLQ SGVPSRFSGSGSGTDFTLTISLQPEDFATYYCQQSYSTPP ITFGQGRLEIKVD	$2.2 * 10^{-7} M^4$



Supplementary Figure 1. Human T cell outgrowth in vivo, and mouse survival and weight (A) total number of human T cells recorded in the mice model described in figure 3. For each (treatment) group or (B) $\gamma\delta$ TCR_{HI}- α CD3_{HI} treatment group CD4+ and CD8+T lymphocytes separate. (C) Survival of the mice until the endpoint at day 35. (D) Body weight of the mice until the endpoint at day 35. Error bars represent SEM (A) or SD (C). N=10 or N=5 (PBMC only).



Supplementary Figure 2. GABs with higher affinity CD3 binding do not induce increased T cell infiltration in tumor tissue. Tumor tissue was collected and infiltrated. Human T cells were visualized and quantified using HNF and CD3 staining and immunofluorescent microscopy. N=5 Error bars represent SD, significance was calculated using student T test. ns= not significant.

Supplementary References

- Li Q, Hapka D, Chen H, Vallera DA, Wagner CR. Self-assembly of antibodies by chemical induction. *Angew Chem Int Ed Engl.* 2008;47(52):10179-82.
- Kjer-Nielsen L, Dunstone MA, Kostenko L, Ely LK, Beddoe T, Mifsud NA, et al. Crystal structure of the human T cell receptor CD3 epsilon gamma heterodimer complexed to the therapeutic mAb OKT3. *Proc Natl Acad Sci US A.* 2004;101(20):7675-80.
- Moore PA, Zhang W, Rainey GJ, Burke S, Li H, Huang L, et al. Application of dual affinity retargeting molecules to achieve optimal redirected T-cell killing of B-cell lymphoma. *Blood.* 2011;117(17):4542-51.
- Smith E, inventoranti-CD3 antibodies, bispecific antigen-binding molecules that bind CD3 and CD20, and used thereof 2017.



CHAPTER 5

Adding help to an HLA-A*24:02 tumor-reactive $\gamma\delta$ TCR increases tumor control

Inez Johanna^{1†}, Patricia Hernández-López^{1†}, Sabine Heijhuurs¹, Wouter Scheper¹, Laura Bongiovanni³, Alain de Bruin^{3,4}, Dennis X Beringer¹, Rimke Oostvogels², Trudy Straetemans^{1,2}, Zsolt Sebestyen¹, and Jürgen Kuball^{1,2*}

¹ Center for Translational Immunology, University Medical Center Utrecht, Utrecht, The Netherlands

² Department of Hematology, University Medical Center Utrecht, Utrecht, The Netherlands

³ Department of Biomolecular Health Sciences, Dutch Molecular Pathology Center, Faculty of Veterinary Medicine, Utrecht University, Utrecht, The Netherlands

⁴ Department of Pediatrics, University Medical Center Groningen, University of Groningen, Groningen, The Netherlands

† These authors have contributed equally to this work and share first authorship

Frontiers in immunology, 2021

Abstract

$\gamma\delta$ T cell receptors ($\gamma\delta$ TCRs) recognize a broad range of malignantly-transformed cells in mainly a major histocompatibility complex (MHC)-independent manner, making them valuable additions to the engineered immune effector cell therapy that currently focuses primarily on $\alpha\beta$ TCRs and chimeric antigen receptors (CARs). As an exception to the rule, we have previously identified a $\gamma\delta$ TCR, which exerts antitumor reactivity against HLA-A*24:02-expressing malignant cells, however without the need for defined HLA-restricted peptides, and without exhibiting any sign of off-target toxicity in humanized HLA-A*24:02 transgenic NSG (NSG-A24:02) mouse models. This particular tumor-HLA-A*24:02-specific V γ 5V δ 1TCR required CD8 α co-receptor for its tumor reactive capacity when introduced into $\alpha\beta$ T cells engineered to express a defined $\gamma\delta$ TCR (TEG), referred to as TEG011, thus it was only active in CD8⁺ TEG011. We subsequently explored the concept of additional redirection of CD4⁺ T cells through co-expression of the human CD8 α gene into CD4⁺ and CD8⁺ TEG011 cells, later referred as TEG011_CD8 α . Adoptive transfer of TEG011_CD8 α cells in humanized HLA-A*24:02 transgenic NSG (NSG-A24:02) mice injected with tumor HLA-A*24:02⁺ cells showed superior tumor control in comparison to TEG011, and to mock control groups. The total percentage of mice with persisting TEG011_CD8 α cells as well as total number of TEG011_CD8 α cells per mice was significantly improved over time, mainly due to a dominance of CD4⁺CD8⁺ double positive TEG011_CD8 α which resulted in higher total counts of functional T cells in spleen and bone marrow. We observed that tumor clearance in the bone marrow of TEG011_CD8 α -treated mice associated with better human T cell infiltration, which was not observed in the TEG011-treated group. Overall, introduction of transgenic human CD8 α receptor on TEG011 improves antitumor reactivity against HLA-A*24:02⁺ tumor cells, and further enhances *in vivo* tumor control.

Introduction

$\gamma\delta$ T cells share the properties of both innate and adaptive immunity and play an essential role in cancer immunosurveillance^{1,2}. Unlike conventional $\alpha\beta$ T cells, $\gamma\delta$ T cells recognize their cognate antigens in an MHC-unrestricted manner, targeting stress-induced and malignantly-transformed self-antigens^{3,4}. As such, $\gamma\delta$ T cells represent an attractive cell subset to substantiate T cell-based immunotherapeutic strategies that still mainly focus on $\alpha\beta$ T cells.

Based on their TCR δ chain repertoire, two major subsets of $\gamma\delta$ T cells can be distinguished: V δ 2⁺ and V δ 2⁻ cells. V δ 2⁺ cells mainly reside in the human peripheral blood, representing up to 5% of total circulating T cells, and sense metabolic changes in tumor cells with intracellular accumulation of phosphoantigens (pAgs) level. V δ 2⁺ T cell recognition is facilitated by butyrophilin (BTN) family molecules, including BTN2A1 and BTN3A1⁵⁻¹⁰. On the other hand, V δ 2⁻ cells mainly localize in mucosal and epithelial tissues, but their antitumor properties are scarcely known⁴. V δ 2⁻ cells recognize broad range of stress-induced ligands, such as the MHC-associated proteins MICA and MICB, foreign lipid antigens presented on CD1c/d molecules in classical HLA-like manner, and CMV-associated UL16-binding protein (ULBP) family members, that are upregulated in stressed or malignant cells¹¹⁻¹⁵.

V δ 1⁺ T cells, one of the major V δ 2⁻ subsets, have been shown to exert antitumor reactivity against leukemia and solid tumors¹⁶⁻²¹, indicating their potential in cancer immunotherapy. Adoptive transfer of *in vitro* expanded V δ 2⁺ cells only showed marginal clinical responses to date^{4,22}, while adoptive transfer of V δ 2⁻ cells is yet to be tested in the clinic²³. Translational efforts using $\gamma\delta$ T cells and their receptors outside the context of allogeneic stem cell transplantation^{24,25} face substantial hurdles, due to their limited proliferative capacity, underestimated diversity in co-receptors expression and function, as well as scarce information on how $\gamma\delta$ TCRs interact with their targets.

To bypass these major drawbacks of translating $\gamma\delta$ T cells-based immune therapies into clinical practice, we developed the concept of TEGs: $\alpha\beta$ T cells

engineered to express a defined $\gamma\delta$ TCR, allowing the introduction of highly tumor-reactive $\gamma\delta$ TCR, both $V\delta 2^+$ ^{26, 27} or $V\delta 2^-$ ^{28, 29} subsets, into proliferatively-proficient $\alpha\beta$ T cells^{27, 30, 31}. This concept did not only allow to select for highly tumor-reactive $\gamma\delta$ TCR, but also within the context of $V\delta 2^+$ TCRs to reprogram both $CD4^+$ and $CD8^+$ $\alpha\beta$ T cells^{26, 27}. Professional help for TCR-engineered $CD8^+$ $\alpha\beta$ T cells by also functionally engineering $CD4^+$ $\alpha\beta$ T cells has not only been shown to be important *in vitro*³² but also to improve clinical responses³³. Within this context, we previously identified an allo-HLA-restricted and tumor-specific $V\gamma 5V\delta 1$ TCR derived from clone FE11, introduced in the TEG concept as TEG011, which was, although not dependent on a defined peptide, selectively targeting HLA-A*24:02⁺ tumor cells without impairing the healthy tissues³⁴. Furthermore, we also highlighted that antitumor reactivity of $V\gamma 5V\delta 1$ TCR derived from clone FE11 requires $CD8\alpha$ as costimulatory receptor and showed that both $CD8\alpha\alpha$ on the original clone FE11 and $CD8\alpha\beta$ on transduced $\alpha\beta$ T cells are capable of providing co-stimulation to the $V\gamma 5V\delta 1$ TCR derived from clone FE11³⁴. Thus, for this very particular $V\gamma 5V\delta 1$ TCR the concept of TEGs would not benefit from reprogramming $CD4^+$ $\alpha\beta$ T cells when only a $V\gamma 5V\delta 1$ TCR is transferred as $CD4$ -transduced TEG011 cells do not elicit antitumor reactivity.

Human $CD8$ is a membrane glycoprotein classified in an immunoglobulin-like super family consisting of hetero- or homodimer of α and β chains, making up for the $CD8\alpha\beta$ or $CD8\alpha\alpha$ co-receptor on the cell surface. $CD8\alpha\beta$ predominantly expressed on $\alpha\beta$ T cells, while $CD8\alpha\alpha$ mainly expressed on the cell membrane of innate immune cells, including macrophages, dendritic cells, natural killer (NK) cells, and $\gamma\delta$ T cells³⁵. Transfer of $CD8$ receptor has been reported for $\alpha\beta$ TCR engineered $\alpha\beta$ T cells to functionally reprogram $CD4^+$ $\alpha\beta$ T cells, when low to intermediate affinity $\alpha\beta$ TCRs are used for engineering³⁶. Within this context, we addressed the implication of $CD8\alpha\alpha$ -dependency of FE11 $\gamma\delta$ TCR in relation to its tumor immunity. Based on this mechanistic basis of antitumor reactivity for TEG011 cells, we hypothesize that the transfer of $CD8\alpha$ receptor can functionally rescue $V\gamma 5V\delta 1$ TCR engineered $CD4^+$ $\alpha\beta$ T cells. Within this context, we explored now as additional approach to improve efficacy of TEG011 therapy the simultaneously co-expressing $V\gamma 5V\delta 1$ TCR derived from clone FE11 together with $CD8\alpha$ receptor in a TEG format, referred

to as TEG011_CD8 α . Importantly, we demonstrate that introduction of transgenic human CD8 α co-receptor into CD4⁺ TEG011 cells successfully enhanced its antitumor efficacy *in vitro* and *in vivo*, and thus did not require CD8 β . Furthermore, we show that the co-expression of CD8 α in CD4⁺ TEG011 provides additional survival signal and facilitates better T cell persistence and infiltration *in vivo*, both of which are essential to sustain long-term tumor control of adoptively transferred TCR-based immunotherapy.

Material and methods

Cell lines

Daudi, SW480, and Phoenix-Ampho cell lines were obtained from ATCC. K562 with HLA-A*24:02-transduced cell line was kindly provided by Fred Falkenburg (Leiden University Medical Centre, the Netherlands) and subsequently transduced with luciferase for *in vivo* imaging purposes. EBV-LCL was kindly provided by Phil Greenberg (Seattle, WA). Phoenix-Ampho and SW480 cells were cultured in DMEM supplemented with 1% Pen/Strep (Invitrogen) and 10% FCS (Bodinco), whereas all other cell lines in RPMI with 1% Pen/Strep and 10% FCS. All cell lines were authenticated by short tandem repeat profiling/karyotyping/iso-enzyme analysis and were passaged for a maximum of 2 months, after which new cell line stocks were thawed for experimental use. Furthermore, all cell lines were routinely verified by growth rate, morphology, and/or flow cytometry and tested negative for mycoplasma using MycoAlert Mycoplasma Kit (Lonza, Breda, The Netherlands). Peripheral blood mononuclear cells (PBMCs) from healthy donors were isolated by Ficoll-Paque (GE Healthcare, Eindhoven, The Netherlands) from buffy coats supplied by Sanquin Blood Bank (Amsterdam, The Netherlands).

Cloning of TEG011_CD8 α and TEGLM1_CD8 α

Clone FE11 was generated as previously described²⁸. FE11 and LM1 (non-functional $\gamma\delta$ 2TCR with length mutation on the complementary determining region 3 (CDR3) of the δ 2-chain³¹) $\gamma\delta$ TCRs were subcloned to pMP71 retroviral vectors containing both γ TCR and δ TCR chains, separated by a ribosomal skipping T2A sequence. pU57 constructs containing a ribosomal

skipping P2A sequence, followed by full-length human CD8 α were purchased from Baseclear (Leiden, The Netherlands). Thereafter, CD8 α was subcloned into pMP71 vector using *Xho*I and *Hind*III restriction sites downstream of γ 115TCR-T2A- δ 115_LM1 sequence to generate a TEGLM1_CD8 α construct that contained *Nco*I and *Xho*I restriction sites up- and downstream of LM1 $\gamma\delta$ TCR chains. *Nco*I and *Xho*I restriction sites were then inserted up- and downstream of FE11 $\gamma\delta$ TCR sequences by site-directed mutagenesis PCR, after which this sequence was ligated to P2A-CD8 α sequence in pMP71 vector using the introduced *Nco*I and *Xho*I sites, generating a TEG011_CD8 α construct (Supplementary Table 1). Where indicated, CD4 $^+$, CD8 $^+$, CD4 $^+$ CD8 $\alpha\alpha^+$ and CD4 $^+$ CD8 $\alpha\beta^+$ TCR-transduced T-cells were sorted using a FACSAria II (BD) flow cytometry to >99% purity. Expression levels of CD8 α mutants were measured by flow cytometry using anti-CD8 α antibody (clones RPA-T8).

Functional T cell assays

IFN γ ELISPOT was performed using anti-human IFN γ mAb1-D1K (I) and mAb7-B6-1 (II) (Mabtech) per the manufacturer's protocol. 15,000 TEG cells (TEG011, TEGLM1, TEG011_CD8 α , or TEGLM1_CD8 α) were co-incubated with 50,000 target cells (E:T ratio 1:3) for 18-24 hours in nitrocellulose-bottomed 96-well plates (Millipore). IFN γ spots were visualized with TMB substrate (Sanquin) and subsequently the number of spots was quantified using ELISPOT Analysis Software (Aelvis). Where indicated, blocking of CD8 α was performed using 10 μ g/ml anti-CD8 α antibody clone OKT8 (eBioscience) and blocking of CD8 β with 10 μ g/ml anti-CD8 β clone 2ST8.5H7 (Abcam).

Retroviral transductions of T cells

TEGs were generated as previously described³⁰. Briefly, Phoenix-Ampho packaging cells were transfected with gag-pol (pHIT60), env (pCOLT-GALV), and pMP71 retroviral constructs containing both γ TCR and δ TCR chains separated by a ribosomal skipping T2A sequence and followed by CD8 α sequence separated by P2A sequence where applicable, using FugeneHD reagent (Promega, Leiden, The Netherlands). PBMCs from a healthy donor pre-activated with 30 ng/mL anti-CD3 (clone OKT3, Miltenyi Biotec) and 50 IU/mL IL-2 (Proleukin, Novartis, Arnhem, The Netherlands) were transduced

twice with viral supernatant within 48 hours, in the presence of 50 IU/mL IL-2 and 6 μ g/mL polybrene (Sigma-Aldrich, Zwijndrecht, The Netherlands). TCR-transduced T cells were expanded by stimulation with anti-CD3/CD28 Dynabeads (500,000 beads/ 10^6 cells; Thermo Fisher Scientific, Breda, The Netherlands) and 50 IU/mL IL-2. Thereafter, transduced T cells were depleted of the non-engineered T cells.

Depletion of non-engineered T cells

Non-engineered T cells was depleted as previously described²⁷. In brief, transduced T cells were incubated with a biotin-labeled anti- $\alpha\beta$ TCR antibody (clone BW242/412; Miltenyi Biotec, Leiden, The Netherlands) and then incubated with an anti-biotin antibody coupled to magnetic beads (anti-biotin MicroBeads; Miltenyi Biotec), most recently reported to preferentially bind to the β TCR chain³⁷. Thereafter, the cell suspension was loaded onto an LD column, and $\alpha\beta$ TCR⁺ T cells were depleted by MACS cell separation per the manufacturer's protocol (Miltenyi Biotec). After depletion, TEGs were expanded using a T cell rapid expansion protocol (REP)³⁰.

Separation of CD4⁺ subsets of TEGs

The separation of CD4⁺ TEGs was performed using CD4 Microbeads (Miltenyi Biotec) as per manufacturer's instructions. Briefly, TEGs that were previously expanded on REP were incubated with magnetic microbeads cells and loaded into LS column for MACS cell separation. Thereafter, CD4⁺ selected or bulk (with CD4:CD8 ratio 50:50) TEGs were expanded separately on the next REP cycle prior to *in vitro* functional assay. TEG expression was monitored prior to functional assays or *in vivo* infusion by flow cytometry using anti- $\alpha\beta$ TCR-APC (clone IP26, eBioscience), anti-pan- $\gamma\delta$ TCR-PE (clone IMM510, Beckman Coulter), anti-CD8-PerCP-Cy5.5 (clone RPA-T8, Biolegend), anti-CD4-PeCy7 (clone TPA-R4, Biolegend), anti-CD4-FITC (clone TPA-R4, Biolegend), and V δ 1-FITC (clone TS8.2, Thermo Fisher Scientific) antibodies.

Animal model

The NOD.Cg-Prkdc^{scid}Il2rg^{tm1Wjl}Tg(HLA-A24)3Dvs/Sz (NSG-A24:02) mice³⁸ were bred and housed in the breeding unit of the Central Animal Facility of

Utrecht University. Experiments were conducted per institutional guidelines after obtaining permission from the local Ethical Committee, and performed in accordance with the current Dutch laws on Animal Experimentation. Mice were housed in individually ventilated cage (IVC) system to maintain sterile conditions and fed with sterile food and water. After irradiation, mice were given the antibiotic ciproxin in the sterile water for the duration of the experiment. Both male and female mice were randomized with equal distribution among the different groups, based on age and initial weight (measure on Day -1) into 10 mice/group. Adult NSG-A24:02 mice (11-20 weeks old) received sub-lethal total body irradiation (1,75 Gy) on day -1 followed by intravenous injection of 1×10^5 K562-HLA-A*24:02 luciferase tumor cells on day 0, and received 2 intravenous injections of TEG011, TEG011_CD8 α or TEGLM1_CD8 α cells on day 1 and 6 as previously reported³⁴. Together with the first TEGs injection, all mice received $0,6 \times 10^6$ IU of IL-2 (Proleukin; Novartis) in 100 μ l incomplete Freund's adjuvant (IFA) subcutaneously and subsequently administered every 3 weeks until the end of the experiment. Mice were monitored at least twice a week for any symptoms of disease (sign of paralysis, weakness, and reduced motility), weight loss, and clinical appearance scoring (scoring parameter included hunched appearance, activity, fur texture, and piloerection). The humane endpoint was reached when mice showed aforementioned symptoms of disease, experienced a 20% weight loss from the initial weight (measured on day -1), developed extramedullary solid tumor masses (if any) reached 2 cm³ in volume and when clinical appearance score 2 was reached for an individual parameter or a total score of 4.

Flow cytometry analysis

The following antibodies were used for flow cytometry analysis: huCD45-PB (clone HI30; Sony Biotechnology), pan- $\gamma\delta$ TCR-PE (clone IMMU510; Beckman-Coulter), mCD45-APC (clone 30-F11, Sony Biotechnology), $\alpha\beta$ TCR-FITC (clone IP26; Biolegend), CD4-PeCy7 (clone RPA-T4, Biolegend), CD8-PerCPy5.5 (clone RPA-T8, Biolegend), PD-1-BV711 (clone EH12.2H7, Biolegend), and TIM3-BV650 (clone F38-2E2, Biolegend). To exclude non-viable cells from the analysis, Fixable Viability Dye eFluor506 was used (eBioscience). All samples were analyzed on a BD LSRFortessa using

FACSDiva Software (BD Biosciences).

Assessment for TEGs persistence

Mouse peripheral blood samples were obtained via cheek vein (max. 50-70 μ l/mouse) once a week. Red blood cell was lysed using 1X RBC lysis buffer (Biolegend) and were then stained with a mixture of antibody panels as listed above. The persistence of TEG cells was counted as absolute cell number tumor-reactive TEG cells expressing following cell surface markers huCD45⁺ $\gamma\delta$ TCR⁺CD8⁺ and huCD45⁺ $\gamma\delta$ TCR⁺CD4⁺CD8⁺ populations or non-reactive TEG cells expressing huCD45⁺ $\gamma\delta$ TCR⁺CD4⁺ marker observed in mouse peripheral blood using Flow-count Fluorospheres (Beckman Coulter) and measured by flow cytometry.

Preparation of single cell suspensions

At the end of the study period, bone marrow (mixed from tibia and femur) and spleen sections were isolated and processed into single cell suspension. Femur and tibia from the hind legs were collected; bone marrow cells were collected by centrifugation of the bones at 10,000 rpm for 15 seconds and resuspension of the cells in phosphate buffer saline (PBS).

A small section of the spleen was minced and filtered through a 70 μ m cell strainer (BD); incubated with 1X RBC lysis buffer cells for maximum 4 minutes, and subsequently cells were washed and resuspended in PBS. Absolute cell number of TEG cells were quantified using Flow-count Fluorospheres and measured from a total of 10⁶ cells stained for the presence of TEG cells in spleen and bone marrow by flow cytometry analysis (BD LSRFortessa).

Histology staining and analysis

Formalin-fixed femur for bone marrow sections were embedded in paraffin and cut into 4 μ m sections. Hematoxylin and eosin (H&E) staining was performed for the femur, for bone marrow section. Tissue sections were evaluated to assess for any differences in the presence, distribution and extension of neoplastic foci indicating tumor tissue. Tissue sections of the femur were evaluated for quantification of tumor tissue by dividing the area

covered by the tumor cells by the total area of bone marrow tissue visible in the section using the ImageJ analysis system software (NHI, Bethesda, Maryland, USA) and expressed as a percentage. Images were taken using an Olympus BX45 microscope with the Olympus DP25 camera and analyzed using DP2-BSW (version 2.2) or ImageJ softwares.

Statistical Analyses

Experimental data were analyzed using GraphPad Prism (GraphPad Software Inc., La Jolla, CA, USA) and shown as mean \pm standard deviation (SD) or standard error of mean (SEM) with * $P < 0.05$; ** $P < 0.01$; *** $P < 0.001$; and **** $P < 0.0001$. Statistical significances between groups were assessed using a non-parametric Kruskal-Wallis test, a two-way ANOVA, and a mixed-effects model with repeated measures where indicated.

Results

Co-transfer of transgenic CD8 α receptor is sufficient to re-establish tumor reactivity of CD4⁺ TEG011 cells

We previously identified an allo-restricted CD8 α -dependent V γ 5V δ 1TCR clone FE11²⁸, which showed *in vitro* antitumor reactivity against HLA-A*24:02-expressing tumor cells³⁴. We therefore investigated whether introduction of CD8 $\alpha\alpha$ or CD8 $\alpha\beta$ along with V γ 5V δ 1TCR derived from clone FE11 could enhance antitumor reactivity of CD8⁺, and also functionally reprogram CD4⁺ TEG011 cells. Hence, we co-transduced T cells with the FE11 $\gamma\delta$ TCR, and with either CD8 α alone or CD8 α together with CD8 β (Supplementary Figure S1). Subsequently, we sorted separate sets of CD4⁺ TEG011 cells that co-expressed either exogenous CD8 $\alpha\alpha$ (CD4⁺CD8 $\alpha\alpha$ ⁺) or CD8 $\alpha\beta$ (CD4⁺CD8 $\alpha\beta$ ⁺) as well as TEG011 cells expressing only endogenous CD4 and CD8 as negative and positive controls for tumor recognition, respectively (Figure 1A). Thereafter, TEG cells were co-cultured with SW480 and EBV-LCL target cells or healthy PBMCs as mock control. Both CD4⁺CD8 $\alpha\alpha$ ⁺ and CD4⁺CD8 $\alpha\beta$ ⁺ TEG011 cells secreted significantly higher levels of IFN γ upon exposure to tumor targets than CD4⁺ TEG011 cells. The acquired antitumor reactivity of CD4⁺CD8 $\alpha\alpha$ ⁺ and CD4⁺CD8 $\alpha\beta$ ⁺ TEG011 cells could be blocked by CD8 α and CD8 β blocking antibodies (Figure 1B), confirming the

strict dependence of FE11 $\gamma\delta$ TCR on introduced CD8 molecules. Taken together, we showed that introduction of CD8 α alone is sufficient to re-establish antitumor reactivity of CD4⁺ T cells expressing FE11 $\gamma\delta$ TCR. Introduction of CD8 β did not further enhance tumor recognition, but was functionally involved in the molecular interaction with its target when present.

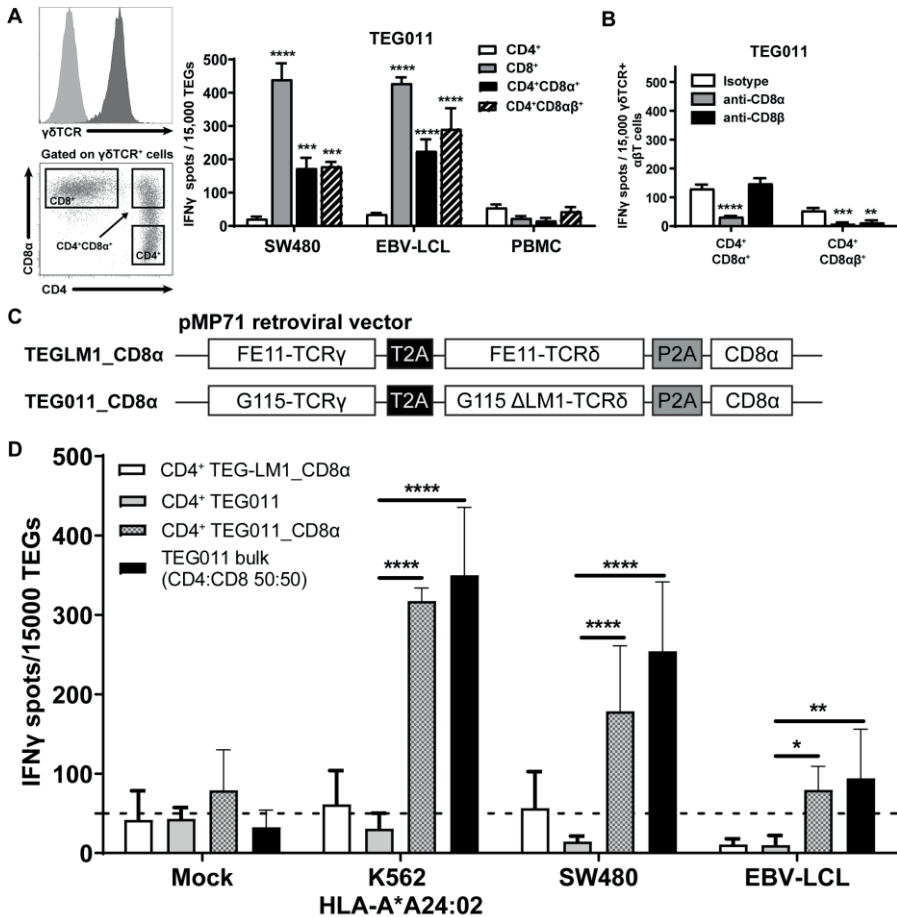


Figure 1 Introduction of transgenic CD8 α receptor on TEG011 improves T cell activation. (A) TEG011 were retrovirally transduced with either CD8 α alone or CD8 α in combination with CD8 β . CD4⁺, CD8⁺, CD4⁺CD8 α ⁺ and CD4⁺CD8 α β ⁺ subsets of T cells were subsequently sorted (left panel is a representative sorting plot for CD4⁺, CD8⁺ and CD4⁺CD8 α ⁺ cells; CD4⁺CD8 α β ⁺ cells were sorted in a similar manner) and tested for recognition of SW480 and EBV-LCL target cells by IFN γ ELISPOT (right panel). Healthy PBMCs were included as untransformed mock control target cells. Data are of representative of four independent experiments and error bars represent mean \pm SEM (**P < 0.01; ***P < 0.001) calculated by two-way ANOVA.

(B) CD8 α and CD8 β blocking on CD4⁺ T cells were transduced with the FE11 $\gamma\delta$ TCR and CD8 α alone, or CD8 α with CD8 β . TEG011 was co-incubated with SW480 target cells in the presence of a control antibody, or CD8 α or CD8 β blocking antibodies. IFN γ production was measured by ELISPOT. Data represent mean \pm SD of replicates for each effector (**P < 0.01; ***P < 0.001; ****P < 0.0001) calculated by two-way ANOVA. **(C)** Schematic diagram of pMP71 retroviral vector constructs containing codon-optimized human $\gamma\delta$ TCR sequences from either clone FE11 (referred as TEG011_CD8 α) or non-functional LM1 chains (referred as TEGLM1_CD8 α) in combination with full length of human CD8 α receptor (top panel). Within the transgene cassettes, individual γ TCR and δ TCR chains have been linked with a self-cleaving theta virus 2A (T2A; black box) ribosomal skipping sequence, while the CD8 α sequence was connected with a porcine teschovirus-1-derived 2A (P2A; grey box) ribosomal skipping sequence. **(D)** CD4⁺ $\alpha\beta$ T cells were transduced with either TEGLM1_CD8 α , TEG011, or TEG011_CD8 α $\gamma\delta$ TCR (as effector cells) and subsequently co-cultured with HLA-A*24:02-expressing target cell lines or healthy T cells (E:T ratio is 1:3) for 18–24 h. TEG011 bulk population with 50:50 ratio of both CD4⁺ and CD8⁺ TEGs and T cells from healthy donor were used as positive and untransformed mock controls, respectively. Antitumor reactivity was measured by IFN γ ELISPOT, where 50 spots/15,000 cells were considered as a positive antitumor response and indicated by the dashed horizontal line. Data are representative of three independent experiments with replicates for each target and error bars represent mean \pm SD (*P < 0.05; **P < 0.01; ****P < 0.0001) calculated by two-way ANOVA.

For clinical administration, co-expression of both CD8 α and the $\gamma\delta$ TCR in one vector is preferred to allow reproducible and cost-effective production processes^{26, 27, 39}. Moreover, co-expressing both CD8 α and the $\gamma\delta$ TCR in one vector can also overcome the difference in transduction efficiency when they were transduced separately. Therefore, we generated new retroviral constructs carrying either FE11 $\gamma\delta$ TCR or a non-functional length mutant clone LM1 $\gamma\delta$ TCR³¹; served as mock control) followed by full-length human CD8 α receptor sequences (TEG011_CD8 α and TEGLM1_CD8 α , Figure 1C). The complete sequence of transgenes for these retroviral constructs are listed in Supplementary Table S1 and S2, respectively. Subsequently, $\alpha\beta$ T cells were transduced with either FE11 $\gamma\delta$ TCR without human CD8 α receptor (TEG011), FE11 $\gamma\delta$ TCR with human CD8 α receptor (TEG011_CD8 α), or LM1 $\gamma\delta$ TCR with human CD8 α receptor (TEGLM1_CD8 α). After TEG expansion, we performed magnetic selection of CD4⁺ T cells for each TEG constructs. To elucidate whether introduction of transgenic CD8 α receptor adequately rescues TEG011 reactivity of non-tumor reactive CD4-transduced cells once delivered by the very same vector, we co-cultured tumor target HLA-A*24:02-transduced CML tumor cells (K562), SW480, and EBV-LVL cells with either CD4⁺ TEG011_CD8 α , CD4⁺ TEGLM1_CD8 α , or CD4⁺ TEG011 (without introduction of the CD8 α receptor). Healthy T cells and TEG011 bulk cells (with CD4:CD8 1:1 ratio) were used as the untransformed mock target and

positive effector control, respectively (Figure 1D). CD4⁺ TEG011_CD8 α cells produced a significantly higher IFN γ level compared to CD4⁺ TEG011, which was equivalent to those of TEG011 bulk cells against all tumor targets, without affecting healthy cells. The equivalent IFN γ level between CD4⁺ TEG011_CD8 α and TEG011 bulk cells comprised of only 50% CD8⁺ TEG011 implied that reprogrammed CD4⁺ TEG011_CD8 α are surprisingly poorer cytokine secretors. Importantly, enhanced tumor recognition was restricted to CD4⁺ TEG011_CD8 α cells and not CD4⁺ TEGLM1_CD8 α mock cells, highlighting the specific role of CD8 α as co-stimulation for the introduced FE11 $\gamma\delta$ TCR. We concluded that introduction of transgenic CD8 α receptor in combination with V γ 5V δ 1TCR derived from clone FE11 allowed reprogramming of CD4⁺ T cells towards HLA-A*24:02-expressing tumor cells *in vitro*, though activity was lower when compared to CD8⁺ TEG011.

TEG011_CD8 α improves *in vivo* tumor control and associates with higher persistence of functional T cells

In previous studies, we have shown TEG011 efficacy against HLA-A*24:02-expressing tumor cells *in vitro* and an extended *in vivo* safety profile as well as peripheral persistence of TEG011, where long-term persistence of TEG associated with reduced probability for developing extramedullary solid tumor masses *in vivo*^{34,40}. To assess the consequence of the additional expression of TEG011_CD8 α , NSG transgenic mice expressing human HLA-A*24:02 (NSG-A24:02) were irradiated, received luciferase-labeled K562 HLA-A*24:02⁺ cells, and subsequently received two intravenous injections of either mock control TEGLM1_CD8 α , TEG011_CD8 α , or TEG011 cells. All infused TEG variants showed comparable $\gamma\delta$ TCR expression, where the transduced $\alpha\beta$ T cells expressed V δ 1⁺ TCR for TEG011 and TEG011_CD8 α (Supplementary Figure S2). Mice were monitored for tumor burden assessed by bioluminescent imaging, T cell persistence and infiltration, as well as any other signs of discomfort. Mice were sacrificed when the humane endpoints were reached (experimental outline Figure 2A). TEG011_CD8 α -treated mice had a significantly lower tumor burden over time compared to the mock control TEGLM1_CD8 α and TEG011-treated groups (Figure 2B), indicating superior tumor control *in vivo* by TEG011_CD8 α . All tumor-bearing mice

eventually developed tumor and measurement of individual mouse indicating tumor growth over time for each treatment group is shown in Figure 2C and 2D. Despite the significant *in vivo* tumor control, we observed only a trend towards an improved overall survival for TEG011_CD8 α -treated mice (Supplementary Figure S3). This could be due to limited treatment window of this mouse model contributed by aggressive tumor growth of K562 HLA-A*24:02-transduced cells.

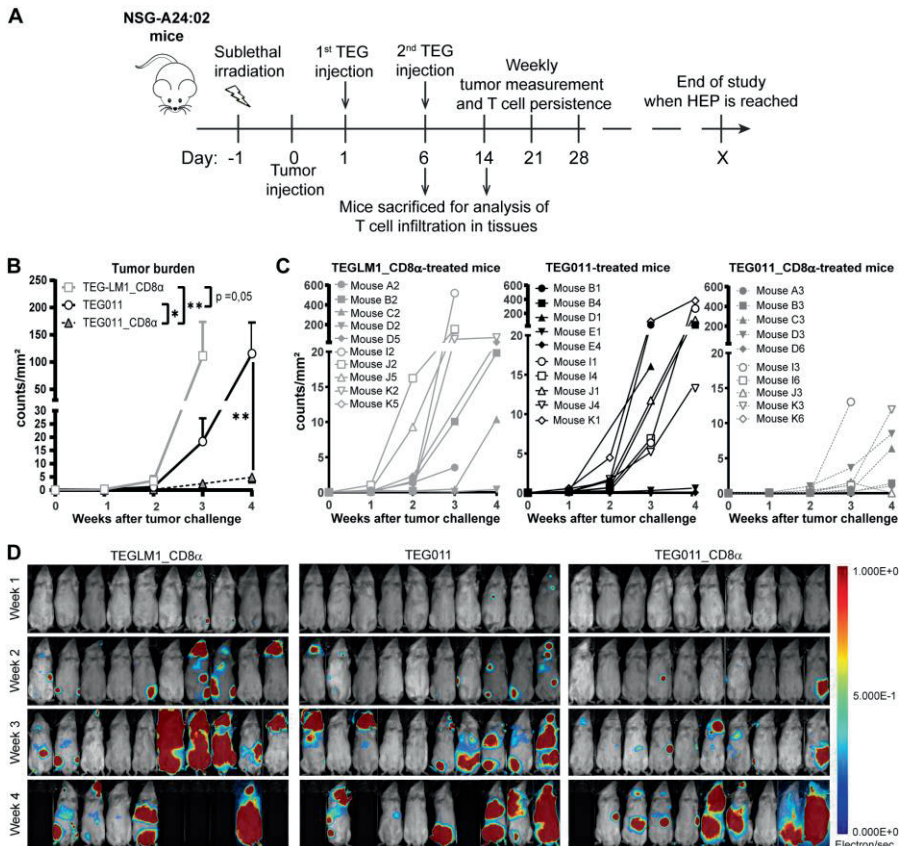


Figure 2 TEG011_CD8 α improves *in vivo* tumor control against HLA-A*24:02⁺ tumor cells. **(A)** Schematic overview of the *in vivo* experiment for NSG-A24:02 tumor-bearing mice. Irradiated mice were intravenously injected with K562-HLA*A24:02-luciferase tumor cells on day 0 followed by two infusions of TEG011, TEG011_CD8 α or TEGLM1_CD8 α mock cells on days 1 and 6. Mice were monitored regularly and sacrificed when the humane endpoint (HEP) was reached. **(B)** Tumor burden for K562-HLA*A24:02-luciferase was assessed *in vivo* measuring integrated signal density per total surface area (count/mm²) by bioluminescence imaging (BLI) with the mouse abdomen facing up. Data are shown only up to week 3 for

the TEGLM1_CD8 α mock-treated group (open light gray rectangle) due to subsequent mouse dropout >50%, while data for TEG011 (open black circle) and TEG011_CD8 α (open black triangle) are shown up to week 4. Data are shown as mean \pm SEM of all mice per group ($n = 10$). Statistical significances were calculated by a mixed-effects model with repeated measure up to week 3 as comparison all treatment group (indicated next to legends) and only between TEG011 and TEG011_CD8 α group for week 4 (indicated on the graph); (* $P < 0.05$; ** $P < 0.01$). **(C)** Tumor burden for individual mouse for each treatment group measured by integrated signal density per total surface area (count/mm²) using BLI. **(D)** Tumor load for individual mouse was evaluated by bioluminescence imaging on week 1 to week 4 using Milabs Optical Imaging (OI) Acquisition and OI-Post processing software (version 2.0). Anaesthetized mice were injected intraperitoneally with 25mg/ml Beetle-luciferin (Promega). Calibrated units were calculated from integrated density of bioluminescence signal (electron/s) as shown by the right bar. The animals were imaged 10 min after luciferin injection. Black areas indicate loss of mice.

As TEG011 cells carry CD8 α -dependent V γ 5V δ 1TCR, we focused our *in vivo* analysis to tumor-reactive CD8-expressing TEG cells (as validated by *in vitro* functional T cell assay in Figure 1D) while taking into account the non-tumor reactive CD4⁺ TEG cells. Therefore, we assessed CD8-expressing TEG cell product properties and persistence by measuring viable huCD45⁺ $\gamma\delta$ TCR⁺CD8⁺ single-positive and huCD45⁺ $\gamma\delta$ TCR⁺CD4⁺CD8⁺ double-positive cells (present in mock control TEGLM1_CD8 α and TEG011_CD8 α only) in mouse peripheral blood using flow cytometry (gating strategy depicted in Supplementary Figure S4). TEG cells persisted up to 4 weeks after infusion in the mouse peripheral blood with biological variations between mice (Figure 3A). To address this interindividual variation in T cell persistence, we analyzed separately the percentage of mice where CD4⁺ and CD8⁺ T cells reached at least 500 cells/ml in the peripheral blood over time, a threshold described previously⁴¹ (Figure S5A). We observed a higher percentage of mice with persisting CD4⁺ and CD8⁺ T cells in TEG011_CD8 α group when compared to mock TEGLM1_CD8 α and TEG011 group. Despite some imbalance in the CD4:CD8 ratio with lower numbers for CD8⁺ TEG011 infused (Supplementary Figure S2), more CD8⁺ TEG011 persisted over time when compared to CD8⁺ single-positive TEG011_CD8 α . Vice versa, endogenous CD4 T cells for TEG011_CD8 α were lower before infusion when compared to TEG011 prior to infusion, while CD4⁺CD8⁺ double-positive TEG011_CD8 α were higher in numbers over time when compared to both CD4⁺CD8⁺ double-positive TEGLM1_CD8 α and CD4⁺ TEG011 cells (Supplementary Figure S5B). As a net effect, we observed more CD8-expressing T cells for TEG011_CD8 α cells

when compared to TEG011 (Figure 3B). Next, we investigated the expression of PD1 and TIM3 on CD8⁺ single-positive cells and CD4⁺ single-positive or CD4⁺CD8⁺ double-positive cells. Higher numbers of T cells expressing PD1 or TIM3 were observed on TEG011_CD8 α cells, as compared to mock TEGLM1_CD8 α and TEG011 cells (Supplementary Figure S6A and B). CD8⁺ single-positive TEG011 and TEG011_CD8 α showed an increased PD1 expression when compared to CD8⁺ single-positive TEG_LM1 (Supplementary Figure S6A). A partial decline of TIM3 expression was most pronounced over time in CD8⁺ single-positive TEG011_CD8 α (Supplementary Figure S6B).

Next, we investigated infiltration of TEG cells into spleen and bone marrow on weeks 1 and 2 after infusion. Specifically, we compared the TEG011 and TEG011_CD8 α groups to elucidate the contribution of transgenic CD8 α co-expression in TEG011 infiltration *in vivo*, and focused on the total sum of CD8-expressing TEG011 cells. We detected a significantly higher number of CD8-expressing TEG cells infiltrating in the spleen and bone marrow of TEG011_CD8 α -treated mice at both time points (Figure 3B). Importantly, we did not observe rapid clearance of CD4⁺CD8⁺ double-positive TEG011_CD8 α cells in these tissues within these time points, whereas CD8⁺ single-positive TEG011 cells were barely detected. Thus, we conclude that CD8 α co-stimulation with TEG011 improves overall *in vivo* tumor control, T cell persistence and infiltration of CD8-expressing TEG011 cells.

TEG011_CD8 α enhanced T cell infiltration and effectively cleared tumor cells in bone marrow

We previously reported an extensive *in vivo* safety profile of TEG011 against healthy tissues that express HLA-A*24:02 molecules, in which no significant histological lesions were observed in major organs, including liver, spleen, and intestine⁴⁰. For histopathology analysis, we collected a femur bone marrow section from each treatment group at the end of the study period to further evaluate antitumor efficacy of the new TEG011_CD8 α cells (Figure 4A). Tissue sections were assessed for the presence and extension of the neoplastic foci composed by round, large, undifferentiated tumor cells. The mock control TEGLM1_CD8 α -treated group showed evident 19,2% neoplastic infiltration,

whereas the TEG011-treated group showed up to 3,4% neoplastic infiltration of a homogeneous population of neoplastic cells in the bone marrow. Interestingly, we did not observe any neoplastic infiltration in the bone marrow

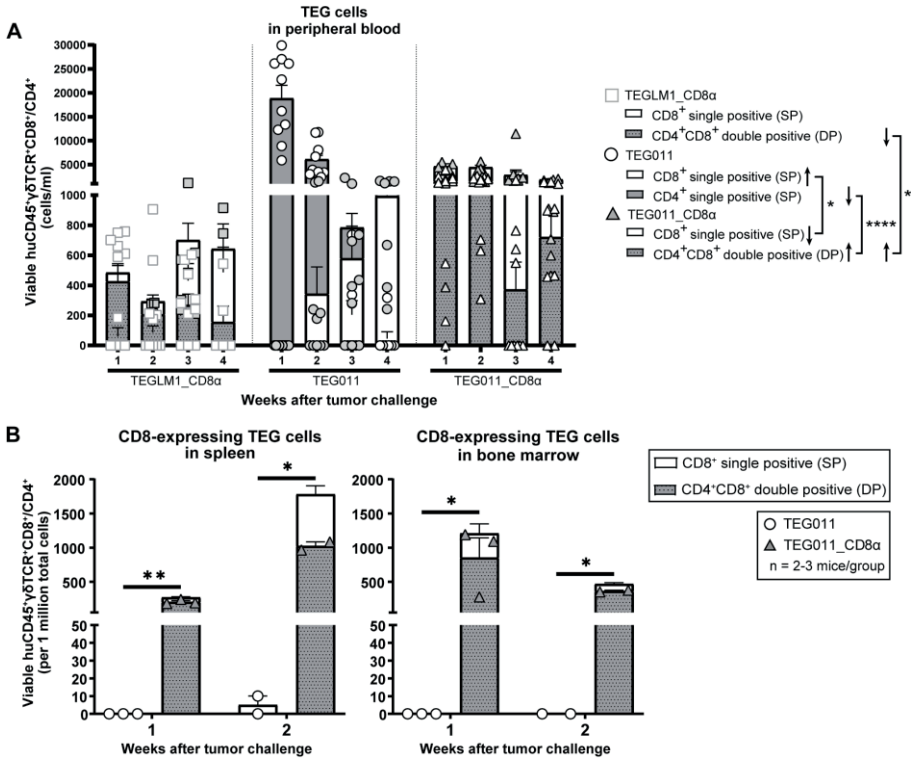


Figure 3 TEG011_CD8a enhances TEG persistence and infiltration. (A) TEG cells were measured in peripheral blood using flow cytometry by quantifying the absolute cell numbers of TEGM1_CD8a mock (open light gray rectangle), TEG011 (open black circle), and TEG011_CD8a (open black triangle) in tumor-bearing mice. TEG cells are distinguished into different cellular compartments: CD8 \cdot single-positive (SP; white stacked bar), CD4 \cdot single-positive (SP; grey stacked bar), and CD4 \cdot CD8 \cdot double-positive (DP; grey dotted stacked bar) cells. Black arrows indicate higher or lower T cell counts observed. Data are shown as mean \pm SEM of all mice per group ($n = 10$ mice). Statistical significances were calculated by a mixed-effects model with repeated measures (* $P < 0.05$; **** $P < 0.0001$). (B) CD8-expressing TEG cells was assessed in spleen and bone marrow by quantifying the total viable cells of huCD45 $\gamma\delta$ TCR \cdot CD8 \cdot and huCD45 $\gamma\delta$ TCR \cdot CD4 \cdot CD8 \cdot per one million single cell suspension by flow cytometry. Cell counts of individual mouse per treatment group are represented by each symbol. Functional TEG011 cells consist of two different cellular compartments: CD8 \cdot single-positive (SP; white stacked bar) and CD4 \cdot CD8 \cdot double-positive (DP; grey dotted stacked bar). Data are shown as mean \pm SEM (* $P < 0.05$; ** $P < 0.01$) calculated by a mixed-effects model with repeated measures.

of mice in the TEG011_CD8 α group and the appearance of bone marrow cell composition and cellularity were normal (Figure 4B). In conclusion, although number of analyzed bone marrows was limited in numbers, our data imply that TEG011_CD8 α effectively cleared tumor cells in bone marrow, emphasizing the role of CD8 α co-stimulation for better *in vivo* tumor control of TEG011 cells. Overall, our data indicate that introduction of transgenic CD8 α on TEG011 cells effectively improves *in vivo* tumor control and better T cell infiltration into bone marrow.

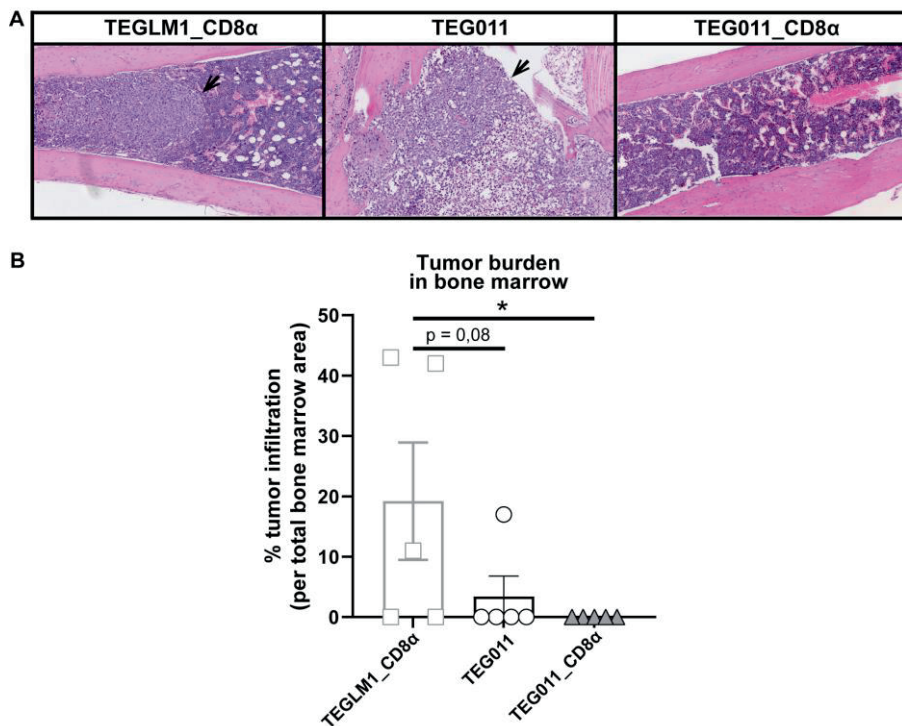


Figure 4 TEG011_CD8 α effectively cleared tumor cells in bone marrow, without a significant difference in tumor infiltration observed in other major organs. **(A)** Representative pictures H&E stained of mouse bone marrow with the presence of neoplastic cells (black arrow) from individual mice of each treatment group (n = 5 mice/group). Magnification:10 \times . **(B)** Percentage cases of tumor infiltration in mouse bone marrow for each treatment group (n = 5mice/group). Calculation was performed by dividing the area covered by the tumor cells per the total area of bone marrow tissue visible in the section using ImageJ. Data are shown as mean \pm SEM (*P < 0.05) calculated by non-parametric Kruskal-Wallis test.

Discussion

TEG011 has been reported to specifically recognize HLA-A*24:02⁺ malignant cells while sparing the HLA-A*24:02-expressing healthy tissues with the requirement of CD8 α co-stimulation^{34, 40}. While TEG011 has shown a favorable efficacy profile *in vivo*, we only observed in approximately 50% of the mice long-term persistence of CD8⁺ TEG011 cells, which could be due to the lack of support by antigen-specific CD4⁺ T cells^{29, 40}. The presence of both tumor-specific CD4⁺ and CD8⁺ $\alpha\beta$ T cells has been reported to significantly improve clinical responses compared to tumor-specific CD8⁺ $\alpha\beta$ T cells alone³³. To further improve the antitumor efficacy of TEG011, we co-expressed a CD8 α co-receptor together with the V γ 5V δ 1TCR derived from clone FE11 in TEG format, referred to as TEG011_CD8 α cells. Introduction of CD8 α receptor is particularly beneficial for TEG011 as this particular $\gamma\delta$ TCR requires the presence of CD8 α as co-receptor for their antitumor reactivity as we published previously^{34, 40}. CD8 α expression has been reported as common feature of $\gamma\delta$ TCR after CMV infection²⁸. These insights imply that also other V δ 1TCR might functionally depend on CD8 α which we could however not investigate in a broader context. Thus, when exploring tumor-reactivity with selected V δ 1TCR for the development of $\gamma\delta$ T cell-based immunotherapies²⁰, the absence of functional reactivity by an introduced V δ 1TCR might not necessarily reflect the absence of binding of the V δ 1TCR to its target but rather the lack of a co-stimulation through e.g., CD8 α or other co-stimulatory molecules. In this study, we reported on the capacity of the introduced CD8 α co-receptor to successfully redirect non-tumor reactive CD4⁺ TEG011 cells *in vivo* and *in vitro* against tumor targets that express HLA-A*24:02 molecules. We now report on more than 80% of mice showing persistence of CD8-expressing T cells after 4 weeks. TEG011_CD8 α cells showed also in absolute numbers higher T cell counts and stable peripheral persistence *in vivo*, which was, however, mainly a consequence of the persistence of CD4⁺CD8⁺ double-positive TEG011_CD8 α and not an improved persistence of CD8⁺ single-positive TEG011_CD8 α . This finding supports the notions that co-expression of CD4⁺ and CD8⁺ T cells provides an additional survival signal for TEG011 cells. This observation is in line with clinical studies for CD19 CAR T cells that

reported that a mixture of both CD4⁺ and CD8⁺ T cells with 1:1 ratio improved tumor remission in B-ALL patients^{42, 43}. Regardless of the precise underlying molecular mechanism, for the first time we observed tumor clearance in the bone marrow by TEG011_CD8 α , but not by TEG011 alone.

Using humanized transgenic mice expressing human HLA-A*24:02, we could study the implication of CD8 α introduction to TEG011, referred to as TEG011_CD8 α , elucidating their improved efficacy *in vivo*. We provide evidence that TEG011_CD8 α effectively cleared tumor cells in bone marrow and elicited better tumor control against human HLA-A*24:02-expressing tumor cells. We cannot entirely exclude that superior tumor control in TEG011_CD8 α may have been caused initially by more CD8 single-positive cells in the TEG011_CD8 α product compared to TEG011 product, as CD4⁺/CD8⁺ ratios could not be entirely controlled in the experimental set up prior to infusion. However, our mouse model also allowed us to investigate TEG011_CD8 α kinetics in the presence of tumor cells; and we observed sustained long-term TEG persistence mainly for $\gamma\delta$ TCR⁺CD4⁺CD8⁺ double-positive and a decline in $\gamma\delta$ TCR⁺CD8⁺ single-positive TEG011_CD8 α cells. Importantly, the sustained peripheral TEG persistence was only observed for TEG011_CD8 α but not TEGLM1_CD8 α , highlighting the key role of a functional tumor-reactive $\gamma\delta$ TCR. This observation rather argues against the classical helper function of $\gamma\delta$ TCR⁺CD4⁺CD8⁺ double-positive TEG011_CD8 α cells within the context of TEG011_CD8 α . Hence, the concurrent expression of CD4⁺ and CD8⁺ co-receptor most likely provided additional survival signal for tumor-specific CD4⁺ T cells, which did not, however, translate into classical helper functions towards CD8⁺ T cells^{40, 44, 45}. CD4⁺ T cells have been reported to avoid expression of inhibitory receptors on CD8⁺ T cells⁴⁶ and as an important cell subset to induce memory T cell formation⁴⁷. Along this line we observed over time reduced expression of TIM3 in CD8⁺ single-positive TEG011_CD8 α cells compared to mock and TEG011 group. CD4⁺CD8⁺ double-positive TEG011_CD8 α cells had lower levels of TIM3 when compared to CD8⁺ single-positive TEG011_CD8 α cells. These data remain difficult to interpret, and most likely simply reflect different regulation and activation of non-tumor reactive CD4⁺ and tumor-reactive CD8⁺ TEG011 cells, respectively. We also acknowledge that xenograft mouse models do not allow

to completely mimic all potential helper roles of human CD4⁺ T cells, due to the lack of human professional antigen presenting cells.

Reprogramming CD4⁺ T cells by genetic engineering has been reported to clinically impact efficacy and toxicity by high affinity receptors, like CARs⁴⁸. V γ 9V δ 2TCR³⁰ and CD8 $\alpha\beta$ independent $\alpha\beta$ TCRs³² have been also reported to reprogram CD4⁺ T cells which have the not only the ability to exert tumor cell killing but also induce maturation of professional antigen presenting cells. Transfer of CD8 $\alpha\beta$ in combination with intermediate affinity tumor reactive $\alpha\beta$ TCR has been reported to support tumor control *in vitro* and *in vivo*^{49, 50} and for high affinity $\alpha\beta$ TCR with artificial signaling domains adding CD8 α alone has been shown to reprogram CD4⁺ T cells³⁶. Within this context, our data show that CD8 $\alpha\alpha$ in combination with a natural $\gamma\delta$ TCR functions serves as co-stimulatory receptor, as opposed to the well-described inhibitory function of CD8 $\alpha\alpha$ on $\alpha\beta$ T cells within the context of a natural $\alpha\beta$ TCR. Expression of that CD8 $\alpha\alpha$ on activated CD4⁺ and CD8 $\alpha\beta$ ⁺ $\alpha\beta$ T cells has been reported to act as corepressor by competing with CD8 $\alpha\beta$ ⁺ cells for p56^{lck} signaling molecule⁵¹. Though we investigated the role of CD8 $\alpha\alpha$ in the TEG concept, our data support the notion that CD8 $\alpha\alpha$ in combination with a $\gamma\delta$ TCR are synergistic on natural $\gamma\delta$ T cells, as activated CD8 $\alpha\alpha$ ⁺ $\gamma\delta$ T cells were reported in supporting control of HIV infection⁵². We have also previously reported significant increases in circulating CD8 $\alpha\alpha$ ⁺ $\gamma\delta$ T cells in CMV-positive population²⁸. Thus, CD8 $\alpha\alpha$ appears to have opposing functions on innate and adaptive immune cells, where it acts as co-stimulatory receptor in the context of a $\gamma\delta$ TCR.

The precise molecular interaction between CD8 $\alpha\alpha$ and its specific ligand in our context remains yet to be unraveled. The CD8 $\alpha\alpha$ receptor has been shown to bind to MHC Class I molecules, including HLA-A*02:01, HLA-A*11:01, HLA-B*35:01, HLA-C*07:02, via protruding α 3 domain loop of MHC molecules with lower affinity than the binding of a TCR-pMHC complex⁵³⁻⁵⁶. Polymorphisms in the MHC α 3 domain contributes to a binding variation of CD8 $\alpha\alpha$ to different HLA molecules, such as HLA-A*24:02. In this context, HLA-A*24:02 is one of the possible ligands for CD8 $\alpha\alpha$ on TEG011, in line with an earlier study that reported CD8 $\alpha\alpha$ interaction with HLA-A*24:02 in a similar

way with HLA-A*02:01, involving binding to the $\alpha 2$ and $\alpha 3$ domains, as well as to the $\beta 2m$ domain of pMHC complex, but with different conformation that suggests CD8 α plasticity⁵⁷. The non-classical MHC molecules are also reported to interact with CD8 α , such as HLA-G and HLA-E⁵⁸. HLA-G is a known ligand for CD8 α , which is expressed on some colorectal cancer⁵⁹⁻⁶¹, while HLA-E is mainly expressed in human endothelial cells and is highly expressed in tumor cells⁵⁸. Other studies also demonstrated the interaction between CD8 and CEACAM5, which support the possibility of CEACAM5 as CD8 α ligands⁶².

Overall, we demonstrate that TEG011 equipped with human CD8 α co-receptor elicits superior tumor control and long-term persistence, which mainly impacted numbers of $\gamma\delta$ TCR⁺CD4⁺CD8⁺ double-positive TEG011_CD8 α cells, and associated with better T cell infiltration. In addition, TEG011_CD8 α cells successfully cleared tumor cells in the bone marrow. In contrast to currently emerging immunotherapy approach using CAR T cells, our strategy allows tumor-specific targeting of HLA-A*24:02-positive cancer patients, irrespective of antigen-specific expression on cell surface and the type of cancer, and thus TEG011_CD8 α therapy has broader applicability towards a substantial amount of cancer patients with HLA-A*24:02-positive haplotype highlighting its therapeutic potential for further clinical application.

Conflict of Interest

DB, ZS and JK are inventors on different patents with $\gamma\delta$ TCR sequences, recognition mechanisms and isolation strategies. JK is cofounder and shareholder of Gadeta (www.gadeta.nl). No potential conflicts of interest were disclosed by the other authors.

Author Contributions

IJ, TS, ZS and JK conceptualized, designed and developed the *in vivo* models. IJ, PH, and SH performed the *in vitro* and *in vivo* experiments. LB and AB performed the histopathology examination of the mouse tissues. DB and RO contributed vital components. IJ analyzed all *in vitro* and *in vivo* data and was

a major contributor in writing the manuscript. IJ, ZS, and JK interpret all *in vitro* and *in vivo* data. IJ and JK wrote the manuscript; all authors read, review and approved the final manuscript.

Funding

Funding for this study was provided by ZonMW 43400003 and VIDI-ZonMW 917.11.337, KWF 6426, 6790 and 7601 to JK; 12586 to TS and JK; 11393 and 13043 to ZS and JK; 11979 to JK and DB.

Acknowledgments

We thank Halvard Boenig (Institute for Transfusion Medicine and Immunohematology, Goethe University, Frankfurt a. M., Germany) for providing PBMCs for feeder cells.

References

1. Dadi, S., et al., Cancer Immunosurveillance by Tissue-Resident Innate Lymphoid Cells and Innate-like T Cells. *Cell*, 2016. **164**(3): p. 365-77.
2. Melandri, D., et al., The gammadeltaTCR combines innate immunity with adaptive immunity by utilizing spatially distinct regions for agonist selection and antigen responsiveness. *Nat Immunol*, 2018. **19**(12): p. 1352-1365.
3. Muro, R., H. Takayanagi, and T. Nitta, T cell receptor signaling for gammadeltaT cell development. *Inflamm Regen*, 2019. **39**: p. 6.
4. Sebestyen, Z., et al., Translating gammadelta (gammadelta) T cells and their receptors into cancer cell therapies. *Nat Rev Drug Discov*, 2020. **19**(3): p. 169-184.
5. Sandstrom, A., et al., The intracellular B30.2 domain of butyrophilin 3A1 binds phosphoantigens to mediate activation of human Vgamma9Vdelta2 T cells. *Immunity*, 2014. **40**(4): p. 490-500.
6. Sebestyen, Z., et al., RhoB Mediates Phosphoantigen Recognition by Vgamma9Vdelta2 T Cell Receptor. *Cell Rep*, 2016. **15**(9): p. 1973-85.
7. Karunakaran, M.M., et al., Butyrophilin-2A1 Directly Binds Germline-Encoded Regions of the Vgamma9Vdelta2 TCR and Is Essential for Phosphoantigen Sensing. *Immunity*, 2020. **52**(3): p. 487-498 e6.
8. Rigau, M., et al., Butyrophilin 2A1 is essential for phosphoantigen reactivity by gammadelta T cells. *Science*, 2020. **367**(6478).
9. Vyborova, A., et al., gamma9delta2T cell diversity and the receptor interface with tumor cells. *J Clin Invest*, 2020. **130**(9): p. 4637-4651.
10. Cano, C.E., et al., BTN2A1, an immune checkpoint targeting Vgamma9Vdelta2 T cell cytotoxicity against malignant cells. *Cell Rep*, 2021. **36**(2): p. 109359.
11. Groh, V., et al., Broad tumor-associated expression and recognition by tumor-derived gamma delta T cells of MICA and MICB. *Proc Natl Acad Sci U S A*, 1999. **96**(12): p. 6879-84.
12. Catellani, S., et al., Expansion of Vdelta1 T lymphocytes producing IL-4 in low-grade non-Hodgkin lymphomas expressing UL-16-binding proteins. *Blood*, 2007. **109**(5): p. 2078-85.
13. Poggi, A., et al., Vdelta1 T lymphocytes from B-CLL patients recognize ULBP3 expressed on leukemic B cells and up-regulated by trans-retinoic acid. *Cancer Res*, 2004. **64**(24): p. 9172-9.
14. Luoma, A.M., et al., Crystal structure of Vdelta1 T cell receptor in complex with CD1d-sulfatide shows MHC-like recognition of a self-lipid by human gammadelta T cells. *Immunity*, 2013. **39**(6): p. 1032-42.
15. Zhao, J., et al., Vdelta1 T cell receptor binds specifically to MHC I chain related A: molecular and biochemical evidences. *Biochem Biophys Res Commun*, 2006. **339**(1): p. 232-40.
16. Schilbach, K., et al., Immune response of human propagated gammadelta-T-cells to neuroblastoma recommend the Vdelta1+ subset for gammadelta-T-cell-based immunotherapy. *J Immunother*, 2008. **31**(9): p. 896-905.

17. Devaud, C., et al., Anti-metastatic potential of human Vdelta1(+) gammadelta T cells in an orthotopic mouse xenograft model of colon carcinoma. *Cancer Immunol Immunother*, 2013. **62**(7): p. 1199-210.
18. Almeida, A.R., et al., Delta One T Cells for Immunotherapy of Chronic Lymphocytic Leukemia: Clinical-Grade Expansion/Differentiation and Preclinical Proof of Concept. *Clin Cancer Res*, 2016. **22**(23): p. 5795-5804.
19. Di Lorenzo, B., S. Ravens, and B. Silva-Santos, High-throughput analysis of the human thymic Vdelta1(+) T cell receptor repertoire. *Sci Data*, 2019. **6**(1): p. 115.
20. Janssen, A., et al., gammadelta T-cell Receptors Derived from Breast Cancer-Infiltrating T Lymphocytes Mediate Antitumor Reactivity. *Cancer Immunol Res*, 2020. **8**(4): p. 530-543.
21. Harty, C., et al., Human gammadelta T cell sensing of AMPK-dependent metabolic tumor reprogramming through TCR recognition of EphA2. *Sci Immunol*, 2021. **6**(61).
22. Deniger, D.C., J.S. Moyes, and L.J. Cooper, Clinical applications of gamma delta T cells with multivalent immunity. *Front Immunol*, 2014. **5**: p. 636.
23. Siegers, G.M. and L.S. Lamb, Jr., Cytotoxic and regulatory properties of circulating Vdelta1+ gammadelta T cells: a new player on the cell therapy field? *Mol Ther*, 2014. **22**(8): p. 1416-1422.
24. de Witte, M.A., et al., alphabeta T-cell graft depletion for allogeneic HSCT in adults with hematological malignancies. *Blood Adv*, 2021. **5**(1): p. 240-249.
25. de Witte, M., et al., Allogeneic Stem Cell Transplantation Platforms With Ex Vivo and In Vivo Immune Manipulations: Count and Adjust. *Hemasphere*, 2021. **5**(6): p. e580.
26. Straetmans, T., et al., GMP-Grade Manufacturing of T Cells Engineered to Express a Defined gammadeltaTCR. *Front Immunol*, 2018. **9**: p. 1062.
27. Straetmans, T., et al., Untouched GMP-Ready Purified Engineered Immune Cells to Treat Cancer. *Clin Cancer Res*, 2015. **21**(17): p. 3957-68.
28. Scheper, W., et al., gammadeltaT cells elicited by CMV reactivation after allo-SCT cross-recognize CMV and leukemia. *Leukemia*, 2013. **27**(6): p. 1328-38.
29. Scheper, W., et al., Hunting for clinical translation with innate-like immune cells and their receptors. *Leukemia*, 2014. **28**(6): p. 1181-90.
30. Marcu-Malina, V., et al., Redirecting alphabeta T cells against cancer cells by transfer of a broadly tumor-reactive gammadeltaT-cell receptor. *Blood*, 2011. **118**(1): p. 50-9.
31. Grunder, C., et al., gamma9 and delta2CDR3 domains regulate functional avidity of T cells harboring gamma9delta2TCRs. *Blood*, 2012. **120**(26): p. 5153-62.
32. Kuball, J., et al., Cooperation of human tumor-reactive CD4+ and CD8+ T cells after redirection of their specificity by a high-affinity p53A2.1-specific TCR. *Immunity*, 2005. **22**(1): p. 117-29.
33. Rosenberg, S.A. and M.E. Dudley, Cancer regression in patients with metastatic melanoma after the transfer of autologous antitumor lymphocytes. *Proc Natl Acad Sci U S A*, 2004. **101 Suppl 2**: p. 14639-45.
34. Kierkels, G.J.J., et al., Identification of a tumor-specific allo-HLA-restricted gammadeltaTCR. *Blood Adv*, 2019. **3**(19): p. 2870-2882.

35. Gibbings, D. and A.D. Befus, CD4 and CD8: an inside-out coreceptor model for innate immune cells. *J Leukoc Biol*, 2009. **86**(2): p. 251-9.
36. Willemsen, R., et al., Redirecting human CD4+ T lymphocytes to the MHC class I-restricted melanoma antigen MAGE-A1 by TCR alpha gene transfer requires CD8alpha. *Gene Ther*, 2005. **12**(2): p. 140-6.
37. Kierkels, G.J.J., et al., Characterization and modulation of anti-alphaTCR antibodies and their respective binding sites at the betaTCR chain to enrich engineered T cells. *Mol Ther Methods Clin Dev*, 2021. **22**: p. 388-400.
38. Najima, Y., et al., Induction of WT1-specific human CD8+ T cells from human HSCs in HLA class I Tg NOD/SCID/IL2rgKO mice. *Blood*, 2016. **127**(6): p. 722-34.
39. Straetmans, T., et al., TEG001 Insert Integrity from Vector Producer Cells until Medicinal Product. *Mol Ther*, 2020. **28**(2): p. 561-571.
40. Johanna, I., et al., TEG011 persistence averts extramedullary tumor growth without exerting off-target toxicity against healthy tissues in a humanized HLA-A*24:02 transgenic mice. *J Leukoc Biol*, 2020. **107**(6): p. 1069-1079.
41. Johanna, I., et al., Evaluating in vivo efficacy - toxicity profile of TEG001 in humanized mice xenografts against primary human AML disease and healthy hematopoietic cells. *J Immunother Cancer*, 2019. **7**(1): p. 69.
42. Guedan, S., et al., Enhancing CAR T cell persistence through ICOS and 4-1BB costimulation. *JCI Insight*, 2018. **3**(1).
43. Turtle, C.J., et al., CD19 CAR-T cells of defined CD4+:CD8+ composition in adult B cell ALL patients. *J Clin Invest*, 2016. **126**(6): p. 2123-38.
44. Morris, E.C., et al., A critical role of T cell antigen receptor-transduced MHC class I-restricted helper T cells in tumor protection. *Proc Natl Acad Sci U S A*, 2005. **102**(22): p. 7934-9.
45. Willemsen, R.A., et al., CD8 alpha coreceptor to improve TCR gene transfer to treat melanoma: down-regulation of tumor-specific production of IL-4, IL-5, and IL-10. *J Immunol*, 2006. **177**(2): p. 991-8.
46. Ahrends, T., et al., CD4(+) T Cell Help Confers a Cytotoxic T Cell Effector Program Including Coinhibitory Receptor Downregulation and Increased Tissue Invasiveness. *Immunity*, 2017. **47**(5): p. 848-861 e5.
47. Shedlock, D.J. and H. Shen, Requirement for CD4 T cell help in generating functional CD8 T cell memory. *Science*, 2003. **300**(5617): p. 337-9.
48. Shah, N.N., et al., CD4/CD8 T-Cell Selection Affects Chimeric Antigen Receptor (CAR) T-Cell Potency and Toxicity: Updated Results From a Phase I Anti-CD22 CAR T-Cell Trial. *J Clin Oncol*, 2020. **38**(17): p. 1938-1950.
49. Bajwa, G., et al., Transgenic CD8alpha co-receptor rescues endogenous TCR function in TCR-transgenic virus-specific T cells. *J Immunother Cancer*, 2020. **8**(2).
50. Yachi, P.P., et al., Altered peptide ligands induce delayed CD8-T cell receptor interaction--a role for CD8 in distinguishing antigen quality. *Immunity*, 2006. **25**(2): p. 203-11.
51. Cheroutre, H. and F. Lambolez, Doubting the TCR coreceptor function of CD8alpha. *Immunity*, 2008. **28**(2): p. 149-59.

52. Omi, K., et al., Inhibition of R5-tropic HIV type-1 replication in CD4(+) natural killer T cells by $\gamma\delta$ T lymphocytes. *Immunology*, 2014. **141**(4): p. 596-608.
53. Gao, G.F., et al., Classical and nonclassical class I major histocompatibility complex molecules exhibit subtle conformational differences that affect binding to CD8 $\alpha\alpha$. *J Biol Chem*, 2000. **275**(20): p. 15232-8.
54. Witte, T., R. Spoerl, and H.C. Chang, The CD8 β ectodomain contributes to the augmented coreceptor function of CD8 $\alpha\beta$ heterodimers relative to CD8 $\alpha\alpha$ homodimers. *Cell Immunol*, 1999. **191**(2): p. 90-6.
55. Chang, H.C., K. Tan, and Y.M. Hsu, CD8 $\alpha\beta$ has two distinct binding modes of interaction with peptide-major histocompatibility complex class I. *J Biol Chem*, 2006. **281**(38): p. 28090-6.
56. Huang, J., et al., Kinetics of MHC-CD8 interaction at the T cell membrane. *J Immunol*, 2007. **179**(11): p. 7653-62.
57. Shi, Y., et al., Plasticity of human CD8 $\alpha\alpha$ binding to peptide-HLA-A*2402. *Mol Immunol*, 2011. **48**(15-16): p. 2198-202.
58. Gavlovsky, P.J., et al., Expression of MHC class I-related molecules MICA, HLA-E and EPCR shape endothelial cells with unique functions in innate and adaptive immunity. *Hum Immunol*, 2016. **77**(11): p. 1084-1091.
59. Yie, S.M., et al., Expression of human leukocyte antigen G (HLA-G) correlates with poor prognosis in gastric carcinoma. *Ann Surg Oncol*, 2007. **14**(10): p. 2721-9.
60. Sanders, S.K., P.A. Gibling, and P. Kavathas, Cell-cell adhesion mediated by CD8 and human histocompatibility leukocyte antigen G, a nonclassical major histocompatibility complex class 1 molecule on cytotrophoblasts. *J Exp Med*, 1991. **174**(3): p. 737-40.
61. Hofmeister, V. and E.H. Weiss, HLA-G modulates immune responses by diverse receptor interactions. *Semin Cancer Biol*, 2003. **13**(5): p. 317-23.
62. Roda, G., et al., Characterizing CEACAM5 interaction with CD8 α and CD1d in intestinal homeostasis. *Mucosal Immunol*, 2014. **7**(3): p. 615-24.

Supplementary figures

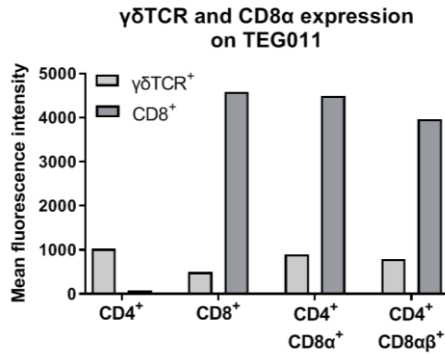


Figure S1. Transgene expression levels on T cells transduced with the FE11 $\gamma\delta$ TCR in combination with CD8 α alone or CD8 α and CD8 β . $\alpha\beta$ T cells were transduced with the FE11 $\gamma\delta$ TCR and with either CD8 α alone, or CD8 α combined with CD8 β . Thereafter, CD4⁺, CD8⁺, CD4⁺CD8 α ⁺ and CD4⁺CD8 $\alpha\beta$ ⁺ TEG011 cells were sorted, and the expression of $\gamma\delta$ TCR and CD8 α was measured by flow cytometry.

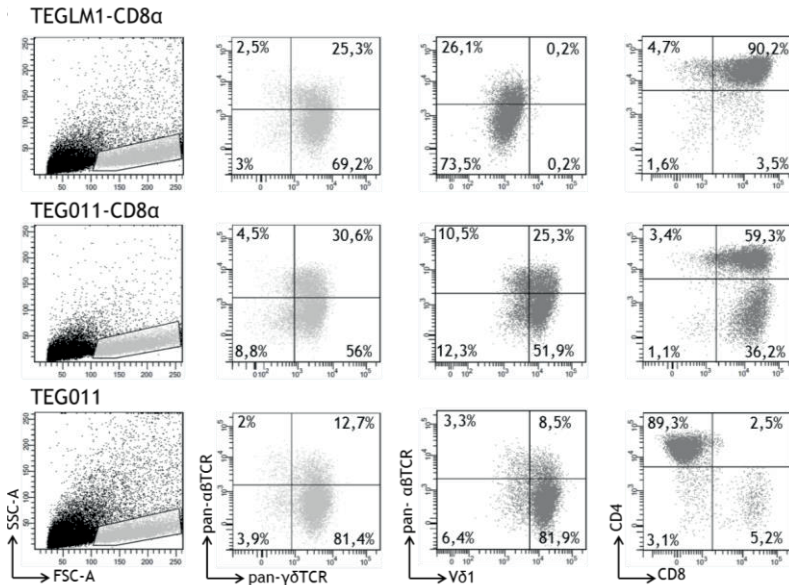


Figure S2. $\gamma\delta$ TCR expression of TEG011, TEG011_CD8 α , and TEGLM1_CD8 α mock. Representative flow cytometry plots for $\gamma\delta$ TCR expression of TEGLM1_CD8 α (top panel), TEG011_CD8 α (middle panel), and TEG011 (bottom panel) prior to infusion into mice after 2 weeks expansion. Representative plots for V δ 1

TCR expression of TEG011 and TEG011_CD8 α were included as a quality control for the flow cytometry panel using pan- $\gamma\delta$ TCR monoclonal antibody.

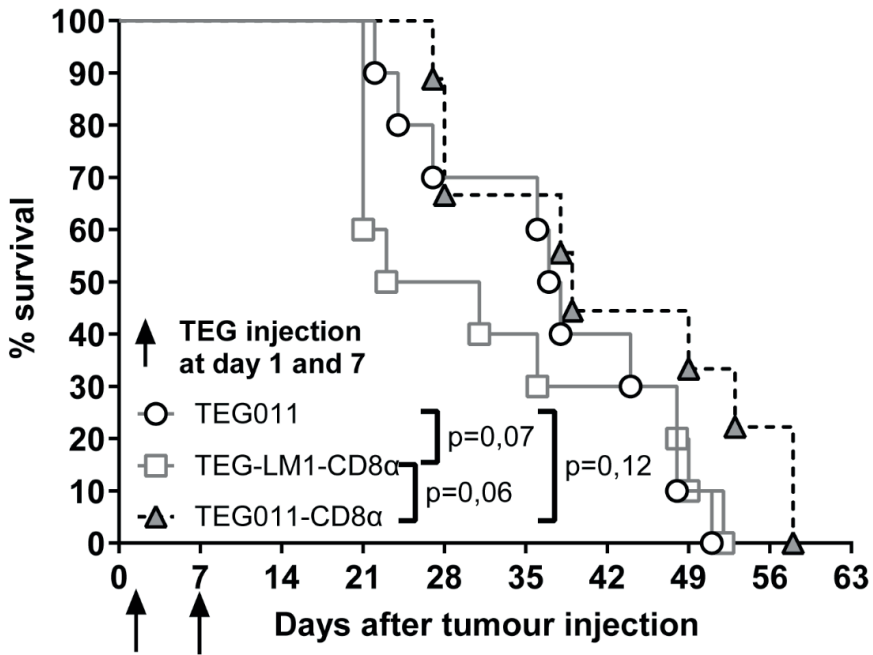


Figure S3. In vivo antitumor reactivity of TEG011_CD8 α in tumor-bearing mice. (A) Overall survival of treated K562-HLA*A24 luciferase tumor-bearing mice for monitoring efficacy was followed for 60 days. Statistical significances were calculated by log-rank (Mantel-cox) test.

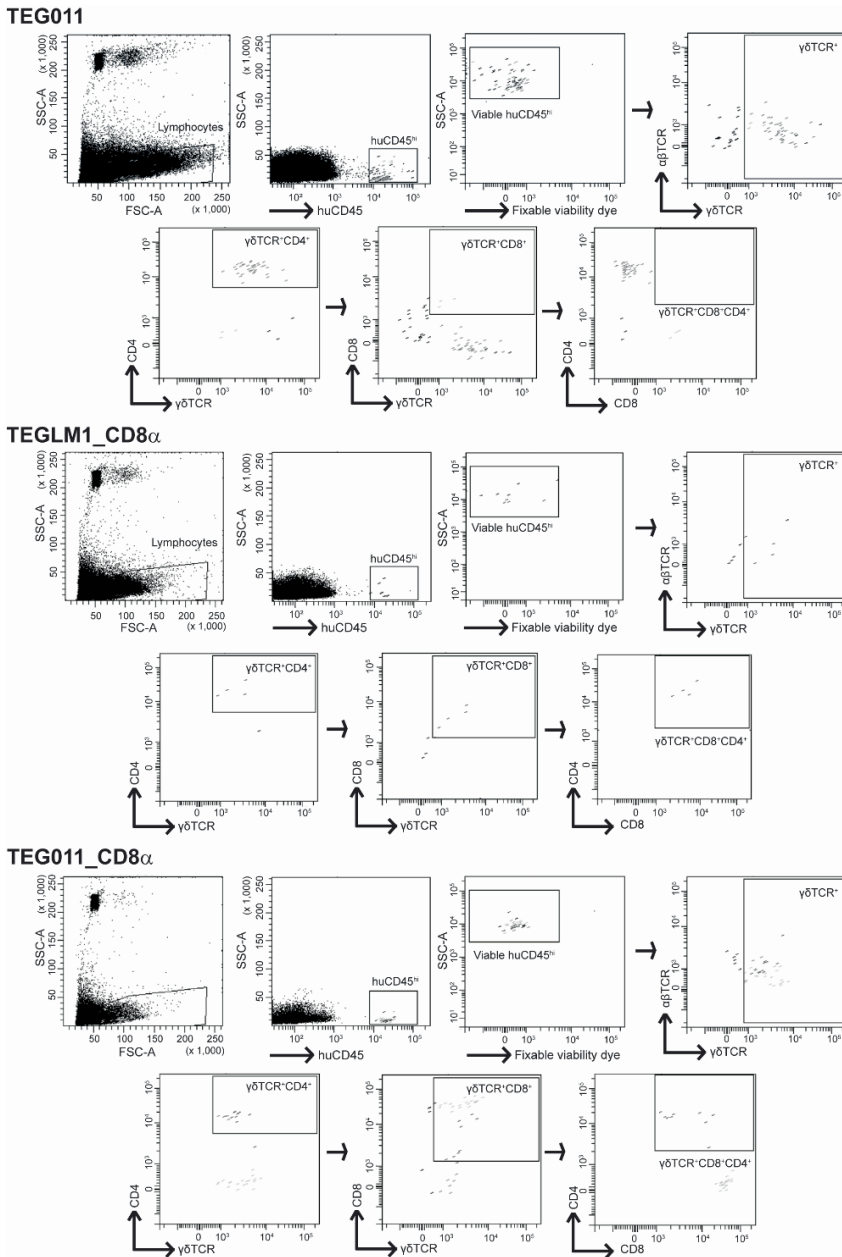


Figure S4. Gating strategy for flow cytometry analysis of TEGs persistence in peripheral blood. (A) Representative flow cytometry plots of peripheral blood in tumor-bearing mice model on Week 2. TEG persistence was measured by quantifying absolute cell number of viable huCD45 $^+$ $\gamma\delta$ TCR $^+$ CD8 $^+$ for TEG011, huCD45 $^+$ $\gamma\delta$ TCR $^+$ CD8 $^+$ single positive and huCD45 $^+$ $\gamma\delta$ TCR $^+$ CD4 $^+$ CD8 $^+$ double positive for TEGLM1_CD8 α and TEG011_CD8 α mock group.

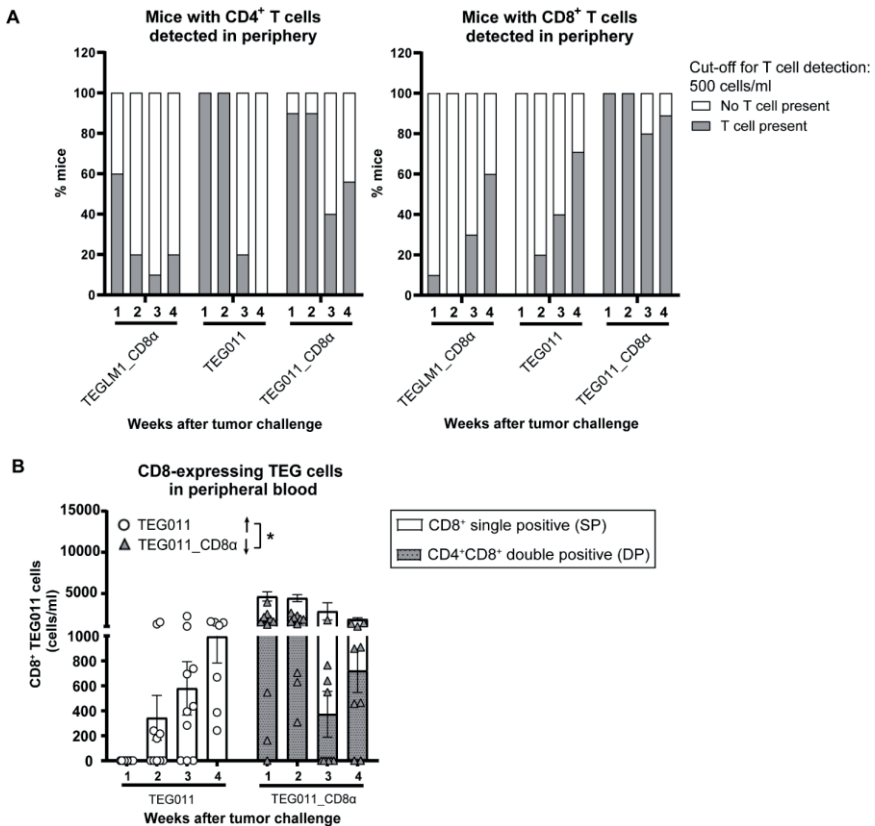


Figure S5. The presence of T cells observed in peripheral blood of individual mice. (A) Percentage of mice with either CD4⁺ T cells (left panel) or CD8⁺ T cells (right panel) where minimum 500 cells/ml T cells are detected (lower grey bar) or less than 500 cells/ml or no T cells are detected (upper white bar) detected in peripheral blood for each treatment group (n = 10 mice/group). **(B)** Overall persistence of CD8⁺ TEG011 cells in periphery. Absolute number of CD8-expressing TEG011 cells were measured in peripheral blood by flow cytometry for TEG011 (open black circle) and TEG011_CD8 α (open black triangle) in tumor-bearing mice. TEG cells are distinguished into two different cellular compartments: CD8⁺ single-positive (SP; white stacked bar) and CD4⁺CD8⁺ double-positive (DP; grey dotted stacked bar). Black arrows indicate higher or lower T cell counts observed. Data represent mean \pm SEM of all mice per group (n = 10 mice). Statistical significances were calculated by a mixed-effects model with repeated measures (*P < 0.05).

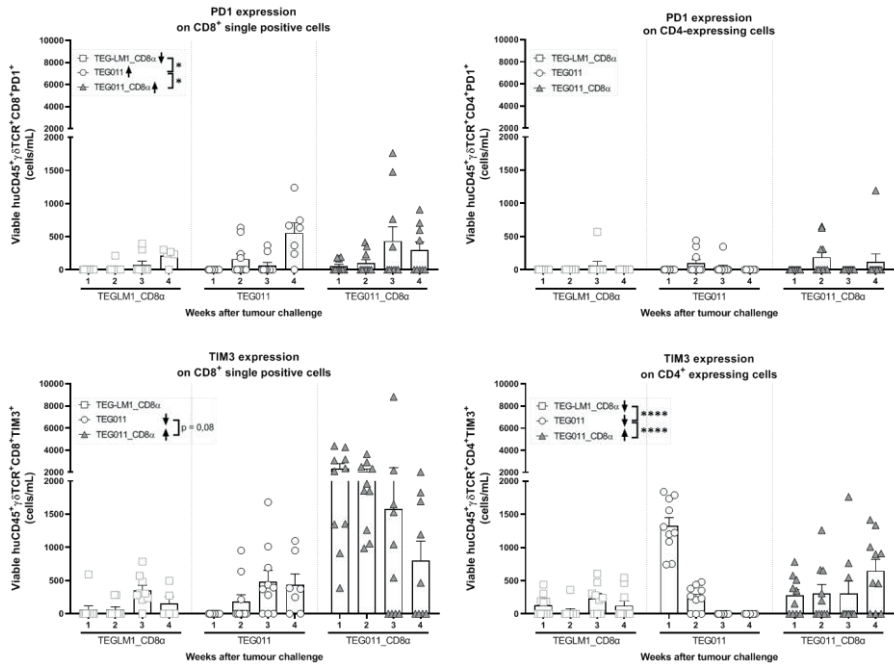


Figure S6. PD1 and TIM3 expression on CD4⁺ and CD8⁺ TEGs. Absolute cell counts of PD1-expressing (A) and TIM3-expressing (B) huCD45⁺γδTCR⁺CD8⁺ single positive cells (left panel) and huCD45⁺γδTCR⁺CD4⁺ single positive or CD4⁺CD8⁺ double positive cells (right panel) were measured by flow cytometry for TEG-LM1_CD8α mock (open light gray rectangle), TEG011 (open black circle), and TEG011_CD8α (grey triangle). Black arrows indicate higher or lower T cell counts observed. Data represent mean ± SEM of all mice per group (n = 10 mice). Statistical significances were calculated by a mixed-effects model with repeated measures (*P < 0.05; ****P < 0.0001).

Supplementary tables

Supplementary Table 1. Complete sequence of TEG011_CD8 α (pMP71-TCR_FE11 γ -T2A-FE11 δ _P2A-CD8 α)

```

>>--TCR FE11 $\gamma$ -->
1081 gctcacttac aggcggccac gcgtggatcc gaattcaccatgggatgggc tctgctggg
>-----TCR FE11 $\gamma$ ----->
1141 ctgctggcct ttctgtctcc tgccagccag aagtccagca acctgggaagg cggcaccaag
>-----TCR FE11 $\gamma$ ----->
1201 agcgtgacca gacctacaag aagcagcgc gagatcacct gtgacctgac cgtgatcaac
>-----TCR FE11 $\gamma$ ----->
1261 gccttctaca tccactggta tctgcaccaa gaaggcaagg cccctcagcg gctgctgtac
>-----TCR FE11 $\gamma$ ----->
1321 tacgatgtgt ccaacagcaa ggacgtgctg gaaagcggac tgagccccgg caagtactac
>-----TCR FE11 $\gamma$ ----->
1381 acccacacac ctgacggtg gtctggatc ctgactctgc ggaacctgat cgagaacgac
>-----TCR FE11 $\gamma$ ----->
1441 tccggcgtgt actactgcgc cacctggat agacccgaga tctactataa gaagtgttc
>-----TCR FE11 $\gamma$ ----->
1501 ggcagcggca ccactcgtgt ggtcacagac aaacagctgg acgccagctg gtcccctaag
>-----TCR FE11 $\gamma$ ----->
1561 cctaccatct tctgccttc tatgccggag acaaagctgc agaagccggg cacctacctg
>-----TCR FE11 $\gamma$ ----->
1621 tgcctgctgg aaaagtctt cccagacgtg atcaagatcc actgggaaga gaagaatcc
>-----TCR FE11 $\gamma$ ----->
1681 aacaccatcc tggcagcca agaggcaac accatgaaga ccaacgacac ctacatgaag
>-----TCR FE11 $\gamma$ ----->
1741 ttacgtggc tgaccgtgcc tgagaagtcc ctggacaaag aacaccggtg catcgtgccg
>-----TCR FE11 $\gamma$ ----->
1801 cacgagaaca acaagaacgg cgtggaccaa gagatcatct tccacctat caagaccgac
>-----TCR FE11 $\gamma$ ----->
1861 gtcatcacia tggaccccaa ggacaactgc tccaaggacg ccaacgatac cctgctgctg
>-----TCR FE11 $\gamma$ ----->
1921 cagctgacaa acaccagcgc ctactacatg tatttgctgc tttgctgaa gtccgtggg
>-----TCR FE11 $\gamma$ ----->
1981 tacttcgcca tcatcatg ctgctgctg cggagaaccg ccttctgctg caatggcgag
----->>-----T2A linker----->>
2041 aaaagctgc acagcggctc tggcagatct ggctctggcg aaggcagagg ctctctgctg
-----T2A linker----->>
2101 acatgtggcg acgtggaaga gaaccccgga cctcgcttaa ttaacatgtt gttcagcagc
>-----TCR FE11 $\delta$ ----->
2161 ctgctgtgcg tttcgtggc cttagctac agcggagca gcgtggcca gaaagtgaca
>-----TCR FE11 $\delta$ ----->

```

```

2221 cagggccagtc cctccgtgtc tatgcctgtg cggaaagccg tgacactgaa ctgcctgtac
>-----TCR FE11 $\delta$ ----->
2281 gagacaagct ggtggttta ctacatcttc tggtaacaagc agctgccagc caaagagatg
>-----TCR FE11 $\delta$ ----->
2341 atctttctga tccggcaggg cagcgacgag cagaatgcca agagcggcag atactccgtg
>-----TCR FE11 $\delta$ ----->
2401 aacttcaaga aagccgcca gtctgtggcc ctgaccatct ctgctctgca actggaagat
>-----TCR FE11 $\delta$ ----->
2461 agcccaagct acttctgctc cctggcgatg tttatggcg cggacctct gtacaccgac
>-----TCR FE11 $\delta$ ----->
2521 aagctgatct tcggcaaggg caccagatg accgtggaa ctagaagcca gcctcacacc
>-----TCR FE11 $\delta$ ----->
2581 aagccttcgg tgtttgtgat gaagaacggc accaacgtgg cctgcctggt caaagagttc
>-----TCR FE11 $\delta$ ----->
2641 taccctaagg acatccggat caacctggtg tccagcaaga agatcaccga gttcgaccoc
>-----TCR FE11 $\delta$ ----->
2701 gccatctgta tcagccctag cggcaagtat aacgccgtga agctgggaa gtacgaggac
>-----TCR FE11 $\delta$ ----->
2761 agcaatagcg tgacctgacg cgtgcagcat gataacaaga ccgtgcacag caccgatttc
>-----TCR FE11 $\delta$ ----->
2821 gaagtgaaaa ccgactccac cgaccacgtg aagcccaaag agacagagaa caccaagcag
>-----TCR FE11 $\delta$ ----->
2881 cccagcaagt cctgccacaa gcctaaggcc atcgtgcaca ccgagaaagt gaacatgatg
>-----TCR FE11 $\delta$ ----->
2941 agcctgacag tctgggcct gagaatgctg ttcgccaaga cagtgccgt gaatttcctg
>-----TCR FE11 $\delta$ ----->>-----P2A linker----->>
3001 ctgaccgcca agctgttctt tctgctcag ggcagcggcg ccacaattt cagcctctg
-----P2A linker----->>-----
3061 aaacaggccg gcagctcga agaaaatcct gacccaatgg ccttaccagt gaccgcctg
>-----CD8 $\alpha$ ----->
3121 ctctgccg tggtcttct gctccacgcc gccagggcca gccagttccg ggtgtcggc
>-----CD8 $\alpha$ ----->
3181 ctggatcga cctggaacct gggcgagaca gtggagctga agtgcagggt gctgctgtcc
>-----CD8 $\alpha$ ----->
3241 aaccggacgt cggctgctc gtggctcttc cagccgcgcg gcgccggcg cagtcccacc
>-----CD8 $\alpha$ ----->
3301 ttctctctat acctctccca aaacaagccc aaggcggccg agggctgga caccagcgg
>-----CD8 $\alpha$ ----->
3361 ttctcggca agaggtggg ggaacacctc gtctctacc tgagcactt ccgccgagag
>-----CD8 $\alpha$ ----->
3421 aacgaggct actatttctg ctggccctg agcaactcca tcatgtactt cagccacttc
>-----CD8 $\alpha$ ----->
3481 gtccggctct tctgccagc gaagcccacc acgacgccag gcggcgacc accaacaccg
-----CD8 $\alpha$ ----->
3541 gcgcccacca tcgctcga gccctgtcc ctgcgccag aggcgtgcc gccagcggc
>-----CD8 $\alpha$ ----->
3601 gggcgcgag tgacacagag gggctggac ttgcctgtg atatctacat ctggcgccc

```

```

>-----CD8 $\alpha$ ----->
3661 ctgcccggga cttgtgggt ccttctctg tcactggta tcacccttta ctgcaaccac
>-----CD8 $\alpha$ ----->
3721 aggaaccgaa gacgttttg caaatgtccc cggcctgtg tcaaatcggg agacaagccc
>-----CD8 $\alpha$ ----->
3781 agccttcgg cgagatacgt ctgatagaa aagcttaaca cgagccatag atagaataaa

```

Supplementary Table 2. Complete sequence of TEGLM1_CD8 α

```

>>--TCR G115y-->
1081 gctcacttac aggcggccac gcgtggatcc gaattcacc atggtgtccct gctgcacgcc
>-----TCR G115y----->
1141 agcaccctgg ccgtgctggg cggcctgtg gtgtatggcg ccggacacct ggaacagccc
>-----TCR G115y----->
1201 cagatcagca gcaccaagac cctgagcaag accgccaggc tggaaatcgt ggtgtccggc
>-----TCR G115y----->
1261 atcaccatca gcgccacctc cgtgtactgg tacagagaga gaccggcga ggtcatccag
>-----TCR G115y----->
1321 ttctgtgtt ccatcagcta cgacggcacc gtcgggaaag agagcggcat ccccagcggc
>-----TCR G115y----->
1381 aagttcagg tggacagaat ccccgagacc agcacctcca cctgacat ccaaacgtg
>-----TCR G115y----->
1441 gagaagcagg acatgccac ctactactgc gccctgtggg aggccagca ggaactggc
>-----TCR G115y----->
1501 aagaaaatca aggtttcgg cctggcacc aagctgatca tcaccgaca gcagctggac
>-----TCR G115y----->
1561 gccgacgtga gcccgaagc taccatctc ctgccagca tcgccgagac caagctcag
>-----TCR G115y----->
1621 aaggccggca cctacctgtg cctgctggaa aagttctcc ccgactgat caagatccac
>-----TCR G115y----->
1681 tggaggaaa agaagagcaa caccatcctg ggcagccagg aaggcaatac catgaaaacc
>-----TCR G115y----->
1741 aacgacacct acatgaagt cagctggctg accgtgcccg agaagagcct ggaacaagag
>-----TCR G115y----->
1801 cacagatgca tegtccggca cgagaacaac aagaacggcg tggaccagga aatcatcttc
>-----TCR G115y----->
1861 cccccatca agaccgatgt gatcacaatg gacccaagg acaactcag caaggacgcc
>-----TCR G115y----->
1921 aacgataccc tgctgctgca gctgaccaac accagcct actacatgta tctcctgctg
>-----TCR G115y----->
1981 ctgctgaaga gcgtgggta cttcgccatc atcacctgt gtctgtgcg gcggaccgcc
>-----TCR G115y----->>-----T2A linker----->
2041 ttctgctgca acggcgaaa gacgtcgac agcggcagcg ggcgcagcg cagcggcgaa

```

```

-----T2A linker-----
2101 ggccgaggca gcctgctgac ctgcggcgat gtggaagaaa accctggccc gcgcttaatt
---->-----TCR G115 $\delta$ _LM1----->
2161 aacatggagc ggatcagcag cctgatccac ctgagcctgt tctggccgg agtgatgagc
>-----TCR G115 $\delta$ _LM1----->
2221 gccatcgagc tggtgcccga gcaccagacc gtgcccgta gcatcggcgt gccccgccacc
>-----TCR G115 $\delta$ _LM1----->
2281 ctgcggtgca gcatgaaggg cgaaggccatc ggcaactact acatcaactg gtacagaaag
>-----TCR G115 $\delta$ _LM1----->
2341 acccagggca acaccatgac cttcatctac cgggagaagg acatctacgg ccctggcttc
>-----TCR G115 $\delta$ _LM1----->
2401 aaggacaact tccagggcga catcgacatc gccaagaacc tggcctgct gaagatcctg
>-----TCR G115 $\delta$ _LM1----->
2461 gccccagcg agagggacga gggcagctac tactgcgctt gcgacaccct ggccaccgac
>-----TCR G115 $\delta$ _LM1----->
2521 aagctgatct tggcaaggg caccgggtg accgtggagc ccagaagcca gcccccacacc
>-----TCR G115 $\delta$ _LM1----->
2581 aagcccagcg tttctgcat gaagaacggc accaacctgg cctgcctggt gaaagagttc
>-----TCR G115 $\delta$ _LM1----->
2641 taccccagg acatccgat caacctggtg tccagcaaga agatcaccga gttcgacccc
>-----TCR G115 $\delta$ _LM1----->
2701 gccatctgca tcagccccag cggcaagtac aacgccgtga agctgggcaa gtacgaggac
>-----TCR G115 $\delta$ _LM1----->
2761 agcaacagcg tgacctgcag cgtgcagcac gacaacaaga ccgtgcacag caccgacttc
>-----TCR G115 $\delta$ _LM1----->
2821 gagtgaaaa ccgactccac cgaccagtg aagcccaaaag agaccgagaa caccaagcag
>-----TCR G115 $\delta$ _LM1----->
2881 cccagcaaga gctgccacaa gcccaaggcc atcgtgcaca ccgagaaggt gaacatgatg
>-----TCR G115 $\delta$ _LM1----->
2941 agcctgaccg tctgggctt cgggatgctg ttcgccaaga cagtggcctg gaacttcctg
>----TCR G115 $\delta$ _LM1--->>-----P2A linker-----
3001 ctgaccgcca agctgttctt cctgctcag ggcagcggcg ccacaaattt cagcctgctg
-----P2A linker----->>-----CD8 $\alpha$ ----->
3061 aaacaggccg gcgacgtcga agaaaatctt ggaccaatgg ccttaccagt gaccgccttg
>-----CD8 $\alpha$ ----->
3121 ctctgccgc tggccttctt gctccacgcc gccaggcca gccagttccg ggtgtcggcg
>-----CD8 $\alpha$ ----->
3181 ctggatcggc cctggaacct gggcgagaca gtggagctga agtgccaggt gctgctgtcc
>-----CD8 $\alpha$ ----->
3241 aaccgacgt cggctgctc gtggcttct cagccgcgcg gcgccgccc cagtcccacc
>-----CD8 $\alpha$ ----->
3301 ttctctctat acctctccca aaacaagccc aaggcggccg agggctgga caccagcgg
>-----CD8 $\alpha$ ----->
3361 ttctcggca agaggttgg ggaacacctt gtctcacc tgagcactt ccgccgagag
>-----CD8 $\alpha$ ----->
3421 aacgaggct actatttctg ctgcgcctg agcaactcca tcatgtact cagccacttc
>-----CD8 $\alpha$ ----->
3481 gtgccgtct tctgcccagc gaagcccacc acgacgccag cggcggacc accaacaccg

```

```

>-----CD8a----->
3541 ggcaccacca tcgcgtcgca gccctgtcc ctgcgccag aggcgtccg gccagcggcg
>-----CD8a----->
3601 ggggcgcag tgcacacgag gggctggac ttgcctgtg atatctacat ctggcgccc
>-----CD8a----->
3661 ctggcggga ctgtgggt cttctcctg tcaactgta tcaccctta ctgcaaccac
>-----CD8a----->
3721 aggaaccgaa gacgttttg caaatgtccc ggcctgtg tcaaatcggg agacaagccc
>-----CD8a----->>
3781 agccttcgg cgagatacgt ctgatatgaa aagcttaaca cgagccatag atagaataaa

```



CHAPTER 6

Dual-targeting of cancer-metabolome and stress antigens impacts transcriptomic heterogeneity and efficacy of engineered T-cells

Patricia Hernández-López^{1†}, Eline van Diest^{1†}, Peter Brazda^{1,2}, Sabine Heijhuurs¹, Angelo Meringa¹, Lauren Hoorens van Heyningen¹, Caterina Riillo^{1,3}, Caroline Schwenzel^{4,5,6}, Marina Zintchenko^{4,5,6}, Inez Johanna¹, Mara J.T. Nicolassen¹, Astrid Cleven¹, Thomas A. Kluiver², Rosemary Millen⁷, Jiali Zheng¹, Effrosyni Karaiskaki¹, Trudy Straetemans¹, Hans Clevers^{2,7#}, Remco de Bree⁸, Hendrik G Stunnenberg², Weng Chuan Peng², Jeanine Roodhart⁹, Susana Minguet^{4,5,6}, Zsolt Sebestyén¹, Dennis X. Beringer^{1x}, and Jürgen Kuball^{1,10x*}

¹Center for Translational Immunology, University Medical Center Utrecht, Utrecht University Utrecht, The Netherlands.

²Princess Máxima Center for Pediatric Oncology, Utrecht, The Netherlands.

³Department of Experimental and Clinical Medicine, Magna Graecia University, Catanzaro, Italy.

⁴Faculty of Biology, University of Freiburg, Freiburg, Germany.

⁵Signalling Research Centres BIOSS and CIBSS, University of Freiburg, Freiburg, Germany

⁶Center of Chronic Immunodeficiency (CCI) and Institute for Immunodeficiency, University Clinics and Medical Faculty, Freiburg, Germany.

⁷Oncode Institute, Hubrecht Institute, Royal Netherlands Academy of Arts and Sciences (KNAW), Utrecht, the Netherlands

⁸Department of Head and Neck Surgical Oncology, University Medical Center Utrecht, Utrecht, The Netherlands

⁹Department of Medical Oncology, University Medical Center Utrecht; Utrecht, The Netherlands.

¹⁰Department of Hematology, University Medical Center Utrecht; Utrecht, The Netherlands.

† These authors contributed equally to this work

x Shared senior authors

Nature Immunology, 2023

Patent application: EP23188032.9CD277 TARGETING COSTIMULATORY RECEPTOR (Hernandez-Lopez co-inventor)

Abstract

Few cancers can be efficiently targeted with engineered T-cell strategies. Here, we explored whether $\gamma\delta$ TCR-mediated cancer-metabolome targeting can be combined with the attack of cancer-associated stress antigens, like NKG2D-ligands or CD277, through the addition of chimeric co-receptors. This strategy overcame suboptimal $\gamma\delta$ TCR-engagement of TEGs ($\alpha\beta$ T-cell engineered to express a defined $\gamma\delta$ TCR) and improved serial killing, proliferation and persistence of TEGs. *In vivo*, the NKG2D-CD28_{WT}-chimera enhanced only liquid tumor control, NKG2D-4-1BB_{CD28TM}-chimera prolonged persistence of TEGs and improved tumor control of liquid and solid tumors. The CD277-targeting chimera (103-4-1BB-chimera) was the most optimal co-stimulation format, mediating eradication of both liquid and solid tumors. Single-cell transcriptomic analysis revealed that NKG2D-4-1BB_{CD28TM} and 103-4-1BB chimeras reprogrammed TEGs through NF- κ B. Due to the competition with naturally expressed NKG2D in CD8⁺ TEGs, NKG2D-4-1BB_{CD28TM} chimera mainly skewed CD4⁺ TEGs towards adhesion, proliferation, cytotoxicity and less-exhausted signatures, while the 103-4-1BB-chimera additionally shaped the CD8⁺ subset towards a proliferative state.

Introduction

Metabolome targeting by transfer of $\gamma\delta$ TCR into $\alpha\beta$ T-cells (TEGs) has been reported to overcome two limitations in the T-cell immunotherapy field, i) the scarceness of targetable tumor antigens for solid tumors and ii) the poor function and high heterogeneity of natural $\gamma\delta$ T-cells in patients. TEGs sense intracellular accumulation of phosphoantigens (pAg) in tumor cells by recognizing an inside-out mechanism involving RhoB¹, BTN2A1²⁻⁴ and the BTN3A-complex (CD277)⁵⁻⁷ through a carefully selected high affinity $\gamma\delta$ TCR (later referred to as TEG001)^{8,9}. TEG001 is currently being explored in a phase I clinical trial (NTR6541)¹⁰ showing complete remission in a patient with refractory acute myeloid leukemia (AML)¹¹. However, antigen recognition is suboptimal for many cancer types, and does not allow for full T-cell activation, especially in solid tumors¹².

Cancer-associated stress antigens like NKG2D-ligands¹³ have been proposed as universal targets for liquid and solid tumors. In the current TEG format, recognition of NKG2D-ligands by NKG2D is limited to a subset of CD8+ TEGs¹⁴. CD277 has been proposed to act not only as a metabolic target, but also as a stress antigen^{15,16}. Utilizing CD277-targeting antibodies in combination with $\gamma\delta$ TCR-based targeting enhanced potency of primary $\gamma\delta$ T-cells¹⁷. However, to date, no objective clinical responses have been observed in patients treated with anti-CD277 antibody monotherapy when relying on the natural $\gamma\delta$ T-cell repertoire¹⁸.

To harvest the full potential of co-targeting the cancer-metabolome and cancer-associated antigens, novel strategies are needed. Probably, a better orchestration of TCR and CAR signaling is required. Within this context, many approaches are currently being explored to make CAR-T cells more $\alpha\beta$ TCR-like to enhance activity¹⁹, or to add to TCR signaling a CAR-like co-stimulation^{20,21}. A recent study revealed a surprisingly high heterogeneity in single-cell behavior of engineered $\alpha\beta$ T-cells, which was associated with distinct transcriptomic profiles and behaviors¹². Also, analyses of CAR-T from long-term survivors imply the importance of understanding different signaling domains and the heterogeneity of engineered immune cells^{22,23}.

Cognizant of the power and limitations of both the $\gamma\delta$ TCR-mediated cancer-metabolome targeting, and stress-targeting, we combined $\gamma\delta$ TCR and chimeric NKG2D and anti-CD277 costimulatory receptors to improve targeting of tumors. By modifying costimulatory signaling, we aimed to also shape transcriptomic heterogeneity and function, including activity at the tumor site, as well as persistence of engineered T-cells. We observed that most of the stress-targeting chimeras impacted function in different readouts and overcame suboptimal $\gamma\delta$ TCR-engagement *in vitro*. However, only the combined expression of the NKG2D-4-1BB_{CD28TM}-chimera with TEG001 substantially altered the transcriptome heterogeneity of CD4⁺ TEGs through NF- κ B signaling pathway. Conversely, the anti-CD277 chimeric co-receptor (so-called 103-4-1BB-chimera) impacted transcriptomic heterogeneity of both CD4⁺ and CD8⁺ TEGs, and mediated superior clinical responses with complete remissions in both liquid and solid tumor *in vivo* models.

Material and Methods

Antibodies and flow cytometry analysis

The following antibodies were used: CD8a-PerCP-Cy5.5 (1:100; clone RPA-T8; 301032), CD4-AF700 (1:40; clone RPA-T4; 300526), $\alpha\beta$ TCR-PE-Cy5 (1:80; clone IP26; 11-9986-42), PD1-BV711 (1:20, clone EH12.2H7; 329928), Granzyme B-APC (1:50; clone QA16A02; 372204) and huNKG2D (clone 1D11; 320802), huCD45RO-AF700 (clone UCHL-1; 304218) from Biolegend. $\gamma\delta$ TCR-PE-Cy7 (1:20; clone IMMU510; B10247) from Beckman Coulter. NKG2D-BV650 (1:40; clone 1D11; 563408), CCR-7-BV711 (1:20, clone 3D12, 563712) and $\gamma\delta$ TCR-APC (1:5; clone B1; 555718) from BD Biosciences. Pan- $\gamma\delta$ TCR-PE (1:10; clone IMMU510; B49176) from Beckman-Coulter. huCD45-PB (1:30; clone HI30; 2120145), mCD45-APC (1:30; clone 30-F11S; 1115560), and huCD69-APC (1:25; clone FN50; 2154550) from Sony Biotechnology. $\alpha\beta$ TCR-FITC (1:10; clone IP26; 11-9986-42) from Invitrogen. CD4-PE-Cy7 (1:100; clone RPA-T4; 25-0049-42), NKG2D-PE (1:25; clone 1D11; 12-5878-42) and Fixable Viability Dye eFluor506 from eBioscience. huCD3 (clone OKT3; 130-093-387) from Miltenyi Biotec.

For the intracellular staining of Granzyme B (GZMB), BD Cytotfix/Cytoperm™ kit from BD Biosciences was used. All samples were analyzed on a BD LSRFortessa or BD Canto using FACS-Diva Software or FlowJo Software (BD Biosciences).

Examples of the gating strategy used in *in vitro* and *in vivo* experiments are shown in Supplementary Figures 1,2,4.

Cell-lines, patient derived organoids and cell culture

Daudi (ATCC CCL-213), K562 (ATCC CCL-243), HL60 (ATCC CCL-240), RPMI-8226 (ATCC CCL-155), SCC9 (ATCC CRL-1629), HEK293 (CRL-1573) and Phoenix-Ampho (ATCC CRL-3213) cells were obtained from ATCC. Phoenix-Ampho and SCC9 cells were cultured in DMEM supplemented with 1% Pen/Strep (Invitrogen) and 10% FCS (Bodinco, Alkmaar, The Netherlands). All other cell-lines were cultured in RPMI with 1% Pen/Strep and 10% FCS. All the cell lines were reauthenticated using the Cell Line Authentication (CLA) Test provided by Eurofins Genomics Europe (Germany) each time a cell line batch was frozen. Primary fresh PBMCs were isolated by Ficoll-Paque (GE Healthcare, Eindhoven, The Netherlands) from buffy coats supplied by Sanquin Blood Bank (Amsterdam, The Netherlands).

Head and neck and liver patient-derived organoids were established and cultured as described previously⁵⁵⁻⁵⁷. Authorizations for head and neck organoids were obtained by the medical ethical committee and biobank research ethics committee of UMC Utrecht (UMCU) at the request of HUB (www.hub4organoids.nl), to ensure compliance with the Dutch Medical Research Involving Human Subjects Act. Patient derived liver organoids were obtained through the Biobank of the Princess Máxima Center for Pediatric Oncology (Utrecht, The Netherlands). The Biobank protocol was approved by the Medical Ethics Committee of the Erasmus Medical Center (Rotterdam, The Netherlands; protocol number MEC-2016-739). The patients and/or their legal representatives participating in the Biobank study signed informed consent. The Biobank and Data Access Committee (BDAC) of the Princess Máxima Center granted approval for the present project (project PMCLAB2020.107). For liver tumor-derived organoids, the culture medium was based on Saltsman et al.⁵⁸ and consisted of the following: Advanced

DMEM/F12 supplemented with 1% penicillin/streptomycin, 1% GlutaMAX, 10 mM HEPES, 0.2% Normocin, 1x B27 supplement, 1x N2 supplement, 1.25 mM N-acetyl-L-cysteine, 10% (vol/vol) RSPO1 conditioned medium, 10 mM nicotinamide, 10 nM recombinant human (Leu15)-gastrin I, 50 ng/mL recombinant human EGF, 100 ng/mL recombinant human FGF10, 25 ng/mL recombinant human HGF, 10 μ M forskolin, 5 μ M A8301, 10 μ M Y27632 and 0.5 nM WNT surrogate⁵⁹.

For co-culture assays using head and neck tumor organoids, organoids were recovered from the BME by resuspension in TrypLE Express and collected in adDMEM/F12+++ . For co-culture assays, liver tumor-derived organoids were released from their BME matrix using dispase. For head and neck organoids: HN1 is T6⁵⁶, HN2 and HN3 have not previously been described.

Construction of chimeric NKG2D receptors

cDNAs for the type I NKG2D co-receptors were synthesized by BaseClear (Leiden, Netherlands). Type II co-receptors were created using overlap extension PCR. Both designs were cloned into pBullet. For the second version of the type I NKG2D chimeric co-receptors, the transmembrane and linker domains of the co-receptors NKG2D-ICOS_{wt} and NKG2D-4-1BB_{wt} were replaced by the transmembrane and linker domains of NKG2D-CD28_{wt} chimera using overlap extension PCR. They were all subcloned into pMP71 already containing $\gamma\delta$ TCR-Cl5, using XhoI and HindIII. All restriction enzymes were supplied by NEB (Massachusetts, USA).

Retroviral transduction of $\alpha\beta$ T-cells and cell-lines

Briefly, packaging cells (Phoenix-Ampho) were transfected with helper constructs gag-pol (pHIT60), env (pCOLT-GALV) and pMP71 or pBullet retroviral vectors containing genes codifying for the different proteins. In the case of human PBMCs, they were pre-activated with anti-CD3 (30 ng/mL; Orthoclone OKT3; Janssen-Cilag) and IL-2 (50 IU/mL; Proleukin, Clinigen). Both PBMCs and cell-lines were transduced twice with a viral supernatant within 48 or 3 hours respectively, in the presence of 6 μ g/mL polybrene (Sigma-Aldrich). For PBMCs 50 IU/mL of IL-2 was added. TCR-transduced T-cells were expanded by stimulation with anti-CD3/CD28 Dynabeads

(500,000 beads/ 10^6 cells; Life Technologies) and IL-2 (50 IU/mL). Thereafter, TCR-transduced T-cells were depleted of the non-engineered $\alpha\beta$ T-cells.

Depletion of non-engineered T-cells

$\alpha\beta$ T-cells transduced with $\gamma\delta$ TCR-Cl5 either alone, or together with NKG2D wild type, or the different NKG2D chimeras were incubated with a biotin-labeled anti- $\alpha\beta$ TCR antibody (clone BW242/412; Miltenyi Biotec, Bergisch Gladbach, Germany) and subsequently incubated with an anti-biotin antibody coupled to magnetic beads (anti-biotin MicroBeads; Miltenyi Biotec). Thereafter, the cell suspension was loaded onto an LD column and $\alpha\beta$ T-cells were depleted by MACS cell separation, per the manufacturer's protocol (Miltenyi Biotec). After depletion, TEGs were expanded, using a T-cell rapid expansion protocol (REP)¹⁴.

Selection of engineered T-cells

After $\alpha\beta$ -depletion, T-cells were selected using human CD4+ or CD8+ microbeads and MS columns (Miltenyi Biotec). The procedure was carried out according to the manufacturer's protocol.

Generation of reporter cell-lines

Lentiviral constructs were generated by inserting $\gamma\delta$ TCR-Cl5 with or without NKG2D-CD28_{WT} or NKG2D-4-1BB_{CD28TM} constructs by Gibson cloning into the lentiviral plasmid using the short EF1 α promoter. Sequence was verified by Sanger sequencing (Eurofin). For lentivirus production, 10^7 HEK293T cells were plated in 20 ml DMEM medium the day prior. HEK293T cells were co-transfected with the respective construct and the packaging plasmids pMD2.G (envelope) and pCMVR8.74 (gag/pol). Cells were then incubated at 37°C and 7.5% CO₂. The supernatant containing the lentiviral particles was collected 24 and 48 hours after transfection. Viruses were concentrated by 10% sucrose gradient (supplemented with 0.5 mM EDTA) centrifugation at 10.000g, 6°C for 4 hours. The virus pellet was resuspended in 100 μ l PBS and stored at -80°C until further use. Jurkat NF κ B and Jurkat NFAT reporter cell-lines expressing GFP under the control of the indicated transcription factor were used in this study⁶⁰. Cell-lines were grown in complete RPMI 1640 medium supplemented with 10% bovine serum and antibiotics at 37°C.

Reporter cell-lines were transduced by adding the concentrated lentivirus to the cell culture. Successful expression of NKG2D and the $\gamma\delta$ TCR was assayed by surface staining and flow cytometric analysis. To this end, cells were incubated for 15 min at 4°C with PE-coupled anti- $\gamma\delta$ TCR antibody coupled to PE (1/200, Life Technologies #MHGD04) and APC-coupled anti-NKG2D (1/200 Biolegend #320807). Cells were measured at the Attune™ NxT Flow Cytometer.

NKG2D ligand staining

The expression of NKG2D ligands in tumor cell-lines and organoids was assessed using Recombinant Human NKG2D Fc Chimera Protein (R&D systems, Abingdon, UK). 10^5 tumor cells were incubated either with 0.5 μ g of NKG2D Fc recombinant protein, or with IgG1-Fc for 30 min. Cells were washed with FACs buffer (1% BSA, 1% Na⁺azide) and a secondary antibody IgG-PE (Southern Biotech, Alabama, USA) was added in a 1:200 dilution. Cells were fixed using 1% PFA in PBS. Samples were measured on a BD LSR Fortessa, and FACSDiva (BD) software was used for data analysis.

Generation of NKG2D knockout TEGs by CRISPR/Cas9

NKG2D knockouts were performed following manufacturer's instructions (Integrated DNA technologies, IDT). In short, 23,8 μ M crRNA:tracrRNA, 9,89 μ M Cas9 nuclease and 1,8 μ M electroporation enhancer were combined with 2×10^6 cells. Cells were pulsed one time with a voltage of 1800 and 20 ms. Two different crRNA guides targeting NKG2D were used (1:1) to generate the KOs: guide 1 (GAAGTTCAAATTCCTTGAC) from Brunello library⁶¹ and guide 2 (AGAGTGATTTTCAACACGA) designed at IDT website (Custom Alt-R™ CRISPR-Cas9 guide RNA) using the first 600 nucleotides of the mRNA (NM_007360.4). As electroporation might influence TEGs fitness, the different TEGs were also electroporated with commercial negative control crRNA guide (IDT), and used in the functional assays as controls. Percentage of NKG2D-KO cells was assessed by flow cytometry on a BD LSR Fortessa, using huNKG2D (clone 1D11; 320802).

Functional T-cell assays

For CD69 expression, 200.000 T-cells per well were incubated in a 96 wells plate precoated with 0,2 ug/ml anti-huCD3 (clone OKT3; 130-093-387, Miltenyi Biotec), 5 µg/ml anti-huNKG2D (clone 1D11; 320802, Biolegend), or a combination of the two. Cells were incubated for 24 hours, after which they were incubated with anti-huCD69-APC (1:25; clone FN50; 2154550) from Sony Biotechnology for 30 min. Cells were washed with FACs buffer (1% BSA, 1% Na⁺azide) and fixed using 1% PFA in PBS. Samples were measured on BD FACs Canto and FACSDiva (BD) software was used for data analysis.

For cytokine detection, 5×10^4 effector T-cells were co-cultured for 18 hours with different tumor cell-lines, or with organoids in a 1:1 or 1:30 effector-to-target ratios (E:T) respectively, in round-bottom 96-well plates, in the presence of pamidronate. After incubation, supernatants were collected, and either frozen, or used to detect IFN γ levels straight away. ELISA was performed using IFN gamma Human Uncoated ELISA Kit (Thermo Fisher Scientific, Massachusetts, USA).

A ⁵¹chromium-release assay for cell-mediated cytotoxicity was previously described⁹. In brief, target cells were labeled for 2 hours with 100 µCu ⁵¹Cr and incubated for 4 to 5 hours with transduced T-cells in five effector-to-target ratios (E:T) between 10:1 and 0.11:1 in the presence of 10-30 µM of pamidronate. Percentage of specific lysis was calculated as follows: (experimental cpm - basal cpm)/(maximal cpm - basal cpm) x100 with maximal lysis determined in the presence of 5% triton, and basal lysis in the absence of effector cells.

For long term serial-killing assays and to assess PD1 and GZMB expression on CD4⁺ TEGs, 5×10^3 RPMI 8226, SCC9 or Fadu tumor cells expressing luciferase-GFP were co-cultured with effector T-cells at 3:1 or 1:1 effector:target ratio in presence of 10 µM pamidronate. To assess the ability of the different constructs to repetitively kill tumor cells, and to mimic chronic antigen exposure, new targets were added every 24 hours. Luciferin was added at 12.5 ug/ml and luminescence signal was measured on a Softmax pro machine at 24, 48, 72 and 96 hours. For PD1 and GZMB analysis, cells were stained after the 4th round of stimulation.

In order to assess proliferation, T-cells were resuspended at 1×10^6 cells/ml using a $2 \mu\text{M}$ solution of CellTrace™ Violet Cell Proliferation Kit (Thermo Fisher Scientific, Massachusetts, USA) in PBS. The cell suspension was incubated for 20 min at 37°C . Cells were washed two times with complete RPMI medium, and resuspended in culture medium. For proliferation after stimulation with antibodies, 200.000 labeled T-cells per well were incubated for 6 days in a 96 wells plate, pre-coated with different concentrations of anti-huCD3 (clone OKT3; 130-093-387, Miltenyi Biotec), anti-huNKG2D (clone 1D11; 320802, Biolegend) or a combination of the two. For the proliferation assay with tumor cell-lines, 2.5×10^5 labeled effector T-cells were co-cultured, together with 2.5×10^5 tumor cells in 48-well plates for 6 days, $100 \mu\text{M}$ pamidronate was added to cultures to boost recognition. On Day 6, cells were analyzed by flow cytometry. For the proliferation assays with organoids, 1×10^5 labeled T-cells were co-cultured with organoids in a E:T ratio of 1:1,5 in 96-U well plate, in the presence of pamidronate ($100 \mu\text{M}$) during 6 days. On Day 6, proliferation was assessed by flow cytometry.

For activation assays using the reporter cell-lines, 100.000 Jurkat reporter cells were incubated with RPMI-8226 or HL60 cells at a 1:1 Effector:Target (E:T) ratio for 24 hours on 96-well plates. Cells were then analyzed by flow cytometry for GFP expression. Samples were measured at the Attune™ NX7 Flow Cytometer. FlowJo was used for data analysis.

3D model

The 3D model was previously described in detail ²⁹. The RPMI 8226 or SCC9 tumor cells were stained with Vybrant DiO or Dil (Thermo Fisher, United States) and seeded in Matrigel (Corning, United States). In the RPMI-8226 experiments multipotent mesenchymal stromal cells (MSCs) were stained with Vybrant DiD (Thermo Fisher, United States) and were added to the model on the same day. After four days, the different TEGs were stained with Vybrant Dil (Thermo Fisher, United States) or CTV and administered to the model, together with and $10 \mu\text{M}$ PAM (Calbiochem, United States). Three and/or six days later, the Matrigel was dissolved using Dispase (Corning, United States) to retrieve the cells from the model. Tumor, T-cells and stromal cells were quantified by FACS, using Flow count Fluorospheres (Beckman Coulter,

United States). Cell numbers were normalized to mock treatment. Luminex was performed on supernatant to measure cytokine levels for IL2, IL4, IL6, IL10, IL17, CCL1, CCL4, CCL7, CCL8, CCL20, CCL22, CCL28, CXCL1, CXCL9, IP10, CXCL12 and GMCSF at days 3 and 6 after TEG administration.

Animal models

NOD.Cg-PrkdcscidIl2rgtm1Wjl/SzJ (NSG) mice originally obtained from Jackson Laboratory (Bar Harbor, ME, USA) were bred and housed in the breeding unit of the Central Animal Facility of Utrecht University or purchased from Charles River Laboratories (Germany). Experiments were conducted under institutional guidelines, after obtaining permission from the Animal Welfare Body Utrecht (nos. 4288-2-12, 4288-2-19, 4288-2-21, 4288-1-10, 16349-1-02) and in accordance with the current Dutch laws on Animal Experimentation. Male and/or female mice were used in the different models, as indicated in the figure legends. Mice were housed under 45–65% humidity and a daily 12/12-h light/dark regime, in sterile conditions, using an individually ventilated cage (IVC) system and fed with sterile food (V1534-703, Ssniff) and water. Irradiated mice were given sterile water with the antibiotic Ciproxin for the duration of the experiment. Mice were randomized with equal distribution by sex (when using male and female). Power analysis was used to determine sample sizes by using G*Power software (F test, ANOVA, Fixed effects, omnibus, one-way). Adult mice (10-19 weeks old) received sublethal total body irradiation (1.75 Gy) on Day -1. On Day 0, depending on the model, NSG mice were injected either intravenously with 5×10^6 RPMI 8226-luciferase cells resuspended in PBS or subcutaneously with $0,5 \times 10^6$ SCC9-luciferase tumor cells resuspended in mixture of matrigel and PBS (1:1). On Days 1 and 7, mice were injected intravenously with 1×10^7 of different engineered T-cells (TEGs). The average CD4+/CD8+ ratio for functional TEGs was approximately 1:1 across all experiments. All mice received 0.6×10^6 IU of IL-2 (Proleukin; Clinigen) in 100 μ l incomplete Freund's adjuvant (IFA) subcutaneously, together with the first TEGs injection, and every 3 weeks until end of experiment. Pamidronate (10mg/kg body weight) was injected intravenously, together with the T-cell injections, and every 3 weeks until the end of the experiment, in order to enhance activation of TEGs as previously reported ¹⁴. Tumor growth was monitored weekly by bioluminescence.

Furthermore, in the subcutaneous model, tumor volumes were measured weekly, and calculated by using the formula $tumor\ volume = 0.4 \times (length \times width^2)$. Maximal allowed tumor size was 1500 mm³, as agreed with the ethics committee, and was not exceeded in these experiments. In the RPMI 8226-luc model, mouse survival was assessed at least twice a week, by monitoring weight loss and symptoms of disease (sign of paralysis, weakness, and reduced motility). For the SCC9 model survival could not be addressed as tumors got ulcerated around day 55, independently of size, and mice need to be sacrificed for ethical reasons.

Assessment for TEGs persistence *in vivo*

Blood samples were obtained via cheek vein (max. 50–70 µl/mouse). Red blood cells were lysed using 1× RBC lysis buffer (Biolegend) and were then stained with a mixture of antibody. To assess persistence of cells in bone marrow we collected femur and tibia from the hind legs. Bone marrow cells were obtained by centrifugation at 9000 x g for 15 sec. Cell pellet was resuspended in PBS. Spleen was collected and processed into single-cell suspension. Spleen was cut in small pieces and filtered through a 70 µm cell strainer (BD). Spleen was incubated with 1× RBC lysis buffer cells for maximum 4 min. After that, spleen filtered cells were washed and resuspended in PBS. 1×10^6 cells were used for staining. The persistence of TEG cells was calculated using Flow-count Fluorospheres (Beckman Coulter) and measured by flow cytometry (BD LSRFortessa).

scRNA-seq sequencing

TEGs were co-cultured together with RPMI 8226 cells (E:T 1:1) in the presence of 10 µM PAM during 48h. After incubation, cells were sorted by expression of $\gamma\delta$ TCR+CD4+ or $\gamma\delta$ TCR+CD8+ (pan- $\gamma\delta$ TCR-PE, clone IMMU510; CD4-PB, clone RPA-T4; CD8-PerCP Cy5.5, RPA-T8) into 384-well PCR plates (BioRad) using ARIA II. Cells were sequenced by Single Cell Discoveries (Utrecht, The Netherlands) according to the SORT-seq method based on CEL-Seq2⁶², and libraries were sequenced with paired end sequencing on Nexseq500 by the Utrecht Sequencing Facility (USEQ, Life Sciences Faculty, Utrecht University). The gene expression matrix was processed and analyzed using the *Seurat* package in R. Before dimensionality reduction and clustering, low-

quality cells (number of genes detected < 200 or mitochondrial UMIs > 30% or ERCC reads > 50%) were excluded. For the NKG2D-chimeras experiment, we collected 2355 single cells with high-quality RNA profiles, representing both the CD4+ and CD8+ subpopulations of TEG001 (TEG), TEG001-NKG2D-CD28_{WT} (NKG2D-CD28) or TEG001-NKG2D-4-1BB_{CD28TM} (NKG2D-4-1BB) cells. CD4-CD8 annotation was based on the surface expression on these surface markers during sorting. For the 103-4-1BB-chimera experiment, we collected 1153 single cells with high-quality RNA profiles, representing both the CD4+ and CD8+ subpopulations of TEG001 (TEG) and TEG001-103-4-1BB (103-4-1BB). To test the differences in overall cluster composition of the chimeras, relative to TEG001 dataset we applied Pearson's Chi-squared test. To investigate the per-cluster differences, we applied `Fisher's Exact Test for Count Data` contrasting the per-cluster relative abundance values of a chimera to the per-cluster relative abundance values of the TEG001 construct. To run these test, we used the *chisq.test* and *fisher.test* function of the *stats* R-package. (Results are summarized in Supplementary table 2, where p-value<0,001 is marked.)

Dimensionality reduction, clustering and visualization

Data were normalized, scaled to 10000 counts, and log-transformed using the *NormalizeData* function of the *Seurat* package. Principal component analysis was performed on the scaled data with the 4000 most variable genes. The number of principal components used was determined using the *ElbowPlot* function. Following Uniform Manifold Approximation and Projection (UMAP) based dimensionality reduction for visualization, we calculated clusters, using the *FindNeighbors* and *FindClusters* functions with the resolution parameter set to 0.3. Marker genes that differentiated between clusters were identified using the *FindAllMarkers* function. We applied gene ontology (GO) over-representation test with *clusterProfiler*⁶³, to identify the terms that were significantly enriched for the cluster marker genes. With regard to the annotation the clusters with biological terms, GO analysis was the primary source, but we also considered canonical marker genes but not necessarily listed in the reference dataset (for example: exhaustion).

Statistical analysis

scRNA-seq statistical analysis was completed as described above, extended with statistical tests applied using the `chisq.test` and `fisher.test` function of the *stats* R-package. All other statistical analyses were performed using GraphPad Prism. Data distribution was assumed to be normal, but this was not formally tested. Exact tests and P values are shown either in graphs or legends. P values > 0.05 were considered not significant (n.s.). All data points were analyzed including outliers unless there were technical errors.

Data Availability

Raw sequencing data for this study have been deposited into Gene Expression Omnibus (GEO): GSE244053 (<https://www.ncbi.nlm.nih.gov/geo/query/acc.cgi?acc=GSE244053>).

Code Availability

In this study, we employed published and publicly available software packages to conduct all data analysis. Source data and scripts for scRNAseq analyses and visualization are deposited in Zenodo (<https://doi.org/10.5281/zenodo.8378941>). Any additional information required to reanalyze the data reported in this manuscript is available from the lead contact upon request.

Results

Co-expression of NKG2D-chimeras rescues suboptimal TEG001 activation

Suboptimal TCR-engagement is often a limitation for TCR-based cancer immune therapies^{8, 24}. To overcome this, we combined cancer-metabolome targeting through TEG001 with targeting of cancer-associated stress antigens, using three different NKG2D-derived chimeric co-receptors. Only type I designs, in combination with CD28 transmembrane domains led to optimal expression of NKG2D-chimeras (Extended data figure 1A-D). The NKG2D-chimeras were created by linking the extracellular domain of NKG2D to the hinge and transmembrane domains of CD28, and the intracellular signaling domain of ICOS, CD28 or 4-1BB (Figure 1A). $\gamma\delta$ TCR chains were combined

with NKG2D_{wt} or with the NKG2D-chimeras, in a tricistronic construct to ensure equimolar expression in engineered primary αβT-cells (Extended data figure 1D). First, we assessed whether engagement of the different NKG2D-chimeras or NKG2D_{wt} could rescue activation of T-cells when TCR-engagement was limited. Suboptimal CD3 stimulation (mimicking suboptimal TCR-engagement), through low concentration of anti-CD3 antibody, combined with stimulation by an anti-NKG2D antibody, increased expression of CD69 in TEG001, only when one of the NKG2D-chimeras or NKG2D_{wt} were co-expressed (Extended data figure 1E). Of note, triggering of the NKG2D-CD28_{wt}-chimera in the absence of TCR-engagement did lead to a small, but significant, upregulation of CD69, which is in line with earlier observations that antibody-induced stimulation of CD28 upregulates CD69²⁵.

IFNγ release but not killing is improved by NKG2D-4-1BB_{CD28TM}-chimera

We next investigated whether the increased signaling induced by the NKG2D-chimeras is preserved when using tumor cells expressing natural NKG2D-ligands for the activation of CD4+ TEG001. A panel of tumor cell-lines was selected based on their reported susceptibility to γ9δ2TCR-mediated recognition^{10, 14} and characterized for NKG2D-ligand expression by utilizing a NKG2D-Fc fusion protein (Extended data figure 2A). Three tumor cell-line phenotypes were identified: (I) **recognized** by TEG001 and **low** NKG2D-ligand expression (Daudi), (II) **recognized** by TEG001 and **high** NKG2D-ligand expression (SCC9, K562 and RPMI-8226) and (III) **not recognized** by TEG001 and **high** NKG2D-ligand expression (HL60).

First, we assessed the impact of the NKG2D-chimeras on IFNγ secretion by CD4+ TEGs in a co-culture with tumor cell-lines expressing high or low levels of NKG2D-ligands under varying pamidronate (PAM) concentrations, which was used to modulate intracellular pAg concentration in the tumor cells²⁶. The most prominent increase in activity was observed for TEG001-NKG2D-4-1BB_{CD28TM}, which secreted higher levels of IFNγ against K562 (NKG2D-ligand high) compared to TEG001 (Extended data figure 2B). This effect was most significant at lower PAM concentrations, implying again that co-stimulation becomes important once TCR-engagement is limited. No IFNγ secretion was

detected when NKG2D_{wt} or the NKG2D-chimeras were co-expressed with a non-functional $\gamma\delta$ 2TCR [10], called TEG-LM1. In contrast, there were no differences in killing observed between CD8+ TEG001 and TEG001 co-

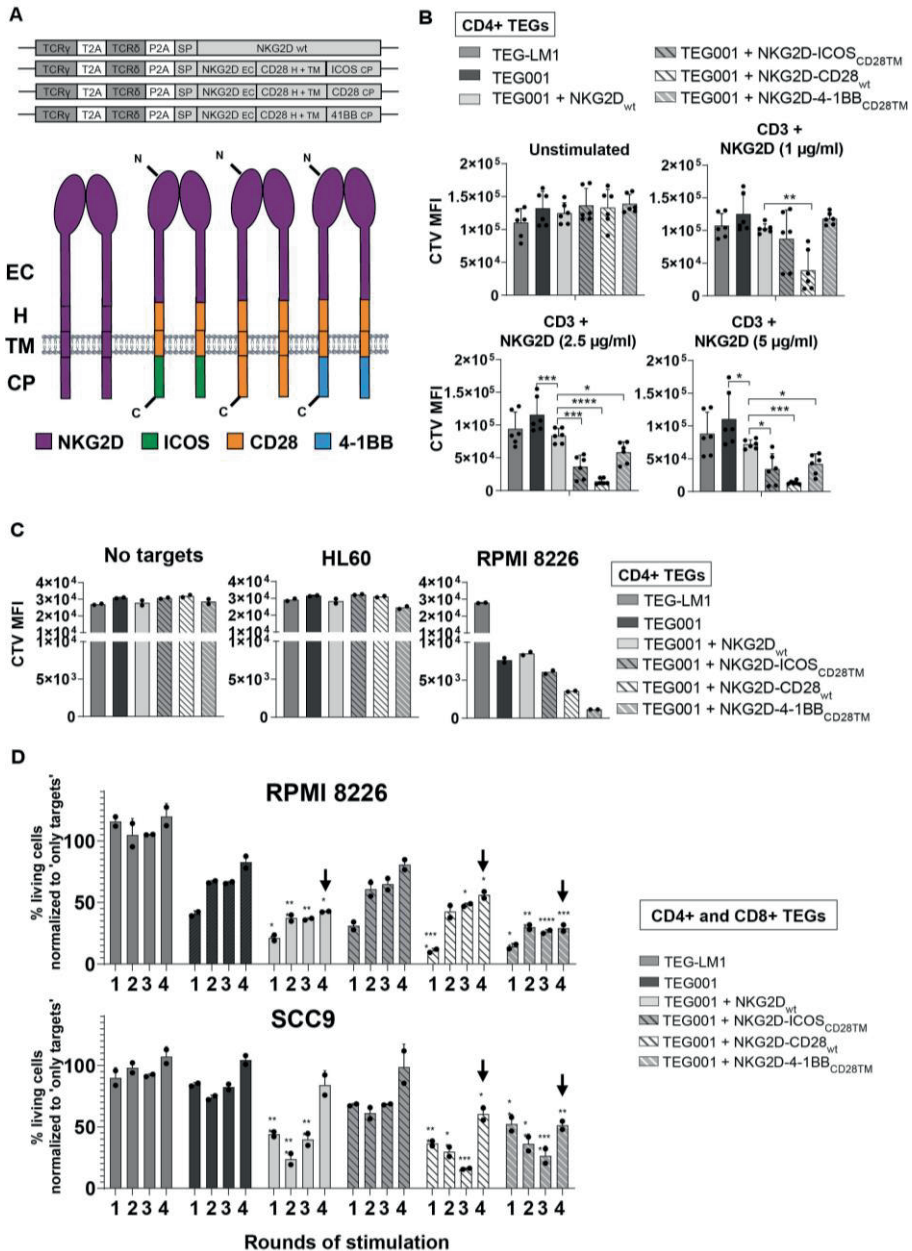


Fig. 1. Introduction of NKG2D chimeras improves proliferation and long-term killing activity of TEGs.

a, Schematic overview of type I chimeras containing CD28 transmembrane (TM) and hinge (H) domains and a $\gamma\delta$ TCR transgene cassette in the retroviral vector pMP71. TCR δ chain was derived from clone 5 and TCR γ from clone 5, and P2A (derived from the porcine teschovirus 1 2A) and T2A (derived from the Thoesea as signa virus) refer to two different 2A ribosomal skipping sequences. NKG2D, ICOS, CD28 and 4-1BB domains are colored in purple, green, orange and blue, respectively; SP, signal peptide; EC, extracellular; CP, cytoplasmic. b, Proliferation of CD4+ transduced T cells after stimulation with anti-CD3 and anti-NKG2D; n = 3 independent experiments with two biological replicates each. Data represent CTV mean fluorescence intensity (MFI) \pm s.d., and significance was calculated using a one-way analysis of variance (ANOVA) with a Holm-Sidak correction for multiple comparisons (NKG2D, 1 μ g ml⁻¹: NKG2D-CD28WT **P = 0.0021; NKG2D 2.5 μ g ml⁻¹: NKG2D_{WT} **P = 0.0063, NKG2D-ICOS_{CD28TM} ***P = 0.0002, NKG2D-CD28_{WT} ****P

expressing the different NKG2D-chimeras or NKG2D_{wt} when using chromium (⁵¹Cr) labeled HL60, Daudi, K562, RPMI-8226 and SCC9 tumor cells (Extended data figure 2C). This data suggests that the short-term killing potential of the CD8+ TEGs is not influenced by these costimulatory chimeras, or that endogenous NKG2D expression by CD8+ TEGs can overrule effects observed with CD4+ TEGs, which lack endogenous NKG2D expression (Extended data figure 3A).

NKG2D-chimeras enhance proliferation overcoming low TCR-ligand density

It has been reported that variations in costimulatory signaling impact proliferation capacity of CAR-T cells²⁷. To assess whether this also holds true when a combined signaling of $\gamma\delta$ TCR and NKG2D-chimeras is used, we examined the proliferation capacity of both CD4+ and CD8+ TEG001 cells co-transduced with NKG2D_{wt} or NKG2D-chimeras using antibody stimulation. Co-expression of NKG2D_{wt} in CD4+ TEGs resulted in an enhanced proliferation, when compared to conventional TEG001 (Figure 1B). Interestingly, co-expression of the NKG2D-chimeras resulted in significantly increased proliferation compared to TEG001-NKG2D_{wt}, emphasizing the importance of the intracellular co-stimulatory signaling domain in the NKG2D-chimeras. Intriguingly, under the most stringent conditions (1 μ g/ml NKG2D antibody) only TEG001-NKG2D-CD28_{wt} showed a significant increase in proliferation compared to TEG001-NKG2D_{wt} (Figure 1B). In CD8+ TEGs with endogenous NKG2D expression, stimulation with the anti-NKG2D antibody induced proliferation of TEG001 and TEG-LM1 compared to unstimulated condition, reducing thus the overall observed differences between the constructs

(Extended data figure 3B). This suggests that the endogenous expression of NKG2D in CD8+ TEGs can overrule the effect of the chimeras.

As differences were more profound in the absence of endogenous NKG2D, and stimulation by anti-NKG2D antibodies could again overestimate the impact of co-receptor signaling, we next focused on the proliferation ability of CD4+ TEGs after stimulation with the natural ligands. As expected, CD4+ TEG001, but not CD4+ TEG-LM1 (mock), were able to proliferate when co-cultured with RPMI-8226 tumor cells (Figure 1C and Extended data figure 3C). In contrast to the antibody-based assay, co-expression of NKG2D_{wt} no longer improved proliferation compared to TEG001. Once more, addition of the NKG2D-chimeras to TEG001 increased proliferation when compared to TEG001-NKG2D_{wt}, highlighting the added benefit of a chimeric co-receptor with additional signaling domains. Despite the high levels of NKG2D-ligands on HL60, none of the engineered T-cells proliferated when co-cultured with these cells, implying that $\gamma\delta$ 2TCR activation is essential for the additive effect of the NKG2D-chimeras.

NKG2D_{wt}, NKG2D-CD28_{wt} and NKG2D-4-1BB_{CD28TM} increase serial killing

Although we did not see enhanced short-term killing when co-expressing the different NKG2D chimeras (Extended data figure 2C), we postulated that co-expression of NKG2D-chimeras would impact TEG serial killing over time, as reported recently for T-cells engineered with a FAS-4-1BB fusion protein²⁰. As serial killing of tumor cells depends on both CD4+ and CD8+ engineered T-cells²⁸, a mixture of CD4+ and CD8+ (1:1) TEGs were challenged every 24 hours with new target cells. Overall, TEG001-NKG2D_{wt}, TEG001-NKG2D-CD28_{wt}, or TEG001-NKG2D-4-1BB_{CD28TM}, showed increased killing ability even after the 4th rechallenge against RPMI-8226, and the latter two also showed increased killing ability against SCC9 (Figure 1D), while TEG001-NKG2D-ICOS_{CD28TM} did not have any additive effect in killing ability when compared to TEG001. In contrast to the chromium-release readout, significant improved killing was observed after one stimulation, probably due to the differences in length of incubation and CD4:CD8 ratio.

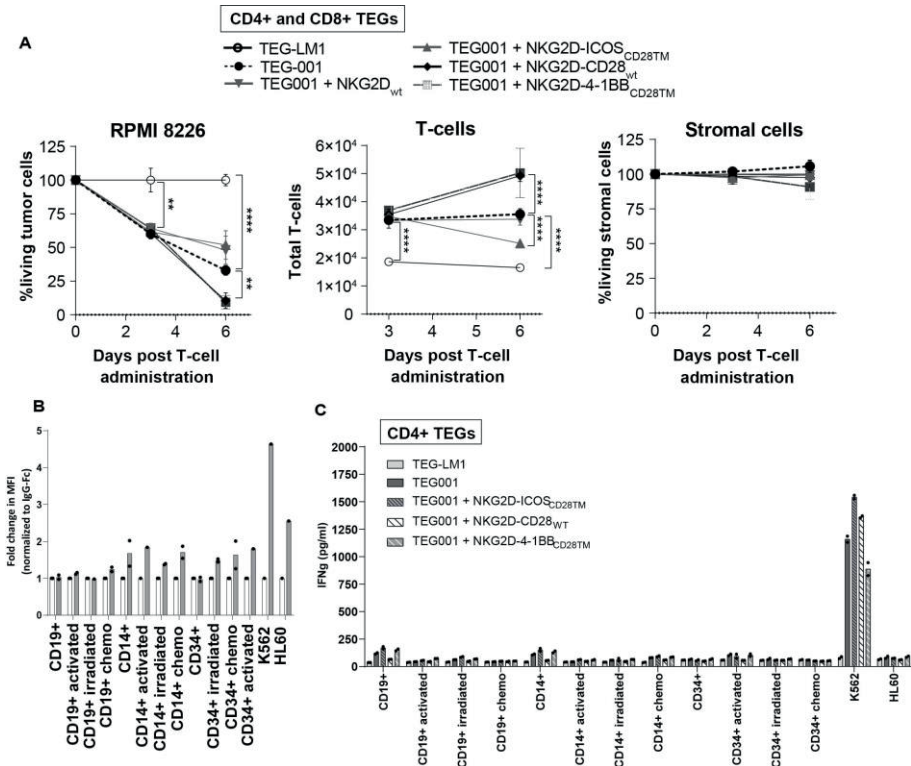


Fig. 2. NKG2D-CD28^{WT} and NKG2D-4-1BB^{CD28TM} improve persistence and tumor targeting without damaging healthy tissue. a, RPMI-8226 tumor cells expressing luciferase and stroma cells were cultured in Matrigel constituting a 3D bone marrow niche. After 4 d, CD4⁺ and CD8⁺ TEGs (at a ratio of 1:1) were added together with 10 μ M PAM. Three and 6 d later, living tumor cells (left), T cells (middle) and stroma cells (right) were quantified by FACS. Tumor and stroma cell numbers were normalized to those in the mock treatment (TEG-LM1) group; n = 2 independent experiments with two biological replicates each. Data represent mean \pm s.d. Significance was calculated using a two-way ANOVA with a Dunnett correction (day 3: TEG-LM1 versus TEG001 **P = 0.0056; day 6: TEG-LM1 versus TEG001 ****P < 0.0001, day 6, TEG-LM1 versus TEG001 ****P < 0.0001, TEG001 versus TEG001-NKG2D-ICOS_{CD28TM} ****P < 0.0001, TEG001 versus TEG001-NKG2D-4-1BB_{CD28TM} ****P < 0.0001. b, Surface expression of NKG2D ligands on healthy hematopoietic cells in resting, activated or stressed states. MFI was measured by flow cytometry using NKG2D-Fc and IgG-Fc fusion proteins. Fold change was calculated per type of cells as MFI measured using the NKG2D-Fc condition (gray) relative to the IgG-Fc condition (white); n = 2 independent experiments. Data represent mean; chemo, chemotherapy. c, CD4⁺ TEG001 cells or TEG001 cells coexpressing NKG2D-ICOS_{CD28TM}, NKG2D-CD28_{WT} and NKG2D-4-1BB_{CD28TM} were cocultured with healthy hematopoietic cells in resting, activated (CD40L, lipopolysaccharide or IFN γ) or stressed (irradiation or a combination treatment with cyclophosphamide and fludarabine) states in the presence of 100 μ M PAM. IFN γ release was measured by enzyme-linked immunosorbent assay (ELISA); n = 2 independent experiments. Data represent mean.

NKG2D-CD28_{WT} and NKG2D-4-1BB_{CD28TM} improve tumor killing in a 3D model

Co-expression of NKG2D-CD28_{WT} or NKG2D-4-1BB_{CD28TM} in TEG001 cells significantly improved TEG001 function. To further explore the benefits of NKG2D-chimeras, we increased the difficulty for the engineered T-cells to target tumor cells by mimicking a physiological tumor microenvironment (TME) in a 3D bone marrow niche model²⁹. After 3 days, TEG001 and TEG001 co-expressing the NKG2D-chimeras significantly increased killing of RPMI-8226 compared to TEG-LM1. No difference in tumor control between the functional constructs was observed (Figure 2A). However, on day 6 TEG001-NKG2D-CD28_{WT} and TEG001-NKG2D-4-1BB_{CD28TM} significantly increased tumor control compared to TEG001. Enhanced T-cell activity of TEG001-NKG2D-CD28_{WT} and TEG001-NKG2D-4-1BB_{CD28TM} on day 6 was also reflected by significantly higher numbers of T-cells compared to TEG001. Luminex analysis of the supernatants revealed a significant increase of chemokines (CCL1, CCL4, CCL8, CCL20, CCL22, CXCL9 and CXCL10) at Day 3 for TEG001-NKG2D-CD28_{WT}, and TEG001-NKG2D-4-1BB_{CD28TM} (Supplementary table 1) suggesting improved interaction of TEGs with the microenvironment in the presence of the chimeras. In summary, the 3D model hinted at the superiority of TEG001-NKG2D-CD28_{WT} and TEG001-NKG2D-4-1BB_{CD28TM}.

Dual-targeting preserves cells derived from healthy tissues

By quantification of the remaining viable stromal cells (MSCs) in the 3D bone marrow niche model, we assessed the impact of the TEG treatment on healthy tissues. TEGs preserved healthy tissues (Figure 2A, right panel) while displaying tumor specificity in the very same experimental set up. To further preclude the potential risk of targeting healthy tissues, we extended the analyses to stressed healthy tissues, which can temporarily upregulate NKG2D-ligands³⁰. Recognition of several healthy donor-derived hematopoietic cell subsets was assessed in resting, stressed (irradiated or treated with cyclophosphamide and fludarabine), or activated (treated with huCD40LT, LPS or IFN γ) states. Upregulation of NKG2D-ligands was observed for all CD14⁺ cells and for the stressed CD34⁺ cells, but not for CD19⁺ cells (Figure 2B). However, upregulation of NKG2D-ligands on healthy cell subsets,

did not result in recognition of targets by TEGs (Figure 2C), suggesting an advantageous safety profile of TEG001 co-expressing NKG2D-chimeras.

NKG2D-4-1BB_{CD28TM} and NKG2D-CD28_{WT} improve *in vivo* targeting of liquid tumors

To assess how TEG001 and TEG001 co-expressing NKG2D-chimeras behave *in vivo*, we established a human multiple myeloma (MM) xenograft model utilizing the same target cells as we used in the 3D model (RPMI-8226) (Figure 3A). Treatment with TEG001-NKG2D-CD28_{WT} or TEG001-NKG2D-4-1BB_{CD28TM} improved tumor control compared to TEG001, while co-expression of NKG2D_{WT} or NKG2D-ICOS_{CD28TM} did not lead to improved tumor control (Extended data figure 4A,B). Importantly, this improved tumor control by TEG001-NKG2D-CD28_{WT} or TEG001-NKG2D-4-1BB also resulted in significantly prolonged survival compared to treatment TEG001 (Figure 3B). The net treatment effect for TEG001 compared to TEG-LM1 treatment was 12 days, while for the groups treated with TEG001-NKG2D-CD28_{WT} or TEG001-NKG2D-4-1BB_{CD28TM} this was more than doubled, with a net treatment effect of 31.5 and 28 days respectively. Bone marrow from sacrificed mice was collected, and the number of TEGs was assessed by FACS (Figure 3C). Interestingly, a significantly higher number of TEG001-NKG2D-4-1BB_{CD28TM} was observed, compared to TEG001 and TEG001-NKG2D-CD28_{WT}, suggesting different dynamics for the different chimeras.

TEG dynamics *in vivo* substantially differ between formats

To further investigate the effect of the introduction of NKG2D-CD28_{WT} and NKG2D-4-1BB in TEG001 on TEG dynamics *in vivo*, the RPMI-8266 MM xenograft model was modified by labeling the TEGs administered in the second injection (Day 7) with CTV (Figure 3D). In line with the long-term survival model, tumor burden was significantly reduced after 2 weeks in mice treated with TEG001-NKG2D-CD28_{WT} when compared to TEG001. TEG001-NKG2D-4-1BB_{CD28TM} also showed marked tumor control when compared to TEG001 (Figure 3E). In line, the number of tumor cells (GFP+) measured by FACS in bone marrow was significantly reduced for TEG001-NKG2D-CD28_{WT}

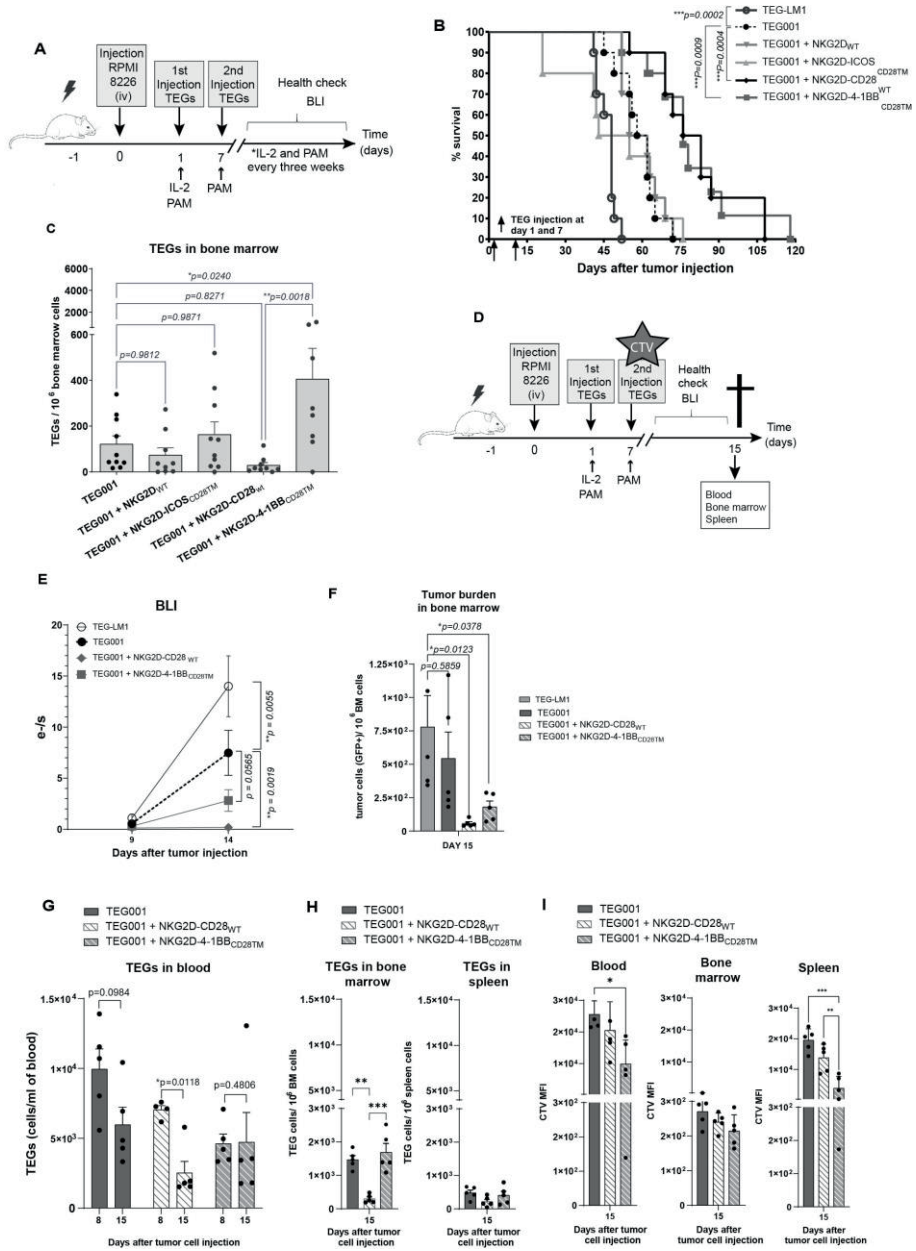


Fig. 3 | In vivo efficacy and proliferation of TEGs coexpressing NKG2D chimeras in an MM model. a, Experimental setup to evaluate in vivo efficacy of TEG001-NKG2D chimeras against RPMI-8226 tumors in male and female NSG mice; i.v., intravenous. b, Survival was assessed by monitoring weight loss and symptoms of disease. Data were generated from one experiment with $n = 10$ mice per treatment. One mouse was censored at day 63 in the TEG001-NKG2D-4-1BB^{CD28TM} group due to non-tumor-related death. Significance was calculated by log-rank (Mantel-Cox) test. c, Comparison between the numbers of TEG001 ($n = 10$ mice), TEG001-NKG2D^{WT} ($n = 9$ mice), TEG001-NKG2D-ICOS^{CD28TM} ($n = 10$ mice), TEG001-

NKG2D-CD28_{WT} (n = 9 mice) and TEG001-NKG2D-4-1BB_{CD28TM} (n = 8 mice) cells in mouse bone marrow. Data represent mean \pm s.e.m. and were generated from one experiment. Significance was calculated by using a one-way ANOVA with a Tukey correction. d, Experimental setup to evaluate *in vivo* proliferation of TEG001-NKG2D chimeras against RPMI-8226 tumors in female NSG mice. e, Tumor burden was measured by BLI. Data were generated from one experiment with n = 5 mice per treatment group. Data represent mean \pm s.e.m. Statistical significance was calculated by a mixed-effects model test with a Dunnett correction for multiple comparisons per time point. f, Tumor burden quantified by the number of GFP+ cells in bone marrow. Data were generated from one experiment with n = 5 mice per treatment group. Data represent mean \pm s.e.m. Significance was calculated by using a one-way ANOVA with a Dunnett correction. g, Comparison between the number of different TEGs in blood. Data represent mean \pm s.e.m. Data were generated from one experiment with n = 5 mice per treatment. Significance was calculated using a paired one-tailed t-test. h, Comparison between the number of different TEGs in bone marrow and spleen. Data represent mean \pm s.e.m. Data were generated from one experiment with n = 5 mice per treatment group. Significance was calculated using a one-way ANOVA with a Bonferroni correction (TEG001 versus TEG001-NKG2D-CD28_{WT} **P = 0.0011; TEG001-NKG2D-CD28_{WT} versus TEG001-NKG2D-4-1BB_{CD28TM} ***P = 0.0003). i, Proliferation of different TEGs was measured by CTV MFI decreases in the blood, bone marrow and spleen. Data represent mean \pm s.d. Data were generated from one experiment with n = 5 mice per treatment group. Significance was calculated using one-way ANOVA with a Bonferroni correction (blood: TEG001 versus TEG001-NKG2D-4-1BB_{CD28TM} *P = 0.0148; spleen: TEG001 versus TEG001-NKG2D-4-1BB_{CD28TM} ***P = 0.0001, TEG001-NKG2D-CD28_{WT} versus TEG001-NKG2D-4-1BB_{CD28TM} **P = 0.0064)

and TEG001-NKG2D-4-1BB_{CD28TM}, compared to TEG-LM1 (Figure 3F). The number of T-cells in peripheral blood was monitored on Days 8 and 15 (1 and 8 days respectively after the 2nd T-cell injection). When comparing the functional TEGs, a significant decrease in the number of T-cells in blood between Days 8 and 15 was observed for TEG001-NKG2D-CD28_{WT} (Figure 3G). Moreover, the number of TEG001 cells was also lower on Day 15 compared to Day 8. In contrast, no drop in T-cell numbers was observed for TEG001-NKG2D-4-1BB_{CD28TM}. Interestingly, mice treated with TEG001-NKG2D-CD28_{WT} also had a lower number of TEGs both in bone marrow and spleen (Figure 3H), when compared to TEG001 and TEG001-NKG2D-4-1BB_{CD28TM}. The analysis of the MFI for CTV implied significantly increased proliferation of TEG001-NKG2D-4-1BB_{CD28TM}, compared to TEG001 in blood and spleen (Figure 3I). Altogether, differences observed between TEG001-NKG2D-CD28_{WT} and TEG001-NKG2D-4-1BB_{CD28TM} in killing at early time points (Figure 3E,F) and in the *in vivo* proliferation rate (Figure 3G-I) suggest that, *in vivo*, TEG001-NKG2D-CD28_{WT} induced strong and fast killing of tumor cells during the first days (Figure 3E,F), followed by the death of these TEGs (Figure 3G-I). By contrast, TEG001-NKG2D-4-1BB_{CD28TM} showed an advantage during chronic-antigen stimulation because of their enhanced capacity to proliferate. Nevertheless, both modes of action resulted in equally improved survival in the long-term MM *in vivo* model (Figure 3A-B).

TEG001-NKG2D-4-1BB_{CD28TM} improves *in vivo* efficacy against solid tumors

Accomplishing tumor control in solid tumors is substantially more challenging than in liquid tumors³¹. To address whether the NKG2D-chimeras could also enhance tumor control against solid tumors, NSG mice were subcutaneously injected with SCC9-luciferase tumor cells and treated on Days 1 and 7 with TEG-LM1 (mock), TEG001, TEG001-NKG2D-CD28_{WT} or TEG001-NKG2D-4-1BB_{CD28TM} (Extended data figure 5A). In this model, TEG001-NKG2D-4-1BB_{CD28TM} was the only design that consistently showed a significant delay in tumor outgrowth assessed by tumor volume and BLI when compared to TEG-LM1 and TEG001 (Extended data figure 5B-C). Our results imply that differences in T-cell dynamics might have different impacts on clinical outcomes for both liquid and solid tumors.

Improved activity of TEG001-NKG2D-4-1BB_{CD28TM} against cancer organoids

As TEG001-NKG2D-4-1BB_{CD28TM} showed the best tumor control in the solid tumor *in vivo* model, we decided to further investigate whether this increased targeting also holds true for a panel of patient-derived tumor organoids, from head and neck cancer (HN), hepatocellular carcinoma (HCC) and hepatoblastoma (HB). The expression of NKG2D-ligands varied amongst the different organoids (Extended data figure 6A). TEG001-NKG2D-4-1BB_{CD28TM} significantly increased IFN γ release against one of the patient-derived organoids (HCC-1) and showed a marked increase against two HB organoids (HB-10 and HB-13) (Extended data figure 6B). Since the most profound effects of NKG2D co-stimulation was on T-cell proliferation (Figure 1C), we assessed T-cell proliferation upon co-culture with different organoids (Extended data figure 6C,D). An increase in proliferation for TEG001-NKG2D-4-1BB_{CD28TM} compared to TEG001 was observed upon co-culturing with most of the organoids. In conclusion, recognition of primary solid tumors by TEG001 can be improved by the addition of NKG2D-chimeras.

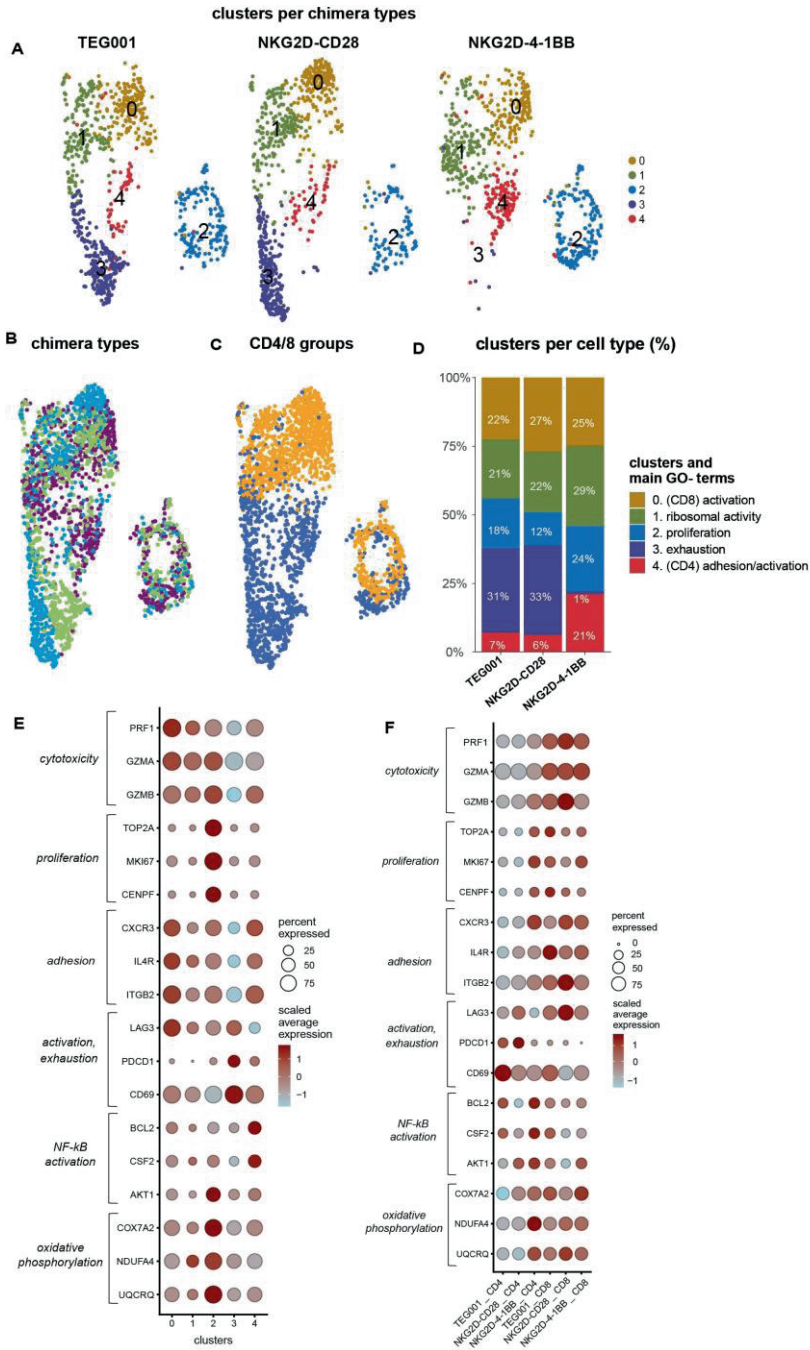


Fig. 4. Single-cell transcriptomic analysis of TEG001, TEG001-NKG2D-CD28_{WT} and TEG001-NKG2D-4-1BB_{CD28TM} cells after incubation with RPMI8226. a–c, Uniform manifold approximation and projection

(UMAP) clustering of TEG001, TEG001-NKG2D-CD28_{WT} and TEG001-NKG2D-4-1BB_{CD28TM} cells (839, 819 and 697 cells; 2,355 cells in total) split by chimera types. Cells are annotated by clusterID (a), chimera types (b) or CD4-CD8 FACS profiles (c). d, Percentage representation of the clusters (annotated by the main GO terms) across the cell types (cluster 0 'CD8 activation' (marker genes: CD8 α , CSF1 and CCL5), cluster 1 'ribosomal activity' (marker genes: RPS27 and RPS29), cluster 2 'proliferation' (marker genes: TOP2A and MKI67), cluster 3 'exhaustion' (marker genes: DUSP1 and PDCD1) and cluster 4 'CD4 adhesion and activation' (marker genes: CD4, IL2RA and PRKAR1A)). e, Density dot plot of the percentage of cells in a cluster that express a given gene ('percent expressed') and the scaled average expression of canonical markers. f, Density dot plot of the percentage of cells from chimera types that express a given gene ('percent expressed') and the scaled average expression of canonical markers

NKG2D-4-1BB_{CD28TM} skews CD4+ TEG001 transcriptomics to less exhaustion

Transcriptomic and functional heterogeneity among engineered T-cells has been described recently¹². To assess whether co-stimulation impacts the profile of a defined subpopulation or skews transcriptomic heterogeneity, we focused on how NKG2D-CD28_{WT} and NKG2D-4-1BB_{CD28TM} Chimeras impacted transcriptomic heterogeneity of TEG001, and whether this could explain the observed functional phenotypes and different behaviors in different tumor models. We carried out FACS-assisted single-cell RNA sequencing (SORT-seq) experiments after antigen encounter on tumor cells (RPMI-8226). Unsupervised clustering of the combined dataset revealed five clusters (Figure 4A). In terms of cluster abundance, the most apparent and significant difference compared to TEG001, was the decline of Cluster3 and enrichment of Cluster4 for TEG001-NKG2D-4-1BB_{CD28TM} (Figure 4A,B, p-values from Fisher's test are shown in Supplementary table 2). The identified clusters were annotated based on the GO-terms associated with their differentially expressed genes (Figure 4D, Supplementary figure 3A, Supplementary table 3). The most apparent difference between all conditions was the absence of Cluster3 and enrichment of Cluster4 for TEG001-NKG2D-4-1BB_{CD28TM} (Figure 4A,B). The CD4-CD8 annotation showed that most of the transcriptomic differences between the chimeras are linked to the CD4+ populations (Figure 4C). The cell frequencies in clusters that were mostly populated with CD8+ T-cells (Cluster0, Cluster1) did not differ between engineered cells (Figure 4D, Supplementary table 4), but Cluster2 (proliferation) was elevated among the TEG001-NKG2D-4-1BB_{CD28TM} cells, in line with the short-term MM xenograft model (Figure 3G-I). As stated above, the major differences were in Cluster3

(exhaustion) and Cluster4 (CD4+ adhesion and activation), where TEG001-NKG2D-4-1BB_{CD28}TM showed the highest representation of the 'CD4+ adhesion and activation' cluster, and the lowest representation of the 'exhaustion' cluster, when compared to the other TEG types. This was confirmed when we repeated the analysis over the CD4+ and CD8+ subsets, separately; in the CD4+ subset, the most significant differences were identified in Cluster0 (exhaustion) and Cluster2 (adhesion) between the TEG001 construct and the 41BB chimera, similarly to the combined dataset (Extended data figure 7A-H, Supplementary table 5).

To better represent the immunological functionalities, we plotted the scaled average expression of canonical marker genes of immunologically relevant biological processes across each cluster (Figure 4E). This reflected the proliferative features of Cluster2, the exhaustion features of Cluster3 and the activation-adhesion features of Cluster4.

Investigating the transcriptomic clusters of the combined dataset revealed the cellular complexities of TEGs and the shifts that were caused by the expression of the chimeras. Next, we studied the differences between the chimera populations by contrasting the chimera types (Supplementary table 6). When plotting the scaled average expression of the same canonical marker across the chimera types (Figure 4F), and splitting the CD4+ and CD8+ populations, the CD4+ subset of the NKG2D-4-1BB chimera stood out from multiple aspects. In this population, we noticed a decreased level of the activation-exhaustion signature and an elevated level in the cytotoxicity signature, represented by GZMA, GZMB and PRF1 expression. To validate whether this 'cytotoxicity/less exhaustion' signature was also present on protein level in engineered CD4+ TEGs, we addressed PD1 and granzyme B expression after repetitive stimulation with target cells (Extended data figure 8A-B). In concordance with the scRNAseq results, CD4+ TEG001-NKG2D-4-1BB_{CD28}TM showed lower PD1 expression (Extended data figure 8A). Granzyme B expression was significantly increased in TEG donors where the percentage of granzyme B-positive TEG001 cells was lower than 40% after tumor-encounter (Extended data figure 8B). Other transcriptional signatures associated with improved CAR-T persistence and survival, like oxidative

phosphorylation³² and NF- κ B activation³³, were enriched in CD4+ TEG001-NKG2D-4-1BB_{CD28TM} cells as well (Figure 4F). An increase in NF- κ B signaling induced by NKG2D-4-1BB_{CD28TM} was confirmed in a reporter-assay with cell-lines expressing the $\gamma\delta$ TCR used for engineering TEG001 (TEG001_R) alone, or in combination with the different NKG2D-chimeras (Extended data figure 8C). No obvious differences were observed in TCR-mediated signaling assessed with NFAT reporter cell-lines. Thus, in addition to the increased proliferation, an enhanced killing machinery, improved metabolic activity, as well as NF- κ B signaling and reduced dependency on PD1 might have contributed to the improved *in vivo* control of solid tumors by TEG001-NKG2D-4-1BB_{CD28TM}.

Endogenous NKG2D impairs NKG2D-4-1BB_{CD28TM} function on CD8+ TEGs

To study whether the limited additional impact of NKG2D chimeras in CD8+ TEGs was due to competition with endogenous NKG2D, NKG2D was knocked-out (KO) in CD8+ TEGs (Extended data figure 9A-C). TEG001-NKG2D-4-1BB_{CD28TM} NKG2D-KO cells showed increased killing and proliferation ability when compared to their negative control counterpart (Extended data figure 9D,E). No differences were observed for TEG001. These results suggest that endogenous expression of NKG2D in CD8+ TEGs hampered activity of the NKG2D-chimeras.

Adding an anti-CD277-chimera improves activity of CD4+ and CD8+ TEGs

To overcome complex knock-out and knock-in strategies, from a product development perspective, we designed a chimeric co-receptor targeting CD277 which is overexpressed on tumor cells of diverse origin³⁴, and closely linked to $\gamma\delta$ 2T-cell activation. We assumed that we would thereby avoid competition of a new co-receptor with endogenous receptors. The design of the new chimeric co-receptor (103-4-1BB-chimera) was based on the NKG2D-4-1BB_{CD28TM}-chimera design by swapping the extracellular domain of NKG2D by the scFv derived from mAb-103.2 directed against CD277¹⁷ (Figure 5A). 103-4-1BB was well expressed in engineered T-cells (Extended data figure 10A), and in this case, CD4+ and CD8+ TEG001-103-4-1BB had improved proliferation activity compared to TEG001 (Extended data figure 10B). To formally confirm that 103-4-1BB-chimera overcome the weakness of

NKG2D-4-1BB_{CD28TM}-chimera which primarily enhanced activity in CD4+ TEGs, we evaluated the killing ability of CD4+ and CD8+ TEGs expressing different chimeras separately and combined in the 3D bone marrow niche model (Figure 5B). As expected, only 103-4-1BB-chimera was able to significantly increase the killing ability of either CD4+ and CD8+ TEGs alone. No differences between the NKG2D-4-1BB_{CD28TM}-chimera and the 103-4-1BB-chimera were observed when they were expressed simultaneously in CD4+ and CD8+, most likely because maximum killing was already reached for TEG001-NKG2D-4-1BB_{CD28TM}. Next, we generated TEG products in 1:1 CD4:CD8 ratios, where either only CD4+ or CD8+ TEGs co-expressed the chimeras (Figure 5C). While once more NKG2D-4-1BB_{CD28TM} only improved killing ability when expressed in CD4+ TEGs, 103-4-1BB was equally potent enhancing killing ability of CD4+ or CD8+ TEGs in both liquid (RPMI-8266) and solid tumors (SCC9). Surprisingly, NKG2D-CD28_{WT}-chimera only enhanced killing activity of TEG001 when expressed on both CD4+ and CD8+, implying some added value when expressed in CD8+ TEGs.

103-4-1BB-chimera impacts the transcriptome of CD4+ and CD8+ TEGs

The 103-4-1BB-chimera improved the killing activity of both CD4+ and CD8+ TEGs. In order to gain insights in how this chimera impacts these cells, we performed scRNA seq after co-culturing TEG001-103-4-1BB cells with RPMI-8226. We observed changes in the transcriptomic profile for both CD4+ and CD8+ TEG001-103-4-1BB cells when compared to TEG001 (Figure 5D-I). CD4+ TEG-103-4-1BB cells skewed towards increased proliferation (Cluster0) and reduced exhaustion (Cluster3) (Figure 5F, Extended data figure 10C, Supplementary table 7). Moreover, stronger NF- κ B and oxidative phosphorylation signatures were observed for CD4+ TEG001-103-4-1BB, in line with previous observations in the NKG2D-4-1BB_{CD28TM} (Extended data figure 10C). Abundance of CD8+ TEG001-103-4-1BB cells was significantly higher in the proliferation cluster (Cluster2) compared to TEG001 (Figure 5I). Again, the oxidative phosphorylation signature was stronger in TEG001-103-4-1BB, compared to TEG001 (Extended data figure 10D).

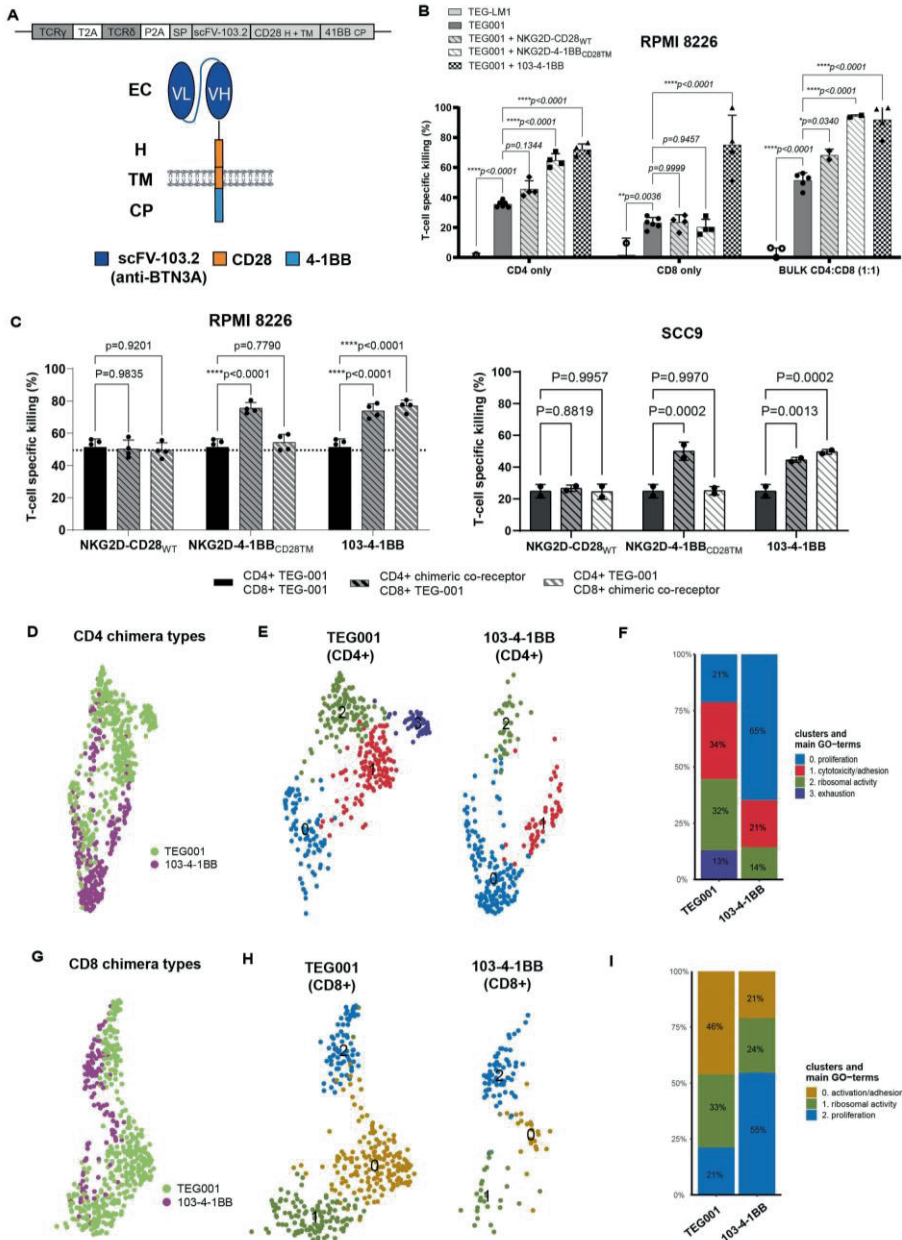


Fig. 5. Addition of the 103-4-1BB chimeric receptor affects the activity and transcriptomic profiles of CD4+ and CD8+ TEGs. **a**, Schematic overview of the anti-BTN3A-derived chimera (103-4-1BB chimera) containing the anti-BTN3A scFV extracellular domain, CD28 transmembrane (TM) domain, hinge (H) domain, 4-1BB intracellular signaling domain (CP) and δ TCR transgene cassette in the retroviral vector pMP71. The TCR δ chain was derived from clone 5, and the TCR γ chain was from clone 5. P2A (derived from

porcine teschovirus 1 2A) and T2A (derived from the *Thosea asigna* virus) refer to two different 2A ribosomal skipping sequences. Anti-CD277-derived scFV (clone 103.2), CD28 and 4-1BB domains are colored in dark blue, orange and clear blue, respectively. b, Tumor killing by only CD4+ TEGs, only CD8+ TEGs or bulk CD4:CD8 (1:1) TEGs in a 3D bone marrow niche. Tumor and cell numbers were normalized to those of the mock treatment (TEG-LM1); n = 2 independent experiments with two biological replicates each. Data represent mean ± s.d. Significance was calculated by twoway ANOVA with a Dunnett correction. c, Tumor killing of RPMI-8226 or SCC9 tumor cells in a 3D bone marrow niche. TEG001 CD4+ T cells were combined 1:1 with TEG001 CD8+ T cells coexpressing the three different chimeras and vice versa (TEG001 CD8+ T cells combined 1:1 with TEG001 CD4+ T cells coexpressing the chimeras) and added to the model as effector cells. Tumor cell numbers were normalized to those of the mock treatment (TEG-LM1); n = 2 independent experiments for RPMI-8226 and n = 1 experiment for SCC9 with two biological replicates each. Data represent mean ± s.d. Significance was calculated by two-way ANOVA with a Dunnett correction. d,e, CD4+ -enriched cells from the TEG001 and TEG001-103-4-1BB (referred to as 103-4-1BB) cell types (400 cells and 244 cells in total, respectively) annotated by clusterID (d) or by chimera types (e). f, Percentage representation of the clusters (annotated by the main GO terms) across the CD4+ chimera types. g,h, CD8+ -enriched cells from the TEG001 and TEG001-103-4-1BB cell types (387 cells and 122 cells in total, respectively) annotated by clusterID (g) or by chimera types (h). i, Percentage representation of the clusters (annotated by the main GO terms) across the CD8+ chimera types

TEG001-103-4-1BB eradicates hematological and solid tumors *in vivo*

Next, we tested whether the increased capacity to kill tumor cells by both CD4+ and CD8+ TEG001-103.2-4-1BB also translates into better tumor control and survival *in vivo*, using the RPMI-8226 MM xenograft model (Figure 6A). The group treated with TEG001-103-4-1BB showed complete inhibition of tumor outgrowth in all mice (Figure 6B), and 100% survival at the time when all TEG001 treated mice had reached the humane endpoint (Figure 6C). A high number of TEG001-103-4-1BB cells, with effector (75%) and central (25%) memory phenotype, were found in the bone marrow of the sacrificed mice, implying long-term persistence (Figure 6D,E). Encouraged by this significant treatment effect, we decided to compare the efficacy of TEG001-103-4-1BB and TEG001-NKG2D-4-1BB_{CD28TM} in a head and neck solid tumor xenograft model (SCC9) side by side (Figure 6F). While TEG001-NKG2D-4-1BB_{CD28TM} was again only able to significantly delay tumor outgrowth compared to TEG001 (Figure 6G), TEG001-103-4-1BB completely eradicated solid tumors.

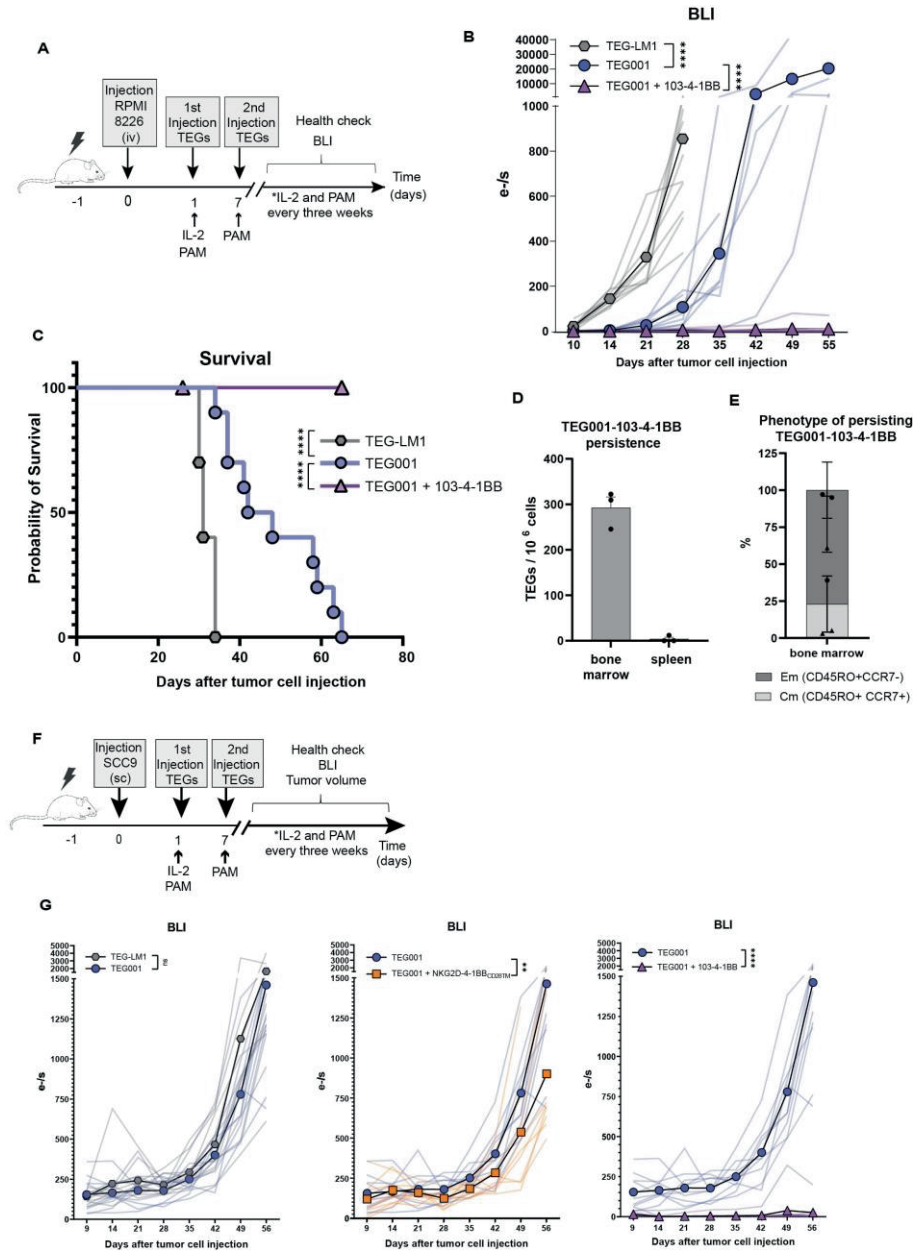


Fig. 6. TEG001-103-4-1BB cells eradicate liquid and solid tumors *in vivo*. a, Experimental setup to evaluate the *in vivo* efficacy of TEG001-103-4-1BB cells against RPMI-8226 tumor cells. Female NSG mice were irradiated at day -1 and injected with 5×10^6 RPMI-8226 luciferase tumor cells intravenously at day 0, followed by 107 TEGs on days 1 and 7 in the presence of PAM. Interleukin-2 (IL-2) and PAM were administered every 3 weeks. b, BLI was measured weekly to assess tumor outgrowth. For BLI, single curves

and mean values are shown for TEG-LM1 (mock; gray), TEG001 (blue) and TEG001-103-4-1BB (purple) cells. Significance was calculated for tumor outgrowth over time using mixed-effect model tests with repeated measures by comparing TEG001 to TEG-LM1 cells (****P<0.0001) or TEG001-103-4-1BB cells (****P<0.0001). c, Survival was assessed by monitoring weight loss and symptoms of disease. Data were generated from one experiment with n = 10 mice per treatment group. One mouse was censored at day 26 in the 103-4-1BB-treated group due to non-tumorrelated death. Significance was calculated by log-rank (Mantel-Cox) test; TEG-LM1 versus TEG001 cells ****P<0.0001; TEG001 versus TEG001-103-4-1BB cells. d, Numbers of TEGs in the bone marrow and spleen were assessed (n = 3 mice per treatment group). Data represent mean \pm s.e.m. e, Memory phenotype (Em, effector memory; Cm, central memory) of persisting TEG001-103-4-1BB cells was assessed by FACS (n = 3 mice per treatment). Data represent mean \pm s.e.m. f, Schematic diagram of the experimental setup to evaluate the efficacy of TEGs coexpressing NKG2D-4-1BB_{CD28TM} or 103-4-1BB chimeras against SCC9 tumors. Male NSG mice were irradiated at day -1 and injected with 0.5×10^6 SCC9 luciferase tumor cells subcutaneously (s.c.) at day 0, followed by 107 TEGs on days 1 and 7 in the presence of PAM. IL-2 and PAM were administered every 3 weeks. Data were generated from one experiment with n = 10 mice per group. g, BLI was measured weekly to assess tumor outgrowth. For BLI, single curves and mean values are shown for TEG-LM1 (mock; gray), TEG001 (blue), TEG001- NKG2D-4-1BB_{CD28TM} (orange) and TEG001-103-4-1BB (purple) cells. Significance was calculated for tumor outgrowth over time using mixed-effect model tests with repeated measures by comparing TEG001 to the rest of the treatments; TEG-LM1 versus TEG001 cells P = 0.8362; TEG001 versus TEG001- NKG2D-4-1BB_{CD28TM} cells **P = 0.0013; TEG001 versus TEG001-103-4-1BB cells ****P<0.0001; NS, no significant.

Discussion

The question of how to target most cancers with a single engineered immune cell strategy is still unsolved. Here, we present a new approach to overcome this substantial drawback, by combining cancer-metabolome targeting, mediated by a defined high affinity $\gamma 9\delta 2$ TCR, with stress-ligand sensing by chimeric NKG2D or anti-CD277 co-stimulatory-receptors, to target tumors of both hematological and solid origin. A side-by-side comparison of different co-stimulatory signaling domains revealed that chimeric receptors signaling via 4-1BB most efficiently overcame suboptimal $\gamma 9\delta 2$ TCR-ligation, and targeted a large range of not only liquid, but also solid tumors. Utilizing $\gamma 9\delta 2$ TCR and CAR-like co-stimulation allowed us to further tweak transcriptomic heterogeneity towards a more favorable transcriptomic profile for CD4+ TEGs when using NKG2D-4-1BB_{CD28TM}-chimera, and for both CD4+ and CD8+ TEGs when utilizing the 103-4-1BB-chimera. CD277-engagement by the 103-4-1BB-chimera was consequently the most powerful co-stimulation in mediating tumor control *in vivo* in liquid and solid tumor models.

Combining targeting of the cancer-metabolome and cancer-associated stress antigens has many strategic advantages, as compared to other currently targeted tumor antigens that have shown clinical responses in phase I clinical trials, in solid tumors like claudin 18.2 in gastric cancer ³⁵, or GD2 for midline glioma ³⁶. Both of the targets, CD277 and NKG2D-ligands, are broadly expressed in many different tumor types, making this dual-targeting strategy a broad-spectrum approach, suitable for treating multiple cancers with a single product. The separation of activation and co-stimulatory signals circumvents the potential risk of activation of TEG001-NKG2D-co-stimulatory chimera by NKG2D-ligands after damage of healthy tissues, which might cause exhaustion of T-cells, when signaling solely depends on NKG2D-engagement, as in NKG2D CARs ³⁷. Another appeal of our strategy is that the addition of the NKG2D-chimeras rescued suboptimal TCR-stimulation mimicked by reduced doses of PAM. Therefore, our approach might be interesting to enhance recognition of tumors that express low TCR-ligand density, not only for $\gamma\delta$ TCR, but also for $\alpha\beta$ TCR-based engineering as addition of these chimeras might reduce the threshold of antigen density required for optimal T-cell activity.

Chronic stimulation of CAR-T has been reported to cause T-cell exhaustion ³⁸, and transcriptomic signatures related with exhaustion correlate with poor clinical CAR-T responses ^{39, 40}. However, comprehensive analysis of heterogeneity in $\alpha\beta$ T-cell behavior is missed in most of these studies. Most recently, we described a high diversity in transcriptomic profiles for engineered immune cells ¹². Different strategies have been explored to shape behavioral cell fate ^{41, 42}, though such studies might underestimate that, depending on the level of T-cell development, deletion or addition of defined genes might have completely different impact on T-cell behavior. Here we aimed to explore how the different chimeras impacted transcriptomic signatures and T-cell phenotypes. Our first observation was that, in line with our *in vitro* results, the main differences in the transcriptomic profiles were observed for the CD4⁺ subset of TEG001-NKG2D-4-1BB_{CD28}TM, in which cells displayed more proliferative, cytotoxic and less exhausted transcriptional signatures, important properties that are associated with long-term tumor control ⁴³. Reduced exhaustion was confirmed by reduction of PD1 upregulation on TEG001-NKG2D-4-1BB_{CD28}TM after chronic antigen

stimulation, which might be directly linked to the induction of chemokines, such as CXCL10, in the tumor microenvironment, as observed in the 3D model experiments and previously reported by others⁴⁴. Moreover, TEG001-NKG2D-4-1BB_{CD28}TM promoted the development of cytotoxic CD4⁺ T-cells, a cell population which has been associated with a good prognosis in cancer patients⁴⁵ and with longevity⁴⁶. Also, in line with reports for 4-1BB bearing CAR-T cells^{47,48}, we observed a beneficial activation of the NF- κ B pathway when using 4-1BB as costimulatory signaling domain within our chimera.

NKG2D-KO experiments suggested that interference of the NKG2D-chimeras with extra- or intracellular T-cell binding partners of the endogenously expressed NKG2D natural receptor mechanistically explain the lack of activity of the NKG2D-chimeras on CD8⁺ TEGs. However, this strategy would complicate the manufacturing process from an ATMP (Advanced therapy medicinal products) production perspective. To avoid extra-engineering steps and overcome the limited activity of the NKG2D-chimeras in CD8⁺ T-cells, we explored 103-4-1BB-chimera as a potential alternative, which indeed reprogrammed CD4⁺ and CD8⁺ T-cells. The fact that the CD277 binding chimera did not inhibit, but enhanced activity of TEG001, implies that this chimera does not hamper the direct or indirect interaction of $\gamma\delta$ TCR with CD277. TEG001-NKG2D-4-1BB_{CD28}TM and TEG001-103-4-1BB CD4⁺ cells were equally potent in the 3D bone marrow assays, implying that different affinities of costimulatory receptors did not impact killing activity. CD277 is, like NKG2D-ligands, expressed in several solid and hematological tumors^{49,50}. The results obtained using the 3D bone marrow, together with the overwhelming observed *in vivo* tumor control, imply that enhancing activity of both CD4⁺ and CD8⁺ T-cells might be essential to exploit the full potential of co-stimulation in the context of a TCR. This would also imply that in ATMP production processes for engineered T-cells, an optimized CD4⁺/CD8⁺ T-cell ratio might be preferable, as reported for CD19-CAR-T (lisocabtagene maraleucel)⁵¹.

Our strategy of an orchestrated dual signaling could make obsolete the most recent efforts of extensive gene editing to avoid expression of checkpoint inhibitors⁵². Our observation contrasts with CAR-T engineering studies

comparing 4-1BB and CD28 costimulatory signals, which favored CD28 against solid tumors⁵³, illustrating that signaling through a single standard CAR substantially differs from efforts where TCRs are used in combination with co-stimulatory CARs⁵⁴. Our data advocate for adding single-cell sequencing, to gain insights on the functional profiling of engineered immune cells early, during the development of novel receptors, as data on transcriptomic heterogeneity can provide important hints for designing potentially superior constructs.

We conclude that the combination of TCR-mediated targeting of the cancer-metabolome, together with chimeric co-receptor targeting of cancer-associated stress ligands opens new possibilities for cancer immunotherapies. On one hand, as our approach relies on the targeting of two types of universal tumor-associated antigens, we increased the number of tumors that can be treated with one single therapy. On the other hand, splitting first (TCR) and second (NKG2D or anti-CD277 chimeric co-receptors) T-cell activation signals overcame limited antigen expression when the TCR was used as the first signal, and resulted in shaping of transcriptomic profiles towards favorable described profiles. However, it is important to equally support both CD4+ and CD8+ T-cells, to achieve the full potential of co-stimulation.

References

1. Sebestyen Z, Scheper W, Vyborova A, Gu S, Rychnavska Z, Schiffler M, et al. RhoB Mediates Phosphoantigen Recognition by V γ 9V δ 2 T Cell Receptor. *Cell Rep.* 2016;15(9):1973-85.
2. Rigau M, Ostrouska S, Fulford TS, Johnson DN, Woods K, Ruan Z, et al. Butyrophilin 2A1 is essential for phosphoantigen reactivity by gammadelta T cells. *Science.* 2020;367(6478).
3. Karunakaran MM, Willcox CR, Salim M, Paletta D, Fichtner AS, Noll A, et al. Butyrophilin-2A1 Directly Binds Germline-Encoded Regions of the Vgamma9Vdelta2 TCR and Is Essential for Phosphoantigen Sensing. *Immunity.* 2020;52(3):487-98 e6.
4. Mamedov MRV, S.; Freimer, J.W.; Das Sahu, A.; Ramesh, A.; Arce, M.M.; Meringa, A.D.; Ota, M.; Chen P.M.; Hanspers, K.; Nguyen, V.Q.; Takeshima, K.A.; Pritchard, J.K; Kuball, J.; Sebestyen, Z.; Adams, E.J.; Marson, A. CRISPR screens decode cancer cell pathways that trigger $\gamma\delta$ T cell detection. *Nature.* 2023(In print).
5. Harly C, Guillaume Y, Nedellec S, Peigne CM, Monkkonen H, Monkkonen J, et al. Key implication of CD277/butyrophilin-3 (BTN3A) in cellular stress sensing by a major human gammadelta T-cell subset. *Blood.* 2012;120(11):2269-79.
6. Hsiao CC, Nguyen K, Jin Y, Vinogradova O, Wiemer AJ. Ligand-induced interactions between butyrophilin 2A1 and 3A1 internal domains in the HMBPP receptor complex. *Cell Chem Biol.* 2022;29(6):985-95.e5.
7. Yuan L, Ma X, Yang Y, Qu Y, Li X, Zhu X, et al. Phosphoantigens glue butyrophilin 3A1 and 2A1 to activate V γ 9V δ 2 T cells. *Nature.* 2023.
8. Vyborova A, Beringer DX, Fasci D, Karaiskaki F, van Diest E, Kramer L, et al. γ 9 δ 2T cell diversity and the receptor interface with tumor cells. *J Clin Invest.* 2020;130(9):4637-51.
9. Gründer C, van Dorp S, Hol S, Drent E, Straetmans T, Heijhuurs S, et al. γ 9 and δ 2CDR3 domains regulate functional avidity of T cells harboring γ 9 δ 2TCRs. *Blood.* 2012;120(26):5153-62.
10. Straetmans T, Grunder C, Heijhuurs S, Hol S, Slaper-Cortenbach I, Bonig H, et al. Untouched GMP-Ready Purified Engineered Immune Cells to Treat Cancer. *Clin Cancer Res.* 2015;21(17):3957-68.
11. de Witte M, Scheepstra J, Weertman N, Daudeij A, van der Wagen L, Oostvogels R, et al. First in Human Clinical Responses and Persistence Data on TEG001: A Next Generation of Engineered A β T Cells Targeting AML and MM with a High Affinity γ 9 δ 2TCR. *Blood.* 2022;140(Supplement 1):12737-9.
12. Dekkers JF, Alieva M, Cleven A, Keramati F, Wezenaar AKL, van Vliet EJ, et al. Uncovering the mode of action of engineered T cells in patient cancer organoids. *Nat Biotechnol.* 2022.
13. Fuertes MB, Domaica CI, Zwimer NW. Leveraging NKG2D Ligands in Immunology. *Frontiers in immunology.* 2021;12:713158.

14. Marcu-Malina V, Heijhuurs S, van Buuren M, Hartkamp L, Strand S, Sebestyen Z, et al. Redirecting alphabeta T cells against cancer cells by transfer of a broadly tumor-reactive gammadeltaT-cell receptor. *Blood*. 2011;118(1):50-9.
15. Harly C, Guillaume Y, Nedellec S, Peigné CM, Mönkkönen H, Mönkkönen J, et al. Key implication of CD277/butyrophilin-3 (BTN3A) in cellular stress sensing by a major human $\gamma\delta$ T-cell subset. *Blood*. 2012;120(11):2269-79.
16. Benyamine A, Loncle C, Foucher E, Blazquez JL, Castanier C, Chrétien AS, et al. BTN3A is a prognosis marker and a promising target for V γ 9V δ 2 T cells based-immunotherapy in pancreatic ductal adenocarcinoma (PDAC). *Oncoimmunology*. 2017;7(1):e1372080.
17. Palakodeti A, Sandstrom A, Sundaresan L, Harly C, Nedellec S, Olive D, et al. The molecular basis for modulation of human Vgamma9Vdelta2 T cell responses by CD277/butyrophilin-3 (BTN3A)-specific antibodies. *J Biol Chem*. 2012;287(39):32780-90.
18. De Gassart A, Le KS, Brune P, Agaagué S, Sims J, Goubard A, et al. Development of ICT01, a first-in-class, anti-BTN3A antibody for activating V γ 9V δ 2 T cell-mediated antitumor immune response. *Sci Transl Med*. 2021;13(616):eabj0835.
19. Mansilla-Soto J, Eyquem J, Haubner S, Hamieh M, Feucht J, Pailton N, et al. HLA-independent T cell receptors for targeting tumors with low antigen density. *Nat Med*. 2022;28(2):345-52.
20. Oda SK, Anderson KG, Ravikumar P, Bonson P, Garcia NM, Jenkins CM, et al. A Fas-4-1BB fusion protein converts a death to a pro-survival signal and enhances T cell therapy. *J Exp Med*. 2020;217(12).
21. Liu X, Ranganathan R, Jiang S, Fang C, Sun J, Kim S, et al. A Chimeric Switch-Receptor Targeting PD1 Augments the Efficacy of Second-Generation CAR T Cells in Advanced Solid Tumors. *Cancer Res*. 2016;76(6):1578-90.
22. Melenhorst JJ, Chen GM, Wang M, Porter DL, Chen C, Collins MA, et al. Decade-long leukaemia remissions with persistence of CD4(+) CAR T cells. *Nature*. 2022;602(7897):503-9.
23. Anderson ND, Birch J, Accogli T, Criado I, Khabirova E, Parks C, et al. Transcriptional signatures associated with persisting CD19 CAR-T cells in children with leukemia. *Nat Med*. 2023;29(7):1700-9.
24. Xia A, Zhang Y, Xu J, Yin T, Lu XJ. T Cell Dysfunction in Cancer Immunity and Immunotherapy. *Front Immunol*. 2019;10:1719.
25. Vandenberghe P, Verwilghen J, Van Vaeck F, Ceuppens JL. Ligation of the CD5 or CD28 molecules on resting human T cells induces expression of the early activation antigen CD69 by a calcium- and tyrosine kinase-dependent mechanism. *Immunology*. 1993;78(2):210-7.
26. Kunzmann V, Bauer E, Feurle J, Weissinger F, Tony HP, Wilhelm M. Stimulation of gammadelta T cells by aminobisphosphonates and induction of antiplasma cell activity in multiple myeloma. *Blood*. 2000;96(2):384-92.

27. Weinkove R, George P, Dasyam N, McLellan AD. Selecting costimulatory domains for chimeric antigen receptors: functional and clinical considerations. *Clin Transl Immunology*. 2019;8(5):e1049.
28. Kuball J, Schmitz FW, Voss RH, Ferreira EA, Engel R, Guillaume P, et al. Cooperation of human tumor-reactive CD4+ and CD8+ T cells after redirection of their specificity by a high-affinity p53A2.1-specific TCR. *Immunity*. 2005;22(1):117-29.
29. Braham MVJ, Minnema MC, Aarts T, Sebestyen Z, Straetmans T, Vyborova A, et al. Cellular immunotherapy on primary multiple myeloma expanded in a 3D bone marrow niche model. *Oncoimmunology*. 2018;7(6):e1434465.
30. Eagle RA, Jafferji I, Barrow AD. Beyond Stressed Self: Evidence for NKG2D Ligand Expression on Healthy Cells. *Curr Immunol Rev*. 2009;5(1):22-34.
31. Majzner RG, Mackall CL. Clinical lessons learned from the first leg of the CAR T cell journey. *Nat Med*. 2019;25(9):1341-55.
32. Kawalekar OU, O'Connor RS, Fraietta JA, Guo L, McGettigan SE, Posey AD, Jr., et al. Distinct Signaling of Coreceptors Regulates Specific Metabolism Pathways and Impacts Memory Development in CAR T Cells. *Immunity*. 2016;44(2):380-90.
33. Philipson BI, O'Connor RS, May MJ, June CH, Albelda SM, Milone MC. 4-1BB costimulation promotes CAR T cell survival through noncanonical NF- κ B signaling. *Sci Signal*. 2020;13(625).
34. Payne KK, Mine JA, Biswas S, Chaurio RA, Perales-Puchalt A, Anadon CM, et al. BTN3A1 governs antitumor responses by coordinating $\alpha\beta$ and $\gamma\delta$ T cells. *Science*. 2020;369(6506):942-9.
35. Qi C, Gong J, Li J, Liu D, Qin Y, Ge S, et al. Claudin18.2-specific CAR T cells in gastrointestinal cancers: phase 1 trial interim results. *Nat Med*. 2022;28(6):1189-98.
36. Majzner RG, Ramakrishna S, Yeom KW, Patel S, Chinnasamy H, Schultz LM, et al. GD2-CAR T cell therapy for H3K27M-mutated diffuse midline gliomas. *Nature*. 2022.
37. Guerra N, Lanier LL. Editorial: Emerging Concepts on the NKG2D Receptor-Ligand Axis in Health and Diseases. *Front Immunol*. 2020;11:562.
38. Gumber D, Wang LD. Improving CAR-T immunotherapy: Overcoming the challenges of T cell exhaustion. *EBioMedicine*. 2022;77:103941.
39. Deng Q, Han G, Puebla-Osorio N, Ma MCJ, Strati P, Chasen B, et al. Characteristics of anti-CD19 CAR T cell infusion products associated with efficacy and toxicity in patients with large B cell lymphomas. *Nat Med*. 2020;26(12):1878-87.
40. Fraietta JA, Lacey SF, Orlando EJ, Pruteanu-Malinici I, Gohil M, Lundh S, et al. Determinants of response and resistance to CD19 chimeric antigen receptor (CAR) T cell therapy of chronic lymphocytic leukemia. *Nat Med*. 2018;24(5):563-71.
41. Scott AC, Dündar F, Zumbo P, Chandran SS, Klebanoff CA, Shakiba M, et al. TOX is a critical regulator of tumour-specific T cell differentiation. *Nature*. 2019;571(7764):270-4.
42. Philip M, Schietinger A. CD8(+) T cell differentiation and dysfunction in cancer. *Nat Rev Immunol*. 2022;22(4):209-23.

43. Lim WA, June CH. The Principles of Engineering Immune Cells to Treat Cancer. *Cell*. 2017;168(4):724-40.
44. Peng W, Liu C, Xu C, Lou Y, Chen J, Yang Y, et al. PD-1 blockade enhances T-cell migration to tumors by elevating IFN- γ inducible chemokines. *Cancer Res*. 2012;72(20):5209-18.
45. Oh DY, Fong L. Cytotoxic CD4(+) T cells in cancer: Expanding the immune effector toolbox. *Immunity*. 2021;54(12):2701-11.
46. Hashimoto K, Kouno T, Ikawa T, Hayatsu N, Miyajima Y, Yabukami H, et al. Single-cell transcriptomics reveals expansion of cytotoxic CD4 T cells in supercentenarians. *Proc Natl Acad Sci U S A*. 2019;116(48):24242-51.
47. Li G, Boucher JC, Kotani H, Park K, Zhang Y, Shrestha B, et al. 4-1BB enhancement of CAR T function requires NF- κ B and TRAFs. *JCI Insight*. 2018;3(18).
48. Hirabayashi K, Du H, Xu Y, Shou P, Zhou X, Fuca G, et al. Dual Targeting CAR-T Cells with Optimal Costimulation and Metabolic Fitness enhance Antitumor Activity and Prevent Escape in Solid Tumors. *Nat Cancer*. 2021;2(9):904-18.
49. Chen S, Li Z, Huang W, Wang Y, Fan S. Prognostic and Therapeutic Significance of BTN3A Proteins in Tumors. *J Cancer*. 2021;12(15):4505-12.
50. Liang F, Zhang C, Guo H, Gao SH, Yang FY, Zhou GB, et al. Comprehensive analysis of BTN3A1 in cancers: mining of omics data and validation in patient samples and cellular models. *FEBS Open Bio*. 2021;11(9):2586-99.
51. Abramson JS, Palomba ML, Gordon LI, Lunning MA, Wang M, Amason J, et al. Lisocabtagene maraleucel for patients with relapsed or refractory large B-cell lymphomas (TRANSCEND NHL 001): a multicentre seamless design study. *Lancet*. 2020;396(10254):839-52.
52. Azangou-Khyavy M, Ghasemi M, Khanali J, Boroomand-Saboore M, Jamalkhah M, Soleimani M, et al. CRISPR/Cas: From Tumor Gene Editing to T Cell-Based Immunotherapy of Cancer. *Front Immunol*. 2020;11:2062.
53. Textor A, Grunewald L, Anders K, Klaus A, Schwiebert S, Winkler A, et al. CD28 Co-Stimulus Achieves Superior CAR T Cell Effector Function against Solid Tumors Than 4-1BB Co-Stimulus. *Cancers (Basel)*. 2021;13(5).
54. Pichler AC, Carrié N, Cuisinier M, Ghazali S, Voisin A, Axisa PP, et al. TCR-independent CD137 (4-1BB) signaling promotes CD8(+)-exhausted T cell proliferation and terminal differentiation. *Immunity*. 2023;56(7):1631-48.e10.

Methods-only references

55. Driehuis, E., K. Kretzschmar, and H. Clevers, *Establishment of patient-derived cancer organoids for drug-screening applications*. *Nat Protoc*, 2020. **15**(10): p. 3380-3409.
56. Driehuis, E., et al., *Oral Mucosal Organoids as a Potential Platform for Personalized Cancer Therapy*. *Cancer Discov*, 2019. **9**(7): p. 852-871.

57. Huch, M., et al., *Long-term culture of genome-stable bipotent stem cells from adult human liver*. *Cell*, 2015. **160**(1-2): p. 299-312.
58. Saltsman, J.A., et al., *A Human Organoid Model of Aggressive Hepatoblastoma for Disease Modeling and Drug Testing*. *Cancers (Basel)*, 2020. **12**(9).
59. Miao, Y., et al., *Next-Generation Surrogate Wnts Support Organoid Growth and Deconvolute Frizzled Pleiotropy In Vivo*. *Cell Stem Cell*, 2020. **27**(5): p. 840-851.e6.
60. Jutz, S., et al., *Assessment of costimulation and coinhibition in a triple parameter T cell reporter line: Simultaneous measurement of NF- κ B, NFAT and AP-1*. *J Immunol Methods*, 2016. **430**: p. 10-20.
61. Doench, J.G., et al., *Optimized sgRNA design to maximize activity and minimize off-target effects of CRISPR-Cas9*. *Nat Biotechnol*, 2016. **34**(2): p. 184-191.
62. Muraro, M.J., et al., *A Single-Cell Transcriptome Atlas of the Human Pancreas*. *Cell Syst*, 2016. **3**(4): p. 385-394.e3.
63. Wu, T., et al., *clusterProfiler 4.0: A universal enrichment tool for interpreting omics data*. *Innovation (Camb)*, 2021. **2**(3): p. 100141.

Acknowledgements

We thank the staff of the Flow Core Facility at the UMC Utrecht for their kind assistance. We thank Wout Megchelenbrink at Princess Máxima Center for Pediatric Oncology, Utrecht for his suggestions related to statistical evaluations. Funding for this study was provided by KWF 6790, and 7601, 11393, 11979, 12586, 13043, 13493, Gadeta and Onco Accelerator (<https://www.oncoaccelerator.nl>) to J.K. SM is supported by the German Research Foundation (DFG) through BIOS - EXC294 and CIBSS - EXC 2189; SFB1479 (Project ID: 441891347 - P15), FOR2799 (MI1942/3-1, Project ID: 395236335) and MI1942/5-1 (Project ID: 501436442).

Author contributions

Conceptualization: PHL, EvD, DB, JK; **Methodology:** PHL, EvD, DB, JK; **Formal analysis:** PB; **Investigation:** PHL, EvD, PB, SH, AM, LHvH, CR, CS, MZ, IJ, MN, AC, TAK, RM, JZ, EK, TS, SM. **Resources:** HC, RdB, HGS, JR, WCP, SM. **Writing-Original draft:** PHL, EvD, PB, ZS, DB, JK. **Supervision:** DB, JK.

Competing interests

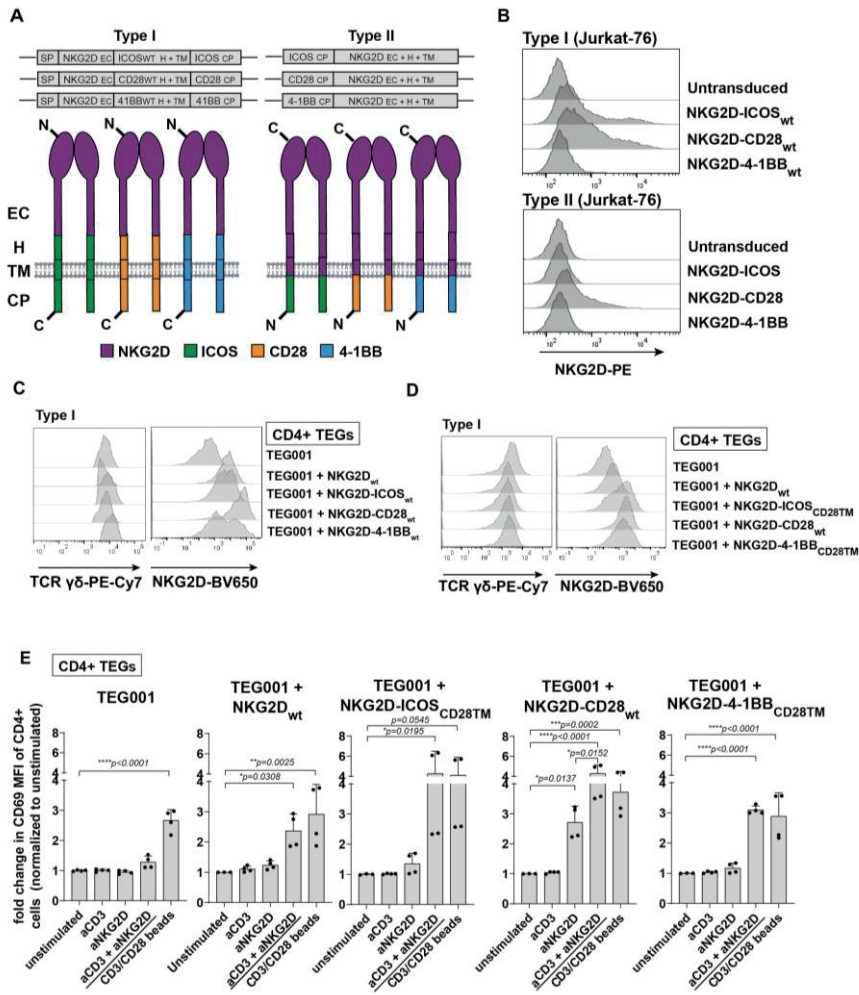
JK is shareholder of Gadeta. JK, ZS, EvD, and DB are inventors on patents with $\gamma\delta$ TCR related topics. JK, ZS, DB, PHL, AM and AC are inventors on patents with CD277 related topics.

For the full disclosure of HC., see <https://www.uu.nl/staff/JCClevers/Additional%20functions>

JR: Advisory role for Merck-Serono, Pierre Fabre, Servier, BMS, Roche, Bayer, GSK (all payments to institution). Institutional scientific grants from Bristol Myers Squibb, Merck, Delphi, HUB4 Organoids, Cleara, Pierre Fabre, Servier, Xilis, GSK. Board member foundation hubrecht organoid biobank.

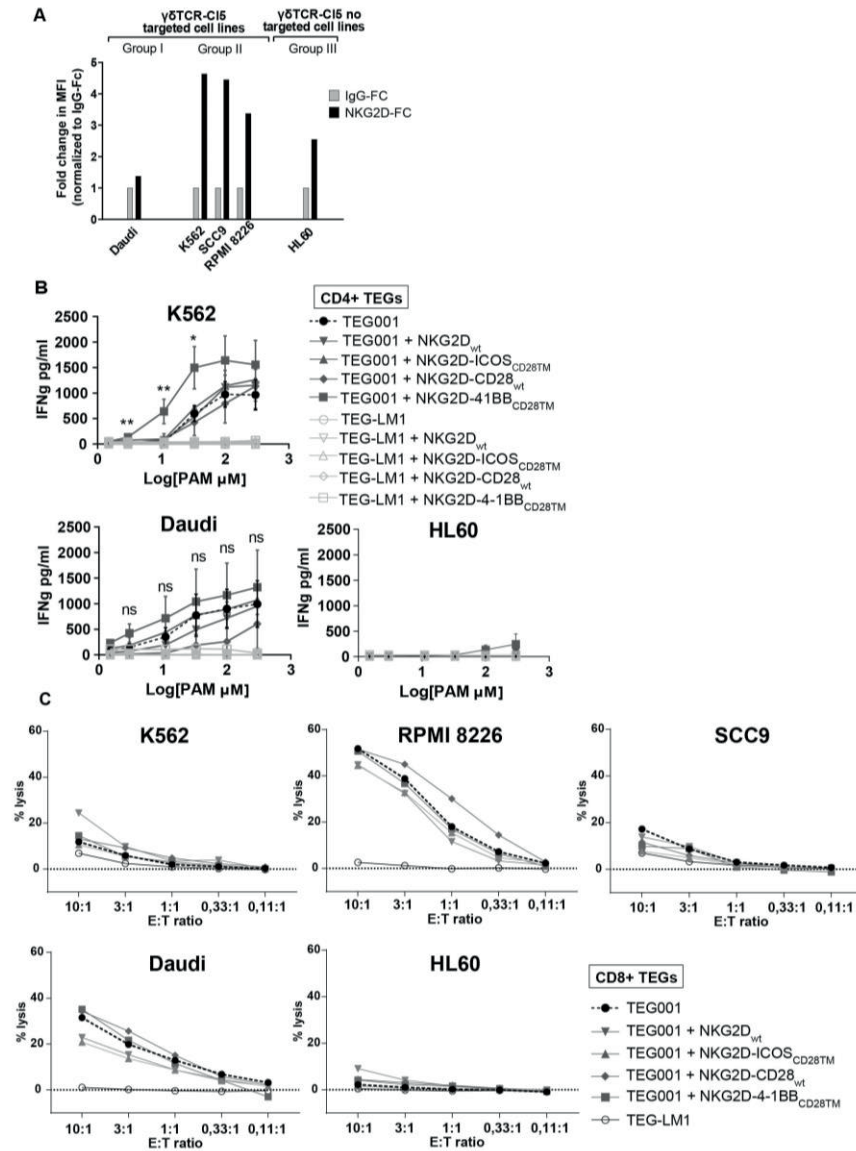
The remaining authors declare no competing interests.

Extended data



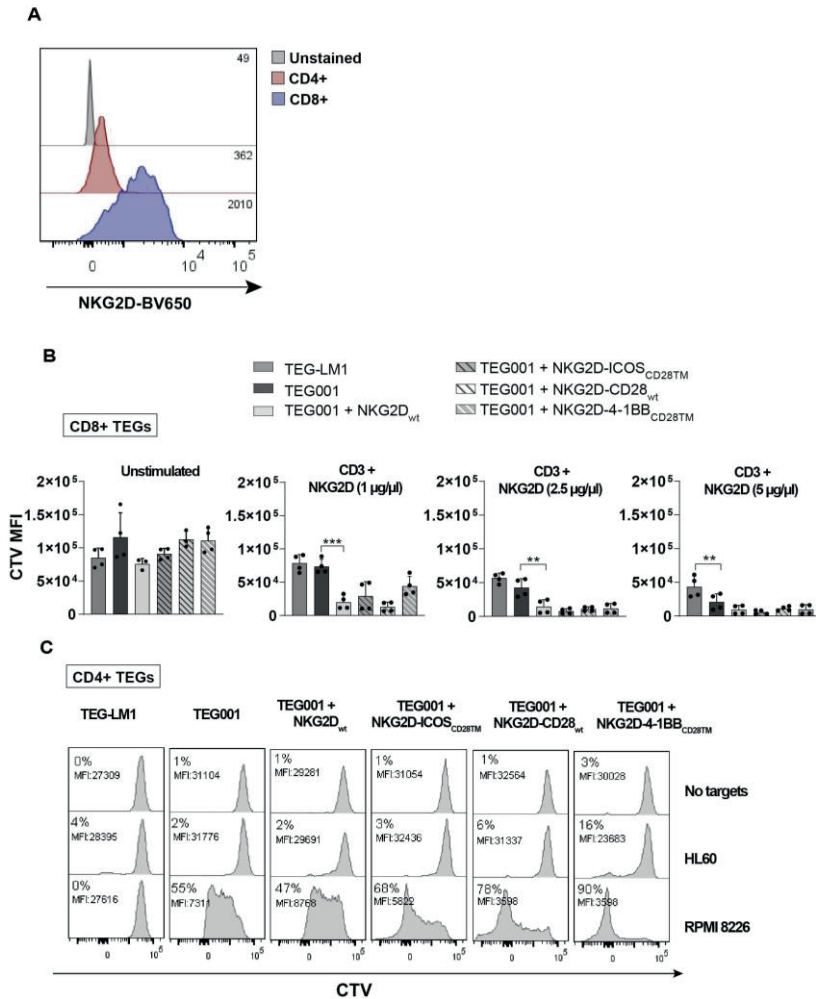
Extended Data Fig. 1. Type I and Type II NKG2D chimeric co-receptors design, expression and activity upon CD3 and NKG2D stimulation. (a) Schematic diagram of Type I and Type II chimeric NKG2D-chimeras. As the natural orientation of NKG2D (a Type II membrane protein) differs from the costimulatory proteins ICOS, CD28 and 4-1BB (all Type I membrane proteins), two different chimeras types were generated. A 'Type I' design with extracellular (EC) domain of NKG2D, and the hinge (H), transmembrane (TM) and cytoplasmic (CP) domains of the different costimulatory proteins, or a 'Type II' design where the cytoplasmic signaling domain of the costimulatory proteins was fused to the transmembrane and extracellular domain of NKG2D. Signal peptide is indicated as SP. N-terminal and C-terminal are represented by N and C respectively. NKG2D, ICOS, CD28 and 4-1BB domains are colored in purple, green, orange and blue respectively. (b) Expression of Type I and Type II chimeric NKG2D co-receptors in Jurkat-

76 cells. For 'Type I' chimeras, differential, but high surface expression was observed, with the strongest surface expression for NKG2D-CD28wt. Of the 'Type II' designs, only NKG2D-CD28wt, was marginally expressed. (c) Surface expression of $\gamma\delta$ TCR-CI5 and Type I NKG2D co-receptors or NKG2D_{wt} on primary CD4+ T-cells after transduction and $\alpha\beta$ depletion. (d) As NKG2D-CD28_{wt} showed increased surface expression, we generated Type I NKG2D co-receptors containing CD28 transmembrane (TM) and hinge (H) domains. Surface expression of $\gamma\delta$ TCR-CI5 and NKG2D_{wt}, or new chimeras containing CD28 TM domain on CD4+ T-cells after transduction and $\alpha\beta$ depletion was assessed. Using the same CD28 hinge and TM for all chimeras resulted in higher and more comparable surface expression. Chimera designs with CD28 hinge and TM (later referred as: NKG2D-ICOS_{CD28TM}, NKG2D-CD28_{wt} and NKG2D-4-1BB_{CD28TM}) were selected for further testing (e) Expression of CD69 on CD4+ TEGs upon stimulation with CD3 (0,2 μ g/ml and/or NKG2D (5 μ g/ml) antibodies, or CD3/CD28 dynabeads. MFI relative to the unstimulated condition is shown. N = 2 independent experiments with two biological replicates each. Data represents mean \pm SD. Significance was calculated using One way ANOVA with Tukey correction for multiple comparisons.

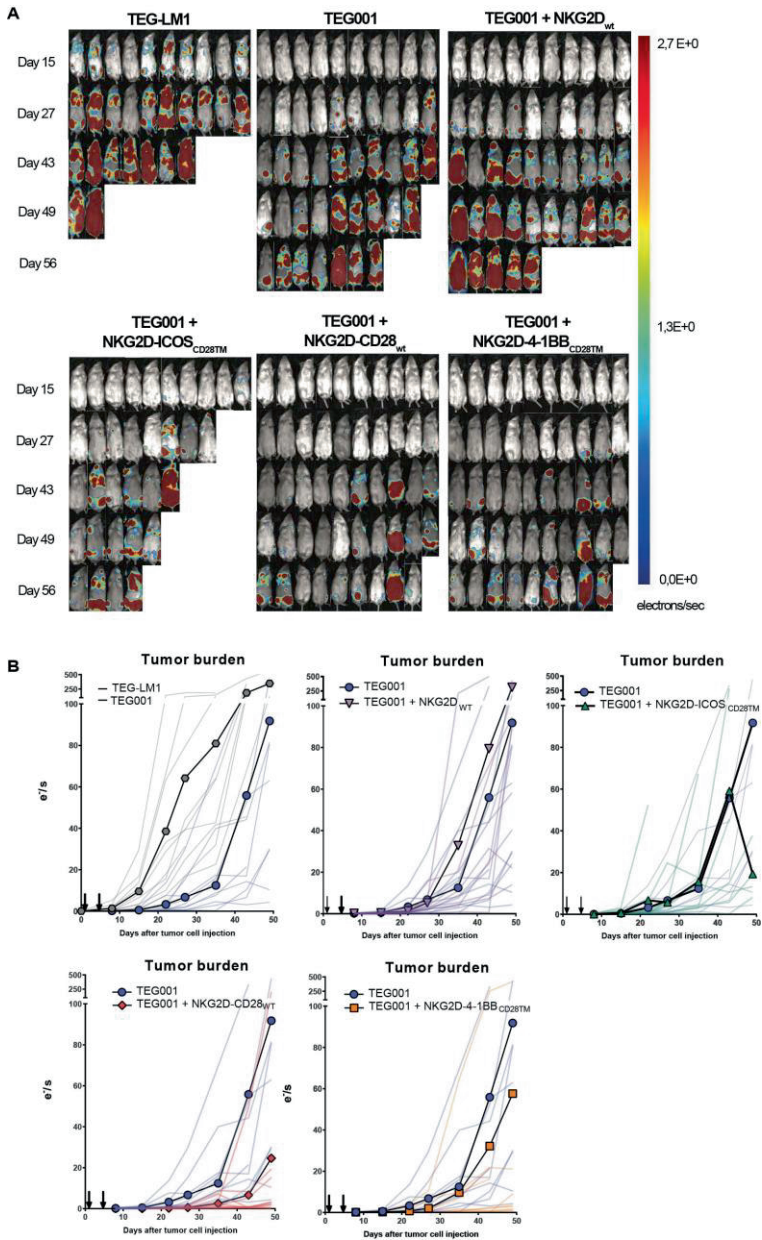


Extended Data Fig. 2. Introduction of NKG2D-4-1BB-chimera increases TEG001 IFN γ release in response to tumor cells, but does not impact short-term killing. (a) Surface expression of NKG2D-ligands in TEG001 targeted (K562, SCC9, RPMI-8226 and Daudi) or no targeted (HL60) tumor cells. MF was measured by flow cytometry using NKG2D-Fc and IgG-Fc fusion proteins. Fold change was calculated per type of cells as MFI, measured using NKG2DFc relative to IgG-Fc condition. (b) Transduced CD4+ T-cells were incubated with K562, Daudi or HL60 at several pamidronate concentrations. After 18 hours,

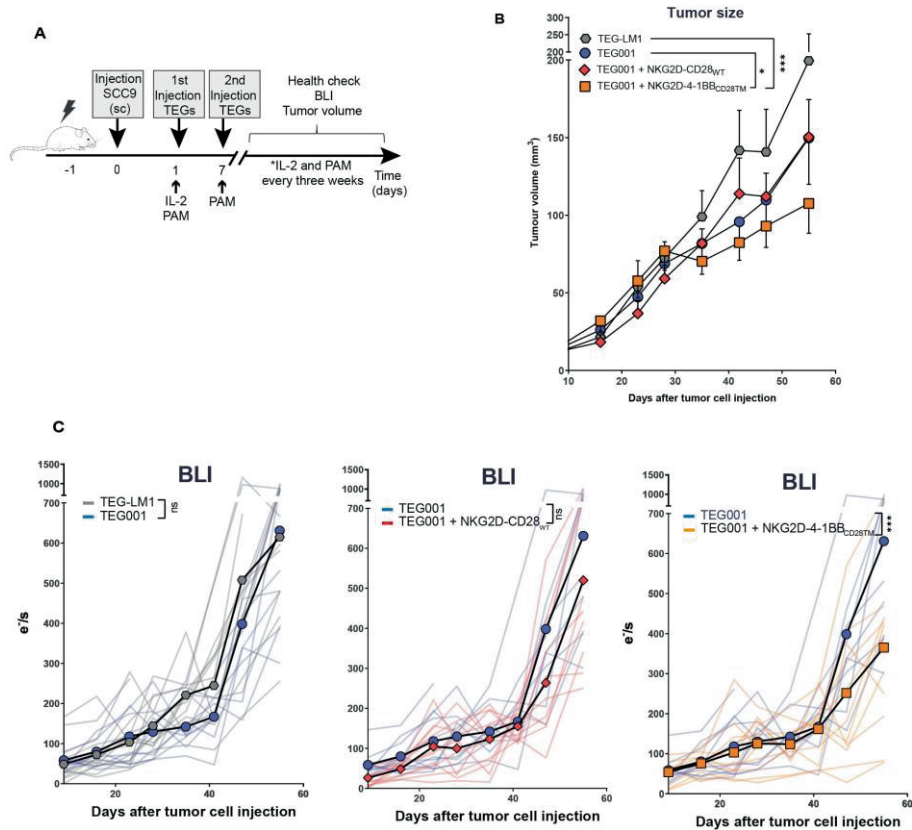
supernatants were harvested and analyzed for IFN γ secretion by ELISA. N = 3 independent experiments. Data represent mean \pm SD, significance was calculated using Two Way ANOVA with Dunnett correction. For K562: 3 μ M PAM (**P = 0.0075), 11 μ M PAM (**P = 0.0075), 33 μ M PAM (*P = 0.0112). (c) Transduced CD8 $^{+}$ (75%) were tested against K562, RPMI-8226, SCC9, Daudi and HL60 in a 51 Cr-release assay (E:T, 10:1, 3:1, 1:1, 0,33:1, 0,11:1). 51 Cr-release was measured in the supernatant after 5 hours. Specific lysis was calculated using the formula (experimental cpm - basal cpm)/(maximal cpm - basal cpm) \times 100 with maximal lysis determined in the presence of 5% triton, and basal lysis in the absence of effector cells. N = 2 independent experiments (for K562, SCC9 and HL60, N = 1 with biological replicates). Data represent mean.



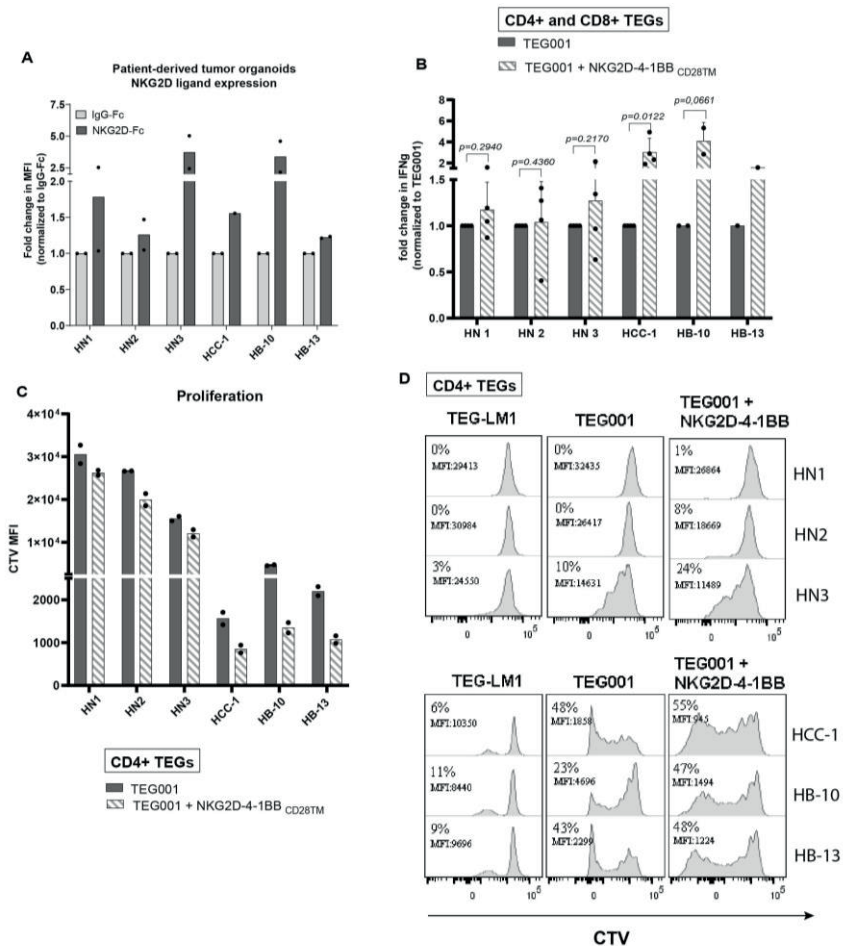
Extended Data Fig. 3. In vitro assessment of TEGs. (a) Surface expression of endogenous NKG2D in CD4+ and CD8+ $\alpha\beta$ T-cells. (b) CD8+ transduced T-cells were labeled with CTV and stimulated with CD3 and NKG2D antibodies for six days. On Day 6, MFI was assessed by flow cytometry. N = 2 independent experiments with two biological replicates each. Data represent Trace violet MFI mean \pm SD, significance was calculated using One Way ANOVA with Holm-sidak. For NKG2D 1 μ g/ml: NKG2D_{wt} (P = 0.0002); For NKG2D 2.5 μ g/ml: NKG2D_{wt} (**P = 0.0012). For NKG2D 5 μ g/ml: TEG-LM1 (**P = 0.0027). (c) CD4+ transduced cells were labeled using CTV and co-cultured with HL60 or RPMI-8226 tumor cells. On Day 6, proliferation was assessed by flow cytometry. Histogram data shows CTV intensity and percentage of proliferating cells, taking LM1 without targets as a control for gating.**



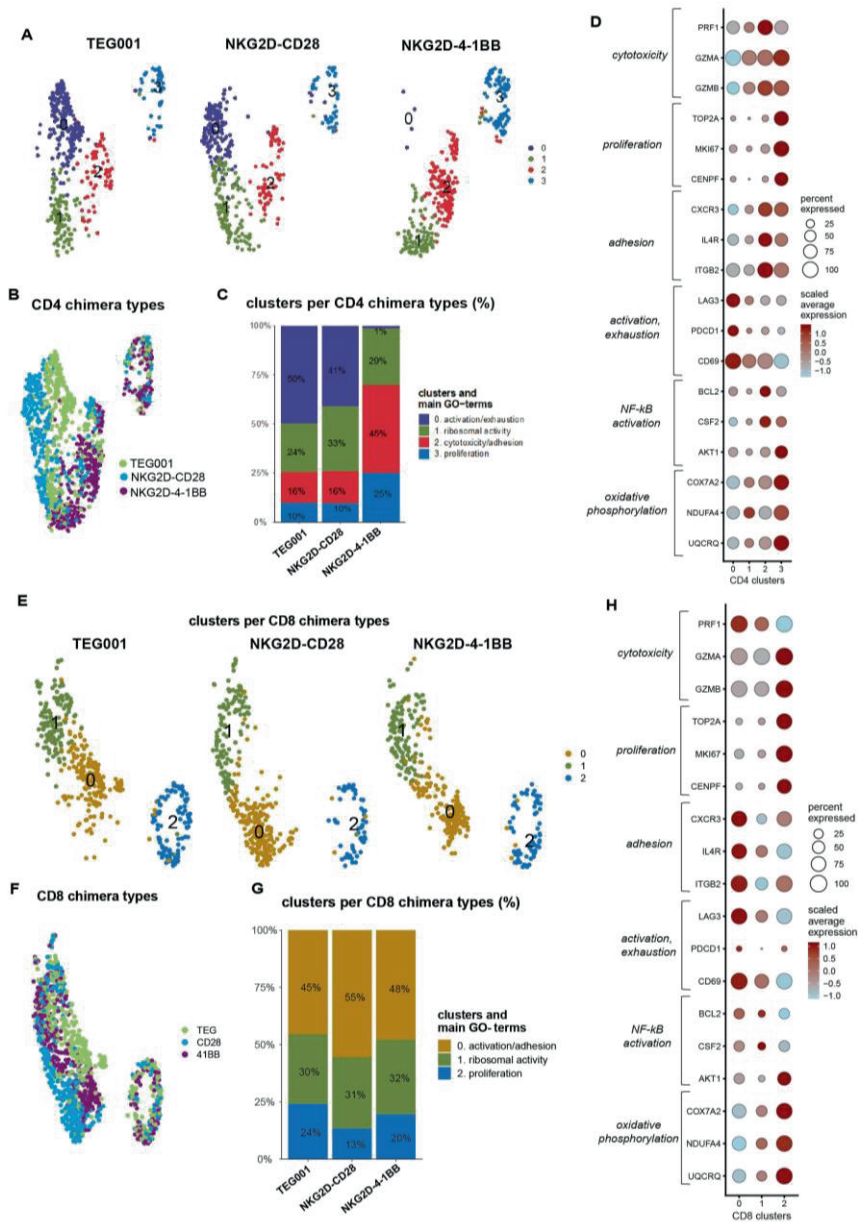
Extended Data Fig. 4. In vivo monitoring of tumor growth by BLI in multiple myeloma xenograft. (a) RPMI-8226-luciferase tumor growth in NSG mice treated with different TEGs. Pictures show BLI signal of all the mice on Days 15, 27, 43, 49, 56. Data generated from one experiment with $N = 10$ mice per treatment. (b) Comparison of BLI signal, including mean and single curves, from mice treated with TEG-LM1 (mock) (grey), TEG001 (blue), TEG001-NKG2D_{wt} (purple), TEG001-NKG2D-ICOS_{CD28TM} (green), TEG001-NKG2D-CD28_{wt} (red), TEG001-NKG2D-4-1BB_{CD28TM} (orange).



Extended Data Fig. 5. Therapeutic effects of TEGs co-expressing NKG2D chimeric co-receptors in a head and neck xenograft model. (a) Schematic diagram of experimental setup to evaluate efficacy of TEGs co-expressing NKG2D-chimeras against SCC9 luciferase tumor. Male and female NSG mice were irradiated and injected s.c. with 0.5×10^6 SCC9 tumor cells. On Days 1 and 7, 107 mice were treated with TEG-LM1 (mock) (N = 12), TEG001 (N = 11), TEG001-NKG2D-CD28_{WT} (N = 11) or TEG-NKG2D-4-1BB_{CD28T} (N = 11). Weekly BLI and bleeding were performed, and IL2 and PAM was administered every three weeks. Data generated from one experiment. (b) Tumor size was measured weekly. Data represent mean \pm SEM. Significance was calculated for tumor outgrowth over time using mixed-effect model test with repeated measures by comparing TEG-LM1 or TEG001 to the rest of the treatments. TEG-LM1 vs TEG001-NKG2D-4-1BB_{CD28T} (**P = 0.0002), TEG001 vs TEG001-NKG2D-4-1BB_{CD28T} (*P = 0.0148). (c) BLI were measured weekly to assess tumor outgrowth. Data represent single curves and mean for TEG-LM1 (mock) (grey), TEG001 (blue), TEG001-NKG2D-CD28_{WT} (red) and TEG001-NKG2D-4-1BB_{CD28T} (orange). Significance was calculated for tumor outgrowth over time using mixed-effect model test with repeated measures by comparing TEG-LM1 or TEG001 to the rest of the treatments. TEG-LM1 vs TEG001 (P = 0.5907), TEG001 vs TEG001-NKG2D-CD28_{WT} (P = 0.5570), TEG001 vs TEG001-NKG2D-4-1BB_{CD28T} (**P = 0.0003).

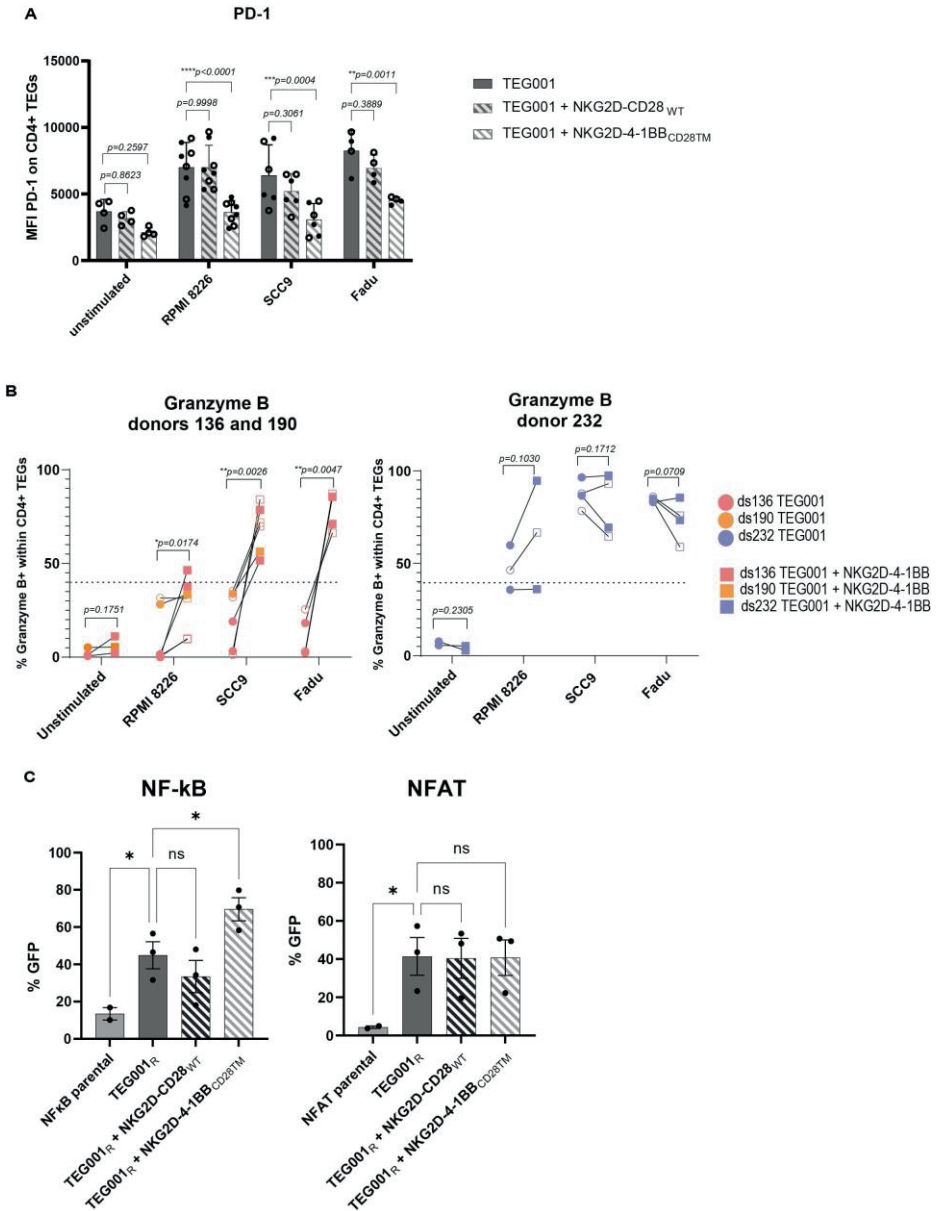


Extended Data Fig. 6. In vitro recognition of patient-derived tumor organoids by TEGs. (a) Surface expression of NKG2D-ligands in patient-derived liver and head neck tumor organoids. MFI was measured by flow cytometry using NKG2D-Fc and IgG-Fc fusion proteins. Data represent the mean of NKG2D-Fc staining, relative to IgG-Fc condition. N = 2 independent experiments for all organoids but HCC pt1 (N = 1) (b) Transduced CD4+ and CD8+ T-cells were incubated with the different organoids with 30-60 μ M PAM. After 18 hours, supernatants were harvested and analyzed for IFN γ secretion by ELISA. Data represent mean of fold change normalized to TEG001 \pm SD. N = 4 (HN1, HN2, HN3, HCC pt1), N = 2 (HB pt10) or N = 1 (HB pt13) independent experiments. Significance was calculated using unpaired one-tailed T test. Data represent mean \pm SD (c) Transduced CD4+ T-cells were labeled with CTV and co-cultured with patient-derived liver and head and neck tumor organoids in presence of 100 μ M PAM. On Day 6 MFI was assessed by flow cytometry. Representative graph of two independent experiments is shown. Data represent Cell Trace violet MFI mean of biological replicates. (d) Histogram data shows CTV intensity and percentage of proliferating cells, taking LM1 without targets as control for gating.



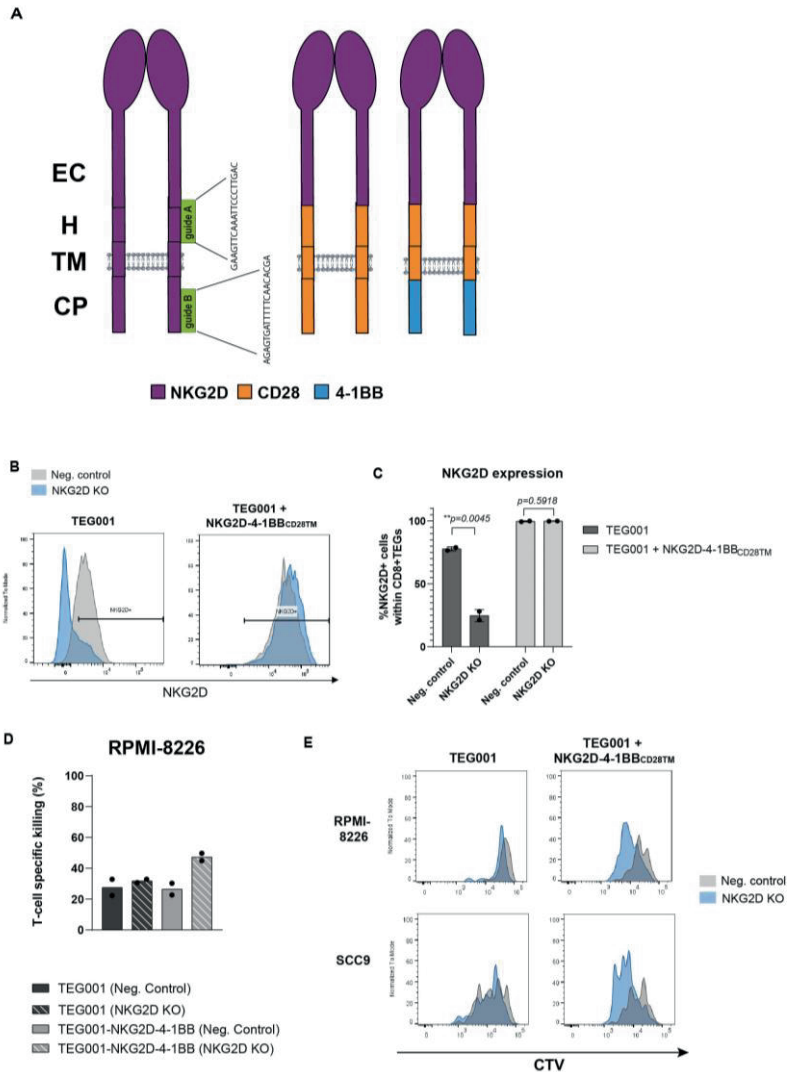
Extended Data Fig. 7. Separated clustering of CD4 and CD8 subsets for the different TEGs. a,b, CD4+ enriched cell from the TEG/CD28/41BB cell types (422, 404 and 351 cells, 1177 cells in total) split by chimera types. Cells are annotated by clusterID (a) or chimera types (b). (c) Percentage representation of the clusters (annotated by the main GO-terms) across the CD4(+) chimera types. (d) Density dot plot of the percentage of cells in a CD4(+) cluster that express a given gene ('percent expressed') and the scaled

average expression of canonical marker. e,f, CD8+ enriched cell from the TEG/CD28/41BB cell types (417, 415, 346, and cells, 1178 cells in total) split by chimera types. Cells are annotated by clusterID (e) or chimera types (f). (g) Percentage representation of the clusters (annotated by the main GO-terms) across the CD8(+) chimera types. (h) Density dot plot of the percentage of cells in a CD8(+) cluster that express a given gene ('percent expressed') and the scaled average expression of canonical marker.



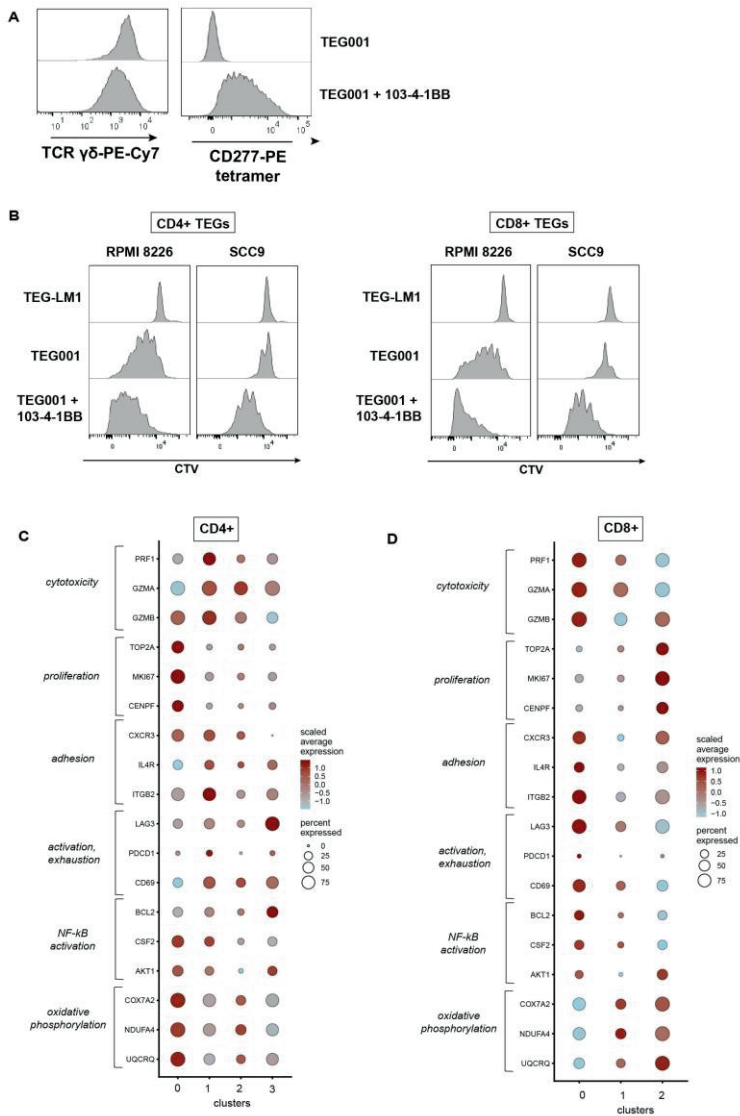
Extended Data Fig. 8. Decreased expression of PD-1 and enhanced expression of granzyme B and NF-κB in TEG001-NKG2D-4-1BB^{CD28TM}. (a) Expression of the exhaustion marker PD-1 (MFI) on CD4+ TEGs assessed by FACS after 4 rounds of stimulation with RPMI-8226, SCC9 or Fadu tumor cells in presence of 10 μM PAM. Opened symbols represent 1:1 E:T conditions. Closed symbols represent 3:1 E:T conditions. Data represent mean ± SD. Significance was calculated using One Way ANOVA with Tukey correction. N = 8 independent experiments for RPMI-8226, N = 6 for SCC9 and N = 4 for Fadu. (b) Percentage of granzyme

B+ cells within CD4+TEG001 and TEG001-NKG2D-4-1BB_{CD28TM} assessed by FACS for three different T-cell donors (ds136 in red; ds190 in orange; ds232 in blue) after 4 rounds of stimulation with RPMI-8226, SCC9 or Fadu in presence of 10 μ M PAM at E:T 3:1 (closed symbols) or 1:1 (opened symbols). Donors 136/190: N = 6 independent experiments for RPMI-8226, N = 6 for SCC9, N = 4 for Fadu; Donor 232: N = 3 independent experiments for RPMI-8226, N = 4 for SCC9, N = 4 for Fadu. Opened symbols represent 1:1 E:T conditions. Closed symbols represent 3:1 E:T conditions. Dotted line represents 40%. Significance was calculated using a one-tailed unpaired t test. (c) Percentage of GFP-positive cells after co-culture of Jurkat NF- κ B and Jurkat NFAT reporter cell lines with RPMI-8226 tumor cells. N = 3 independent experiments. Data represents mean \pm SEM. Statistical significance was calculated using One Way ANOVA followed by Fisher's LSD test comparison. For NF- κ B: NF- κ B parental (*P = 0.0247), TEG001-NKG2D-CD28_{WT} (P = 0.2842), TEG001-NKG2D-4-1BB_{CD28TM} (*P = 0.0405). For NFAT: NFAT parental (*P = 0.0377), TEG001-NKG2D-CD28_{WT} (P = 0.9387), TEG001-NKG2D-4-1BB_{CD28TM} (P = 0.9624).



Extended Data Fig. 9 | Knock-out (KO) of endogenous NKG2D improves killing and proliferation activity of in CD8+ TEG001-NKG2D-4-1BB. (a) Schematic overview showing annealing of crRNA guides (guide A and guide B) and NKG2D. (b, c) Percentage of NKG2D+ cells within CD8+TEG cells after electroporation with a negative control crRNA guide (grey) or NKG2D crRNA guides (blue). For TEG001, the percentage of NKG2D+ cells was reduced from 77% in the negative control to 21% after KO. Due to the high expression of the NKG2D chimera, the KO percentage on TEG001-NKG2D-4-1BB_{CD28}TM could not be assessed by FACS. As the percentage of KO cells in TEG001 was similar amongst biological replicates, the same efficiency was assumed for TEG001-NKG2D-4-1BB_{CD28}TM. Significance was calculated using a two-tailed unpaired t test. Data represents mean \pm SD. N = 2 independent experiments. (d) RPMI-8226 tumor cell line expressing luciferase and stroma cells were cultured in Matrigel constituting 3D bone marrow niche. After

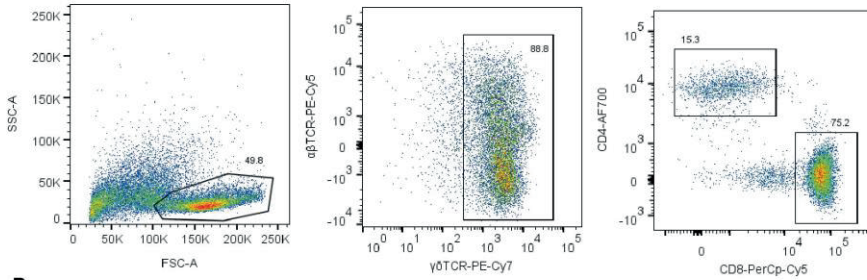
four days, CD8+ negative control and NKG2D-KO TEGs were added, together with PAM (10 μ M PAM). Six days later, living tumor cells were quantified by FACS. Tumor cell numbers were normalized to mock treatment (TEG-LM1). N = 1 with biological replicates. Data represent mean \pm SD. (e) Negative control (gray) and NKG2D KO (blue) CD8+TEGs were stained with CTV and co-cultured with RPMI-8226 or SCC9 (1:1, E:T) in presence of 100 uM pam. After 6 days, proliferation was assessed by FACS



Extended Data Fig. 10. Addition of 103-4-1BB-chimera to TEG001 impacts transcriptomics and proliferation capacity of CD4+ and CD8+ TEGs. a) Surface expression of $\gamma\delta$ TCR-CI5 and 103-4-BB chimeric receptor on T-cells after transduction and $\alpha\beta$ depletion, assessed by flow cytometry. (b) Transduced CD4+ and CD8+ T-cells were labeled with CTV and co-cultured with RPMI-8226 and SCC9 tumor cells in presence of 100 μ M PAM. On Day 6, MFI was assessed by flow cytometry. Representative histograms of two independent experiments are shown. (c) Density dot plot of the percentage of cells in a CD4+ cluster that express a given gene ("percent expressed"), and the scaled average expression of canonical marker. (d) Density dot plot of the percentage of cells in a CD8+ cluster that express a given gene ("percent expressed") and the scaled average expression of canonical marker.

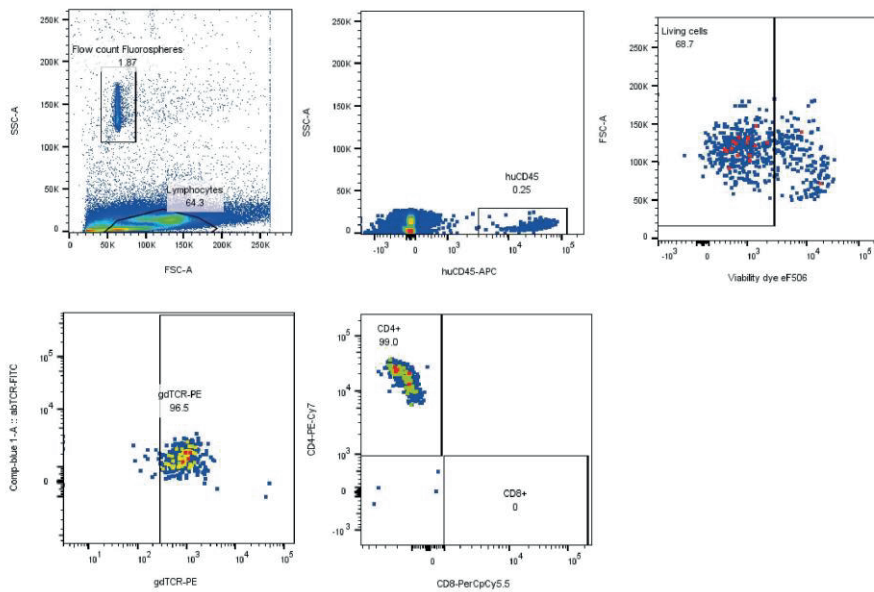
Supplementary figures

A

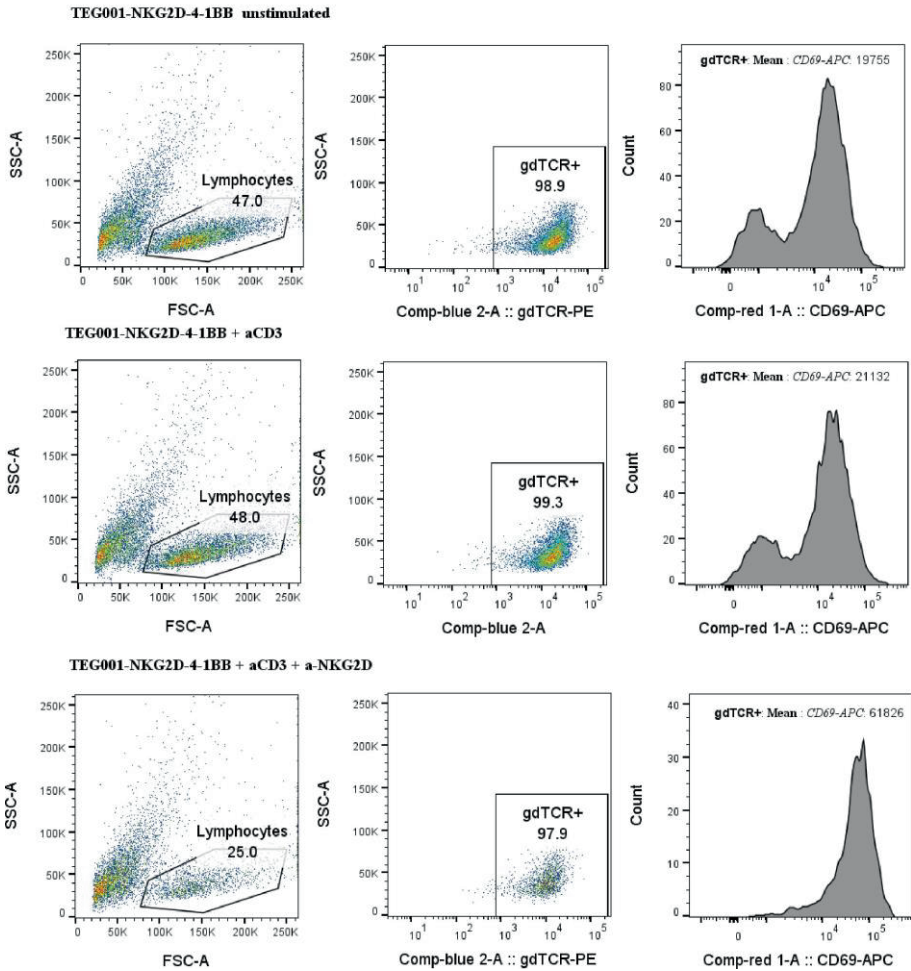
Gating of TEGs for *in vitro* experiments:

B

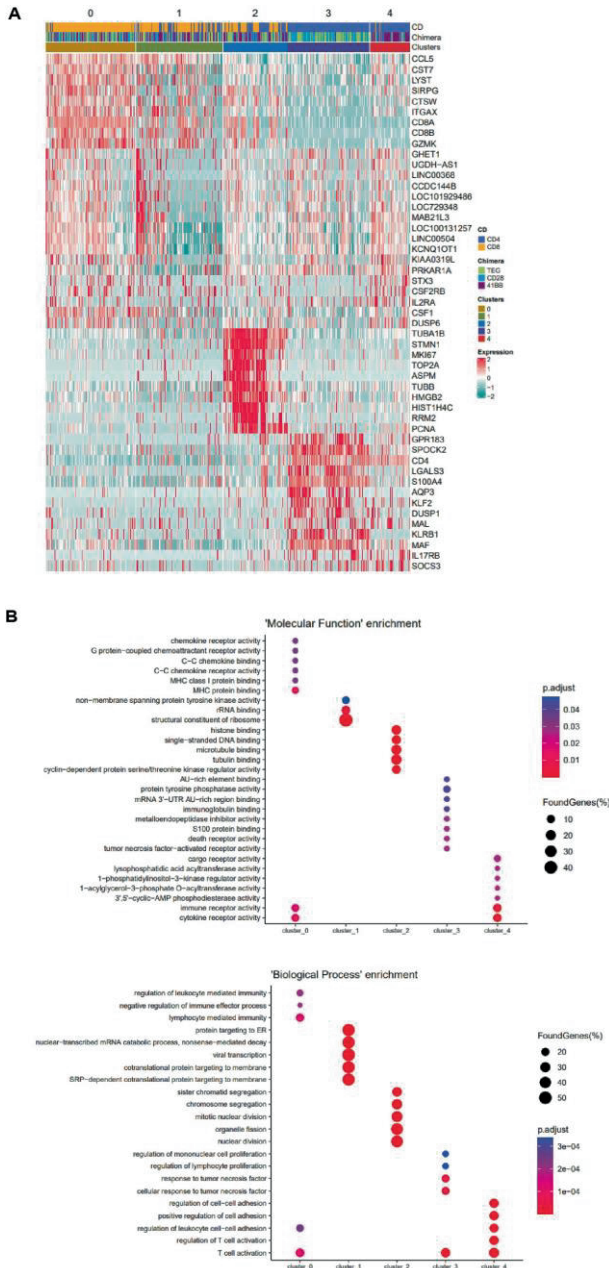
Gating of TEGs in mice samples:



Supplementary figure 1. Gating strategy for TEGs. (A) Example of gating strategy for TEGs used in *in vitro* experiments (B) Example of gating strategy for TEGs measured in mice samples

Gating of CD69 upregulation experiment:

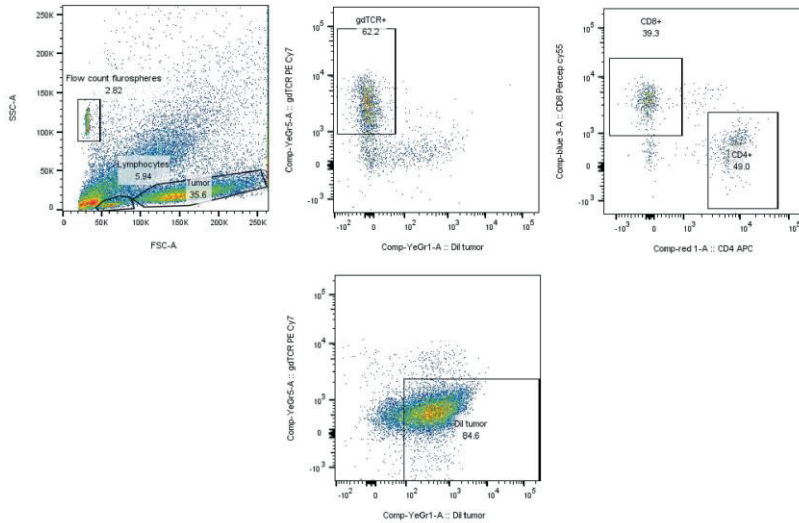
Supplementary figure 2. Gating strategy for the assessment of CD69 upregulation after stimulation with antibodies. Example of gating strategy and FACS plots for CD69 upregulation for non-stimulated TEG001-NKG2D-4-1BB and after stimulation with only antiCD3 antibody or a combination of anti-CD3 and anti-NKG2D antibodies



Supplementary figure 3. Expression of cluster marker genes for the analysis of TEG001, TEG001-CD28_{WT} and TEG001-4-1BB_{CD28TM} after incubation with RPMI-8226 (in Figure 4) (A) Heatmap displaying the top 10 marker genes per clusters. (B) Overrepresented GO terms (category: molecular function, biological pathway) per clusters in Figure 4.

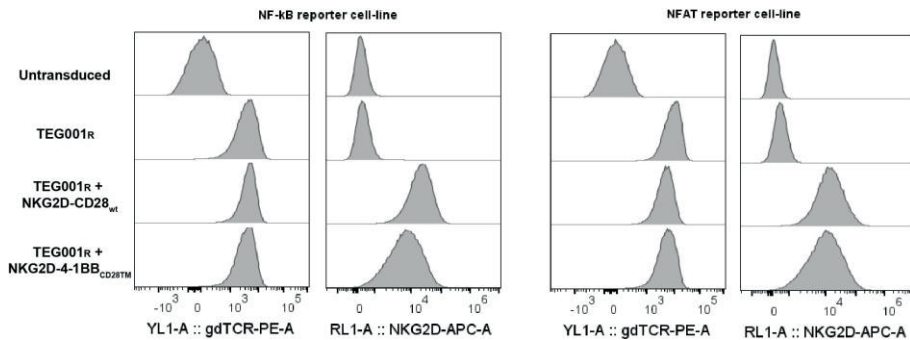
A

Example of gating for 3D model experiments:



B

gdTCR and chimeras expression in Jurkat reporter cell-line:




Supplementary figure 4. Gating strategy for 3D model experiments. (A) Example of gating strategy for the experiments performed using the 3D model. (B) Expression of $\gamma\delta$ TCR-Cl5 (TEG001R) and NKG2D-chimeras on Jurkat NF- κ B and Jurkat NFAT reporter cell-lines.

Supplementary tables

Supplementary table 1. Cytokine and chemokine production after co-culturing of TEGs and RPMI-8226 in a 3D model system

Day 3

	IL2			IL4			IL6			IL10			IL17		
	mean	SD	P value	mean	SD	P value	mean	SD	P value	mean	SD	P value	mean	SD	P value
TEG001	2.3	1.0		0.4	0.0		3057.2	199.7		127.4	5.3		15.3	0.2	
TEG001-NKG2D WT	2.5	2.0	0.8165	0.6	0.2	0.3953	3037.0	223.2	0.9999	139.0	1.5	0.0047	12.5	2.2	0.5614
TEG001-NKG2D-IC05	1.0	0.2	0.8166	0.4	0.2	0.9976	3301.4	83.2	0.6735	174.1	0.5	0.1508	11.5	0.2	0.3275
TEG001-NKG2D-CD28	6.5	2.2	0.1891	0.6	0.1	0.55	4130.1	288.9	0.0144	184.2	15.8	0.5001	17.0	0.4	0.8578
TEG001-NKG2D-4-1BB	8.1	0.7	0.0519	0.7	0.1	0.2255	4659.0	266.2	0.0045	179.4	12.8	0.2861	14.8	4.3	0.9974




	I309 (CCL1)			MIP1b (CCL4)			MCP3 (CCL7)			MCP2 (CCL8)			MIP3a (CCL20)			MDC (CCL22)		
	mean	SD	P value	mean	SD	P value	mean	SD	P value	mean	SD	P value	mean	SD	P value	mean	SD	P value
TEG001	8.9	3.6		15.1	0.3		129.7	12.6		20.5	1.1		49.1	6.0		42.0	7.0	
TEG001-NKG2D WT	8.2	0.5	0.9999	25.6	5.0	0.8775	109.1	19.8	0.9010	21.2	1.9	>0.9999	54.3	3.7	0.5888	67.0	17.1	0.1594
TEG001-NKG2D-IC05	16.5	15.5	0.7956	38.1	16.9	0.4133	123.2	0.7	0.9981	23.3	3.5	0.9999	52.8	0.4	0.7983	39.9	4.5	0.9986
TEG001-NKG2D-CD28	76.6	8.6	0.2397	79.6	26.4	0.0198	284.1	61.8	0.0739	71.8	21.8	0.0144	59.2	6.4	0.2189	106.5	11.2	0.0697
TEG001-NKG2D-4-1BB	49.7	4.9	0.0134	151.5	7.2	0.0007	210.1	21.1	0.1308	53.7	9.1	0.0744	68.8	0.2	0.0163	48.7	7.0	0.9092

	CCL28			GRO1a (CXCL1)			MIG (CXCL9)			IP10 (CXCL10)			SDF1a (CXCL12)			GMCSF		
	mean	SD	P value	mean	SD	P value	mean	SD	P value	mean	SD	P value	mean	SD	P value	mean	SD	P value
TEG001	OR<	OR<	n.a	915.3	64.0		33.1	3.4		216.9	45.1		8.0	0.8		19.1	0.4	
TEG001-NKG2D WT	OR<	OR<	n.a	925.8	22.0	0.9998	36.5	10.0	0.9990	205.2	26.6	>0.9999	5.8	6.8	0.9835	21.3	0.9	0.9633
TEG001-NKG2D-IC05	OR<	OR<	n.a	968.8	40.1	0.8646	49.0	1.2	0.8174	283.4	44.9	0.9990	1.0	0.0	0.5786	22.0	1.7	0.9074
TEG001-NKG2D-CD28	OR<	OR<	n.a	1011.5	124.1	0.3874	315.4	39.7	<0.0001	2260.0	785.6	0.0073	7.3	8.2	0.9998	44.8	5.7	0.0066
TEG001-NKG2D-4-1BB	OR<	OR<	n.a	998.0	65.9	0.6390	255.5	9.9	0.0001	1804.5	204.2	0.0211	10.5	6.2	0.9687	57.1	8.0	0.0011

Day 6

	IL2			IL4			IL6			IL10			IL17		
	mean	SD	P value	mean	SD	P value	mean	SD	P value	mean	SD	P value	mean	SD	P value
TEG001	115.2	63.6		22.0	6.0		100000.0	0.0		727.3	5.4		80.1	30.9	
TEG001-NKG2D WT	36.4	0.2	0.1235	9.6	0.4	0.0591	100000.0	0.0	>0.9999	605.2	50.9	0.8165	37.4	7.8	0.095
TEG001-NKG2D-IC05	32.2	4.7	0.1054	4.2	1.9	0.0147	100000.0	0.0	>0.9999	621.4	7.1	0.8731	29.2	3.7	0.0526
TEG001-NKG2D-CD28	54.5	2.0	0.2479	14.4	2.8	0.2454	9722.9	1	0.6487	600.9	23.7	0.8006	38.0	3.4	0.0994
TEG001-NKG2D-4-1BB	47.2	19.1	0.1870	14.1	4.6	0.2272	100000.0	0.0	>0.9999	733.4	240.4	>0.9999	38.3	8.0	0.102



	I309 (CCL1)			MIP1b (CCL4)			MCP3 (CCL7)			MCP2 (CCL8)			MIP3a (CCL20)			MDC (CCL22)		
	mean	SD	P value	mean	SD	P value	mean	SD	P value	mean	SD	P value	mean	SD	P value	mean	SD	P value
TEG001	453.5	14.0		958.7	224.8		33969.0	31265.8		11162.9	22306.1		5.8	0.9		2125.0	69.3	
TEG001-NKG2D WT	426.6	2.7	0.8849	1598.5	15.1	0.9635	17541.9	1698.3	0.4122	4914.3	1244.7	0.1411	978.7	64.2	0.0726	1943.9	135.0	0.8692
TEG001-NKG2D-IC05	346.7	27.4	0.0720	1077.6	145.3	0.9999	15029.3	600.4	0.3645	1382.6	1082.6	0.0962	248.1	75.4	0.6499	875.2	425.6	0.0113
TEG001-NKG2D-CD28	408.3	69.3	0.5400	2787.2	2833.3	0.5009	27556.5	4294.7	0.6455	6629.6	1637.0	0.1705	300.4	419.4	0.5145	2062.7	242.0	0.9963
TEG001-NKG2D-4-1BB	480.0	7.5	0.8490	3799.4	650.8	0.0748	47413.2	38949.9	0.9964	10109.2	6035.1	0.2507	638.2	210.1	0.0878	3021.8	202.2	0.2540

	CCL28			GRO1a (CXCL1)			MIG (CXCL9)			IP10 (CXCL10)			SDF1a (CXCL12)			GMCSF		
	mean	SD	P value	mean	SD	P value	mean	SD	P value	mean	SD	P value	mean	SD	P value	mean	SD	P value
TEG001	38.0	19.2		2692.5	18621.7		15718.1	2821.3		9915.9	637.3		544.5	445.2		659.3	126.8	
TEG001-NKG2D WT	10.8	13.4		9284.1	492.0	0.3593	14374.6	1400.8	0.9999	8507.7	1614.2	0.6435	121.1	48.1	0.2721	537.4	24.6	0.3236
TEG001-NKG2D-IC05	17.2	11.4	0.1286	6615.6	587.2	0.2677	14912.5	2657.7	>0.9999	6662.7	5.5	0.1328	96.3	6.7	0.2362	490.0	16.0	0.1448
TEG001-NKG2D-CD28	29.9	22.9	0.3262	23005.0	13085.2	0.9847	12411.9	2482.5	0.9978	9342.4	372.8	0.9610	117.1	22.3	0.2660	570.3	26.7	0.5453
TEG001-NKG2D-4-1BB	6.5	4.4	0.0604	3799.4	2885.8	0.6768	39072.6	33455.4	0.4302	9405.3	2252.2	0.9726	115.2	96.2	0.2631	590.1	72.1	0.7116

Supplementary table 2. p-values of the Fisher's Exact Test, comparing cluster abundances to the same clusters in TEG001, related to Figure 4.

	cluster abundances per chimera			p-values (versus TEG001)	
	TEG001	CD28	41BB	CD28	41BB
Cluster0	22%	27%	25%	0.0400	0.2770
Cluster1	21%	22%	29%	0.7215	4.76E-04
Cluster2	18%	12%	24%	2.72E-04	0.0095
Cluster3	31%	33%	1%	0.3702	2.42E-66
Cluster4	7%	6%	21%	0.4919	1.03E-15

p-values (chi-square) 0.003 8.73E-64

Supplementary table 3. Top 50 differentially expressed genes per clusters (related to Figure 4A,E)

rank	Cluster_0	Cluster_1	Cluster_2	Cluster_3	Cluster_4
1	CD8A	LINC00504	TUBA1B	KLRB1	CD4
2	GZMK	KCNQ10T1	STMN1	SPOCK2	MAL
3	CD8B	LOC100131257	HIST1H4C	S100A4	STX3
4	LYST	UGDH-AS1	TOP2A	DUSP1	IL17RB
5	CSF1	LINC00368	TUBB	LGALS3	IL2RA
6	ITGAX	LOC729348	MKI67	CD4	CSF2RB
7	SIRPG	LOC101929486	RRM2	KLF2	SOCS3
8	CCL5	MAB21L3	HMGB2	AQP3	DUSP6
9	CTSW	CCDC144B	ASPM	MAF	KIAA0319L
10	CST7	GHET1	PCNA	GPR183	PRKAR1A
11	IVNS1ABP	LOC101928103	NUSAP1	FOS	MALAT1
12	AOAH	LINC00506	CENPF	CD44	TRAT1
13	SIGLEC17P	ROR1-AS1	HMG2	RGS1	RDH10
14	RNF125	F5	CDK1	S100A6	TMEM173
15	NRX1	ZNF471	KIAA0101	TIMP1	ADGRG1
16	PRF1	LOC101926889	TMPO	LIMS1	SOS1
17	DUSP2	LOC55338	TK1	ZFP36	SORL1
18	SLAMF7	NRX1	DHFR	PTPN13	CD5
19	BCL2L11	LOC101928118	MCM7	NEAT1	LPCAT2
20	GZMA	FER	DUT	RORA	STT3B
21	FOXP3	RPS27	CENPE	TNFRSF25	CD40LG
22	IL2RB	LOC101929415	H2AFZ	CCL20	FOXP3
23	EOMES	LOC105372751	ASF1B	JAML	GNPDA1
24	CCR2	LOC101928936	FEN1	TNFRSF1B	MBOAT7
25	NCAM1	RPS29	CCNA2	CDC42EP3	LPAR6
26	LRRN3	LOC100129434	CKS2	LTK	TNF
27	LAG3	ZIM2-AS1	PRC1	CTSH	ARID5B
28	MCTP2	RPL23	PTMA	CDC25B	PDE7B
29	GLIPR1	HCST	SMC4	COL5A3	GATA3
30	NDVIP2	RPS17	TPX2	CD28	CISH
31	CD101	CCL5	H2AFX	CD40LG	NCDN
32	PRKCQ-AS1	ZNF480	CDKN2C	AHNAK	PDE7A
33	CD84	LOC102724434	CCNB2	CBLL1	CTSB
34	IL4R	RPS15A	HMGB1	CD52	CCDC50
35	HCST	COMMD6	SMC2	ZFP36L1	LGALS8
36	PTCH1	RPL41	TUBB4B	FAM65B	RAP2B
37	RASA1	RPS20	TUBA1C	S1PR4	TXNIP
38	ITGB2	RPL9	CKS1B	MIAT	AH1
39	ARHGAP25	ZNF37BP	ZWINT	PDCD1	CEACAM1
40	ARAP2	RPL38	H2AFV	IFI44	IL10RA
41	FYB	CCR3	BIRC5	KIAA1551	BCL2
42	TESPA1	MIDN	UBE2S	LZTFL1	ADAM19
43	APMAP	IMPAD1	DEK	B3GALT2	CD6
44	TOP1	PTK2B	NUCKS1	CD69	ANXA1
45	HOPX	RPL23A	GTSE1	ADD3	CNPB
46	EGLN3	RPL30	UBE2C	ODC1	SLC20A1
47	CRIM1	LINC00342	NCAPD2	PLEC	LAT
48	SERPINB9	ANKRD20A9P	ATAD2	KLF6	SNAP47
49	CXCR3	PTPRCAP	MCM5	CD6	EGR1
50	SAMD3	BCL2L11	RACGAP1	FOSB	BTG1

Supplementary table 4. p-values of the Fisher's Exact Test, comparing the per-cluster relative abundance values of CD4+ and CD8+ T-cells, related to Figure 4C.

	total count	CD4 count	CD8 count	CD4 %	CD8 %	pvalue
Cluster0	581	24	557	4%	96%	6.49E-264
Cluster1	566	191	375	34%	66%	4.99E-28
Cluster2	415	173	242	42%	58%	2.24E-06
Cluster3	534	534	0	100%	0%	NA
Cluster4	259	256	3	99%	1%	5.45E-142

Supplementary table 5. p-values of the Fisher's Exact Test, comparing the per-cluster relative abundance values of CD4+ and CD8+ T-cells, related to Extended data figure 7A-H.

CD4+	cluster abundances per chimera			p-values (versus TEG001)	
	TEG001	CD28	41BB	CD28	41BB
Cluster0	50%	41%	1%	0.0101	7.54E-62
Cluster1	24%	33%	29%	0.0073	0.1873
Cluster2	16%	16%	45%	0.8507	7.37E-19
Cluster3	10%	10%	25%	1.0000	3.22E-08

CD8+	cluster abundances per chimera			p-values (versus TEG001)	
	TEG001	CD28	41BB	CD28	41BB
Cluster0	45%	55%	48%	0.0044	0.5156
Cluster1	30%	31%	32%	0.8211	0.5339
Cluster2	24%	13%	20%	8.46E-05	0.1397

Supplementary table 6. Top 50 differentially expressed genes per chimera types (related to Figure 4B,F).

rank	TEG	CD28	41BB	TEG	CD28	41BB
	CD4	CD4	CD4	CD8	CD8	CD8
1	FOS	SPOCK2	TNF	DUSP2	CD8A	GZMK
2	DUSP1	KLRB1	CD4	SLAMF7	CD8B	CD8A
3	RGS1	LYZ	TUBA1B	CD8A	NKG7	CD8B
4	GPR183	CD4	HMGB2	RNF125	CCL5	CTSW
5	FOSB	S100A4	HLA-DQA1	EGR2	GZMK	GZMA
6	CD69	AQP3	CLDND1	ITGAX	GZMB	ITGAX
7	S100A4	TIMP1	STMN1	EOMES	LAG3	AIF1
8	ZFP36	KLF2	HLA-DRA	RCBTB2	SIRPG	TARP
9	CD40LG	MAF	TUBB	NKG7	CTSW	SIRPG
10	KLF6	LGALS3	MAL	DUSP6	PRF1	BCL2L11
11	CD4	CD6	ITM2A	CD8B	CST7	CLDND1
12	ZFP36L1	LIMS1	TMEM200A	GZMA	SIGLEC17P	CD7
13	PTPN13	NEAT1	PDE7A	MMP25	GNLY	HOPX
14	LGALS3	CD52	CXCR3	IL4R	ITGAX	EGLN3
15	KLF2	CBLL1	NCDN	NCAM1	CSF1	PTK2B
16	SPOCK2	ODC1	HNRNPD	CD84	IL2RB	LRRN3
17	S100A6	COL5A3	HLA-DRB1	KRAS	LYST	NDFIP2
18	EGR1	ITM2C	RRM2	IVNS1ABP	NCR3	ENTPD1
19	CD44	CD70	OAS3	CTSW	HCST	FOXP3
20	SOS1	IL17RB	SH3BGRL3	IRF1	AOAH	BANF1
21	RORA	FAM65B	CLU	ACSL6	EOMES	AOAH
22	SAT1	CDC25B	PRKAR1A	EGR1	ITGB2	HLA-DMA
23	IFI44	PDCD1	CCT5	HCST	CD84	NCAM1
24	MAF	CD44	SLC20A1	PRKCQ-AS1	LOC101928103	MICAL2
25	TGFBR3	CD28	S100A11	LRRN3	FOXP3	EOMES
26	AHNAK	FLNA	MKI67	GSTP1	GZMA	TESC
27	CTSH	S1PR4	RDH10	ARAP2	CYFIP2	COTL1
28	JUNB	P2RX4	TRAT1	GZMK	FYB	CSF1
29	LZTFL1	CCL20	WEE1	GZMH	CD101	NKG7
30	ZNRF1	S100A6	COX17	CRIM1	RAB27B	MT2A
31	SOCS3	TNFRSF1B	PDE3B	IER2	EPAS1	MT-ND1
32	KLRB1	FBXL16	PGK1	PHLDA1	CCR3	SV2A
33	TNFRSF25	RNASET2	DUT	LYST	GLIPR1	MT-ATP6
34	JAML	CD5	HSP90AB1	CCDC144B	SAMD3	PRF1
35	JUN	SYNE2	HERC5	FOSB	KPNA4	TSPAN5
36	B3GALT2	GPR183	SMC1A	PRKCQ	MMP25	RBPJ
37	NFKBIZ	CDC42EP3	COX8A	HOXB2	CXCR3	TEX30
38	HLA-DRA	CAMK1D	KIAA0101	GATA3	ACP5	ARID1A
39	TNFRSF1B	MAL	CD74	NFKBIZ	BCL2L11	C12orf75
40	CXCR6	GPX1	SOD1	PRRC2C	LCP2	MT-CO2
41	KDSR	ITGB1	TRAPPC1	ANP32A	CCDC144B	TUBA1B
42	BTG2	MIAT	PATL1	USP28	IVNS1ABP	CD38
43	KIAA1551	ADD3	HLA-DPA1	JUNB	G6PD	PPIA
44	IER2	SELPLG	RAB1A	PRF1	BTN3A1	CLEC2B
45	TMEM167A	LAPTM5	PKM	CD48	BBX	GPX4
46	HLA-DRB1	LYAR	TXN	GZMB	CCR2	LAI2
47	CMTM6	PLEKHG3	ARF3	HEG1	CCR1	RNF138
48	MAL	PBXIP1	PCNA	AOAH	KLRG1	BHLHE40
49	TIMP1	FCMR	RBX1	BATF	SATB1	HNRNPC
50	CDC42EP3	MXD1	LDHA	MT-RNR1	AGTRAP	GSTP1

Supplementary table 7. p-values of the Fisher's Exact Test, comparing cluster abundances to the same clusters in TEG001 (of the matching CD4/8 group), related to Figure 5D,G.

CD4+	cluster abundances per chimera		p-values (versus TEG001)
	TEG001	103_41BB	103_41BB
Cluster0	21%	65%	1.96E-28
Cluster1	34%	21%	3.38E-04
Cluster2	32%	14%	8.78E-07
Cluster3	13%	0%	NA

CD8+	cluster abundances per chimera		p-values (versus TEG001)
	TEG001	103_41BB	103_41BB
Cluster0	46%	21%	6.34E-07
Cluster1	33%	24%	0.1089
Cluster2	21%	55%	2.55E-11



CHAPTER 7

Characterization and modulation of anti- $\alpha\beta$ TCR antibodies and their respective binding sites at the β TCR chain to enrich engineered T cells

G.J.J. Kierkels^{1*}, E. van Diest^{1*}, P. Hernández-López^{1*}, W. Scheper^{1*}, A.C.M. de Bruin¹, E. Frijlink¹, T. Aarts-Riemens¹, S.F.J. van Dooremalen¹, D.X. Beringer¹, R. Oostvogels², L. Kramer¹, T. Straetmans¹, W. Uckert³, Z. Sebestyén¹, J. Kuball^{1,2}

¹Center for Translational Immunology, University Medical Center Utrecht, Utrecht University, Heidelberglaan 100 3584 CX, The Netherlands

²Department of Hematology, University Medical Center Utrecht, Heidelberglaan 100 3584 CX, The Netherlands

³Max-Delbrück-Centrum für Molekulare Medizin (MDC), Robert-Rössle-Str. 10 13125, Berlin, Germany

*Equally contributed

Molecular Therapy; Methods & Clinical Development, 2021

Abstract

T cell engineering strategies offer cure to patients and entered clinical practice with chimeric antibody-based receptors, $\alpha\beta$ T cell receptors ($\alpha\beta$ TCR)-based strategies are however lagging behind. To allow a more rapid and successful translation to successful concepts also using $\alpha\beta$ TCRs for engineering, incorporating a method for the purification of genetically modified T cells, as well as engineered T cell deletion after transfer into patients, could be beneficial. This would allow to increase efficacy, reduce potential side effects, and improve safety of newly, to be tested, lead structures. By characterizing the antigen binding interface of a GMP-grade anti- $\alpha\beta$ TCR antibody, usually used for depletion of $\alpha\beta$ T cells from stem cell transplantation products, we developed a strategy which allows for the purification of untouched $\alpha\beta$ TCR engineered immune cells by changing two amino acids only in the TCR β chain constant domain of introduced TCR chains. Vice versa, we engineered an antibody, which targets an extended mutated interface of nine amino acids in the TCR β chain constant domain, and provides the opportunity to further develop depletion strategies of engineered immune cells.

Introduction

The FDA approval of the first engineered T cells expressing chimeric antigen receptors has paved the way for new cellular interventions in the clinic ^{1,2}. A next wave of cell therapy will come with T cell receptor (TCR) engineered T cells specific for targets on both solid and hematological malignancies ³. Most clinical trials using $\alpha\beta$ TCR engineered T cells are directed against cancer/testis antigens, such as NY-ESO-1 ⁴. Although the clinical response rates are very encouraging, only a small proportion of the patients benefit from these novel treatments^{5, 6}. Disappointing response rates can be partially attributed to the presence of non- and poorly- engineered T cells in the administered cell product ⁷. These non- and poorly- engineered T cells can hamper the therapeutic efficiency of engineered immune effector cells because of e.g. insufficient expression of the introduced receptor, mispairing of introduced $\alpha\beta$ TCR with endogenous $\alpha\beta$ TCR ⁸, or by competition for endogenous homeostatic cytokines ^{7,9}. Furthermore, in an allogenic setting, the presence of T cells still expressing the endogenous $\alpha\beta$ TCR can lead to severe graft versus host disease. Purification of engineered T cells before infusion can overcome these hurdles, ultimately resulting in enhanced *in vivo* activity. Current methods for purification of engineered T cells often depend on the expression of artificial molecules such as truncated CD34 ¹⁰ or truncated NGFR ¹¹, in addition to the tumor specific receptor. However, bigger transgene cassettes used to introduce multiple proteins are relatively difficult to express, and additional transgenes can add immunogenic properties to the engineered cell product ¹². Besides purification of engineered T cells to increase effectivity, elimination of engineered T cells after adoptive transfer might be needed, in case of cytokine release syndrome ¹³ or off-target toxicities e.g. due to peptide mimicry ^{5, 14}, expression of the antigen at low levels in healthy tissues ¹⁵, or mispairing of introduced with endogenous $\alpha\beta$ TCR chains resulting in unwanted specificities ⁸. A currently explored solution for the elimination of transferred cells, is the co-expression of HSV-TK along with the transgene of interest ¹⁶, mainly limited by the immunogenicity and relatively large size of the HSV-TK gene ¹⁷. An alternative elegant solution is to introduce a myc-tag into the $\alpha\beta$ TCR sequence itself, followed by *in vivo* depletion through myc-specific antibodies ¹⁸. However, introducing artificial

genes into the $\alpha\beta$ TCR might alter downstream signaling by modifying e.g. its glycosylation¹⁹. Selection of engineered T cells and subsequent *in vivo* elimination achieved with a single marker, which has previously been described for CD20²⁰, would be favorable, due to the relatively small transgene cassette, and therefore better expression. Even better would be a method where the introduced tumor specific TCR could also be used for both purification and *in vivo* depletion, and thereby combines all three properties in one gene: tumor specificity, a selection opportunity of cells expressing the transgene at high levels, as well as an *in vivo* depletion option, which allows for the elimination of the engineered immune cells in case of toxicities caused by the introduced receptor. Within this context we have explored a strategy based on the recent development of purified $\alpha\beta$ T cells engineered to express a defined $\gamma\delta$ T cell receptor (TEGs)²¹⁻²⁹. In this strategy we took advantage of the observation that an anti-human $\alpha\beta$ TCR antibody used for the purification of TEGs does not cross-react with $\gamma\delta$ TCR chains, and can thereby differentiate between engineered and non-engineered cells. This anti-human $\alpha\beta$ TCR antibody is routinely used to deplete $\alpha\beta$ TCR T cells from apheresis products using CliniMACS depletion before allogeneic stem cell transplantation^{3, 30}. Here we describe the translation of the TEG purification procedure into a purification procedure for $\alpha\beta$ TCR engineered T cells. We also provide the rationale for the additional development of elimination strategies of engineered immune cells by further modulating the binding site to be selectively targeted by a second independent antibody.

Materials and Methods

Cells and cell lines

Phoenix-Ampho cells (CRL-3213) were obtained from ATCC and cultured in DMEM (Thermo Fisher Scientific, Breda, The Netherlands) containing 1% Pen/Strep (Invitrogen by Thermo Scientific, Breda, The Netherlands) and 10% FCS (Bodinco, Alkmaar, The Netherlands). The TCR β ^{-/-} Jurkat cell line (a derivative of Jurkat J.RT3-T3.5 cells³¹), a kind gift from Erik Hooijberg (VU Medical Center, Amsterdam, The Netherlands), TCR β ^{-/-} Jurkat-76, a kind gift from Miriam Heemskerk (LUMC, Leiden The Netherlands) and the T2 cell line (ATCC CRL-1992) were cultured in RPMI 1640 + GlutaMAX (Thermo Fisher

Scientific, Breda, The Netherlands) containing 1% Pen/Strep and 10% FCS. Cell lines were authenticated by short tandem repeat profiling/karyotyping/isoenzyme analysis. All cells were passaged for a maximum of 2 months, after which new seed stocks were thawed for experimental use. In addition, all cell lines were routinely verified by growth rate, morphology, and/or flow cytometry and tested negative for mycoplasma using MycoAlert Mycoplasma Kit (Lonza, Breda, The Netherlands). Peripheral Blood Mononuclear Cells (PBMCs) were obtained from Sanquin Blood Bank (Amsterdam, The Netherlands) and isolated by Ficoll-Paque (GE Healthcare, Eindhoven, The Netherlands) from buffy coats. PBMCs were cultured using the previously described Rapid Expansion Protocol (REP; ³²) in RPMI containing 5% non-typed human serum (Sanquin Blood Bank, Amsterdam, The Netherlands), 1% Pen/Strep (Invitrogen by Thermo Scientific, Breda, The Netherlands) and 50 μ M Gibco™ β -Mercaptoethanol (Fisher scientific, Thermo Fisher Scientific, Breda, The Netherlands) (collectively called HuRPMI).

Cloning of TCR chains into single retroviral vectors

The “minimally murinized” V α 16.1 and V β 4.1 chains from an NY-ESO1₁₅₇₋₁₆₅/HLA*02 specific TCR, respectively named M2.2.3 and M1.KA,4.1, were generated as previously described ³³. Additional partially murinized (regions or single residues) TCR chains were ordered from GeneArt (Life Technologies, Thermo Fisher Scientific, Breda, The Netherlands) or constructed via mutagenesis PCR. Cysteine modified chains were designed as reported previously ³⁴. Variants of chimeric $\alpha\beta/\gamma\delta$ TCRs were composed using the IMGT database ³⁵. Sequences were codon optimized and ordered in an industrial resistance-gene harboring vector or as DNA strings (Geneart Life Technologies, Thermo Fisher Scientific, Breda, The Netherlands). DNA strings were processed using the TA TOPO cloning kit (Thermo Fisher Scientific, Breda, The Netherlands) and cloned into the pCR™2.1-TOPO® vector, according to the manufacturer’s protocol. All TCR chains were cloned separately into the retroviral vector pMP71 between the EcoRI and NotI restriction sites, using the indicated restriction enzymes and T4 DNA ligase (all

from New England Biolabs, Ipswich MA, United States). Transformation of ligated constructs was performed in JM109 competent E. Coli (Promega, Leiden, The Netherlands), and subsequent plasmid DNA isolation was conducted using Nucleobond® PC500, according to the manufacturer's protocol (Macherey-Nagel, Düren, Germany).

Retroviral transduction of primary T cells and T cell lines

Phoenix-Ampho packaging cells were transfected using Fugene-HD (Promega, Leiden, The Netherlands) with env (pCOLT-GALV), gagpol (pHIT60), and separate pMP71 constructs containing α or β chains from a NY-ESO1₁₅₇₋₁₆₅/HLA-A*02 specific TCR (isolated from clone ThP2³⁶) kindly provided by Wolfgang Uckert³⁷, or containing TCR γ (G115)-T2A-TCR δ (G115)LM1²¹. PBMCs (preactivated with 50 IU/ml IL-2 (Proleukin, Novartis, Arnhem, The Netherlands) and 30 ng/ml anti-CD3 (clone OKT-3, Miltenyi Biotec, Bergisch Gladbach, Germany), CD4/CD8 T cells selected from PBMCs with REAlease CD4/CD8 (TIL)microbead kit (Miltenyi Biotec, Bergisch Gladbach, Germany) preactivated with anti-CD3/CD28 Dynabeads bead to T cell ratio 1:5 (Thermo Fisher Scientific, Breda, The Netherlands) and 1.7×10^3 IU/ml of MACS GMP Recombinant Human interleukin (IL)-7, and 1.5×10^2 IU/ml MACS GMP Recombinant Human IL-15 (Miltenyi Biotec, Bergisch Gladbach, Germany), Jurma or Jurkat-76 cells were transduced twice within 48 hours with viral supernatant in 6-well plates (4×10^6 cells/well) in the presence of 50 IU/ml IL-2 (PBMCs only), 1.7×10^3 IU/ml IL-7, 1.5×10^2 IU/ml IL-15 and CD3/CD28 dynabeads 1:5 bead to T cell ratio (CD4/CD8 selected T cells only) and 6 μ g/ml polybrene (all) (Sigma-Aldrich, Munich, Germany). After transduction, primary T cells were expanded by the addition of 50 μ l/well anti-CD3/CD28 Dynabeads (Thermo Fisher Scientific, Breda, The Netherlands) and 50 IU/ml IL-2 or 1.7×10^3 IU/ml IL-7, 1.5×10^2 IU/ml IL-15.

Purification of engineered T cells by MACS depletion of poorly and non-engineered immune cells

Transduced primary T cells were incubated with biotin-labeled anti-human $\alpha\beta$ TCR antibody (clone BW242/412; Miltenyi Biotec, Bergisch Gladbach, Germany), followed by incubation with an anti-biotin antibody coupled to magnetic beads (anti-biotin MicroBeads; Miltenyi Biotec, Bergisch Gladbach,

Germany)²¹. Next, the cell suspension was applied to an LD column in a QuadroMACS™ Separator. $\alpha\beta$ TCR-positive T cells were depleted by MACS cell separation according to the manufacturer's protocol (Miltentyi Biotec, Bergisch Gladbach, Germany).

In silico TCR modelling

The structure of different murinized constant domains was predicted using SWISS-MODEL³⁸ on the modeled template of the β chain of the human JKF6 T-cell receptor (PDB entry code: 4ZDH). The structure of the murinized constant domains when binding H57-597 was modeled on the template of the β chain of the murine N15 T-cell receptor (PDB entry code: 1NFD)³⁹. Structure visualizations were performed using PyMol Molecular Graphics System⁴⁰.

Chimeric antibody production and purification

Hamster-human (IgG1) chimeric H57-597 antibody was generated using Lonza expression vectors (pEE14-4-kappaLC, pEE14-4-IgG1)^{41, 42}. The antibody was produced by transient transfection of HEK293F cells with the heavy chain coding plasmid, the light chain coding plasmid and pAdVantage (Accession Number U47294; Promega, Leiden, The Netherlands), using 293fectin transfection reagent (Invitrogen, Thermo Scientific, Breda, The Netherlands) following the manufacturer's instructions. Antibody-containing supernatant was harvested 4 days after transfection and purified by affinity chromatography using HiTrap Protein G HP antibody purification columns (GE Healthcare, Eindhoven, The Netherlands).

Sequencing

DNA sequences of cloning intermediates and final constructs in pMP71 were verified by Barcode Sequencing (Baseclear, Leiden, The Netherlands). 75 μ g plasmid DNA and 25 pmol primer specific for the pCR™2.1-TOPO® vector or pMP71 vector were premixed in a total of 20 μ l and sent to Baseclear for Sanger sequencing.

Flow cytometry

Cells were stained with V β 4-FITC (TRBV29-1, clone WJF24; Beckman Coulter, Brea, California), $\alpha\beta$ TCR-PE (clone BW242/412; Miltentyi Biotec,

Bergisch Gladbach, Germany) CD3-PB (clone UCHT1; BD), CD4-PeCy7 (clone RPA-T4; eBioscience, Thermo Fisher Scientific, Breda, The Netherlands), CD8-APC (clone RPA-T8; BD), CD8-PB (clone SK1; Biolegend, San Diego, California), or RPE-conjugated NY-ESO-1₁₅₇₋₁₆₅ HLA*02:01 (SLLMWITQV) pentamer (ProlImmune, Oxford, United Kingdom). Samples were fixed using 1% PFA in PBS, measured on a FACSCanto-II flow cytometer (BD, Eysins, Switzerland), and analyzed using FACSDiva (BD, Eysins, Switzerland) or FlowJo (BD, Eysins, Switzerland) software.

ELISA

Effector and target cells (E:T 50,000:50,000) were incubated for 16 hours after which supernatant was harvested. IFN γ ELISA was performed using ELISA-ready-go! Kit (eBioscience, Thermo Fisher Scientific, Breda, The Netherlands) following the manufacturer's instructions.

MMAE ADC construction

Chimeric H57-MC-VC-PAB-MMAE was constructed using a kit from CellMosaic, (Woburn, Massachusetts) following the manufacturer's instructions.

Statistical analysis

Statistical analyses were performed using GraphPad Prism 8.3.0 for Windows (GraphPad Software, La Jolla, California). Differences between groups was calculated using a one- or two tailed paired T test (Figure 3, 5) or a repeated measure One-way Anova (Figure 4). Normal distribution of input data was assumed.

Results

Anti-human $\alpha\beta$ TCR binds an epitope on the TCR β chain of human $\alpha\beta$ cells

The GMP-grade anti-human $\alpha\beta$ T cell receptor (TCR) monoclonal antibody clone BW242/412 (from now on referred to as anti-human $\alpha\beta$ TCR) recognizes a common determinant of the human TCR α/β -CD3 complex, which has not yet been characterized. In order to allow for further epitope mapping of the

interface between the anti-human $\alpha\beta$ TCR clone BW242/412 and a human $\alpha\beta$ TCR, we first tested the antibody's ability to bind to murine $\alpha\beta$ TCRs. Therefore, Jurma T cells, a TCR-deficient T cell line, were transduced with human $\alpha\beta$ TCRs directed against the cancer/testis antigen NY-ESO-1157-165 37 or with a murine nonsense $\alpha\beta$ TCR composed of the TCR α chain of an MDM2-specific $\alpha\beta$ TCR 43, and the TCR β chain of a p53-specific $\alpha\beta$ TCR 44. Specific binding of the anti-human $\alpha\beta$ TCR was only observed to the human (α HuHu/ β HuHu) but not the murine (α MuMu/ β MuMu) TCR transduced Jurma cells (Figure 1A). To rule out that parts of the human variable domain of the $\alpha\beta$ TCR bind to the anti-human $\alpha\beta$ TCR antibody, the human NY-ESO-1 $\alpha\beta$ TCR variable domain was grafted on the murine constant domain to create a chimeric $\alpha\beta$ TCR (α HuMu/ β HuMu). Replacing only the human TCR α and TCR β constant domains by murine equivalents completely abrogated binding of anti-human $\alpha\beta$ TCR, to levels resembling binding to a fully murine $\alpha\beta$ TCR (α MuMu/ β MuMu). This indicates that the human constant domain contains the binding epitope. Comparable transgenic expression of murine and human TCRs was confirmed by anti-MuTCR β and anti-V β 4 respectively (Figure 1A). Infusion of T cells expressing TCRs with complete murine constant domains into patients can generate immunogenic effects, and lead to a decreased persistence of the engineered cells in vivo 45. To minimize these undesirable effects, we aimed to map the minimal amount of murine residues needed to disrupt binding of anti-human $\alpha\beta$ TCR, by making use of previously described chimeric-TCR α and β chains, with mutational blocks covering all amino acid differences between the constant regions of human and mouse $\alpha\beta$ TCRs 37. We tested three NY-ESO-1 TCR α chain variants, and four NY-ESO-1 TCR β chain variants, each containing one murine domain, flanked by complete human amino acid sequences. Every TCR α chain was paired with the fully human TCR β chain (β HuHu) (Figure 1B), and every TCR β chain was paired with the fully human TCR α chain (α HuHu) (Figure 1C) and introduced into Jurma cells, after which binding of anti-human $\alpha\beta$ TCR was determined by flow cytometry. Antibody binding was significantly impaired in T cells expressing the $\alpha\beta$ TCR, which includes murine domain 3 (β HuM3), while none of the other chimeric $\alpha\beta$ TCRs substantially impaired anti-human $\alpha\beta$ TCR binding (Figure 1B and C). β HuM3 TCR expression was confirmed by staining for anti-V β 4, and was comparable to α HuHu/ β HuHu (Supplementary Figure 1) These results

indicate that domain 3 of the TCR β chain (β HuM3) dictates the binding of anti-human $\alpha\beta$ TCR.

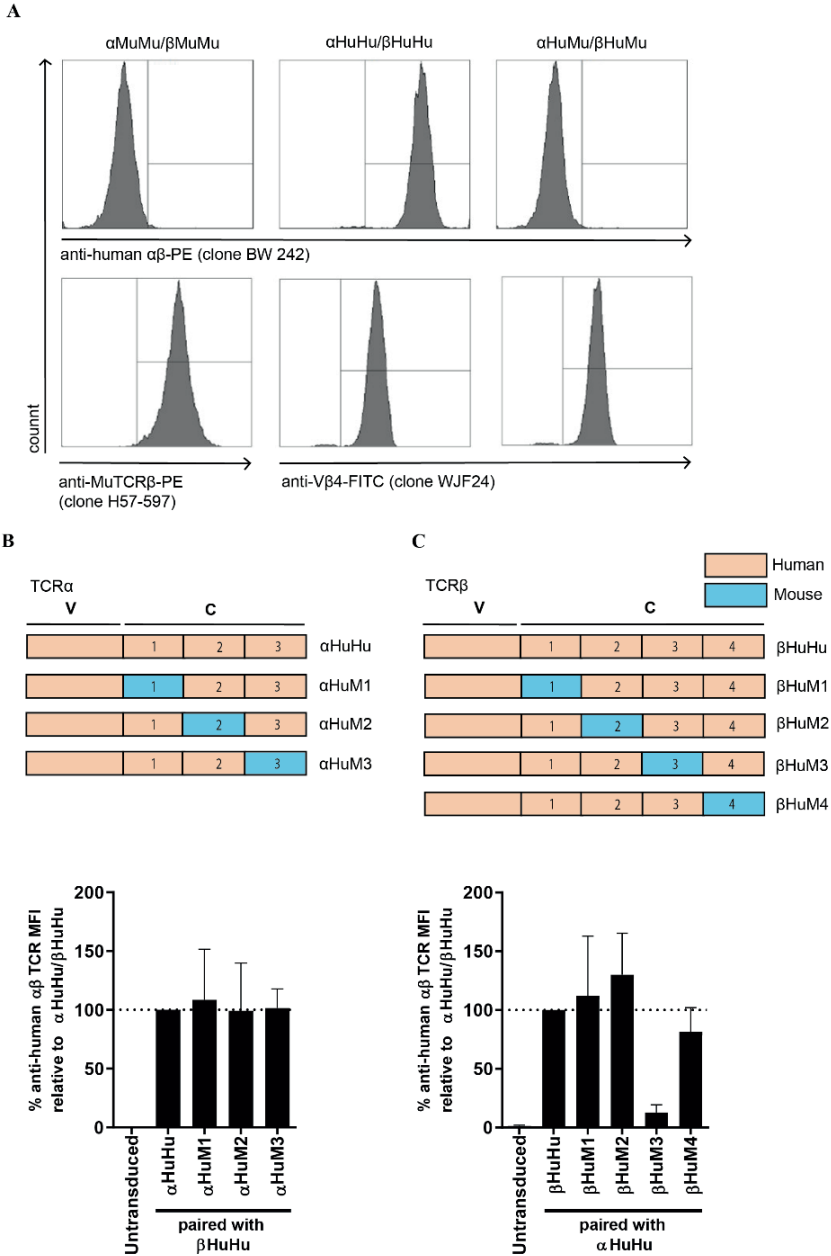


Figure 1. Partial murinization of the TCR β chain constant domain abrogates binding of the anti-human $\alpha\beta$ TCR antibody clone BW242/412. (A) Jurma cells were transduced with fully murine (α MuMu/ β MuMu), fully human NY-ESO-1 specific (α HuHu/ β HuHu) or chimeric $\alpha\beta$ TCR, in which the α - and β - constant domains were murine, and the variable domains were human NY-ESO-1 specific. Binding of anti-human $\alpha\beta$ TCR, anti-MuTCR β and V β 4 was assessed by flow cytometry. Schematic representation of the constructed variable (V) and constant (C) domains of $\alpha\beta$ TCRs that cover all amino acid differences in the (B) TCR α chain and (C) TCR β chain (upper panels). The constant domain of the TCR α and β chain have been divided in respectively 3 or 4 different regions, based on the comparison of human and murine regions revealing clustered differences flanked by homologous regions as described.³⁵ Jurma cells were transduced with the different murinized $\alpha\beta$ TCRs after which anti-human $\alpha\beta$ TCR antibody binding was assessed by flow cytometry, the bar graphs (B&C lower panels) show the anti-human $\alpha\beta$ TCR MFI relative to the fully human TCR. Untransduced Jurma cells served as a negative control. The data correspond to 2 independent experiments and a representative figure is shown (A) or as average with standard deviation (B+C)

Anti-human $\alpha\beta$ TCR binding can be abrogated by mutating 2 residues

Analysis of the sequence of domain 3 of the TCR β chain constant domain revealed eleven residues which are non-homologous between murine and human species (Supplementary Figure 2). To determine which residues are essential for anti-human $\alpha\beta$ TCR binding, we constructed eleven variants of the TCR β chain, in which each one of the non-homologous amino acids was replaced by the murine counterpart. These eleven constructs were paired with the completely human α TCR chain (α HuHu), introduced in Jurma cells, and tested for binding by the anti-human $\alpha\beta$ TCR antibody. Of the eleven generated mutants, the substitutions of ‘human’ glutamic acid (E108) to the ‘murine’ lysine (K), ‘human’ threonine (T110) to the ‘murine’ proline (P), and ‘human’ aspartic acid (D112) to the ‘murine’ glycine (G), showed a substantial abrogation of anti-human $\alpha\beta$ TCR binding (Figure 2A). However, none of these substitutions was sufficient to induce total abrogation, as shown by the TCR consisting of α HuHu/ β HuM3 (Figure 2A). Therefore, we constructed TCR β chains with a combination of the aforementioned mutations. The TCR β chains with a D112G mutation combined with E108K or T110P were both effective in abrogating binding of the anti-human $\alpha\beta$ TCR antibody (Figure 2B), which can be explained by a substantial decrease in bulkiness, thus a decrease in size of these residues (Figure 2C and Supplementary Table 1). For further engineered T cell experiments, the combination of T110P and D112G murinization was selected.

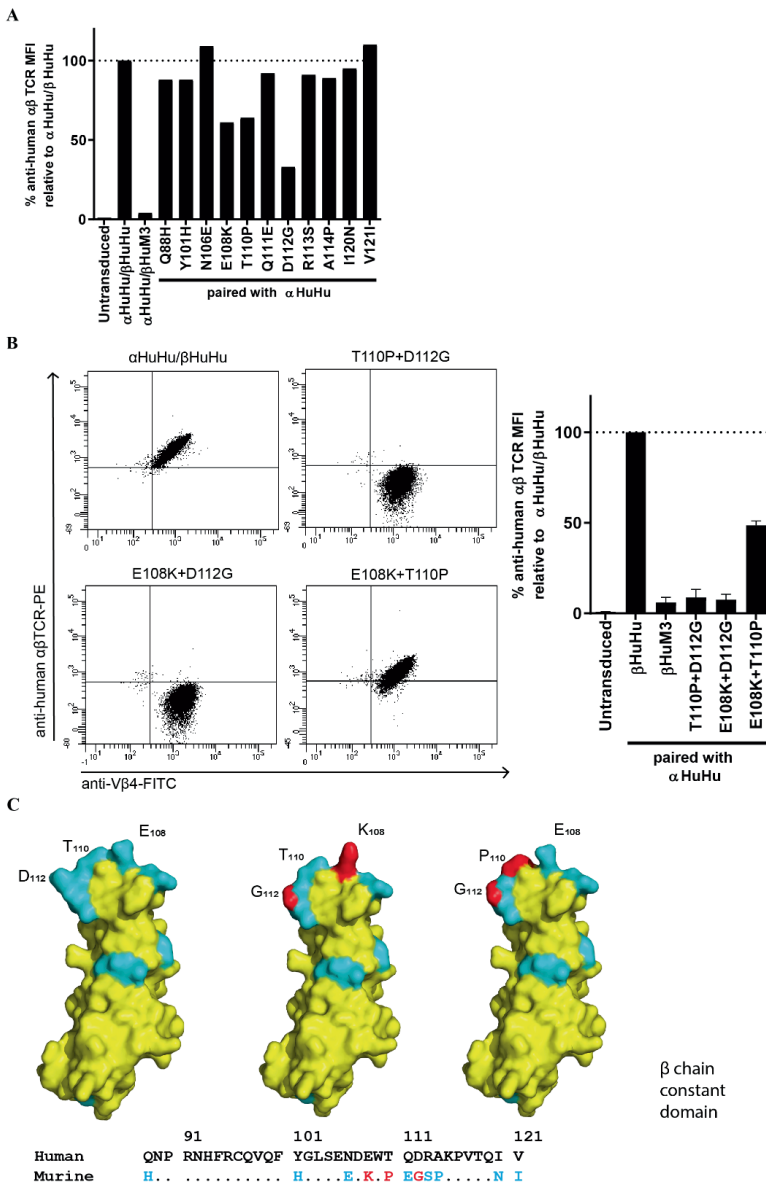


Figure 2. A combination of two specific murine amino acids in the TCR β chain constant domain is sufficient to abrogate binding of the anti-human α TCR antibody clone BW242/412. (A) Jurma cells were transduced with α TCRs containing single murine amino acid substitutions in the 3rd domain of the β chain, after which binding of the anti-human α TCR antibody was assessed using flow cytometry. Untransduced Jurma cells served as a negative control while fully human α TCR transduced Jurma cells

served as a positive control. (B) Jurma cells were transduced with $\alpha\beta$ TCRs containing combinations of murine amino acids in the 3rd domain of the β chain, after which binding of anti-human $\alpha\beta$ TCR antibody was assessed using flow cytometry. (C) Visualization of the eleven non-homologous amino acids between human and mouse β chain 3rd domain in cyan using SWISS-MODEL ⁵⁷ on the modeled template of the β chain of the human JKF6 T-cell receptor (PDB entry code: 4ZDH). Effective single murine amino acid substitutions are displayed in red. The data correspond to 1 experiment (A) or 2 independent experiments shown with representative image (B) and average with standard deviation (B bar graph).

Enrichment of $\alpha\beta$ TCR engineered T cells utilizing fragments of murine $\alpha\beta$ TCR chains

Murine $\alpha\beta$ TCRs, or residues derived from murine $\alpha\beta$ TCRs introduced into human $\alpha\beta$ TCRs, and expressed in human T cells, have been reported to outcompete endogenous human TCR chains ^{33, 46, 47}. These murine and murinized $\alpha\beta$ TCRs preferentially pair with each other, thereby decreasing the occurrence of mispairing with endogenous human $\alpha\beta$ TCRs. Therefore, we utilized single murine amino acids to enhance the expression of introduced TCRs ³³. These “minimally murinized” constant domain variants (from now on referred to as mm) contain murine amino acids which are both critical and sufficient to improve pairing between the two chains ³³. Next, we introduced the above-identified murine residues (T110P+D112G) in the TCR β chain constant domain in order to test whether this was sufficient to disrupt the binding of anti-human $\alpha\beta$ TCR in human primary T cells. To test this concept, healthy donor T cells were transduced with mm NY-ESO-1 specific $\alpha\beta$ TCRs as a negative control, or mm NY-ESO-1 specific $\alpha\beta$ TCRs, including the two identified mutations T110P+D112G. Magnetic-activated cell sorting (MACS) depletion using anti-human $\alpha\beta$ TCR resulted an increased cell fraction not able to bind anti-human $\alpha\beta$ TCR after an expansion of two weeks, in order to assess stability of the phenotype (Figure 3A). However, we also observed outgrowth of

a

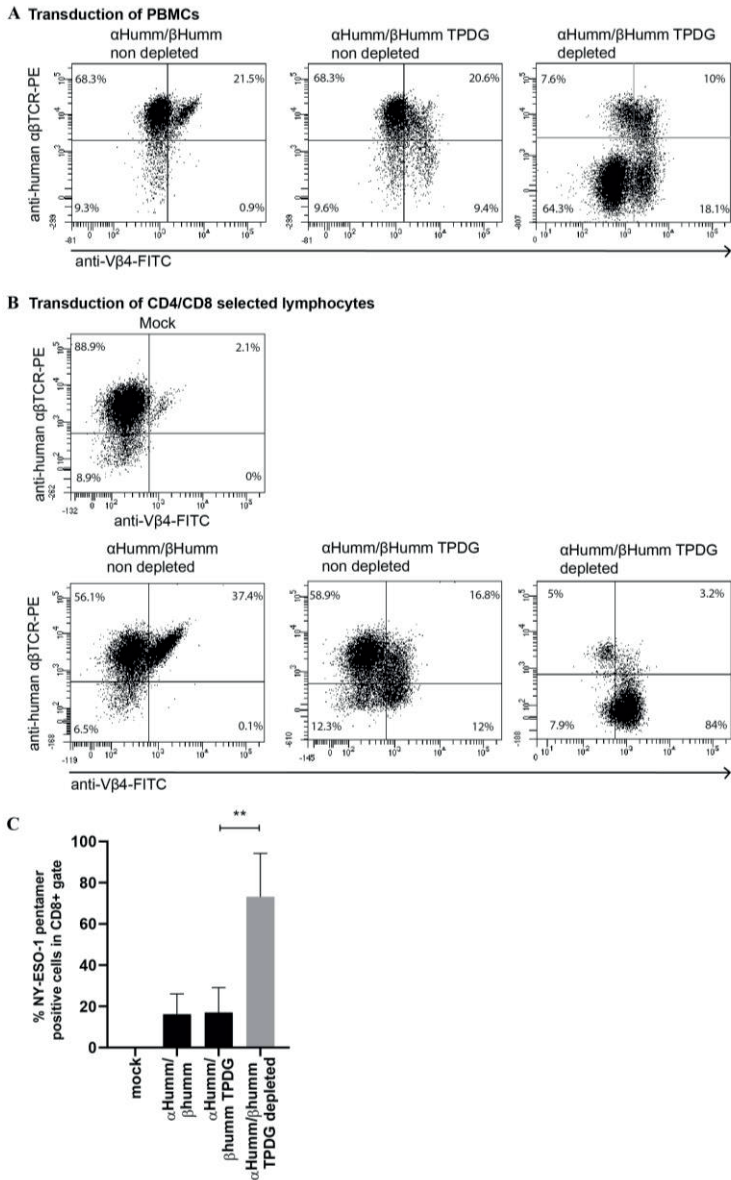


Figure 3. Primary $\alpha\beta$ T cells engineered with murinized $\alpha\beta$ TCRs can be successfully selected by using anti-human $\alpha\beta$ TCR antibody clone BW242/412 to deplete non- and poorly engineered immune cells. (A) PBMCs were transduced with minimally murinized $\alpha\beta$ TCRs with (middle panel) and without (left panel) the “TPDG” mutations. Primary $\alpha\beta$ T cells with the “TPDG” mutations were MACS-depleted and expanded (right-panel). Endogenous $\alpha\beta$ TCR expression and expression of the introduced $\alpha\beta$ TCR without the “TPDG” mutations were determined by flow cytometry using anti-human $\alpha\beta$ TCR antibody, expression of the introduced β TCR chain was assessed with an anti-V β 4 antibody. (B) Prior to transduction with minimally murinized $\alpha\beta$ TCRs T cells were selected from PBMCs using CD4/CD8 MACS selection. (CD4/CD8+) (C)

Expression of correctly paired $\alpha\beta$ TCR chains was assessed before and after depletion and expansion by NY-ESO-1 pentamers (CD8+) for both transduction strategies combined. The data correspond to 3 independent experiments and are shown as representative figure (A+B) or as average with standard deviation (C). Statistical significance (* $p \leq 0.05$, ** $p \leq 0.01$) was calculated using a paired T test.

large fraction of $V\beta 4$ and $\alpha\beta$ TCR negative cells, mainly consisting of NK and $\gamma\delta$ T cells, as reported previously²². To further increase purity of engineered immune cells, T cells were selected by CD4/CD8 MACS from PBMCs prior to the transduction. This indeed prevented the outgrowth of NK and $\gamma\delta$ T cells after $\alpha\beta$ TCR depletion and expansion (Figure 3B). Next, we quantified the fraction of NY-ESO-1₁₅₇₋₁₆₅ HLA*02:01 pentamer positive cells before and after depletion, showing a significant increase in pentamer positive cells after depletion (Figure 3C), further proving successful enrichment of engineered immune cells when using T110P+D112G modified $\alpha\beta$ TCRs.

Enrichment strategy within the context of alternative $\alpha\beta$ TCR stabilization procedures

Multiple alternative strategies to prevent $\alpha\beta$ TCR chain mispairing and thereby increase the expression of the introduced tumor specific $\alpha\beta$ TCR have been reported. E.g., adding an additional cysteine residue, to introduce a disulfide bridge between the α and β chains, has been shown to increase expression and decrease mispairing³⁴. Also, human $\gamma\delta$ TCRs introduced in human T cells do not pair with endogenous $\alpha\beta$ TCRs³². Therefore, it was attractive to use $\gamma\delta$ TCR transmembrane domains for engineering $\alpha\beta$ T cells in a similar way. We tested whether our enrichment strategy could also be combined with these alternative pairing solutions. Firstly, we constructed an NY-ESO-1 specific TCR with an additional disulfide bridge by the mutation of one specific residue in each chain; T48C in TCRC α and S57C in TCRC β ³⁴. Secondly, we constructed an NY-ESO-1 specific TCR with the same additional disulfide bridge, and with a human $\gamma\delta$ TCR trans-membrane domain. These TCRs were compared to the previously used minimally murinized (mm) TCR strategy (schematic representation Figure 4A). To later make use of the $\alpha\beta$ TCR depletion method, we introduced the mutations T110P+D112G in the β chains. We then assessed the expression of the different TCRs in primary T cells by measuring the percentage of $V\beta 4+$ and NY-ESO-1₁₅₇₋₁₆₅ HLA*02:01 pentamer+ cells within the CD8+ population (Figure 4B). All three conditions

resulted in a NY-ESO-1₁₅₇₋₁₆₅ HLA*02:01 pentamer+ CD8+ fraction comparable in size to the V β 4+ CD8+ fraction, indicating that in all cases the introduced TCR chains are preferentially paired (Figure 4B and Supplementary Figure 3). A modest, but significant, increase in expression of the introduced TCR was observed when using a combination of cysteine bridge and $\gamma\delta$ -transmembrane domain when compared to the mm variant (Figure 4C). The increase in expression of V β 4 was associated with an increase of the single V β 4 positive cells to V β 4/ endogenous $\alpha\beta$ TCR double positive cells (Figure 4D), indicating that the combination of cysteine bridge and $\gamma\delta$ -transmembrane domain was most potent in the downregulation of the endogenous $\alpha\beta$ TCR. Next, the three different conditions were $\alpha\beta$ TCR depleted in the same way as before, and the percentage of V β 4+ cells (Figure 5A) and NY-ESO-1₁₅₇₋₁₆₅ HLA*02:01 pentamer+ cells within the CD8+ population (Figure 5B) was measured by flow cytometry, showing successful enrichment for transduced cells in all conditions. After depletion however, we did not see significant differences in %V β 4 or pentamer positive cells between the three tested constructs. In summary, all three described methods were suitable for creating preferential pairing and subsequent purification by our $\alpha\beta$ TCR depletion method with a slight advantage of the combination of cysteine bridge and $\gamma\delta$ -transmembrane domain when assessed by TCR expression.

Augmented in vitro tumor cell recognition by purified engineered T cells

To assess whether purified NY-ESO-1₁₅₇₋₁₆₅ $\alpha\beta$ TCR engineered T cells were superior in target cell recognition compared to non-purified cells, we pulsed T2 cells with multiple concentrations of NY-ESO-1₁₅₇₋₁₆₅ peptide. Purified engineered T cells showed a stronger response to the peptide loaded T2 cells than the non-purified cells. Furthermore, we observed that IFN γ release associated with positivity for the different introduced TCRs (Figure 5C). Purification also resulted in the improved recognition of endogenously processed and presented peptide in the NY-ESO-1 positive tumor cell lines Saos-2 and U226 when assessed by IFN γ release (Figure 5D). As we observed varying, and only minor differences between the three strategies (Figure 4 and 5), and wanted to introduce as little changes as possible in engineered TCRs, the mm approach was used in the next set of experiments to prevent mispairing and increase expression of the introduced TCR as reported³³. The

placement of these 9 murine amino acids, not on the surface but rather buried within the TCR, makes it unlikely that they would cause immunogenicity of the mmTCR as suggested by Sommermeyer et al ³³.

Developing an antibody recognizing the introduced mutated region

The infusion of engineered T cells can potentially be toxic, due to the occurrence of cytokine release syndrome ¹³ or the off-target toxicity of the receptor used ¹⁴. To be able to deplete infused engineered T cells *in vivo* when deemed necessary, we first aimed to raise an antibody specific for the T110P+D112G murinized variant of the $\alpha\beta$ TCR, by immunizing three Wistar rats with a human-mouse chimeric peptide. Despite the fact that antibodies were formed against the chimeric peptide (Supplementary Figure 4A), no antibody binding to surface-expressed $\alpha\beta$ TCRs could be detected (Supplementary Figure 4B). Therefore, we assessed if the commercially available anti-murine TCR β chain antibody clone H57-597 (from now on referred to as anti-MuTCR β), was able to bind the murinized $\alpha\beta$ TCRs on Jurkat-76 cells generated so far. Jurkat-76 cells expressing the T110P+D112G murinized variant of the $\alpha\beta$ TCR (indicated by β Humm 2/11; two out of the eleven non-homologous amino acids in the 3rd domain are murinized) were not bound by anti-MuTCR β , however, Jurkat-76 cells expressing the β HummM3 murinized variant of the $\alpha\beta$ TCR (indicated by β Humm 11/11; all eleven non-homologous amino acids in the 3rd domain are murinized) were bound by anti-MuTCR β (Figure 6A). To limit the amount of murine amino acids introduced, we also constructed a variant in which 9/11 non-homologous amino acids in the 3rd domain are murinized (Supplementary Figure 4C). Both 11/11 and 9/11 non-homologous murine amino acids in β chain of domain 3 were sufficient to reestablish binding of anti-MuTCR β , however, not to the same extent as the HuMu $\alpha\beta$ TCR (Figure 6A). Surprisingly, 9/11 caused a higher MFI than 11/11. Structural analyses suggested that this differential binding could be a consequence of the fact that 9/11 contains one less negatively charged residue, and therefore results in a more focused

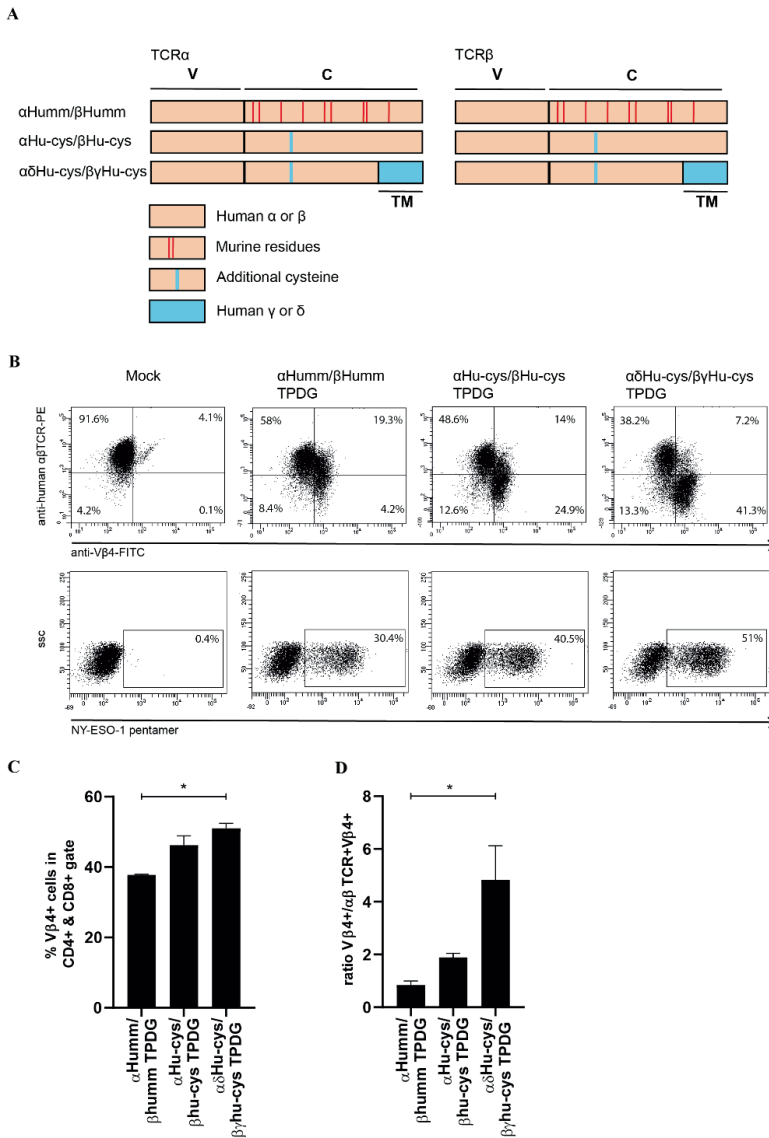


Figure 4. Efficacy of different strategies to induce preferential pairing of introduced α and β TCR chains. (A) Schematic representation of the three different methods for creating preferential pairing between the introduced α and β TCR chains. TM indicates the transmembrane domain, V the variable domain and C the constant domain. (B) Primary $\alpha\beta$ T cells were transduced with the 3 differentially modified $\alpha\beta$ TCRs as indicated in (A) and expression of the introduced β TCR was determined by an anti-V β 4 antibody. Pairing of the introduced α and β TCR chains were assessed by NY-ESO-1 pentamers (C) percentage V β 4+ cells was quantified for the differently modified $\alpha\beta$ TCRs (D) ratio between V β 4 single positive/ V β 4/ $\alpha\beta$ TCR double positive cells was determined. The data correspond to 2 independent experiments and are shown as

representative figure (B) or as average with standard deviation (C+D). Statistical significance (* $p \leq 0.05$, ** $p \leq 0.01$) was calculated using a One-way ANOVA.

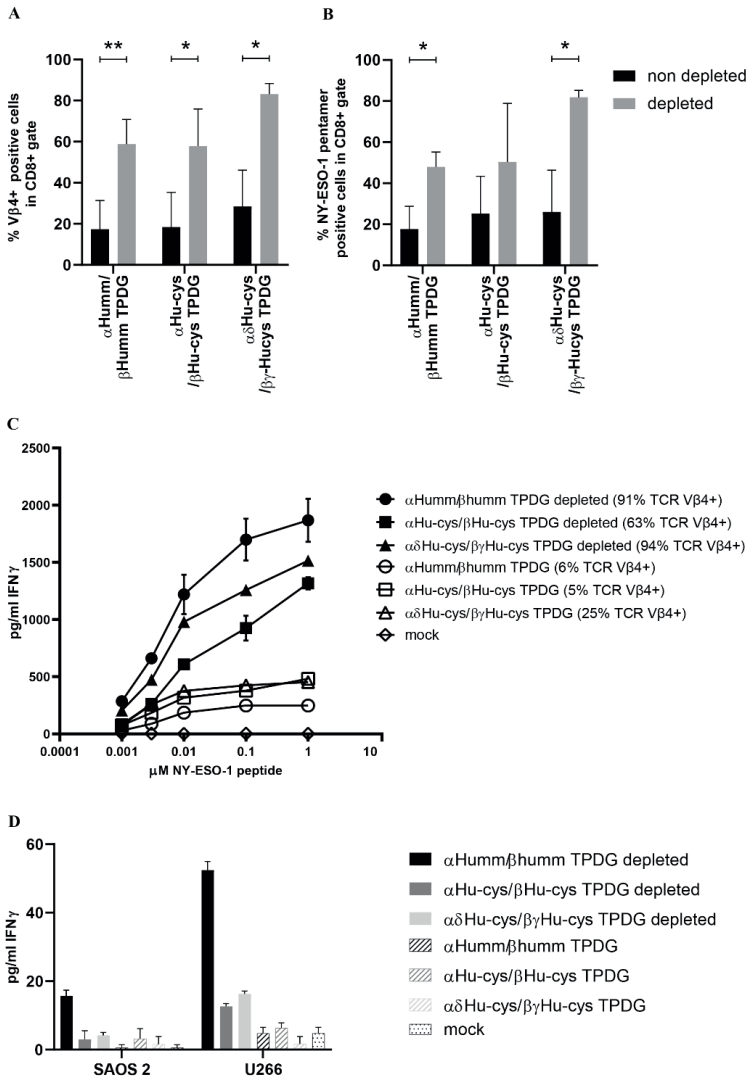


Figure 5. Depletion of non- and poorly- engineered T cells within the context of different preferential $\alpha\beta$ TCR pairing strategies. Primary $\alpha\beta$ T cells were transduced with the 3 differently modified $\alpha\beta$ TCRs as indicated in Figure 4A and depleted with the anti-human $\alpha\beta$ TCR antibody clone BW242/412. (A) Directly before and after depletion, expression of the introduced β TCR was determined by an anti-V β 4 antibody. (B) Expression of appropriately paired introduced α and β TCR chains was determined by NY-ESO-1 pentamers. (C+D) Functionality of purified or non-purified engineered immune cells was assessed in a stimulation assay after co-incubation with NY-ESO-1₁₅₇₋₁₆₅ peptide pulsed T2 cells (C) or tumor cell lines with

endogenous expression of NY-ESO peptide (D). IFN γ production was measured in the supernatant by ELISA. The data correspond to 3 (A, B) or 2 (C, D) independent experiments and are shown as average with standard deviation (A, B) or representative figure (C, D). Statistical significance (* $p \leq 0.05$, ** $p \leq 0.01$) was calculated using a one tailed paired T test.

electrostatic potential to attract the lysine on CDR1 of anti-MuTCR β (Figure 6B). To confirm that the anti-MuTCR β antibody binds to the V β 4+ cells, a co-staining was performed with both antibodies on transduced primary T cells. The MFI of anti-MuTCR β -PE was plotted for the V β 4+ gated cells, this showed that the anti-MuTCR β antibody bound best to the 9/11 or complete murine constant domain (Figure 6C). As expected, there was no binding to the 2/11 variant but surprisingly also not to the 11/11 variant. This might suggest some interference when both antibodies are used in a co-staining, mainly affecting the suboptimal anti-muTCR β binding to the 11/11 variant.

Since the clone of anti-MuTCR β antibody is of Armenian Hamster origin and presumably induces severe side effects once administered to humans, comparable to anti-thymocyte globulin,⁴⁸ we aimed to generate a humanized variant of anti-MuTCR β . We generated chimeric variants of anti-MuTCR β (H57-597, PDB entry code: 1NFD) by exchanging the hamster IgG2 constant domain for the human IgG1 constant domain (referred to as chimeric anti-MuTCR β). We tested binding of this newly constructed antibody in engineered Jurkat-76 cells, which resulted in specific antibody binding to the 9/11 murinized TCR β chain expressed on Jurkat-76 (Supplementary Figure 5). To determine the capacity of the chimeric anti-MuTCR β antibody to bind to primary T cells expressing the murinized $\alpha\beta$ TCRs, we conjugated this antibody and an isotype control, to Alexa Fluor 488 (AF488), and determined binding by flow cytometry. The chimeric anti-MuTCR β antibody was able to bind both 9/11 and 11/11 murinized TCRs and, as observed in Figure 6A, the binding to 9/11 was stronger than to 11/11 (Figure 6D). To assess if the chimeric variant of anti-MuTCR β was able to selectively deplete engineered T cells *in vitro*, the antibody was coupled to monomethyl auristatin E (MMAE), a cell cycle inhibitor, using the protease cleavable linker VC-PAB,⁴⁹ to create an antibody-drug conjugate (ADC). Jurkat-76 cells transduced with different murinized TCRs were incubated with multiple concentrations of the ADC. The highest

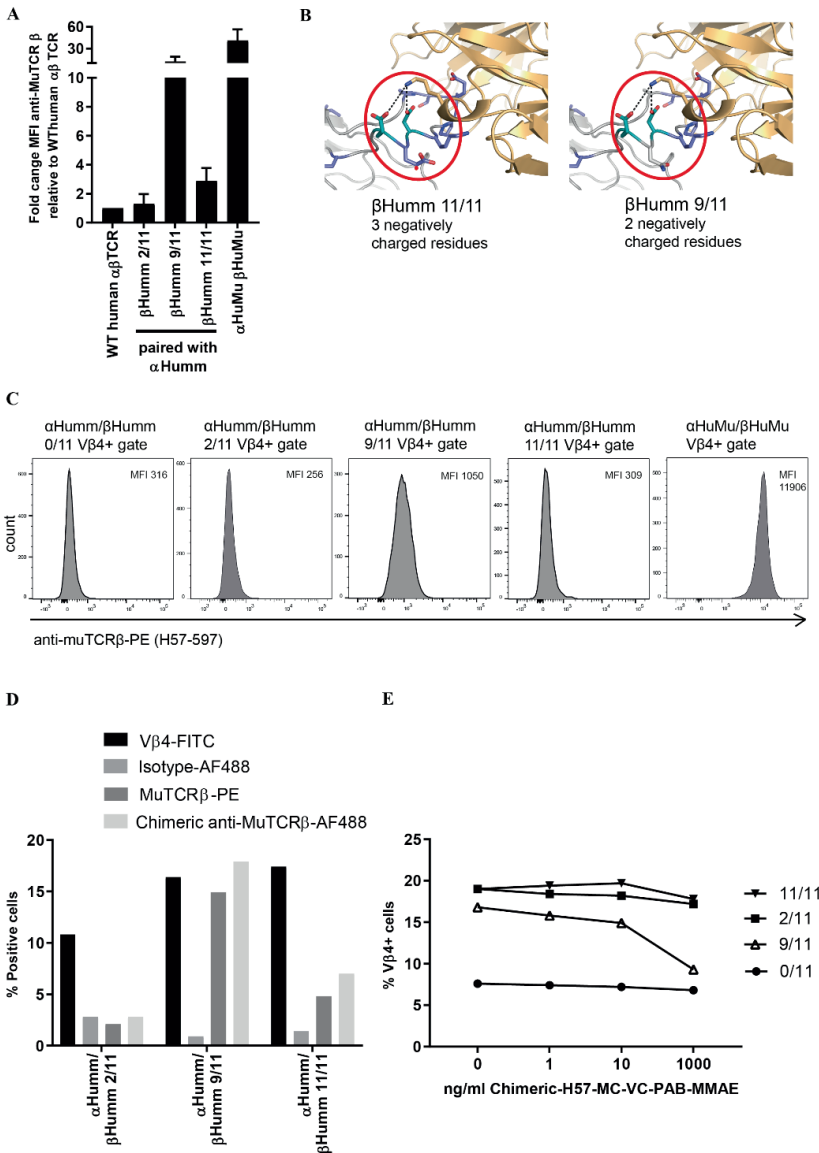


Figure 6. Opportunities for depletion of engineered T cells by using a mutation-specific antibody. (A) Jurkat-76 cells were transduced with 5 different murinized $\alpha\beta$ TCRs to assess binding of anti-MuTCR β . Wild-type (WT) $\alpha\beta$ TCR transduced Jurkat-76 cells served as a negative control, while Jurkat-76 transduced with a TCR containing a complete murine constant domain served as a positive control. (B) The structure of the murinized constant domains (β Humm 11/11 and β Humm 9/11) when binding of H57-597 was modeled on the template of the β chain of the murine N15 T-cell receptor (PDB entry code: 1NFD)⁵³. (C) Primary $\alpha\beta$ T cells were transduced with the 5 different murinized $\alpha\beta$ TCRs and a co-staining was performed with anti

muTCR and anti V β 4 antibodies. Cells were first gated for V β 4 positivity, and plots of the anti muTCR MFH in V β 4 positive gate are shown (D) Primary $\alpha\beta$ T cells expressing 3 different murinized $\alpha\beta$ TCRs were used to assess binding of wild-type and chimeric anti-MuTCR β . Anti-V β 4 and anti-Human IgG1-AF488 isotype were included as a positive and a negative control respectively. (E) Jurkat-76 expressing 4 different murinized $\alpha\beta$ TCRs were incubated with chimeric H57-MC-VC-PAB-MMAE for 24 hours and then stained with an anti-V β 4 antibody. The data correspond to 1 experiment (C), 2 independent experiments (D, E) for which a representative figure is shown or 3 independent experiments (A) shown in a bar graph representing average and standard deviation.

concentration of chimeric H57-MC-VC-PAB-MMAE led to a decrease of V β 4 positivity in the 9/11 condition only (Figure 6E). This specific decrease indicated that the ADC is able to selectively deplete 9/11, and not 11/11 $\alpha\beta$ TCR engineered Jurkat-76 *in vitro*, most likely due to the weaker binding of the engineered antibody to the 11/11 $\alpha\beta$ TCR (Figure 6D). However, depletion was far from complete, indicating that although this binding site is interesting it is far from being developed for a kill-strategy.

Discussion

The main finding of our study is that replacing only two amino acids within the constant domain of the TCR β chain allows for the purification of $\alpha\beta$ TCR engineered T cells with GMP-ready tools,⁵⁰ without the need for additional complex genetic engineering. The very same region on the TCR β chain can also serve as a targeting interface for antibodies, which can be used to develop strategies to eliminate engineered immune cells. These new insights provide the molecular basis for developing select-kill strategies for increasing purity and augmenting safety of $\alpha\beta$ TCR engineered T cells, with only minor engineering steps.

A sufficient down-regulation of the endogenous $\alpha\beta$ TCR chains by the introduced $\alpha\beta$ TCR chains is essential for this method to work. Therefore, strategies interfering with endogenous $\alpha\beta$ TCRs or utilizing knock out of the α or β locus to enhance expression of introduced $\alpha\beta$ TCRs⁵¹ will benefit from this strategy. However, engineering of T cells via ZFN, CRISPR or TALENs⁵² requires additional engineering steps and therefore is an additional hurdle for GMP grade production. We accomplished dominance of the introduced receptors by using a previously described method where human residues are

replaced by key murine counterparts³⁷. Furthermore, we successfully assessed whether the introduction of an additional disulfide bridge⁸ or the exchange of the human $\alpha\beta$ TCR transmembrane domain for the human $\gamma\delta$ TCR counterpart²¹ could also lead to enhanced expression. Thus, we found, in line with our recently published solution for TEGs²¹, an elegant and minimalistic strategy to purify $\alpha\beta$ TCR engineered T cells.

We observed, as reported previously for purification of TEGs^{21, 22}, that $\alpha\beta$ cells double positive for endogenous and introduced TCR are also depleted. This is most likely due to the high affinity of the GMP-grade depletion antibody to the natural β TCR chain. This resulted in a substantial loss of engineered immune cells with residual endogenous $\alpha\beta$ TCR expression. Although the purified population represented only a small fraction of the initial population, we have shown when using this process for $\gamma\delta$ TCRs engineered immune cells, that the recovery is sufficient to reach therapeutic cell numbers in a full GMP grade process²². Furthermore, we observed enrichment of NK and $\gamma\delta$ T cells after depletion, previously reported for $\gamma\delta$ TCRs engineered immune cells²² and transplantation products⁵³ as well. Therefore, selection of CD4⁺ and CD8⁺ T cells prior to transduction is recommended when applying our strategy. Selection of CD4⁺ and CD8⁺ T cells is used already successfully during the full grade GMP production process of approved CAR T products⁵⁴. Overall, our strategy can further improve the current practice for infused engineered products that harbor only between 15-55% engineered immune cells^{55, 56}, since the lack of purity of infusion products can become a major clinical obstacle in terms of efficacy²¹ as well as toxicity^{13, 57}.

Many tumor-associated antigens targeted by $\alpha\beta$ TCR gene therapy are not exclusively expressed on tumor cells⁵⁸. Thus, depending on the type of antigen targeted by the introduced $\alpha\beta$ TCR, depletion strategies can be useful. This is illustrated by multiple clinical trials, which have led to devastating results caused by off-target or on-target but off-tumor toxicities^{5, 14}. Preclinical strategies to predict off-target toxicities by affinity enhanced TCRs provide an important tool to minimize these risks⁵⁹. However, these strategies are not infallible, and therefore an additional safe guard would be extremely valuable when e.g. targeting novel antigens or antigens which are also partially

expressed on healthy tissues. Methods described so far for introducing a safety switch in engineered T cell products rely on the introduction of additional genes for the expression of (truncated) targetable proteins, the introduction of inducible caspase proteins⁶⁰ or sensitivity to ganciclovir in the case of the widely used HSV-TK suicide gene¹⁷. The strategy described here, using minimal murine amino acid substitutions, is not only suitable for creating an untouched population of purified T cells, but also has the potential to develop strategies which will allow an *in vivo* depletion when needed. However, to accomplish this goal, the two identified murine amino acids that enable $\alpha\beta$ TCR depletion needed to be expanded with an additional seven amino acids, to create a chimeric TCR β chain with a total of nine murine amino acids. The major advantage of our strategy, as compared to strategies using e.g. myc-tags introduced into the TCR α chain¹⁸, would be its combined property as a selection and a safeguard system, as well as its use of natural $\alpha\beta$ TCR domains, which most likely do not affect signaling or impair pairing. However, a major remaining limitation of our approach at this stage is the reduced binding efficacy of our engineered depletion antibody to the murine mutants when compared to the murine wild type, implying that further engineering of the TCR domain or affinity maturation of the antibody will be needed to enable translation of this strategy into an efficient killing strategy *in vivo*. As binding of the antibody is also partially driven by residues in the C β -TCR M1 domain³⁹, additional introduction of several murine amino acids in this domain could therefore be considered.

In conclusion, the murinization of two specific residues in the TCR β constant domain allows for the untouched isolation of $\alpha\beta$ TCR engineered T cell products, and can be easily introduced in existing GMP-procedures. When a safeguard of engineered immune cells is required, mutating an additional seven human amino acids to murine residues in the TCR β constant domain allows for binding of an antibody, which has the potential to, after further optimization, selectively recognize engineered T cells. However, the second step will require additional engineering of the TCR-antibody interface as well as carefully selecting the appropriate killing mechanism to reach its full potential.

Acknowledgement

We acknowledge the support by the flow cytometry facility at the UMC Utrecht. Cell lines and derivatives have been provided by Erik Hooijberg and Miriam Heemskerk as well as Edite Antunes and Matthias Theobald.

Funding

Funding for this study was provided by ZonMW 43400003 and VIDI-ZonMW 917.11.337, KWF 6426, 6790 and 7601, to JK; 12586 to TS and JK; 11393 and 13043 to ZS and JK; 11979 to JK and DB.

Conflict of Interest Statement

GK, DB, ZS and JK are inventors on different patents with $\gamma\delta$ TCR sequences, recognition mechanisms and isolation strategies. JK is the scientific cofounder and a shareholder of Gadeta (www.gadeta.nl). No potential conflicts of interest were disclosed by the other authors.

References

1. Chabannon C, Kuball J, Bondanza A, Dazzi F, Pedrazzoli P, Toubert A, et al. Hematopoietic stem cell transplantation in its 60s: A platform for cellular therapies. *Sci Transl Med.* 2018;10(436).
2. McGrath E, Chabannon C, Terwel S, Bonini C, Kuball J. Opportunities and challenges associated with the evaluation of chimeric antigen receptor T cells in real-life. *Curr Opin Oncol.* 2020;32(5):427-33.
3. de Witte MA, Kierkels GJ, Straetemans T, Britten CM, Kuball J. Orchestrating an immune response against cancer with engineered immune cells expressing alphabetaTCRs, CARs, and innate immune receptors: an immunological and regulatory challenge. *Cancer Immunol Immunother.* 2015;64(7):893-902.
4. Gnjjatic S, Nishikawa H, Jungbluth AA, Gure AO, Ritter G, Jager E, et al. NY-ESO-1: review of an immunogenic tumor antigen. *Adv Cancer Res.* 2006;95:1-30.
5. Morgan RA, Chinnasamy N, Abate-Daga D, Gros A, Robbins PF, Zheng Z, et al. Cancer regression and neurological toxicity following anti-MAGE-A3 TCR gene therapy. *J Immunother.* 2013;36(2):133-51.
6. Rapoport AP, Stadtmauer EA, Binder-Scholl GK, Goloubeva O, Vogl DT, Lacey SF, et al. NY-ESO-1-specific TCR-engineered T cells mediate sustained antigen-specific antitumor effects in myeloma. *Nat Med.* 2015;21(8):914-21.
7. de Witte MA, Jorritsma A, Kaiser A, van den Boom MD, Dokter M, Bendle GM, et al. Requirements for effective antitumor responses of TCR transduced T cells. *J Immunol.* 2008;181(7):5128-36.
8. Kuball J, Dossett ML, Wolf M, Ho WY, Voss RH, Fowler C, et al. Facilitating matched pairing and expression of TCR chains introduced into human T cells. *Blood.* 2007;109(6):2331-8.
9. Abad JD, Wrzensinski C, Overwijk W, De Witte MA, Jorritsma A, Hsu C, et al. T-cell receptor gene therapy of established tumors in a murine melanoma model. *J Immunother.* 2008;31(1):1-6.
10. Fehse B, Richters A, Putimtseva-Scharf K, Klump H, Li Z, Ostertag W, et al. CD34 splice variant: an attractive marker for selection of gene-modified cells. *Mol Ther.* 2000;1(5 Pt 1):448-56.
11. Orchard PJ, Blazar BR, Burger S, Levine B, Basso L, Nelson DM, et al. Clinical-scale selection of anti-CD3/CD28-activated T cells after transduction with a retroviral vector expressing herpes simplex virus thymidine kinase and truncated nerve growth factor receptor. *Hum Gene Ther.* 2002;13(8):979-88.
12. Lamers CH, Willemsen R, van EP, van Steenbergen-Langeveld S, Broertjes M, Oosterwijk-Wakka J, et al. Immune responses to transgene and retroviral vector in patients treated with ex vivo-engineered T cells. *Blood.* 2011;117(1):72-82.
13. Neelapu SS, Tummala S, Kebriaei P, Wierda W, Gutierrez C, Locke FL, et al. Chimeric antigen receptor T-cell therapy - assessment and management of toxicities. *Nat Rev Clin Oncol.* 2018;15(1):47-62.

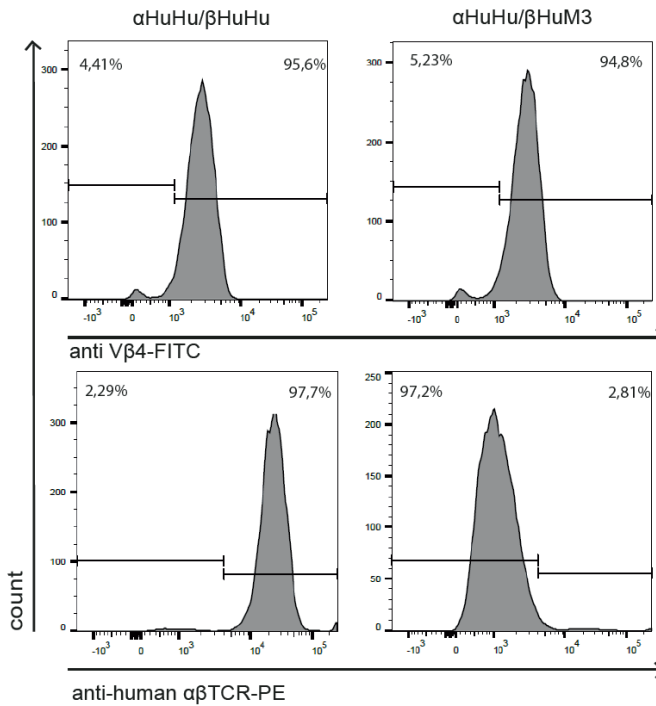
14. Linette GP, Stadtmauer EA, Maus MV, Rapoport AP, Levine BL, Emery L, et al. Cardiovascular toxicity and titin cross-reactivity of affinity-enhanced T cells in myeloma and melanoma. *Blood*. 2013;122(6):863-71.
15. Linette GP, Stadtmauer EA, Maus MV, Rapoport AP, Levine BL, Emery L, et al. Cardiovascular toxicity and titin cross-reactivity of affinity-enhanced T cells in myeloma and melanoma. *Blood*. 2013;122(6):863-71.
16. Traversari C, Markt S, Magnani Z, Mangia P, Russo V, Ciceri F, et al. The potential immunogenicity of the TK suicide gene does not prevent full clinical benefit associated with the use of TK-transduced donor lymphocytes in HSCT for hematologic malignancies. *Blood*. 2007;109(11):4708-15.
17. Traversari C, Markt S, Magnani Z, Mangia P, Russo V, Ciceri F, et al. The potential immunogenicity of the TK suicide gene does not prevent full clinical benefit associated with the use of TK-transduced donor lymphocytes in HSCT for hematologic malignancies. *Blood*. 2007;109(11):4708-15.
18. Kieback E, Charo J, Sommermeyer D, Blankenstein T, Uckert W. A safeguard eliminates T cell receptor gene-modified autoreactive T cells after adoptive transfer. *Proc Natl Acad Sci USA*. 2008;105(2):623-8.
19. Kuball J, Hauptrock B, Malina V, Antunes E, Voss RH, Wolf M, et al. Increasing functional avidity of TCR-redirected T cells by removing defined N-glycosylation sites in the TCR constant domain. *JExpMed*. 2009;206(2):463-75.
20. Introna M, Barbui AM, Bambacioni F, Casati C, Gaipa G, Borteri G, et al. Genetic modification of human T cells with CD20: a strategy to purify and lyse transduced cells with anti-CD20 antibodies. *Hum Gene Ther*. 2000;11(4):611-20.
21. Straetmans T, Gründer C, Heijhuurs S, Hol S, Slaper-Cortenbach I, Böning H, et al. Untouched GMP-Ready Purified Engineered Immune Cells to Treat Cancer. *Clin Cancer Res*. 2015;21(17):3957-68.
22. Straetmans T, Kierkels GJJ, Doorn R, Jansen K, Heijhuurs S, Dos Santos JM, et al. GMP-Grade Manufacturing of T Cells Engineered to Express a Defined gammadeltaTCR. *Front Immunol*. 2018;9:1062.
23. Sebestyen Z, Prinz I, Dechanet-Merville J, Silva-Santos B, Kuball J. Translating gammadelta (gammadelta) T cells and their receptors into cancer cell therapies. *Nat Rev Drug Discov*. 2020;19(3):169-84.
24. Straetmans T, Janssen A, Jansen K, Doorn R, Aarts T, van Muyden ADD, et al. TEG001 Insert Integrity from Vector Producer Cells until Medicinal Product. *Mol Ther*. 2020;28(2):561-71.
25. Vyborova A, Beringer DX, Fasci D, Karaiskaki F, van Diest E, Kramer L, et al. gamma9delta2T cell diversity and the receptor interface with tumor cells. *J Clin Invest*. 2020;130(9):4637-51.
26. Johanna I, Hernandez-Lopez P, Heijhuurs S, Bongiovanni L, de Bruin A, Beringer D, et al. TEG011 persistence averts extramedullary tumor growth without exerting off-target toxicity against healthy tissues in a humanized HLA-A*24:02 transgenic mice. *J Leukoc Biol*. 2020;107(6):1069-79.

27. Janssen A, Villacorta Hidalgo J, Beringer DX, van Dooremalen S, Fernando F, van Diest E, et al. $\gamma\delta$ T-cell Receptors Derived from Breast Cancer-Infiltrating T Lymphocytes Mediate Antitumor Reactivity. *Cancer Immunol Res.* 2020;8(4):530-43.
28. Johanna I, Straetemans T, Heijhuurs S, Aarts-Riemens T, Norell H, Bongiovanni L, et al. Evaluating in vivo efficacy - toxicity profile of TEG001 in humanized mice xenografts against primary human AML disease and healthy hematopoietic cells. *J Immunother Cancer.* 2019;7(1):69.
29. Kierkels GJJ, Scheper W, Meringa AD, Johanna I, Beringer DX, Janssen A, et al. Identification of a tumor-specific allo-HLA-restricted $\gamma\delta$ TCR. *Blood Adv.* 2019;3(19):2870-82.
30. Schumm M, Lang P, Bethge W, Faul C, Feuchtinger T, Pfeiffer M, et al. Depletion of T-cell receptor α/β and CD19 positive cells from apheresis products with the CliniMACS device. *Cytotherapy.* 2013;15(10):1253-8.
31. Aarnoudse CA, Kruse M, Konopitzky R, Brouwenstijn N, Schrier PI. TCR reconstitution in Jurkat reporter cells facilitates the identification of novel tumor antigens by cDNA expression cloning. *Int J Cancer.* 2002;99(1):7-13.
32. Marcu-Malina V, Heijhuurs S, van Buuren M, Hartkamp L, Strand S, Sebestyen Z, et al. Redirecting $\alpha\beta$ T cells against cancer cells by transfer of a broadly tumor-reactive $\gamma\delta$ T-cell receptor. *Blood.* 2011;118(1):50-9.
33. Sommermeyer D, Uckert W. Minimal amino acid exchange in human TCR constant regions fosters improved function of TCR gene-modified T cells. *J Immunol.* 2010;184(11):6223-31.
34. Kuball J, Dossett ML, Wolf M, Ho WY, Voss RH, Fowler C, et al. Facilitating matched pairing and expression of TCR chains introduced into human T cells. *Blood.* 2007;109(6):2331-8.
35. IMGT®, the international ImMunoGeneTics information system®. <http://www.imgt.org>.
36. Kronig H, Hofer K, Conrad H, Guillaume P, Muller J, Schiemann M, et al. Allorestricted T lymphocytes with a high avidity T-cell receptor towards NY-ESO-1 have potent anti-tumor activity. *Int J Cancer.* 2009;125(3):649-55.
37. Sommermeyer D, Uckert W. Minimal amino acid exchange in human TCR constant regions fosters improved function of TCR gene-modified T cells. *J Immunol.* 2010;184(11):6223-31.
38. Bertoni M, Kiefer F, Biasini M, Bordoli L, Schwede T. Modeling protein quaternary structure of homo- and hetero-oligomers beyond binary interactions by homology. *Sci Rep.* 2017;7(1):10480.
39. Wang J, Lim K, Smolyar A, Teng M, Liu J, Tse AG, et al. Atomic structure of an $\alpha\beta$ T cell receptor (TCR) heterodimer in complex with an anti-TCR fab fragment derived from a mitogenic antibody. *EMBO J.* 1998;17(1):10-26.
40. Schrodinger, LLC. The PyMOL Molecular Graphics System, Version 1.8. 2015.
41. Boross P, Lohse S, Nederend M, Jansen JH, van Tetering G, Dechant M, et al. IgA EGFR antibodies mediate tumour killing in vivo. *EMBO Mol Med.* 2013;5(8):1213-26.

42. Meyer S, Evers M, Jansen JHM, Buijs J, Broek B, Reitsma SE, et al. New insights in Type I and II CD20 antibody mechanisms-of-action with a panel of novel CD20 antibodies. *Br J Haematol*. 2018;180(6):808-20.
43. Stanislawski T, Voss RH, Lotz C, Sadovnikova E, Willemsen RA, Kuball J, et al. Circumventing tolerance to a human MDM2-derived tumor antigen by TCR gene transfer. *Nat Immunol*. 2001;2(10):962-70.
44. Kuball J, Schmitz FW, Voss RH, Ferreira EA, Engel R, Guillaume P, et al. Cooperation of human tumor-reactive CD4+ and CD8+ T cells after redirection of their specificity by a high-affinity p53A2.1-specific TCR. *Immunity*. 2005;22(1):117-29.
45. Davis JL, Theoret MR, Zheng Z, Lamers CH, Rosenberg SA, Morgan RA. Development of human anti-murine T-cell receptor antibodies in both responding and nonresponding patients enrolled in TCR gene therapy trials. *Clin Cancer Res*. 2010;16(23):5852-61.
46. Voss RH, Kuball J, Theobald M. Designing TCR for Cancer Immunotherapy. *Methods MolMed*. 2005;109:229-56.
47. Voss RH, Kuball J, Engel R, Guillaume P, Romero P, Huber C, et al. Redirection of T cells by delivering a transgenic mouse-derived MDM2 tumor antigen-specific TCR and its humanized derivative is governed by the CD8 coreceptor and affects natural human TCR expression. *ImmunolRes*. 2006;34(1):67-87.
48. Admiraal R, Nierkens S, de Witte MA, Petersen EJ, Fleurke GJ, Verrest L, et al. Association between anti-thymocyte globulin exposure and survival outcomes in adult unrelated haemopoietic cell transplantation: a multicentre, retrospective, pharmacodynamic cohort analysis. *Lancet Haematol*. 2017;4(4):e183-e91.
49. Caculitan NG, Dela Cruz Chuh J, Ma Y, Zhang D, Kozak KR, Liu Y, et al. Cathepsin B Is Dispensable for Cellular Processing of Cathepsin B-Cleavable Antibody-Drug Conjugates. *Cancer Res*. 2017;77(24):7027-37.
50. Locatelli F, Merli P, Pagliara D, Li Pira G, Falco M, Pende D, et al. Outcome of children with acute leukemia given HLA-haploidentical HSCT after alpha T-cell and B-cell depletion. *Blood*. 2017;130(5):677-85.
51. Provasi E, Genovese P, Lombardo A, Magnani Z, Liu PQ, Reik A, et al. Editing T cell specificity towards leukemia by zinc finger nucleases and lentiviral gene transfer. *NatMed*. 2012;18(5):807-15.
52. Gaj T, Gersbach CA, Barbas CF, III. ZFN, TALEN, and CRISPR/Cas-based methods for genome engineering. *Trends Biotechnol*. 2013.
53. Handgretinger R, Schilbach K. The potential role of gammadelta T cells after allogeneic HCT for leukemia. *Blood*. 2018.
54. Shah NN, Highfill SL, Shalabi H, Yates B, Jin J, Wolters PL, et al. CD4/CD8 T-Cell Selection Affects Chimeric Antigen Receptor (CAR) T-Cell Potency and Toxicity: Updated Results From a Phase I Anti-CD22 CAR T-Cell Trial. *J Clin Oncol*. 2020;38(17):1938-50.

55. Lock D, Mockel-Tenbrinck N, Drechsel K, Barth C, Mauer D, Schaser T, et al. Automated Manufacturing of Potent CD20-Directed Chimeric Antigen Receptor T Cells for Clinical Use. *Hum Gene Ther.* 2017;28(10):914-25.
56. Hodi FS, O'Day SJ, McDermott DF, Weber RW, Sosman JA, Haanen JB, et al. Improved survival with ipilimumab in patients with metastatic melanoma. *N Engl J Med.* 2010;363(8):711-23.
57. Smith M, Zakrzewski J, James S, Sadelain M. Posttransplant chimeric antigen receptor therapy. *Blood.* 2018;131(10):1045-52.
58. Schmitt TM, Stromnes IM, Chapuis AG, Greenberg PD. New Strategies in Engineering T-cell Receptor Gene-Modified T cells to More Effectively Target Malignancies. *Clin Cancer Res.* 2015;21(23):5191-7.
59. Bijen HM, van der Steen DM, Hagedoorn RS, Wouters AK, Wooldridge L, Falkenburg JHF, et al. Preclinical Strategies to Identify Off-Target Toxicity of High-Affinity TCRs. *Mol Ther.* 2018.
60. Di Stasi A, Tey SK, Dotti G, Fujita Y, Kennedy-Nasser A, Martinez C, et al. Inducible apoptosis as a safety switch for adoptive cell therapy. *N Engl J Med.* 2011;365(18):1673-83.

Supplementary figures and tables



Supplementary Figure 1. α huhu/ β huM3 murinized TCR is expressed at the cell surface. (A) Jurma cells were transduced with the α huhu/ β huhu and α huhu/ β huM3 murinized TCR after which TCR expression was confirmed with an anti-V β 4 antibody (upper panel) and binding of the anti-human $\alpha\beta$ TCR antibody was assessed (lower panel), by flow cytometry. The data correspond to 2 independent experiments and a representative figure is shown.

TCR α

	1							
	1	11	21	31	41		51	61
Hu	IQN	DFAVYQ	LRDSKSSDKS	VCLFTDFDSQ	TNVSQSKDSD	VYITDKTVLD	MRSMDFKSNS	AVAWSNKSD
Mu	***E***	*K*PR*O*ST	L*****	I**PKTME*G	TE*****		*KA**S**G	*I**OTS*

	2			3				
	71	81	91	101	111		121	131
Hu	ACANAFNNSI	IPEDTFFPSP	ESSCDV	KVFLVE	KSFETDTNLN	FQNLSVIGER	ILLKLVAGFN	LLMTRLRLWSS
Mu	T*QDI*K---	-ETNAT**S	DVE**	AT*T*	*****M**	*****M*I	*****	*****

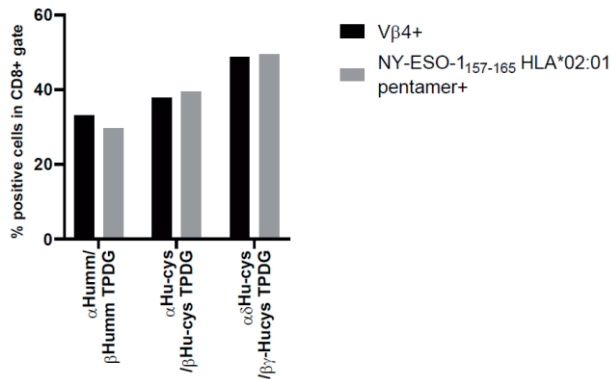
TCR β

	1						2		
	1	11	21	31	41	51	61		
Hu	EDL	KNVFPPE	VAVFEPSEAE	ISHTQKATLV	CLATGFY	PDH	VELSWWVNGK	EVHSGVSTDP	QPLKEQPALN
Mu	**R**T**K	*SL***K**	*ANK*****	**R**F**	*****	*****	*****	*****	*AY*---S*

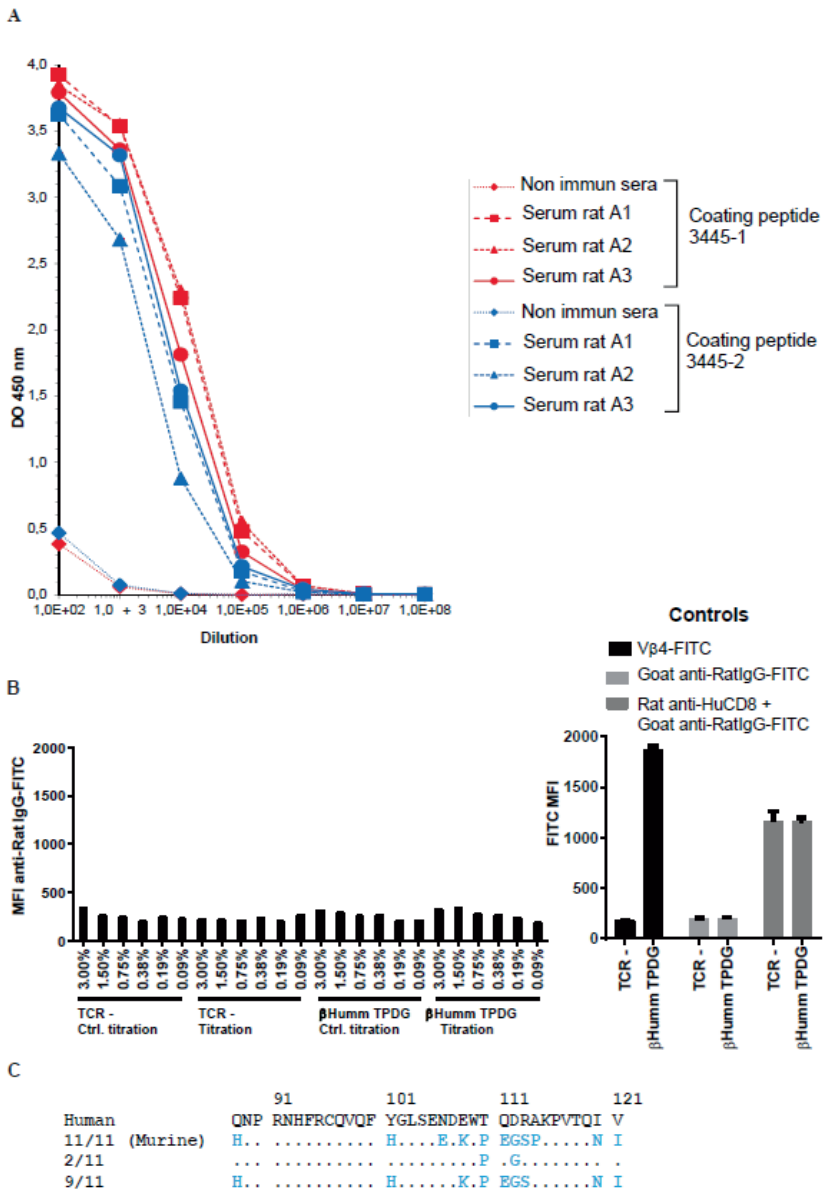
	3								
	71	81	91	101	111	121	131		
Hu	DSR	YCLSSRL	RVSATFW	QNP	RNHFRCQQQF	YGLSENDEWT	QDRAKPVTVI	VSAAEWGRAD	CGFTSESYQQ
Mu	Y*-	*****	*****H**	*****	H***E*K*P	EGSP*****	I	*****	**T**A**H*

	4			
	141	151	161	171
Hu	GVLSATILYE	ILLGKATLYA	VLVSALVIMA	MVKRKDSRG
Mu	*****	*****	***G+***	**K*N*---

Supplementary Figure 2. Extensive homology between human and murine TCR chains. Sequence alignment of the Human (Hu) and Murine (Mu) TCR α (upper panel) or β (lower panel) constant chains. The three (TCR α) or four (TCR β) TCR constant regions with clustered Hu-Mu sequence differences are indicated above the alignment.

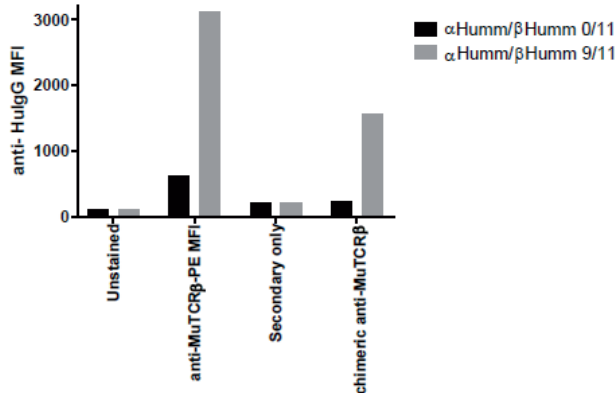


Supplementary Figure 3. Comparable efficacy of different strategies to induce preferential pairing of introduced α and β TCR chains. Primary α TCR cells were transduced with the 3 differentially modified α β TCRs and expression of the introduced β TCR was determined by an anti-V β 4 antibody. Pairing of the introduced α and β TCR chains was assessed by staining with NY-ESO-1 pentamers. The data correspond to 2 independent experiments and a representative figure is shown.



Supplementary Figure 4. Attempting to raise an antibody specific for the T110P+D112G murinized variant of the α TCR by immunizing 3 Wistar rats with a human-mouse chimeric peptide. (A) Determining the presence of peptide-specific antibodies in the serum of the immunized rats. (B) Assessing the ability of the generated antibodies to bind surface-expressed TCRs. α Humm/ β Humm TPDP transduced or non-transduced Jurkat-76 cells were incubated with the indicated percentage of rat serum, after which flow cytometry using anti-RatIgG-FITC was performed. In the controls panel, the functionality of this

secondary antibody was confirmed by staining the Jurkat-76 cells with rat anti-HuCD8 followed by anti-RatIgG-FITC. Expression of the TCR was confirmed using anti-V β 4-FITC. (C) Sequence alignment of the human and murine 3rd domain of the TCR β chain and the constructed 2/11 and 9/11 murinized variants.



Supplementary Figure 5. Chimeric anti-MuTCR β antibody binds to primary T cells expressing the murinized TCR containing 9 out of 11 murine residues in the 3rd domain of the β chain. Jurkat-76 cells were transduced with 2 different $\alpha\beta$ TCRs, containing 0/11 or 9/11 murine residues in the 3rd domain of the β chain, to assess binding of the newly generated chimeric and CDR grafted anti-MuTCR β antibodies. As negative controls, unstained and secondary antibody only conditions were used. As a positive control, wild-type PE-conjugated anti-MuTCR β was used. The data correspond to 2 independent experiments and a representative figure is shown.

Supplementary Table 1 Differences between the eleven human-mouse non-homologous amino acids in the third domain of the β chain (β M3). In red the mutations that abrogated binding of the anti-human $\alpha\beta$ TCR antibody

Mutation	Change in		
	Size	Charge	Hydrophobicity
Q ₈₈ H	-	Uncharged to positive charge	Hydrophilic to hydrophobic
T ₁₀₁ H	-	Uncharged to positive charge	-
N ₁₀₆ E	-	Uncharged to positive charge	-
E ₁₀₈ K	-	Negative to positive charge	Slightly more hydrophilic
T ₁₁₀ P	Less bulky	Uncharged	-
Q ₁₁₁ E	-	Uncharged to positive charge	-
D ₁₁₂ G	Less bulky	Negative charge to uncharged	Less hydrophobic
R ₁₁₃ S	Less bulky	Positive charge to uncharged	-
A ₁₁₄ P	-	Uncharged	Less hydrophobic
I ₁₂₀ N	-	Uncharged	Hydrophobic to hydrophilic
V ₁₂₁ I	-	Uncharged	-



CHAPTER 8

Summarizing discussion

Improving T-cell therapy for cancer

Exploiting the intrinsic ability of the immune system to combat cancer has revolutionized the way we treat cancer¹. Chimeric antigen receptor T-cell therapies (CAR T-cell) have shown promising results in the treatment of hematological malignancies. However, targeting of solid tumors still remains a challenge, mainly due to the intrinsic characteristics of their microenvironment and the difficulties to select an appropriate antigen to target^{2, 3}. **In chapter 1**, main hurdles of targeting solid tumors (antigen dilemma, T-cell fitness and tumor microenvironment) and potential T-cell engineering solutions are extensively discussed.

The use of V γ 9 δ 2-TCRs for the treatment of cancer

Selection of tumor antigens for adoptive T-cell therapy remains a challenge, especially in the context of solid tumors, in which potential targetable tumor associated antigens (TAA) are typically also expressed by healthy tissues⁴. One strategy to overcome antigen selection limitation is the use of V γ 9 δ 2-TCRs, which are able to recognize tumors in an HLA-independent way by sensing altered metabolism of the target cells^{5, 6}. Other advantages of these TCRs are the ability to discriminate between healthy and tumor tissue, as well as their capacity to target a broad range of both hematological and solid tumors. Therefore, the use of V γ 9 δ 2-TCRs to target tumor cells constitutes a promising approach to develop new therapies against cancer and is pursued by many commercial players in the field⁷. However, to date, clinical trials using primary V γ 9 δ 2T-cells have not shown efficacy, so new approaches are needed^{6, 8}. In this thesis two main strategies to harness $\gamma\delta$ TCRs in cancer immunotherapy have been developed and refined: GABs (Gamma delta TCR anti-CD3 Bispecific molecules) and TEGs ($\alpha\beta$ T-cell engineered with a defined $\gamma\delta$ TCR). For the latter design, namely TEGs, we recently reported that one infusion of TEGs was sufficient to induce a complete remission in a patient suffering from acute myeloid leukemia⁹.

Developing $\gamma\delta$ TCR-bispecifics (GABs)

T-cell engagers, commonly known as bispecifics, constitute a promising approach to treat tumors^{10,11}. Bispecific T-cell engagers are molecules that consist of two arms: one that binds to the tumor side (typically an antibody derived scFV directed against a TAA) and another arm that binds to T-cells, in most of the cases an anti-CD3 scFV^{10,12,13}. Consequently, bispecifics are able to attract T-cells in close proximity to tumors, allowing for the formation of an artificial immune synapse that results in the killing of the tumor by the T-cells¹⁴. Advantages of bispecifics when compared to other T-cell based therapies, such as CAR-T or TCR-based therapies, are the lower costs, and the fact that they are an off-the-shelf treatment¹⁵, thus time to infusion is shorter when compared with other immune therapies such as CAR-T cells, in which cells need to be engineered prior to infusion. The shorter time to administration makes them a great option for patients that need to be treated quick.

In **chapter 3** the development of $\gamma\delta$ TCRs anti-CD3 bispecifics (so called GABs) is reported. GABs harness the ability of V γ 9 δ 2-TCRs to recognize tumors in an HLA independent way, by fusing the extracellular domain of a V γ 9 δ 2-TCR to an anti-scFV-CD3, via a flexible linker. In this thesis we demonstrated that GABs were able to target several types of solid and hematological tumors *in vitro*, without harming healthy tissues. Moreover, GABs showed significantly increased tumor control *in vivo* in a subcutaneous multiple myeloma xenograft model. In addition, we observed that TCR affinity impacted GABs efficacy. Therefore, increasing the affinity of the $\gamma\delta$ TCR might lead to enhanced anti-tumor responses. However, affinity maturation of V γ 9 δ 2-TCRs is challenging in practice, as interaction between these TCRs and their target (BTN2A1/BTN3A1-3 complex) is not completely elucidated yet¹⁶.¹⁷. Hence, in **chapter 4** we aimed to improve GABs efficacy by tuning the affinity of the anti-CD3 binding arm. GABs containing different affinity anti-CD3 scFVs were tested. We observed that GABs containing the high affinity anti-CD3 scFV UCHT1 showed improved efficacy *in vitro* and *in vivo*. The improved *in vivo* efficacy of GABs carrying high affinity anti-CD3 scFV opposes to many publications in which high affinity of the anti-CD3 binding arm was related to diminished efficacy *in vivo*, in part due to an impaired tumor

distribution^{18, 19}. These differences in functionality between GABs and regular bispecifics bearing high affinity anti-CD3 scFV, could be explained by the different design of GABs when compared to typical bispecifics. In most of the studied bispecifics, the tumor binding domain is constituted by a high affinity anti-scFV (KD in nanomolar range), while in GABs the extracellular domain of a V γ 9 δ 2-TCR with a low affinity ~40-100 μ M is used^{20, 21}. We observed that GABs carrying the high affinity anti-CD3 scFV were bound to T-cells longer than those that carried the medium affinity anti-CD3 scFV. The prolonged binding of GABs to T-cells when using a high affinity anti-CD3 domain might have influenced the persistence of GABs in the mice, explaining the increased anti-tumor response. Moreover, contrary to other reports, the high affinity anti-CD3 did not induce release of cytokines related to cytokine release syndrome (CRS) nor induced weight loss in mice when compared to the medium affinity anti-CD3 OKT3, suggesting that GABs utilizing high affinity anti-CD3 binders might be safe. These promising results establish the bases for a new generation of $\gamma\delta$ -TCR based bispecifics, which constitute an alternative to more costly and time-consuming strategies such as CAR-T or TEGs.

Challenges in preclinical *in vivo* testing of GABs and future considerations from chapter 3 and 4

Utilization of mouse models is key to bring new immune therapies to clinic. However, evolutionary divergence of TCR γ and TCR δ loci between rodents and primates as well as the absence of BTN2A1-BTN3A molecules in rodents, difficult the selection of suitable preclinical mouse models for the study $\gamma\delta$ -TCR based therapies^{22, 23}. Therefore, further investigation is needed, especially in terms of improving preclinical models that successfully translate results obtained in animal models to cancer patients²⁴. For example, studying biodistribution of GABs *in vivo*, as well as PK/PD, might help to further understand the differences observed *in vivo*, which would help improving the design of GABs to achieve stronger efficacy. However, up to date the most typical *in vivo* models that are used to investigate bispecifics activity rely on the engraftment of huPBMCs into immune compromised mice (typically NSG mice). Although PBMC-engrafted mouse models are usually sufficient to

evaluate efficacy, they cannot be used to assess other important preclinical aspects such as safety (as the expression of the target is typically restricted to the tumor), biodistribution, the effect of the bispecific treatment in other immune cells (as these mice are not fully immune competent) or long-term effect of bispecifics (as the study window is limited to 4-5 weeks due to the development of GVHD in the mice engrafted with PBMCs). Moreover, differences between PBMC donors have been reported, and can highly impact the results²⁵. Alternatively, engraftment of huCD34 cells into NSG mice could be used to evaluate long-term effect of bispecifics, as well as their effect in other immune subsets, as immune cells develop within the mouse instead of in a human, recognizing the host as self and preventing the development of GVHD. Even if huCD34+ humanized mice could help to elucidate the effect of GABs in other immune subsets, as well as, the long term efficacy of GABs, huCD34+ humanized mice models are time-consuming and cannot be used to address safety or biodistribution²⁶. One option to increase the knowledge of GABs in terms of impact on other immune subsets and biodistribution might be the use of syngeneic models, in which immunocompetent mice are used. However, the use of syngeneic models requires the production of surrogate mouse counterparts of GABs, meaning developing GABs containing an anti-mouse-CD3 antibody²⁷. However, as shown in chapter 4, differences in anti-CD3 affinity highly impacts GABs activity, not only in terms of efficacy but also in influencing T cell viability. Thus, it might be challenging to get an anti-mouse-CD3 scFV that mimics the affinity and kinetics of the human one. One intermediate approach is the use of human CD3 transgenic mice²⁸. These are immune competent mice in which the lymphocytes express human CD3. Engrafting human tumors in immunocompetent mice is not possible due to xenogenic immune rejection. Therefore, establishment of a mouse derived tumor transduced to express the BTN2A1-BTN3A complex (needed for human V γ 9 δ 2TCR-mediated recognition) into these mice, and treatment with GABs afterwards could help to understand biodistribution and PK/PD of these molecules. However, due to the lack of BTN2A1-BTN3A1 expression in mice results might differ from biodistribution in humans. Hence, the most optimal approach to fully address safety and PK/PD of GABs are non-human primates, as already used by others developing concepts targeting BTN3A or making use of V δ 2T-cells^{29, 30}, however this is, in practice, challenging from an ethical and

economic point of view. In conclusion, combination of different models might help gaining knowledge on GABs properties, which would lead to improved designs in the future.

Towards a new generation of TEGs by addition of co-receptors

TEGs ($\alpha\beta$ T-cells engineered to express a defined $\gamma\delta$ TCR) were developed in our group to overcome the hurdles observed when using primary $\gamma\delta$ T-cells in patients, such as low expansion^{5,31}. TEGs combine the ability of V γ 9 δ 2TCRs to target tumor cells independently of HLA, with the ability of $\alpha\beta$ T-cells to expand and persist in patients. TEGs have been shown to be able to target both hematological and solid tumors without harming healthy tissues³¹. However, to date, clearance of tumors has not been achieved in mouse preclinical models by TEG001^{32,33}, so further improvement is required.

In **chapter 5** we aimed to improve the activity of TEG011 ($\alpha\beta$ T-cells expressing a V γ 5 δ 1-TCR) by co-expressing CD8a in CD4+ cells. The activation of the V γ 5 δ 1TCR used in TEG011 (so-called FE11), is dependent on the CD8 co-receptor, meaning that CD4+ $\alpha\beta$ T-cells transduced with a V γ 5 δ 1-TCR are not functional. Therefore, we hypothesized that addition of CD8 to CD4-TEG011 would improve efficacy of TEG011. Indeed, co-expression of CD8a into CD4+ TEG011, increased efficacy as well as persistence of TEG011. Due to the intrinsic tumor killing capacity of CD8+ T-cells, most of engineering efforts of the last decades have been focused on improving CD8+ T-cell efficacy. However, it has been recently described that CD4+ cells are key to achieve long-term responses in patients³⁴. These results emphasize the importance of engineering CD4+ T-cells to achieve sustained responses, and to increase efficacy of T-cell based immunotherapies. Hence, it would be interesting to extend our approach to other $\alpha\beta$ TCR based therapies such as NY-ESO or gp100 receptors that recognize tumor peptides in HLA-class I. CD8 co-receptor is key for T-cell activation by stabilizing interactions of TCR and HLA-I. Thus, as these tumor specific TCRs are HLA-class-I restricted, transfer of these into $\alpha\beta$ T-cells mainly impact CD8s, as the lack of the CD8 co-receptor in CD4+ cells impair the interaction between the TCR and the peptide/HLA-I complex reducing their anti-tumor activity³⁵. Therefore, transferring of CD8a

in combination with an anti-tumor specific $\alpha\beta$ -TCRs, such as NY-ESO or gp100, into CD4+ T-cells could improve $\alpha\beta$ TCR based therapies, by improving the activity of the CD4+ fraction.

In **chapter 6** we aimed to improve the efficacy of the clinical candidate TEG001. Contrary to TEG011, TEG001 anti-tumor efficacy relies on a V γ 9 δ 2-TCR (so called C15). Recognition of tumor cells by V γ 9 δ 2-TCRs is HLA independent, as it is mediated by the recognition of the butyrophilins BTN2A1 and BTN3A1-3 on the surface of tumor cells. Therefore, we developed a different strategy to enhance the efficacy of TEG001 by co-expressing NKG2D-chimeric co-receptors with the aim of improving T-cell activation signal 2 (co-stimulation), as it has been described as key to enhance anti-tumor efficacy of T-cell based therapies³⁶⁻³⁸. Different NKG2D chimeras were created by fusing the extracellular domain of the activating receptor NKG2D, which recognized stress antigens that are expressed mainly by tumor cells, to the costimulatory domains of the three different co-stimulatory proteins: ICOS, CD28 and 4-1BB. The three chimeras were tested both *in vitro* and *in vivo*, and different results were obtained. Only the NKG2D-CD28 and NKG2D-4-1BB chimeras were able to significantly improve the survival of mice in a multiple myeloma xenograft model, while the chimera comprising the ICOS domain did not confer any additive effect *in vivo*. Lack of activity of the NKG2D-ICOS chimera *in vivo* might be due to the absence of the transmembrane domain of ICOS in the chimera's design, as CD28 transmembrane and hinge domains were used in all the chimeras due to its superiority in expression. However, it has been described that ICOS signaling is mediated by its transmembrane domain³⁹, which might explain the poor performance of TEGs carrying the NKG2D-ICOS chimera *in vivo*. Hence, using of the transmembrane domain of ICOS in our chimera's, in combination with different intracellular domains, could lead to different results. However, on the other hand, expression when using ICOS domain was rather low compared to CD28, which would heighten the complexity of the engineering process.

Although both NKG2D-CD28 and NKG2D-4-1BB chimeras showed equal improved survival when compared with TEG001, only TEG001-NKG2D-4-1BB was able to improve tumor control in a solid tumor xenograft model. Due to its

intrinsic characteristics, microenvironment of solid tumors makes them more challenging to treat with immunotherapy when compared to hematological malignancies. One of the main hurdles when treating solid tumors is the immunosuppressive environment, which is able to inhibit the activity of T-cells through the activation of checkpoint molecules such as PD-1, inducing T-cell exhaustion and impairing T-cell fitness^{36, 40}. As shown in the scRNA seq data, and later confirmed by FACS, TEGs carrying the chimera NKG2D-4-1BB showed lower expression of exhaustion markers. The different T-cell fitness state between TEGs might explain the differences found in efficacy against hematological and solid tumors for both chimeras (NKG2D-CD28 and NKG2D-4-1BB). Furthermore, NKG2D-4-1BB showed enrichment in signatures related to long-term persistence such as oxidative phosphorylation, proliferation and NF- κ B signaling^{41, 42}. Altogether, the data suggest that combination of these two signatures could have contributed to the improved anti-tumor efficacy observed for NKG2D-4-1BB in the solid tumor model.

RNA seq analysis and experiments performed in the 3D model revealed that the NKG2D chimeras were only able to reprogram CD4+ cells. Knocking out of endogenous NKG2D in CD8+ cells improved the activity of the NKG2D-4-1BB chimera. These data suggest some interference between endogenous NKG2D and the NKG2D-chimeras. One explanation would be competition for the ligands between both receptors, however seems unlikely when comparing the expression levels of the endogenous and introduced receptors, as the expression of the NKG2D chimeras is considerably higher than the expression of the endogenous NKG2D. Other option is that the NKG2D chimeras might dimerize with the endogenous NKG2D, leading to alterations in the dimer interface that could affect the binding of the ligands or impair the signaling of the chimeras. Disruption of the binding pocket of NKG2D has been described to reduce the affinity for their ligands and could explain the lower additive effect observed for the NKG2D chimeras in the CD8+ cells⁴³.

To avoid extra-engineering steps that would complicate the production process, and with the aim of exploiting the full activity of both CD4+ and CD8+ cells, we decided to develop another chimeric co-receptor directed against

the stress antigen CD277 (103-4-1BB) that does not interfere with endogenous natural receptors. The 103-4-1BB chimera was able to reprogram both CD4+ and CD8+ cells and eradicate hematological and solid tumors *in vivo*. These impressive results suggest that tweaking of both subsets is key to achieve robust anti-tumor responses. Nevertheless, as previously reported by others for PD1⁴⁴, differences in binding affinity between the NKG2D-4-1BB-chimera (0.5-1.1 μM)⁴⁵ and the 103-4-1BB-chimera (10 nm)⁴⁶ cannot be excluded as a reason for the differences observed in efficacy. Therefore, substitution of the extracellular domain of the NKG2D-chimeras for an anti-NKG2D-ligand scFV such as anti-MICA (at expenses of restricting the recognition to only one NKG2D ligand), or affinity maturation of NKG2D could be explored in the future, although high binding affinity between NKG2D and its ligands has been described as detrimental for its activity⁴⁷.

Improving purity and safety of $\alpha\beta$ -TCR based therapies

High purity of the T-cell based therapy products has been described as key to achieve tumor control⁴⁸. In **chapter 7** we describe a novel method to enrich $\alpha\beta$ TCR engineered T-cells by modification of two amino acids of the constant domain of the TCR β chain of the introduced TCR. Introduction of only two murine amino acids abrogated the binding of an anti-human- $\alpha\beta$ TCR antibody, allowing the depletion of not engineered $\alpha\beta$ T-cells, and increasing the purity of the final product. Moreover, increasing the number of mutated amino acids to 9 allowed for the destruction of the engineered T-cells by using an anti-mouse-TCR β antibody conjugated to the cell cycle inhibitor MMAE. Hence, mutating binding sites at the TCR β chain of the introduced $\alpha\beta$ TCR addresses two limitations of $\alpha\beta$ TCR-based therapies with a single modification in the TCR β chain, namely *in vitro* selection and later *in vivo* depletion. However, although the enrichment of the engineered product through depletion of non-engineered $\alpha\beta$ T-cells was highly efficient, the *in vitro* results obtained when selectively killing the engineered cells with the anti-mouse-TCR β antibody were rather modest, and will probably not be sufficient for an *in vivo* setting. Therefore, further efforts need to be made to improve the efficiency of this strategy, by, for example, increasing the affinity of the anti-mouse-TCR β antibody. Moreover, it has been shown that immunogenicity impacts

persistence of T-cell based therapies, which is associated with impaired long-term responses^{49, 50}. Although minimal murinization of the $\alpha\beta$ TCR was used in chapter 7, we cannot completely exclude that the addition of the 9 murine counterpart amino acids to the introduced $\alpha\beta$ TCRs induces immunogenicity when infused in patients. Hence, increasing the affinity of the β chain-binding antibody might also help to reduce the number of amino acids that need to be mutated for the selective killing strategy.

Conclusion

In conclusion in this thesis we provide insights for the development and improvement of the next generation of $\gamma\delta$ TCR and $\alpha\beta$ TCR based therapies. First, we developed a new concept by generating $\gamma\delta$ TCR based bispecifics that were able to redirect $\alpha\beta$ T-cells towards a broad panel of hematological and solid tumors. Second, we improved the potency of two previously described $\alpha\beta$ T-cells engineered to express a $\gamma\delta$ TCR (TEG011 and TEG001) by introducing natural or chimeric co-receptors and improving performance of CD4 and/or CD8s. Last, we described a novel method to increase purity of engineered T-cells by murinization of the introduced $\alpha\beta$ TCR.

References

1. Finck, A.V., et al., *Engineered cellular immunotherapies in cancer and beyond*. Nat Med, 2022. **28**(4): p. 678-689.
2. Sterner, R.C. and R.M. Sterner, *CAR-T cell therapy: current limitations and potential strategies*. Blood Cancer J, 2021. **11**(4): p. 69.
3. Rafiq, S., C.S. Hackett, and R.J. Brentjens, *Engineering strategies to overcome the current roadblocks in CAR T cell therapy*. Nat Rev Clin Oncol, 2020. **17**(3): p. 147-167.
4. Wagner, J., et al., *CAR T Cell Therapy for Solid Tumors: Bright Future or Dark Reality?* Mol Ther, 2020. **28**(11): p. 2320-2339.
5. Sebestyen, Z., et al., *RhoB Mediates Phosphoantigen Recognition by V γ 9V δ 2 T Cell Receptor*. Cell Rep, 2016. **15**(9): p. 1973-85.
6. Sebestyen, Z., et al., *Translating gammadelta ($\gamma\delta$) T cells and their receptors into cancer cell therapies*. Nat Rev Drug Discov, 2020. **19**(3): p. 169-184.
7. Dolgin, E., *Unconventional gammadelta T cells 'the new black' in cancer therapy*. Nat Biotechnol, 2022. **40**(6): p. 805-808.
8. Buccheri, S., et al., *Efficacy and safety of $\gamma\delta$ T cell-based tumor immunotherapy: a meta-analysis*. J Biol Regul Homeost Agents, 2014. **28**(1): p. 81-90.
9. de Witte, M.A.S., J.; 1, Weertman, N.; Daudeij, A.; , van der Wagen, L.; Oostvogels, R.; de Haar, C.; Prins, H.J.; Dohmen, W.W.C; Bartels-Wilmer,C.M.; Johanna, I; Sebestyen, Z.; Kuball, J.; Straetemans, T., *First in human clinical responses and persistence data on TEG001: a next generation of engineered $\alpha\beta$ T cells targeting AML and MM with a high affinity $\gamma\delta$ 2TCR*. ASH confidential and under embargo until 04 11 2022 2022.
10. Labrijn, A.F., et al., *Bispecific antibodies: a mechanistic review of the pipeline*. Nat Rev Drug Discov, 2019. **18**(8): p. 585-608.
11. Li, H., P. Er Saw, and E. Song, *Challenges and strategies for next-generation bispecific antibody-based antitumor therapeutics*. Cell Mol Immunol, 2020. **17**(5): p. 451-461.
12. Goebeler, M.E. and R.C. Bargou, *T cell-engaging therapies - BiTEs and beyond*. Nat Rev Clin Oncol, 2020. **17**(7): p. 418-434.
13. Blanco, B., C. Domínguez-Alonso, and L. Alvarez-Vallina, *Bispecific Immunomodulatory Antibodies for Cancer Immunotherapy*. Clin Cancer Res, 2021. **27**(20): p. 5457-5464.
14. Morcos, P.N., et al., *Quantitative Clinical Pharmacology of T-Cell Engaging Bispecifics: Current Perspectives and Opportunities*. Clin Transl Sci, 2021. **14**(1): p. 75-85.
15. Subklewe, M., *BiTEs better than CAR T cells*. Blood Adv, 2021. **5**(2): p. 607-612.
16. Mamedov, M.R.V., S.; Freimer, J.W.; Das Sahu, A.; Ramesh, A.; Arce, M.M.; Meringa, A.D.; Ota, M.; Chen P.M.; Hanspers, K.; Nguyen, V.Q.; Takeshima, K.A.; Pritchard, J.K; Kuball, J.; Sebestyen, Z.; Adams, E.J.; Marson, A., *CRISPR screens decode cancer cell pathways that trigger $\gamma\delta$ T cell detection*. Nature, 2023(In print).

17. Vyborova, A., et al., *gamma9delta2T cell diversity and the receptor interface with tumor cells*. J Clin Invest, 2020. **130**(9): p. 4637-4651.
18. Mandikian, D., et al., *Relative Target Affinities of T-Cell-Dependent Bispecific Antibodies Determine Biodistribution in a Solid Tumor Mouse Model*. Mol Cancer Ther, 2018. **17**(4): p. 776-785.
19. Bortoletto, N., et al., *Optimizing anti-CD3 affinity for effective T cell targeting against tumor cells*. Eur J Immunol, 2002. **32**(11): p. 3102-7.
20. Willcox, B.E. and C.R. Willcox, *γδ TCR ligands: the quest to solve a 500-million-year-old mystery*. Nat Immunol, 2019. **20**(2): p. 121-128.
21. Deseke, M. and I. Prinz, *Ligand recognition by the γδ TCR and discrimination between homeostasis and stress conditions*. Cell Mol Immunol, 2020. **17**(9): p. 914-924.
22. Kazen, A.R. and E.J. Adams, *Evolution of the V, D, and J gene segments used in the primate gammadelta T-cell receptor reveals a dichotomy of conservation and diversity*. Proc Natl Acad Sci U S A, 2011. **108**(29): p. E332-40.
23. Adams, E.J., S. Gu, and A.M. Luoma, *Human gamma delta T cells: Evolution and ligand recognition*. Cell Immunol, 2015. **296**(1): p. 31-40.
24. Fox, B.A., et al., *Defining the critical hurdles in cancer immunotherapy*. J Transl Med, 2011. **9**: p. 214.
25. Yang, J., et al., *Simultaneous evaluation of treatment efficacy and toxicity for bispecific T-cell engager therapeutics in a humanized mouse model*. Faseb j, 2023. **37**(6): p. e22995.
26. Li, Z., X. Yang, and X. Song, *Humanized Mouse Models for Cancer Immunotherapy: A Focus on Human PBMC and HSPC Reconstitution*, in *Animal Models for the Development of Cancer Immunotherapy*. 2022. p. 211-249.
27. Wang, F., et al., *Design and characterization of mouse IgG1 and IgG2a bispecific antibodies for use in syngeneic models*. MAbs, 2020. **12**(1): p. 1685350.
28. Belmontes, B., et al., *Immunotherapy combinations overcome resistance to bispecific T cell engager treatment in T cell-cold solid tumors*. Sci Transl Med, 2021. **13**(608).
29. Lameris, R., et al., *A bispecific T cell engager recruits both type 1 NKT and Vγ9Vδ2-T cells for the treatment of CD1d-expressing hematological malignancies*. Cell Rep Med, 2023. **4**(3): p. 100961.
30. De Gassart, A., et al., *Development of ICT01, a first-in-class, anti-BTN3A antibody for activating Vγ9Vδ2 T cell-mediated antitumor immune response*. Sci Transl Med, 2021. **13**(616): p. eabj0835.
31. Johanna, I., et al., *Evaluating in vivo efficacy - toxicity profile of TEG001 in humanized mice xenografts against primary human AML disease and healthy hematopoietic cells*. J Immunother Cancer, 2019. **7**(1): p. 69.
32. Dekkers, J.F., et al., *Uncovering the mode of action of engineered T cells in patient cancer organoids*. Nat Biotechnol, 2023. **41**(1): p. 60-69.
33. Straetemans, T., et al., *Untouched GMP-Ready Purified Engineered Immune Cells to Treat Cancer*. Clin Cancer Res, 2015. **21**(17): p. 3957-68.

34. Melenhorst, J.J., et al., *Decade-long leukaemia remissions with persistence of CD4(+) CAR T cells*. *Nature*, 2022. **602**(7897): p. 503-509.
35. Tan, M.P., et al., *Human leucocyte antigen class I-redirected anti-tumour CD4(+) T cells require a higher T cell receptor binding affinity for optimal activity than CD8(+) T cells*. *Clin Exp Immunol*, 2017. **187**(1): p. 124-137.
36. Long, A.H., et al., *4-1BB costimulation ameliorates T cell exhaustion induced by tonic signaling of chimeric antigen receptors*. *Nat Med*, 2015. **21**(6): p. 581-90.
37. Guedan, S., et al., *Enhancing CAR T cell persistence through ICOS and 4-1BB costimulation*. *JCI Insight*, 2018. **3**(1).
38. Kowolik, C.M., et al., *CD28 costimulation provided through a CD19-specific chimeric antigen receptor enhances in vivo persistence and antitumor efficacy of adoptively transferred T cells*. *Cancer Res*, 2006. **66**(22): p. 10995-1004.
39. Wan, Z., et al., *Transmembrane domain-mediated Lck association underlies bystander and costimulatory ICOS signaling*. *Cell Mol Immunol*, 2020. **17**(2): p. 143-152.
40. Verma, N.K., et al., *Obstacles for T-lymphocytes in the tumour microenvironment: Therapeutic challenges, advances and opportunities beyond immune checkpoint*. *EBioMedicine*, 2022. **83**: p. 104216.
41. Kawalekar, O.U., et al., *Distinct Signaling of Coreceptors Regulates Specific Metabolism Pathways and Impacts Memory Development in CAR T Cells*. *Immunity*, 2016. **44**(2): p. 380-90.
42. Philipson, B.I., et al., *4-1BB costimulation promotes CAR T cell survival through noncanonical NF- κ B signaling*. *Sci Signal*, 2020. **13**(625).
43. Thompson, A.A., et al., *Identification of small-molecule protein-protein interaction inhibitors for NKG2D*. *Proc Natl Acad Sci U S A*, 2023. **120**(18): p. e2216342120.
44. Jiang, G., et al., *Dual CAR-T cells to treat cancers co-expressing NKG2D and PD1 ligands in xenograft models of peritoneal metastasis*. *Cancer Immunol Immunother*, 2023. **72**(1): p. 223-234.
45. Spear, P., et al., *NKG2D ligands as therapeutic targets*. *Cancer Immun*, 2013. **13**: p. 8.
46. Palakodeti, A., et al., *The molecular basis for modulation of human V γ 9V δ 2 T cell responses by CD277/butyrophilin-3 (BTN3A)-specific antibodies*. *J Biol Chem*, 2012. **287**(39): p. 32780-90.
47. Zuo, J., et al., *A disease-linked ULBP6 polymorphism inhibits NKG2D-mediated target cell killing by enhancing the stability of NKG2D ligand binding*. *Sci Signal*, 2017. **10**(481).
48. de Witte, M.A., et al., *Requirements for effective antitumor responses of TCR transduced T cells*. *J Immunol*, 2008. **181**(7): p. 5128-36.
49. Wagner, D.L., et al., *Immunogenicity of CAR T cells in cancer therapy*. *Nat Rev Clin Oncol*, 2021. **18**(6): p. 379-393.
50. Khan, A.N., et al., *Immunogenicity of CAR-T Cell Therapeutics: Evidence, Mechanism and Mitigation*. *Front Immunol*, 2022. **13**: p. 886546.



APPENDICES

Summary

Nederlandse samenvatting

Acknowledgements

List of publications

Curriculum vitae

Summary

Immunotherapy to treat cancer

Cancer is a disease caused by the uncontrolled division of aberrant cells. It constitutes one of the main causes of death worldwide and can affect any organ. Conventional treatments used to treat cancer patients include surgery, chemotherapy, or radiotherapy. However, these treatments are not always effective, and some patients cannot benefit from them. In addition, some of these therapies induce numerous side effects impairing patients' quality of life. In an attempt to overcome these difficulties, other therapeutic options are being developed in the recent years. Immunotherapy constitutes a new form of cancer treatment. It relies on the use of the patient's immune system to fight cancer. The immune system is formed by different organs, cells and proteins that protect the body against infections and cancer while preserving healthy cells. Immunotherapy make use of these cells and proteins to eliminate cancer cells.

T cells as anti-tumor therapy

T cells are a type of cells that play a crucial role in the immune system protecting the body from infections and participating in the body's response to cancer. Therefore, due to their intrinsic characteristics, T cells are currently being explored in the immunotherapy field as new therapeutic agent against cancer.

There are two different types of T cells: $\alpha\beta$ T cells and $\gamma\delta$ T cells. They are named after a protein that they contain in their membrane called TCR, that is responsible for recognizing infected or cancer cells. $\alpha\beta$ T cells contain an $\alpha\beta$ -TCR while $\gamma\delta$ T cells have a $\gamma\delta$ -TCR. As they contain different TCR types, they recognize infected or tumor cells in a different way. $\gamma\delta$ T cells often recognize infected or tumor cells directly, by sensing metabolic alterations that typically occur in these cells, while $\alpha\beta$ T cells usually require help of other cells (antigen-presenting cells) to recognize protein fragments from invaders or tumors.

In this thesis we made use of T cells' ability to recognize and kill tumor cells to generate new immunotherapeutic treatments as well as developing different strategies to improve their efficacy.

In **Chapter 1** main hurdles encountered when using T cell-based immunotherapies to treat solid tumors are described. Furthermore, different approaches to overcome these limitations are discussed, as for example the use of $\gamma\delta$ T cells or costimulatory receptors.

Bispecific T cell engagers using $\gamma\delta$ -TCRs

Bispecific T cell engagers are artificial proteins that can simultaneously bind two different proteins: one that is present in the tumor and the other one that is present in the T cell. Bispecifics are injected into the patients, where they will be able to bring T cells (treatment) close to tumor cells, facilitating the elimination of the tumor by the immune system.

In **Chapter 3** we developed a bispecific molecule so-called GAB that is able to bind to $\alpha\beta$ -T cells and tumor simultaneously. To make the GABs, we linked a soluble $\gamma\delta$ -TCR that can recognize different types of tumor cells to an antibody that is able to bind to a protein that is present in the membrane of $\alpha\beta$ T cells called CD3. In this way, GABs were able to work as connectors between T cells and tumors, resulting in the killing of the tumor cells both *in vitro* and *in vivo*.

One way to further improve the efficacy of GABs is to increase the binding strength (called affinity) between GABs and T cells. For that, in **Chapter 4** we generated different GABs in which the affinity of the antibody binding CD3 (on T cells) was tuned. We observed that higher affinity was associated with increased efficacy of the treatment *in vitro* and *in vivo*.

Use of $\gamma\delta$ -TCRs in TEG format

As explained above, $\gamma\delta$ T cells possess unique characteristics that made them promising for cancer treatment. However, up to date, the use of primary $\gamma\delta$ T cells in patients has not been successful, and no clinical responses have been observed. One of the reasons that explain this failure is the low ability of $\gamma\delta$ T

cells to divide in the patients, resulting in poor responses. To overcome this hurdle, we developed the concept of TEGs. TEGs are $\alpha\beta$ -T cells in which a $\gamma\delta$ -TCR is introduced. In this way best properties of both type of T cells are combined: a $\gamma\delta$ -TCR that directly recognizes tumor cells and an $\alpha\beta$ -T cell as a carrier, that preserves the ability to properly divide.

TEGs (specifically the so-called candidate TEG001) are being already tested in a clinical trial. In short, $\alpha\beta$ -T cells are extracted from the patient by a process called apheresis. After that, the $\alpha\beta$ -T cells are modified in the lab to introduce a $\gamma\delta$ -TCR (called CI5), generating the final product TEG001. This product is infused again into the patient as treatment against the tumor.

Use of co-receptors to improve TEGs

Although T cells rely on their TCR to get activated, the signal provided by this receptor is not enough to achieve robust anti-tumor responses. T cells express other secondary receptors called co-receptors that provide them with extra signals that are key to achieve full activation.

In this thesis we explored the addition of co-receptors to TEGs to further improve their activity.

In **chapter 5** we aimed to increase the efficacy of TEG011 by adding a CD8 α co-receptor. We know from previous work that the $\gamma\delta$ TCR that is used to generate TEG011 needs the co-receptor CD8 α in order to function. CD8 α is however lacking in a specific subset of $\alpha\beta$ T cells called CD4s, meaning that TEG011-CD4+ cells are not functional. Therefore, introduction of CD8 α into TEG011 allowed also the TEG011-CD4+ cells to be functional. We observed that addition of this receptor to TEG0011 improved efficacy in mice bearing tumors.

In **chapter 6** we developed several chimeric costimulatory receptors (CCR). CCRs were able to bind antigens that are expressed by stressed cells (such as tumor cells) and provide the T cells with extra signals that improved efficacy of the treatment. Addition of these novel co-receptors to TEG001 resulted in improved efficacy *in vivo*, inducing even complete cure of mice bearing liquid and solid tumors.

Improving purity of T cell therapy products

Although immunotherapy using T cells has reinvented the way we treat cancer, not all the patients respond to this type of treatment. One of the reasons of this failure might be explained by the low purity of the therapeutic product that is administered. When T cells are extracted from the patient and modified in the lab, not all the T cells are successfully altered, meaning that not all the T cells that are re-injected into the patient will be able to successfully recognize and kill tumor cells. Therefore increasing purity of the administered product would result in improved treatment effect. In **chapter 7** we developed an strategy to increase the purity of the engineered products. In short, we added some modifications to the sequence of the anti-tumor specific TCR that is introduced into the $\alpha\beta$ -T cells. These modifications in the TCR allowed us to distinguish and enrich the T cells that were successfully modified by eliminating the non-modified ones from the product.

Finally, in **chapter 8** the findings of the other chapters are discussed in the context of the current literature.

Nederlandse samenvatting

Immunotherapie als behandeling tegen kanker

Kanker is een ziekte die veroorzaakt wordt door een ongecontroleerde deling van afwijkende cellen en kan ieder orgaan aantasten. Het vormt wereldwijd een van de belangrijkste doodsoorzaken. Conventionele behandelingen die worden gebruikt om kankerpatiënten te behandelen zijn onder meer een chirurgische ingreep, chemotherapie of radiotherapie. Deze behandelingen zijn echter niet altijd effectief, waardoor er zijn dus nog steeds veel kankerpatiënten die niet kunnen worden genezen. Bovendien hebben de meeste kankermedicijnen vervelende bijwerkingen die de kwaliteit van leven van patiënten aantasten. Om deze redenen zijn er de afgelopen jaren andere behandelingen ontwikkeld. Immunotherapie is een nieuwe vorm van kankerbehandeling, die het immuunsysteem van de patiënt gebruikt om kanker te bestrijden. Het immuunsysteem wordt gevormd door verschillende organen, cellen en eiwitten die het lichaam beschermen tegen infecties en kanker, zonder gezonde cellen te beschadigen. Immunotherapie maakt gebruik van deze cellen en eiwitten om kankercellen op te ruimen.

T cellen als anti-tumor therapie

T cellen zijn immuun cellen die cruciaal zijn in de bescherming van het lichaam tegen infecties, maar ze spelen ook een belangrijke rol in het opruimen van kankercellen. Daarom wordt er op het gebied van immuuntherapie, momenteel onderzoek gedaan naar T cellen als nieuw therapeutisch middel tegen kanker.

Er bestaan twee verschillende soorten T cellen: $\alpha\beta$ T cellen en $\gamma\delta$ T cellen. Het unieke kenmerk van T cellen is hun T cel receptor, een eiwit op hun oppervlakte, waarmee ze geïnfekteerde of kankercellen kunnen herkennen. $\alpha\beta$ T cellen hebben een $\alpha\beta$ -TCR terwijl $\gamma\delta$ T cellen een $\gamma\delta$ -TCR hebben. Het grote verschil tussen de twee type T-cellen is de manier waarop ze geïnfekteerde of kankercellen herkennen. $\gamma\delta$ T cellen herkennen geïnfekteerde of kankercellen vaak direct, doordat ze subtiele veranderingen in de metabole staat van deze cellen herkennen. Terwijl $\alpha\beta$ T cellen hulp nodig hebben van andere cellen

(antigeen presenterende cellen) om stukjes eiwit van indringers of tumoren te herkennen.

In dit proefschrift hebben we gebruik gemaakt van het vermogen van T cellen om kankercellen te herkennen en op te ruimen om nieuwe immunotherapie behandelingen te ontwikkelen, en we hebben verschillende strategieën bedacht om de werkzaamheid te verbeteren.

In **hoofdstuk 1** worden de belangrijkste hindernissen van het gebruik van T cel gebaseerde immunotherapie voor de behandeling van solide tumoren beschreven. Verder worden er verschillende strategieën besproken om T cel immunotherapie te verbeteren, bijvoorbeeld het gebruik van $\gamma\delta$ T cellen of co-stimulerende receptoren.

Bi-specifieke T cel binders met behulp van $\gamma\delta$ -TCRs

Bi-specifieke T cel binders zijn kunstmatige eiwitten die gelijktijdig twee verschillende eiwitten kunnen binden: een die aanwezig is op de tumor, en een die aanwezig is op de T cel. Deze bi-specifieke eiwitten worden in de patiënt geïnjecteerd, waar ze T cellen en tumorcellen dicht bij elkaar brengen. Dit zorgt ervoor dat de T cellen actief worden en de kankercellen gaan aanvallen.

In **hoofdstuk 3** hebben we een nieuw bi-specifiek molecuul ontwikkeld, GAB genaamd, die tegelijkertijd aan $\alpha\beta$ T cellen en aan tumorcellen kan binden. Om deze GABs te maken hebben we een $\gamma\delta$ -TCR, die verschillende soorten tumorcellen kan herkennen, gekoppeld aan een antistof. Deze antistof kan binden aan een eiwit dat aanwezig is op het membraan van $\alpha\beta$ T cellen, CD3 genaamd. Op deze manier werken GABs als verbinder tussen T cellen en tumorcellen, wat resulteert in het opruimen van de tumorcellen zowel *in vitro* (in een testbuis) als *in vivo* (in een muis model).

Een manier om de GABs verder te verbeteren is door de bindingssterkte (affiniteit) tussen de GABs en de T cellen te verhogen. Daarvoor hebben we in **hoofdstuk 4** verschillende GABs gemaakt waarin we de affiniteit van het antilichaam aan CD3 (op T cellen) hebben aangepast. We laten, zowel *in vitro* als *in vivo*, zien dat de GABs met een hoge bindingsaffiniteit aan T cellen, beter werken dan GABs met een lagere T cel bindingsaffiniteit.

Het gebruik van $\gamma\delta$ -TCRs in het TEG concept

Zoals hierboven uitgelegd, bezitten $\gamma\delta$ T cellen unieke eigenschappen waardoor ze veelbelovend zijn als behandeling tegen kanker. Tot op heden is het gebruik van primaire $\gamma\delta$ T cellen bij patiënten echter niet succesvol. Een verklaring hiervoor is dat primaire $\gamma\delta$ T cellen in patiënten vaak uitgeput zijn waardoor ze zich niet meervermenigvuldigen. Om deze reden hebben we het concept van TEGs ontwikkeld. TEGs zijn $\alpha\beta$ T cellen die genetisch gemodificeerd worden om een $\gamma\delta$ -TCR tot expressie te brengen. Met deze techniek is het mogelijk om de beste kwaliteiten van beide celtype te combineren: een $\gamma\delta$ -TCR die direct tumorcellen kan herkennen, en een $\alpha\beta$ T cel als drager die het vermogen om zich te vermenigvuldigen behoudt.

TEGs (met name de zogenaamde kandidaat TEG001) worden al getest in klinische studies. Hierbij worden $\alpha\beta$ T cellen worden uit het bloed van de patiënt gehaald (dit proces noemen we aferese), waarna ze vervolgens in het lab gemodificeerd worden om een $\gamma\delta$ -TCR (Cl5 genaamd) tot expressie te brengen, dit resulteert in het eindproduct TEG001. Dit product wordt via een infuus teruggegeven aan de patiënt als behandeling tegen de tumor.

Het gebruik van co-receptoren om TEGs te verbeteren

Hoewel T cellen afhankelijk zijn van hun TCR om geactiveerd te worden, is het signaal van deze receptor niet voldoende om een krachtige anti-tumor respons te bereiken. T cellen brengen ook andere secundaire receptoren tot expressie: de co-stimulatie receptoren. Deze receptoren voorzien de T cellen van extra signalen die essentieel zijn om volledige activering te bereiken.

Om de activiteit van TEGs te verbeteren hebben we in dit proefschrift het toevoegen van co-receptoren aan TEGs onderzocht.

In **hoofdstuk 5** beschrijven we een manier om de effectiviteit van TEG011 te verbeteren door het toevoegen van een CD8 α co-receptor. We hebben gezien dat de $\gamma\delta$ -TCR die gebruikt is om TEG011 te maken, de CD8 α co-receptor nodig heeft om te functioneren. CD8 α ontbreekt echter in CD4 T cellen, dit is een specifieke subset van $\alpha\beta$ T cellen. Dit betekent dat TEG011-CD4+ cellen niet functioneel zijn. Daarom zorgt de introductie van CD8 α in TEG011 dat

TEG0011-CD4+ cellen ook functioneel zijn. We hebben in muizen met een tumor gezien, dat toevoegen van deze co-receptor aan TEG011 de werkzaamheid verbeterd.

In **hoofdstuk 6** hebben we verschillende chimere co-stimulerende receptoren ontwikkeld (CCR). CCRs kunnen antigenen binden die gestreste cellen tot expressie brengen (zoals tumorcellen) en voorzien de T cellen van extra signalen die de werkzaamheid van de behandeling verbeteren. Het toevoegen van deze nieuwe co-receptoren aan TEG001 resulteerde in een verbeterde werkzaamheid in vivo, we zagen zelfs volledige genezing in muizen met een tumor.

Verbeteren van de zuiverheid van T cel therapie producten

Hoewel T cel immunotherapie een veelbelovende behandeling is voor patiënten met kanker, reageren niet alle patiënten op deze behandeling. Een lage zuiverheid van het toegediende T cel product zou hiervoor een verklaring kunnen zijn. Wanneer T cellen uit het bloed van de patiënt worden gehaald en het in lab worden gemodificeerd worden niet alle T cellen succesvol gewijzigd. Dit betekent dat niet alle T cellen die terug in de patiënt worden geïnjecteerd, in staat zullen zijn om tumorcellen te herkennen en op te ruimen. Het verhogen van de zuiverheid van het toegediende product zal daarom resulteren in een verbeterd effect van de behandeling. In **hoofdstuk 7** bespreken we een techniek om de zuiverheid van het gemodificeerde T cel product te verhogen. In het kort, we hebben een paar veranderingen (mutaties) aangebracht in de geïntroduceerde kankerreactieve TCR, waardoor deze onderscheiden kan worden van de originele TCR van de T cellen. Hierdoor is het mogelijk alleen de gemodificeerde cellen, die nu kankerreactief zijn, terug te geven aan de patiënt als therapie.

Ten slotte worden in **hoofdstuk 8** de resultaten van de andere hoofdstukken in een breder perspectief geplaatst door vergelijkingen te maken met de huidige literatuur.

Acknowledgments

Dear **Jurgen**, thank you for all your support and guidance throughout my PhD. I have always admired your ability to balance clinics, following up on the multiple projects of the lab and still make some time to look out for people. Thanks for being always open for discussions and listening to my opinion even when we did not agree (because it ´s okay to disagree ;)). Thanks also for the opportunity to continue in the group after my PhD, hopefully we can still publish some more data, although I hope it takes us fewer versions than the never-ending NKG2D paper.

Dear **Dennis**, I have really enjoyed working with you all these years. Thanks for your endless patience, guidance, support and for always having a kind answer (even when things were not working). I enjoyed all the scientific discussions we had, from which I always learnt something new. I have always admired how you always came up with the right answer/explanation to all my (most of the times stupid) questions. You are a great supervisor, and I was very lucky to have you around. I hope we can still work together for some time so you can also improve your Spanish (as we all know that my Dutch won´t get any better).

Dear **Zsolt**, I can say you were my first contact with the lab as I had my first interview with you. Although we have not work closely together, you were always willing to give input for my different projects as well as for the papers, so thanks a lot for that! I also enjoyed the meetings we had together and all the conversations about Spain. Thanks also for being the only one trying to pronounce my name right (in the Spanish way) ;)

Dear **Sabine**, you are probably the person I have spent more time with over the last 5 years. Thanks for your hard work with the mice, as well as for listening to me whenever I needed to vent my frustrations, that really helped me going through my PhD. I had a lot of fun working with you, and I admire your professionalism and your dedication. Looking forward to more crazy conversations and hearing about those countless (but necessary) dresses, and who knows, maybe the IV injection company dream will come true someday ;).

Dear **Eline**, what began as a bit of help with an *in vivo* experiment turned into 4 first-shared author papers. Despite some frustrating moments (GABs mouse model), I really enjoyed it. You are a great scientist and I have learnt a lot from you. And, although I will always remember the GABs mouse model as the most frustrating moment of my PhD, I can say that I will also remember the day that we made it work as one of the happiest moments of these years. I wish you all the luck in your career, you really deserve it!

Dear **Inez**, thanks for all the help with the mice during these years. You are hard worker and were always willing to help not only with mice but with whatever question I came to you. Also, I had a lot of fun working with you, and I will never forget the time that we were the only ones around during the pandemic (I think you were the only person I saw during weeks). I wish you all the luck in your next career step, we will miss you and I hope we keep in touch!

Dear **Caterina**, even if you joined the lab in my last year of PhD, we still managed to work quite a lot together! Grazie for all the help with the resubmission experiments and being always willing to help. I enjoyed our lunches, the walks back home and all the Spanish-Italian lessons. Best of luck in 'your new lab' ;) I am sure your hard work will pay off!

All other Kuball group members: **Astrid**, I enjoyed a lot all the chats, lunches, and coffees. I wish you all the best in your new job (glad you are still around) and finishing your thesis; you are the next one!. Dear young **Jiali**, I had a lot of fun working with you! Thanks for all your hard work and help with the hybridomas, for all the tips about restaurants and the friendly reminders about my age ;). **Tineke**, thanks for being always approachable for whatever question I had and for all the nice chats at ML2! **Ivana**, grazie mille for all the Italian lessons and late lunches! I had a lot of fun listening to your proficient Spanish. **Trudy**, I appreciate all the input you gave for the *in vivo* experiments, thanks for that! **Peter**, thanks a lot for all your help analyzing and helping me understand the RNA seq data. I enjoyed a lot the discussions we had for the NKG2D paper. **Konstantinos**, thanks for livening up the long pipetting sessions at ML2 with our 'complaining' chats. Best of luck in finishing the PhD!. **Lucrezia**, thanks for always being there to complain about the Dutch weather. Our best moment during the PhD? Definitely exploring the natural bridge in Canada. Good luck

with finishing the PhD! **Mara**, glad we survived to the 7-eleven! Thank you for all the help with the long sortings and translations in Canada, I really enjoyed a lot our time there. Best of luck with the PhD. **Froso**, thank you for all the help with several papers, and specially for your kindness and for being always willing to help without complaining. **Angelo**, thanks for the help with the 3D model experiments! Good luck with the last steps of your PhD. **Anniek**, thank you for all the help and clear explanations about statistics. Best of luck with the PhD! **Laia**, thanks for all the jamón and turrón, I wish you all the best in your PhD journey! **Annet** and **Naomi**, thanks for helping whenever I had a question about protocols or panels, I also enjoyed all the nice chats we had!

Thanks to **all other CTI colleagues**, and specially to my office roommates: **Emma, Kim, Thomas, Dilara, Flores**, thanks for all the chats and all the help when I struggled with Dutch language (which happened quite often).

To all the people I met during this journey and that ended up becoming friends and my family in Utrecht:

Coral, qué hubiese sido de mi sin ti el primer año. Muchas gracias por todos los planes de turismo, las risas, cenas, anécdotas surrealistas, caminos en bici y en definitiva por estar siempre ahí y escucharme cuando necesitaba desahogarme. **Cris B**, lo que comenzó como una emboscada por parte de Coral, ha terminado en interminables horas de risas, viajes y sobre todo macumbas. Gracias por apuntarte a todo (incluyendo viajes a Amersfoort diluviando), y por escuchar mis audios eternos quejándome de todo un poco. **Laura**, gracias por dejarme formar parte de 'tu erasmus', por todas las fiestas, anécdotas, viajes y por acogerme en Pamplona todos los años. **Alba**, tu fuiste mi primer contacto en Utrecht! Gracias por todos los momentos y por enseñarnos Dublin y todas las risas de St. Patricks day. **Cris P**, gracias por todas las cenas, fiestas y risas. Siempre recordaré las navidades del atleti en tu casa, y los viajes en coche escuchando musicote. Gracias también por tomarte mi próximo cumple tan enserio ;). **Andrea**, gracias por todas las noches de sushi, fiestas y risas. También por las visitas cada vez que vuelves. Nos vemos prontito! **Juan**, gracias por todas las charlas sobre política y música, y por todas las risas. **Mauri**, gracias por el máster en bombas de humo y por todas las anécdotas. **Carlota**, gracias por apuntarte a un bombardeo sin

pensarlo, por todas las noches en los amigos, festivales y macumbas, y...viva la M30!. **Lucía y Lorena**, compañeras de macumbas, conciertos y salseos de famosos, gracias por todas las risas más que necesarias durante el PhD.

A mis amigos de España: **Marina, Sandra, Zahira, Isma, Jorge y David**, gracias por todos los viajes, fiestas y por siempre intentar hacer un hueco para verme cada vez que vuelvo aunque a veces sea difícil cuadrar agendas. También por las visitas (express en algunos casos), que espero que sean más pronto. **Leylita, Iñigo y Paula**, aunque no nos veamos muy frecuentemente es guay seguir en contacto después de tantos años. Gracias por todas las conversaciones recordando anécdotas del hospital y de nada por todos los audios cantando 'felices los cuatro' (tendréis versión en directo en unos meses). **Alicia y Luismi**, gracias por todos los meses que pasamos en Oslo y por seguir preocupándoos por mi estos años de PhD. Espero poder visitaros pronto. **Elenay Sergio**, gracias por los audios compartiendo frustraciones del PhD y poniéndonos al día, y por los largos cafés en Madrid. Nos vemos pronto por el norte!

A toda mi familia por apoyarme durante estos años lejos de casa. En especial a mis padres. **Mamá y Papá**, gracias por todas las visitas, por venir cada vez que necesitaba ayuda con las mudanzas, por las videollamadas, todos los viajes al aeropuerto y sobre todo por preverme con toneladas de Jamón. También por apoyarme allá donde voy y en lo que hago.

List of publications

This thesis:

Meringa, A. D.*, Hernández-López, P.*, Cleven, A.*, de Witte, M., Straetemans, T., Kuball, J., Beringer, D. X., & Sebestyén, Z. (2023). Strategies to improve $\gamma\delta$ TCRs engineered T-cell therapies for the treatment of solid malignancies. *Frontiers in immunology*, 14, 1159337. <https://doi.org/10.3389/fimmu.2023.1159337>.

van Diest, E.*, Hernández López, P.*, Meringa, A. D., Vyborova, A., Karaiskaki, F., Heijhuurs, S., Gumathi Bormin, J., van Dooremalen, S., Nicolassen, M. J. T., Gatti, L. C. D. E., Johanna, I., Straetemans, T., Sebestyén, Z., Beringer, D. X.#, & Kuball, J#. (2021). Gamma delta TCR anti-CD3 bispecific molecules (GABs) as novel immunotherapeutic compounds. *Journal for immunotherapy of cancer*, 9(11), e003850. <https://doi.org/10.1136/jitc-2021-003850>

van Diest, E.*, Hernández-López, P.*, Nicolassen, M., Bongiovani, L., de Bruin, A., Karaiskaki, E., Bots, K., Heijhuurs, S., Kumari, A., Straetemans, T., Beringer D.X.#, Kuball, J#. Impact of CD3 binding affinity on the potency of Gamma delta TCR Anti-CD3 Bispecific T cell engagers (GABs). Manuscript in preparation.

Johanna, I.*, Hernández-López, P.*, Heijhuurs, S., Scheper, W., Bongiovanni, L., de Bruin, A., Beringer, D. X., Oostvogels, R., Straetemans, T., Sebestyén, Z., & Kuball, J. (2021). Adding Help to an HLA-A*24:02 Tumor-Reactive $\gamma\delta$ TCR Increases Tumor Control. *Frontiers in immunology*, 12, 752699. <https://doi.org/10.3389/fimmu.2021.752699>

Hernández-López, P.*, van Diest, E.*, Brazda, P., Heijhuurs, S., Meringa, A., Hoorens van Heyningen, L., Riillo, C., Schwenzel, C., Zintchenko, M., Johanna, I., Nicolassen, MJT., Cleven, A., Kluiver, TA., Millen, R., Zheng, J., Karaiskaki, F., Straetemans, T., Clevers, H., de Bree, R., Stunnenberg, HG., Peng, WC., Roodhart, J., Minguet, S., Sebestyén, Z., Beringer, DX.#, Kuball, J#. Dual targeting of cancer metabolome and stress antigens affects transcriptomic heterogeneity and efficacy of engineered T cells. *Nat Immunol.* 2023 Nov 27. doi: 10.1038/s41590-023-01665-0. Epub ahead of print. PMID: 38012415.

- Patent: EP23188032.9CD277 TARGETING COSTIMULATORY RECEPTOR (Hernandez-Lopez co-inventor)

Kierkels, G. J. J.*, van Diest, E.*, Hernández-López, P.*, Scheper, W.*, de Bruin, A. C. M., Frijlink, E., Aarts-Riemens, T., van Dooremalen, S. F. J., Beringer, D. X., Oostvogels, R., Kramer, L., Straetemans, T., Uckert, W., Sebestyén, Z., & Kuball, J. (2021). Characterization and modulation of anti- $\alpha\beta$ TCR antibodies and their respective binding sites at the β TCR chain to enrich engineered T cells. *Molecular therapy. Methods & clinical development*, *22*, 388–400. <https://doi.org/10.1016/j.omtm.2021.06.011>

*These authors share first authorship

#These authors share senior authorship

Other

Johanna, I., Hernández-López, P., Heijhuurs, S., Bongiovanni, L., de Bruin, A., Beringer, D., van Dooremalen, S., Shultz, L. D., Ishikawa, F., Sebestyén, Z., Straetemans, T., & Kuball, J. (2020). TEG011 persistence averts extramedullary tumor growth without exerting off-target toxicity against healthy tissues in a humanized HLA-A*24:02 transgenic mice. *Journal of leukocyte biology*, *107*(6), 1069–1079. <https://doi.org/10.1002/JLB.5MA0120-228R>

van Diest, E., Nicolassen, M. J. T., Kramer, L., Zheng, J., Hernández-López, P., Beringer, D. X., & Kuball, J. (2023). The making of multivalent gamma delta TCR anti-CD3 bispecific T cell engagers. *Frontiers in immunology*, *13*, 1052090. <https://doi.org/10.3389/fimmu.2022.1052090>

Astrid Cleven, Angelo D. Meringa, Domenico Fasci, Thijs Koorman, Peter Brazda, Tineke Aarts, Inez Johanna, Dennis X Beringer, Patricia Hernandez-Lopez, Sabine Heijhuurs, Tomohiro Mizutani, Sangho Lim, Maarten Huismans, Jochem Bernink, David Vargas Dias, Wei Wu, Esther San Jose, Jelle Schipper, Nikos Tskakirakis, Lauren Hoorens van Heyningen, Annick Nouwens, Lucrezia Gatti, Trudy Straetemans, Hugo Snippert, Jeanine Roodhart, Patrick Derksen, Jarno Drost, Maarten Altelaar, Albert Heck, Hans Clevers, Jurgen Kuball, Zsolt Sebestyén. PI3K-AKT1-mTOR activity and BTN3A1 phosphorylation are required for early cancer immune surveillance via V γ 9V δ 2TCR T cells. Manuscript in preparation.

Curriculum vitae

Patricia Hernández López was born on the 11th of May 1994 in Madrid, Spain. In 2016 she completed her bachelor's degree in Health Biology at the University of Alcalá. During her bachelor's degree program, she undertook a five-month internship at Alberto Sols Biomedical Research Institute under the supervision of Prof.Dr.Antonio Villalobo, where she studied the role of Grb7 in cancer. Subsequently, Patricia started a master's degree in Therapeutic Targets of Cell Signalling: Research and Development at the University of Alcalá. As part of the program, Patricia performed a four-month internship at the Research Institute of Hospital 12 the Octubre under the supervision of Prof.Dr.José Luis Rodríguez Peralto and Yolanda Ruano, studying the application of Comparative Genomic Hybridization in melanoma. After obtaining her MSc, she joined the lab of Dr.Lorena Arranz at the Centre for Molecular Medicine of Norway (NCMM) as a Scientific assistant, where she worked on projects related to stem cells and cancer. In 2018, she started her PhD at the Center for Translational Immunology (CTI) at the University Medical Center Utrecht, under the supervision of Prof.Dr. Jürgen Kuball and Dr.Dennis Beringer. Here she worked on the development and improvement of new immunotherapeutic concepts such as $\gamma\delta$ TCR bispecifics and the use of chimeric costimulatory receptors to enhance T cell based therapies. The results of this work are discussed in this thesis.

